ANNUAL PROGRESS REPORT OF 1992

(Grant No. NAGW-2924)

of

THE CENTER FOR AEROSPACE RESEARCH
- A NASA CENTER OF EXCELLENCE
AT
NORTH CAROLINA AGRICULTURAL AND
TECHNICAL STATE UNIVERSITY

for

the performance period
of
January 1, 1992 to December 31, 1992

submitted to

Futron Corporation
c/o National Aeronautics and Space Administration
7315 Wisconsin Avenue, Suite 400W
Bethesda, Maryland 20814-3202
Attn: HBCU Research Center Program Manager

submitted by

Steven H.-Y Lai, Ph.D., P.E.
Principal Investigator and Center Director
Department of Mechanical Engineering
North Carolina A&T State University
Greensboro, North Carolina 27411
Tel: 919-334-7620, Fax: 919-334-7417

Date Submitted: December 12, 1992

TABLE OF CONTENT

THE CENTER FOR AEROSPACE RESEARCH
A NASA CENTER OF RESEARCH EXCELLENCE

1. EXECUTIVE SUMMARY

This is the first annual project report of NASA Grant No. NAGW-2924. This report documents the efforts and outcomes of our research and educational programs at NASA-CORE in NCA&TSU. The goal of the Center was to establish a quality aerospace research base and to develop an educational program to increase the participation of minority faculty and students in the areas of aerospace engineering.

The major accomplishments of this Center in the first year can be summarized in terms of three different areas, namely, the center's research programs area, the center's educational programs area, and the center's management area. In the center's research programs area, we focus on developing capabilities needed to support the development of the aerospace plane and high speed civil transportation system technologies. A research plan is in place. Each center participant is assigned with a specific research topic in line with the center's hypersonic research. More than twenty (20) technical papers are published or being submitted for publications. In the center's educational programs area, we developed an aerospace engineering option program ready for university approval. Two aerospace engineering courses are being offered this semester. In the center's management area, we are able to develop our long-range plans for the next two years. At this point, we have successfully recruited minority students and faculty researchers needed for the program. One tenure track faculty member and two adjunct research associates are recruited by the center in various research areas. Twenty (20) U.S. citizen students are recruited to the program. Among them eighteen (18) students are African-Americans. We are pleased with our development and wish to continue with our effort.

A. MAJOR ACCOMPLISHMENTS IN RESEARCH PROGRAMS

The NASA-CORE at NCA&TSU provides a common focus for basic research and innovation that link aerospace engineering disciplines in a productive way. The Center focuses its research on the development of the hypersonic plane and high speed civil transportation system technologies by integrating four interdisciplinary components into an effective system. These components include Aerospace Structures, Controls and Guidance, Computational Fluid Dynamics and Human Engineering.

The center has initiated a number of sequenced and coordinated projects that focus on hypersonic research to support high speed transportation and single-stage-to-orbit plane technologies. These research capture the integrated aspects of structures, controls, fluids interaction and human-machine interface that are required for the initial and evolutionary aerospace research. A list of center researchers and their associated research tasks are given in Table 1.

Table 1 - The Center Researchers and Research Tasks

Research Components	Participants	Research Tasks
Structures	E. Abu-Saba M. McGinley J.Y. Shen Res.Assoc./Lai	A. Estimate Structural Dynamics of Vehicle B. Design/Fabricate Structural Test Article and Validate Design in Laboratory Facility C. Study Structural Design of Hypersonic Vehicle D. Refine Integrated Design (Structure/Control)
Controls	A. Homaifar Y.D. Song D. Dunn Res.Assoc./Lai	A. Determine Optimal Flight Path for Lunch to Orbit B. Calculate Flight Dynamics of Hypersonic Vehicle (@ Subsonic & Hypersonic Cond.) C. Study Vibration Characteristics of Vehicle D. Incorporate Deformation Effects into Flight Dynamics and Control Analysis
Fluids	S. Chandra G. Elbert K. Jones Hassan/McRae	A. Develop New Approaches for Turbulence Modeling for High Speed Compressible Flows B. Radiation Heat Transfer for Hypersonic Chemically Reacting Flows C. Design/Fab 6 DOF Balance for Wind Tunnel and Measure Low Speed Aerodynamics of Vehicle in Tunnel D. Research on Improving CFD Algorithm for Better Accuracy and Efficiency For Hypersonic Flows
Human Engineering	S. Ntuen E. Park J. Deeb J. Kim	A. Develop Flight Simulator for Hypersonic Vehicle B. Study NASP Handling Qualities C. Study Effects of Flexibility on Handling Qualities D. Study Effects of Flexibility on Control System Performance

Structures Research

The goal of the structures research group is to develop accurate analytical and experimental models for hypersonic vehicles to be powered at Mach 4 or above. The group's long range research focuses are to (1) establish the geometric parameters for an hypersonic plane, (2) specify materials and component sizes for the various components of an hypersonic plane, (3) apply aerodynamic and thermal forces to the structures, (4) establish analytical models for a hypersonic plane and determine its dynamic characteristics, (5) provide the dynamic model to the guidance and controls group, (6) establish test procedures and perform tests to verify theoretical results, (7) train graduate and undergraduate students to perform specific tasks in the development of the above, and (8) develop the structural laboratory to enable the structures group to provide governmental and private clients with appropriate expertise in the area of aircraft structures.

The structures group is currently working on the following tasks including (1) evaluation of the accuracy of the plane truss-beam model, (2) modification of the plane

truss-beam model to improve the accuracy of prediction, (3) expanding of the analytical model to three dimensional models, (4) modification of computer programs to incorporate the expanded model, (5) provide the guidance and controls group with rough analytical hypersonic plane models with stiffness and mass matrices, (6) preparation of two technical articles for publication.

The structures group holds group meetings once every two weeks. A joint meeting with controls groups was established. The objective is to develop a realistic structures-controls integrated model through group interaction. It is expected that the group will also interact with the CFD and the human engineering groups to acquire aerothermal loading data and requirements for handling quality to build a complete system model. The structures group currently work closely with the Spacecraft Controls and Controls Technology groups at NASA Research Centers.

In summary, we value our structures research group as one of the important areas for hypersonic research. At this stage, the group has an excellent head start. One hypersonic prototype plane model was constructed and ready for experimentation. One research associate, Dr. Ji-Yao Shen, was hired on the project. Dr. Shen's expertise is in space structures modeling. His expertise will benefit the structures group in characterizing the dynamics of hypersonic planes. Four undergraduate students are recruited in this program. They work closely with both Drs. Abu-Saba and McGinley. Two technical paper have been published by the group and one is in preparation.

Controls Research

In order to achieve the objectives stated in the NASA-CORE proposal, the controls group has divided their research tasks into four categories: (1) the study of optimal trajectory and maneuvability of hypersonic vehicles, (2) The study of flight dynamics at both subsonic and supersonic range, (3) The investigation of smart materials for high speed sensing and controls, (4) The applications of intelligent controllers for hypersonic vehicle control.

The control group is currently offering a course, Linear Systems and Controls, for the Center. The group will offer another new course in Flight Vehicle Stability and Controls next semester. The group is currently developing a Control Systems Laboratory to be used for both course teaching and research.

In summary, we view the controls group as a vital and productive group. The group is pleased to hire Dr. Y.D. Song as a senior research fellow. Dr. Song will help the group in various research tasks stated above, specifically in the design of controllers incorporating flight dynamics for hypersonic and supersonic vehicles. Two graduate students and three undergraduate students are recruited to the program. They work closely with both Drs. Homaifar and Lai. The group would like to congratulate on the graduation of Mr. Ed. McCormick, an MSEE student, partially sponsored by the NASA-CORE.

The controls group holds a weekly meeting to discuss research projects and share research outcomes. The group meets with structures group once every two weeks to discuss the integrated model for hypersonic research. Five technical papers were published, two submitted for Journal publication, and another two are in preparation.

Advanced Fluid Dynamics Research

The focus of research in the CFD area is two-fold: (1) to develop new approaches for turbulence modeling so that high speed compressible flows can be studied for applications to entry and re-entry flows, and (2) to perform research to improve CFD algorithm accuracy and efficiency. The short range plans for CFD group are (1) modeling of the pressure dilatation term as well as the compressible dissipation term and using the SPARK code to predict useful parameters such as the shear layer growth rate for compressible high speed turbulent flows, and (2) development of efficient numerical algorithms for high speed flow fields. It is hoped that a new research associate can be hired in early 1993 to initiate research in this vital area.

During 1992, Dr. Chandra supervised the M.S. thesis work of one graduate student (Cheryl Sellers). Both Dr. Chandra and Ms. Sellers spent the bulk of the summer in 1991 and 1992 in NASA Langley Research Center at Theoretical Flow Physics Branch. Ms. Sellers focussed on the study of compressibility effects in modeling turbulent high speed mixing layers. The accomplishments to date are: (1) incorporation of the extension of the compressibility dissipation model of Sarkar et al. of ICASE in the SPARK code using two-equation turbulence modeling, (2) extensive literature review to delineate work done or being done in the study of compressibility effects in turbulent shears flows, (3) comparison of results in (1) with the results of a large number of experimental and analytical studies.

The CFD group will continue association with the Theoretical Flow Physics Branch at the NASA Langley Research Center (LaRC). It is anticipated that Dr. Chandra and/or one faculty member and two students will spend most of 1993 summer at LaRC. Such an association enables faculty and students to (a) use the LaRC technical library; (b) interact with faculty and students from NCSU and other universities; and (c) interact with NASA and ICASE researchers and facilities on a daily basis.

Dr. Chandra is the area coordinator of the CFD research. A research associate, Dr. Gregory Elbert, is recruited aboard on October 15. The new research associate will initiate our effort in the area of radiation heat transfer for hypersonic chemically reacting flows and will, therefore, complement the turbulence modeling work for high speed flows. Detailed short-range and long-range plans will be developed for work in the radiation heat transfer area after the new person joins our center. Mr. Kenneth Jones has joined the ME Department this fall as a tenure-track faculty member. He is scheduled to defend his Ph.D. dissertation at NCSU in early September and is expected to be an asset to the CFD area in CORE by virtue of his experimental/analytical background in CFD research. Mr. Jones plans to apply for participation in one of the NASA/ASEE summer institutes in 1993 with

the objective of becoming closely associated with appropriate NASA facilities and personnel. Dr. Chandra, Mr. Jones and the new research associate will work closely with Drs. Hassan and McRae of NCSU in accordance with the attached subcontract, which delineates the long-range research plan for the CFD area.

A course in computational fluid dynamics is being offered by Dr. Chandra this fall. This course will have a mix of undergraduate ME Seniors and graduate students. Dr. Hassan A. Hassan will offer an advanced course in combustion and reacting flows at NCSU in spring. Some faculty members and graduate students in the CFD area at NCA&TSU will enroll in this course if their schedules permit. The group will continue recruitment efforts with the objective of enticing two graduate students and two undergraduate students by January 1, 1993, (2) offering an advanced course in CFD at NCA&TSU in Spring 1993,

A paper entitled "Study of Compressibility Effects in Turbulent Shear Flows" was presented at the ASME Fluids Engineering Conference, 1992. Ms. Sellers defended her M.S. thesis on August 10, 1992. She has been admitted to the Ph.D. program in ME at the University of Illinois and has begun her doctoral studies this fall. Dr. Jones published a paper entitled "Boundary Layer Study on Nozzle Wall at Hypersonic Velocities," in AIAA conference. Dr. Elbert has two papers to be published in the near future.

Human Engineering Research

The research of HE group is to study the existing handling quality studies and the information in order to develop a prototype training simulator model for hypersonic aircraft. The research platform adopted in this study follows the NASA task statements: (1) develop flight simulator for hypersonic vehicle, (2) study NASP handling qualities, and (3) study effects of flexibility on handling qualities and on Control System Performance.

Following the above statement of work, the group has developed three research strategies involving: (1) the study of existing handling quality studies and the associated aircraft and develop flight simulation data characterization, (2) the development of a profile for flight simulation data acquisition based on objective statement #1 above, and (3) the development of a simulator and an embedded expert system platform which can be used in handling quality experiments for hypersonic aircraft/flight simulation training. The development of a successful knowledge-driven flight simulator shall have at least three utilities. These are: (1) flight data characterization, (2) the derivation of real-time pilot rating over a set of flight test data, and (3) the derivation of aircraft performance data over a set of defined environment and aerodynamic parameters.

The Human Engineering Systems group has come up with a research plan listed as follows: (1) development of theoretical model for human-pilot response in hypersonic aircraft system (short term), (2) purchase and installment of flight simulation platform (short term), (3) experimental test (validation) of the human pilot response models (long term), (4) experimental test of human pilot (subjects) in hypersonic aircraft handling

qualities (long term), (5) 3-D Visual and Motion system reconstruction for flight simulator (long term), (6) handling quality database for pilot performance simulation (short term), (7) expert system platform to support flight simulation and handling quality experiments in hypersonic aircraft domain (long term).

The HE group is able to attract one graduate student and two undergraduate students to the program. A bi-weekly group meeting is held by the HE group. At this stage, one paper published and three hypersonic research related technical papers are being prepared for publication.

PUBLICATIONS

Center Director

1. H.Y. Lai, 1992, "Dynamic Characterization, Monitoring and Control of High-Speed Rotating Beam-Mass Structures Via Piezo-Embedded Techniques," Space Exploration Science and Technologies Research, Vol. AD-Vol. 31, pp. 131-134.
2. H.Y. Lai, 1992, "Smart Sensing and Control of A High Speed Rotating Piezo-Embedded Graphite-Epoxy Beam-Mass System," submitted for publication in the ASME J. of Engineering For Industry.

Aerospace Structures

1. J.Y. Shen, E. G. Abu-Saba, W. M. McGinley, and L. W. Taylor, Jr., 1993, "Piecewise Continuous Timoshenko Beam Model for the Dynamic Analysis of Tapered Beam-Like Structures", Submitted to the 1st SES-ASME-ASCE Joint Meeting, Univ. of Virginia.
2. E. G. Abu-Saba, J. Y. Shen and W. M. McGinley, 1993, "Lumped Mass Modelling for the Dynamic Analysis of Aircraft Structures", Submitted to the 1st SES-ASME-ASCE Joint Meeting, University of Virginia.
3. J. Y Shen, J. K. Huang and L. W. Taylor, Jr., 1992, "Likelihood Estimation for Distributed Parameter Models of Large Beam-Like Structures", Journal of Sound and Vibration, 155(3), pp. 467-480.

Controls and Guidance

1. A. Homaifar and E. McCormick, 1992, "A New Approach for the Design and Implementation of Fuzzy Controllers", The IEEE Proceedings of the Southeastern Symposium on System Theory, and Third Annual Symposium on CSA.
2. A. Homaifar, H.Y. Lai, and Ed McCormick, 1992, "Design Optimization of Turbofan Engines Using Genetic Algorithms," submitted for publication in the Journal of Applied Mathematics.
3. Y. D. Song, et al, 1992, "Robust Motion Tracking Control of Robotics Arms Based on the Generalized Energy Accumulation Principle," Proceedings, IEEE Int. Conf. on Decision and Control.
4. Y. D. Song, et al, 1992, "System Stability and Performance Analysis Based on Generalized Energy Accumulation: Part II - Applications," Proceedings, IEEE Int. Conf. on Decision and Control.
5. Y. D. Song, et al, 1992, "Nonlinear Robust Controller Design for Multi-Robotics Systems with Unknown Payloads," Proceedings, the Fourth NASA Conf. on Muli-Robot Systems.
6. Vance E. McCormick, 1992, "Full Design of Fuzzy Controllers Using Genetic Algorithms," M.S. Thesis, Department of Electrical Engineering.

Computational Fluid Dynamics

1. Chandra, S., 1992, "Study of Compressibility Effects in Turbulent Shear Layers", ASME Fluids Engineering Conference, Los Angles, CA, June 21-23, Abstract published in "Fluids Engineering 1992 - Abstracts, FED-Vol. 133, ASME/Fluids Engineering Division, 1992".
2. Jones, K.M., DeJarnette, F. R., Griffith, W.C., and Yanta, W. J., 1992, "Boundary Layer Study on Nozzle Wall at Hypersonic Velocities", AIAA Paper No. 92-4013, presented at the AIAA 17th Aerospace Ground Testing Conference, Nashville, TN, July 6-8, 1992.
3. Sellers, C. and Chandra, S., "Compressibility Effects in Modeling Turbulent High Speed Mixing Layers", Accepted for Presentation at the 1993 ASME Forum on Turbulent Flows, Washington, DC, June 1993.
4. Elbert, G. J. and Cinnella, P., "Truly Two-Dimensional Algorithms for Radiative Non-equilibrium Flows", 13th International Conference on Numerical Methods in fluid Dynamics, Rome, Italy, July 1992.
5. Elbert, G. J. and Cinnella, P., "Axisymmetric Radiative Heat Transfer Calculations for Flows in Chemical Non-equilibrium", AIAA Paper 93-0139, 31st Aerospace Sciences Meeting, Reno, Nevada, January 1993.
6. Sellers, C., "Compressibility Effects in Modeling High Speed Turbulent Mixing Layers", M. S. Thesis, Department of Mechanical Engineering, North Carolina A&T State University, 1992.

Human Engineering

1. Kim, J.H., Yoon, S.H., Park, E.H. and Ntuen, C.A., 1992, "Recognition of Partially Occluded Threat Objects Using the Annealed Hopfield Network," Proc. of SPIE OE/Technology Conference.
2. Ntuen, C.A., Information Theoretic Models of Human-Machine Interaction, Submitted, International Journal for Information Sciences.
3. Ntuen, C.A., Park, E.H., Deeb, J.M., Geiger, C., Mansfield, E. and Winchester, W., 1993, "Development of Flight Simulation, Database Using Handling Quality Studies," Submitted, 15th Annual Conference on Computers and Industrial Engineering.
4. Ntuen, C.A., 1993, "A New Approach To Modeling Human Response Errors In Synthetic Flight Simulator Domain," Submitted, 15th Annual Conference on Computers and Industrial Engineering.

B. MAJOR ACCOMPLISHMENTS IN EDUCATIONAL PROGRAMS

Concurrent with the above research effort is an academic program designed to prepare students for careers with direct relevance to aerospace engineering. The center plans to offer a sequence of courses in the areas of aerospace engineering including flight vehicle structural design, controls and guidance, aerodynamics, and system performance. Dr. William J. Craft serves as the head of the educational committee. He coordinates the educational and training aspects of the program which will eventually lead to an established aerospace engineering program in the Department of Mechanical Engineering.

The Center for Aerospace Research will have both a positive and significant impact upon this institution's recently authorized Ph.D. Program in both Electrical and Mechanical Engineering. Historically, North Carolina A&T State University has been most successful in attracting high academic ability minority students. Of the more than 1200 students enrolled in the School of Engineering, better than 85% are minorities. North Carolina A&T State University ranks first or second annually in the production of black engineers receiving degrees at the baccalaureate level. Recent graduate program admissions data indicates that more than 30% of all students admitted to these programs at our institution

are African-American. Many of these graduate students will have heavy involvement with ongoing research tasks associated with the Center of Aerospace Studies funded by NASA. Graduate programs of study in aerospace engineering will be offered leading to degrees at the masters level. Once these students are in the program, they are eligible for graduate fellowships supported through the Center, thereby providing a natural progression for a high number of these students to obtain Ph.D.s in Mechanical and Electrical Engineering.

1. Curriculum Development

Undergraduate Aerospace Option

Work on the educational component of the NASA Center of Excellence began in earnest in May'92 when funds for release time first became available to the group. This report covers the period of activity through August 14, 1992. During the summer months, undergraduate and graduate curriculums for aerospace options were developed as part of the proposal requirement. Both of these curricula are described in detail in sections following this general overview.

The undergraduate aerospace option presented particular difficulties since, at least in the near term, it must exist as an option within the current mechanical engineering program and must meet all of the accreditation criteria for mechanical engineering programs as specified by the Accreditation Board for Engineering and Technology (ABET). We have attempted to construct an aerospace program option that: 1) meshes well with the existing mechanical engineering curriculum; 2) meets the required ABET criteria and; 3) provides sufficient background in aerospace engineering to allow a graduate to work in the aerospace field while retaining sufficient fundamental mechanical engineering training to permit a graduate to function well as a mechanical engineer if he/she does not enter the aerospace field.

The aerospace option includes ten courses that are unique to the option as contrasted with the standard mechanical engineering curriculum. Aerospace related courses begin in the second semester of the junior year while the first five semesters remain unchanged from the existing ME program. One of the most critical ABET criteria is the requirement that all engineering programs must include a minimum of 16 credit hours of engineering design content including a capstone design course in the senior year. The proposed aerospace option curriculum outline indicates design content credit hours in parentheses beside the course credit hour column. With some difficulty, 16 credits of design content were maintained in the program.

It is important to note that the aerospace option is in the proposal stage. Both the curriculum outline and the new courses proposed for the option must go through a lengthy approval process involving the Department of Mechanical Engineering, the School of Engineering, the University Faculty Senate and the University Faculty Forum. This process, which normally requires an entire academic year, must be completed before information on

Table 2 - Aerospace Engineering Curriculum Phase-in Time Table

Course No. & Titles	Time Table	Instructor	Supporting Laboratories
EE 410 - Linear Systems and Controls	Fall, 1992	Homaifar	E.E. Controls Lab.
ME 655 - Computational Fluid Dynamics	Fall, 1992	Chandra	M.E. Fluids Lab.
EE 410 - Linear Systems and Controls	Spring, 1993	Song	E.E. Controls Lab.
ME 415 - Aero and Gas Dynamics	Spring, 1993	Jones	CORE CFD/Design Lab.
ME 422 - Aero Vehicle Structures I	Spring, 1993	Shen	A.E. Structures Lab.
ME 576 - Propulsion Systems	Fall, 1993	Jones	CORE Propulsion Lab.
ME 651 - Aero Vehicle Stability and Controls	Fall, 1993	Song	E.E. Controls Lab.
ME 578 - Flight Vehicle Performance	Fall, 1993	Ntuen	I.E. System Engrng Lab.
EE 668 - Automatic Control Systems	Fall, 1993	Homfaifar	E.E. Controls Lab.
ME 415 - Aero and Gas Dynamics	Spring, 1994	Jones	CORE CFD/Design Lab.
ME 653 - Aero Vehicle Flight Dynamics	Spring, 1994	Lai	CORE Systems Lab.
ME 580 - Aero Vehicle Design	Spring, 1994	Shen	CORE Design/CFD Lab.
ME 652 - Aero Vehicle Structure I	Spring, 1994	Abu-Saba	CORE Structures Lab.
EE 410 - Linear Systems and Controls	Spring, 1994	Homaifar	CORE Controls Lab.

the option can be included in the University Bulletin. Nevertheless, a phase-in plan has been implemented beginning with the current Fall'92 semester. This is possible since one of the courses currently exists (ELEN 410 Linear Systems and Control) and others can be offered on a temporary basis under a Special Topics course number. The phase-in time table is shown below. Under this plan, current first semester juniors can begin the option in Fall'92 and graduate under the option in May'94, assuming that the plan gains eventual approval from all requisite university committees.

There are currently two ME students enrolled in ELEN 410 and 9 students enrolled in MEEN 655 including four undergraduates. The number of students who enter the option should increase significantly next year when it can be officially advertised and promoted through the University Bulletin and the Mechanical Engineering Undergraduate Handbook and brochure.

Graduate Aerospace Option

Creation of an aerospace option under the Master of Science in Mechanical Engineering program is significantly less complicated than the undergraduate option since ABET accreditation issues are not involved. The five new aerospace courses at the 600 level that are being proposed will be open to both undergraduate and graduate students. Undergraduates can take them as technical electives (two required) and graduate students can take them as part of the eight courses required under the MSME thesis option. Graduate students will round out their programs with existing 600 and 700 level courses as listed later in the section detailing the graduate aerospace engineering option which includes examples of two possible programs of study. The undergraduate aerospace option will provide a firm foundation for continuing study with aerospace specialization at the MS level. The graduate students in this option will be actively involved with the ongoing research of the center.

2. Student Involvement

Two undergraduate students are currently supported under the educational component of the NASA-CORE. These are Miss Shiryl White and Miss Kimberly Musgrave, both mechanical engineering juniors. Both students work 10 hours per week under the supervision of Dr. Craft. Miss White's efforts are split about equally between clerical and research activities. Her research work involves investigating possible finite element models for orthotropic braids used in composite materials for aircraft and spacecraft applications. The purpose of the research is to develop better modeling techniques to determine global material properties.

Miss Musgrave is also doing both clerical and research work. Her research involves running a finite element computer model of a composite sandwich shell for varying cases of skin and core thickness to find a minimum weight composite structure with adequate strength characteristics for possible application as an aerobrake.

Two additional undergraduate students are currently supported by the Center to help develop laboratory tools. These two students are Miss Monica Smith and Mr. Jerry Hoggard. Miss Monica Smith is working with Dr. Lai to develop computer programs for NASP simulation. This includes the development of NASP plane model and the computation of flight dynamics. Mr. Hoggard's effort is to develop analytical and numerical procedures to compute the optimal trajectory using the NASP plane model.

3. Faculty Involvement

Dr. William Craft, Chairman of Mechanical Engineering, heads the educational component of the Center. Other faculty involved with the educational component include Dr. David Klett, Undergraduate Program coordinator, and Dr. Hsin-Yi Lai, Center Director.

Mr. Kenneth Jones was hired as a new faculty member in support of the Educational Component. He has many years experience working in the aerospace area and is currently completing the requirements for the PhD in aerospace engineering from North Carolina State University. His research work is in CFD and experimental hypersonic flow and his expertise will be an important complement to the CFD efforts currently underway as part of the center and also in helping to develop new laboratories in Propulsion and Aerodynamics. Dr. Jones will teach the Aerodynamics course during Spring '92. Other faculty involved in teaching aerospace courses this academic year include:

1. Dr. Suresh Chandra, Prof. of Mech. Engr. - Teaching Computational Fluid Dynamics, Fall '92
2. Dr. Abdollah Homaifar, Assoc. Prof. of Elec. Engr. - Teaching Linear Systems and Controls, Fall '92 and Spring '93
3. Dr. Shen, Adjunct Asst. Prof. of Mech. Engr. - Teaching Aero Vehicle Structures I, Spring '93

AEROSPACE OPTION IN MECHANICAL ENGINEERING (Effective Fall'93)

FALL SEMESTER Course	cr	SPRING SEMESTER Course	cr
		FRESHMAN YEAR	
ENGL 100 Ideas & Expres I	3	ENGL 101 Ideas & Expres II	3
HIST Elec	3	MATH 132 Calculus II	4
HATH 131 Calculus I	4	GEEN 102 Comp Prog for Engrs	2
GEEN 100 Intro. to Engineering	2	CHEM 101 Gen. Chem. I	3
GEEN 101 Intro. Engr Graphics	2	CHEM 111 Gen. Chem. I Lab	1
SOC SCI Elec	3	HISTORY Elective	3
		HEALTH/PE Elective	1
Total	17	Total	17
		SOPHOMORE YEAR	
PHYS 241 Gen. Phys. I	4	MEEN 210 Num Methods in ME	2
PHYS 251 Gen. Phys. I Lab	1	PHYS 242 Gen. Physics II	4
MATH 231 Calculus III	4	PHYS 252 Gen. Physics II Lab	1
ECON 300 Prin of Economics	3	MATH 331 Appl. Engr. Math I	3
MEEN 226 Manuf. Processes	2	MEEN 335 Statics	3
HUMANITIES Elective	1	MEEN 360 Materials Science	2
Total	17	MEEN 300 Mech Engr Lab I	2
		Total	17
		JUNIOR YEAR	
MATH 332 Appl. Engr. Math II	3	*ELEN 410 Linear Sys & Contrl	3
ELEN 200 Elec. Circuit Anal.	3	MEEN 440 Mechanism Des & Anal	3 (1.5)
ELEN 206 Circuits Lab	1	*MEEN 415 Aerodynamics	3 (0.5)
MEEN 336 Strength of Matrl.	3	*MEEN 422 Aero Veh Structures I	3 (1)
MEEN 337 Dynamics	3	MEEN 474 Engineering Design	3 (2)
MEEN 441 Thermodynamics I	3	MEEN 400 Mech Engr Lab II	1
HEALTH/PE ELECTIVE	1	Total	16
Total	17		
		SENIOR YEAR	
MEEN 560 Mod. Engr. Materials	3 (1)	MEEN 562 Heat Transfer	3 (1)
MEEN 565 Machine Design	3 (2)	MEEN 581 Mechanical Vibration	3 (1)
* MEEN 576 Propulsion	3 (1)	* MEEN 580 Aero Veh. Design	3 (3)
* MEEN 577 Aero & Propulsion Lab	1	* AEROSPACE Elective	3 (1)
* MEEN 578 Flight Veh. Perform.	3 (1)	HUMANITIES Elective	3
* AEROSPACE Elective	3	Total	15
Total	16	(Numbers in Parentheses Indicate Design Credits)	

TECHNICAL ELECTIVES

* MEEN 651 Aero. Veh. Structures II	3 (1)
* MEEN 652 Aero. Veh. Stab. & Cont.	3 (1)
* MEEN 653 Aero. Veh. Flight Dyn.	3
* MEEN 654 Advanced Propulsion	3 (1)
* MEEN 655 Computation Fluid Dyn.	3
MEEN 656 Boundary Layer Theory	3
ELEN 668 Automatic Control Theory	3

CONTENT

Engineering Design:	16
Engineering Science:	52
Math. and Basic Sci:	35
Humanities & Soc Sci:	18
Other:	11
Total Credit Hours:	132

C. MAJOR ACCOMPLISHMENTS IN CENTER MANAGEMENT

The NASA-CORE at NCA&TSU is managed by the Center Director. Dr. Steven H.-Y. Lai is the Director with responsibility for overall coordination of the program. He manages the Center and integrates all components into a productive team. Ms. Jocelyn Foy is newly hired with the center as a Graduate Student Recruiter and the Director's Assistant. She helps the center recruit minority graduate students and establish a board of directors consisting of the Dean of School of Engineering, the Department Heads of participating faculty, and two representatives from collaborating NASA Centers and aerospace industries. The board has a rotating Chairman, elected by the members for a one year period.

1. Center's Management Plan

A detailed two-year management plan for the center is listed in Table 3. The following are what have been accomplished in the first year. These accomplishments include (1) development of both long-range and short-range plans for the Center, (2) recruiting of six graduate students and thirteen undergraduate students to the program, (3) recruiting of one tenure-track faculty and two adjunct research associates to assist research in various areas, (4) hiring of one recruiter/industrial specialist for student recruitment, (5) renovation of center offices and hiring one full-time secretary, (5) participation of the outreach program NU-SPIN to visit on November 22, (6) preparation for the site visit of the technical monitor team on October 27, (7) Submission of the annual area report and three technical papers from each group by December 10, and (8) Submission of the annual report and renew the contract by December 30,

Several important tasks are to be accomplished in the next six months. These are: (1) hiring an associate director to establish Industrial Advisory Group (IAG) before March, 1993, (2) preparation of an aerospace brochure by Mach 31, 1993, (3) Publication of the first issue of NASA-CORE newsletter by June 30, 1993, (4) preparation for the first NASA-CORE symposium on A&T campus, and (6) submission of the proposal to the U.N.C. system to establish the Center For Aerospace Research before June 30, 1993.

2. Center's Personnel Involvement

In the past six months, the area coordinators of the NASA-CORE have worked diligently to recruit faculty researchers and minority students at both undergraduate and graduate levels. Within the limit of area budget provided by the center, we were able to recruit two research associates and one student recruiter to the center. One tenure track faculty position was provided to the center by the university as part of match commitment. Dr. Kenneth Jones joined us in hypersonic CFD area to fill that position. With the addition of new participants in various areas of hypersonic research, the center can now be operated more productively. The proposed work is now conducted by fifteen faculty members from NCA&TSU, and two faculty members from NCSU. The personnel involved in the center are listed in Table 4.

Table 3 - Progress Chart of the NASA-CORE at NCA&TSU

	Q1 1992	Q2 1992	Q3 1992	Q4 1992	Q1 1993	Q2 1993	Q3 1993	Q4 1993
Project Planning	X							
HBCU Orientation	X							
Grant Initialization		X						
Research Planning		X						
Student Recruitment		X						
Curriculum Develop.			X					
Office & Lab Renovation			X					
Personnel Hiring			X					
Semi-annual Report (9/15/92)			X					
MU-SPIN on Campus (11/6/92)				X				
2 Aero. Courses Offered				X				
Center Proposal to N.C.(11/30)				X				
Annual Site Visit (10/27/92)				X				
Annual Report (10/31/92)				X				
Contract Renewal (11/13/92)				X				
Associate Director					X			
Attend Seminars					X			
Aro. Industry Contact					X			
3 Aero. Courses Offered					X			
First NASA-CORE Symposium						X		
Outreach Program Seminars						X		
Summer Seminars Services						X		
PIs Seek for Funding							X	
PIs Travel to NASA R.C.							X	
3 Aero. Courses Offered							X	
IAG Meeting							X	
Annual Site Visit								X
Annual Report Due								X
Contract Renewal								X

Table 4 - The Current Status of Personnel Involvement

Group	Faculty	Students
Center	Steven Lai Jocelyn Foy (Grad. Recruitment; New)	Darryl Bowe (M.S.) Monica Smith (B.S.) Jerry Hoggard (B.S.)
Structures	Elias Abu-Saba William McGinley Ji-Yao Shen (Research Associate; New)	James Cox (B.S.) Raymond Dobbins (B.S.) Eddie Fitts (B.S.) Jerome Redmond (B.S.)
Controls	Abdollah Homaifar DeRome Dunn Y.D. Song (Research Assoc.; New)	Ed McCormick (M.S.) Kevin Barnhart (M.S.) John Hogans (M.S.) Christen Williams (B.S.) Lamark Chance (B.S.) Nikki Smith (B.S.)
C.F.D.	Suresh Chandra Kenneth Jones (Assistant Prof.; New) Gregory Elbert (Research Assc.; New) Hassan Hassan (NCSU Subcontractor) Scott McRae (NCSU Subcontractor)	Cheryl Sellers (M.S.) Michael Gray (B.S.)
M.M.I.	Celestine Ntuen Eui Park Joe Deeb Jung Kim	Woodrow Winchester (M.S) Christopher Geiger (B.S.) Erika Mansfield (B.S.)
Education	William Craft David Klett	Shiryl White (B.S.) Kimberly Musgrave (B.S.)

3. Center's Program Activities

The dirctor calls for area coordinator meeting on the first Tuesday of every months. The management of the center is discussed. The center policy is made with the consent of area coordinators. Each area is asked to hold a regular meeting to discuss the technical information and exchange research finding. The meeting is held eith bi-weekly or monthly. Distinguished guest speakers are invited to campus to educate our students and educators. These speakers are well-known and well-respected scholars in the area of Hypersonic Research. The details of the 1992 program activity are listed in Table 5.

4. Strategies to Recruit Underrepresented Minority Students

The majority of our undergraduate students are African Americans. We are recruiting our current undergraduate mechanical engineering students to enter the aerospace option through announcements about the program in classes and on bulletin boards. Certain aerospace courses have been offered under special topic headings for the current Fall '92 semester, and about six undergraduate students have enrolled in these courses. When the program option receives university approval and can be officially

advertised, a brochure will be printed describing the aerospace engineering option and it will be included in the Mechanical Engineering Undergraduate Handbook and the University Bulletin. The brochure, in particular, can be used as a recruiting tool at university days, etc. Ms. Jocelyn Foy is currently hired by the Center as a student recruiter. Her job is to recruit minority students to the aerospace engineering program for the Center.

The aerospace options in the BSME and MSME programs are currently under development and must pass a lengthy university approval process during the Spring '93 semester, before being officially offered beginning in Fall '93. Tracking of students in the aerospace options will begin at that time.

Table 5 - Meeting and Seminars Conducted by the NASA-CORE

Group	Meeting Date	Speakers/Presenters	Presentation Topics
Center	08/25/92 10/07/92 11/19/92 11/20/92	I.M. Blankson L.W. Taylor W.B. Gao B. Wakim	Hypersonic Research Aircraft Design Sensitivity Analysis Global Linearization and Motion Control of Nonlinear Mechanical Systems NASA-Goddard MU-SPIN Training Workshop
Center	1st Tues. of the Month	area coordinators	Center Management
Structures	bi-weekly	area members (faculty and students)	Technical Discussion, Progress Report, Student Presentation
Controls	bi-weekly	area members (faculty and students)	Technical Discussion, Progress Report, Student Presentation
CFD	monthly	area members (faculty)	Technical Discussion, Progress Report
MMI	bi-weekly	area members (faculty and students)	Technical Discussion, Progress Report, Student Presentation
Education	monthly	area members (faculty)	Technical Discussion, Progress Report

5. Program Impact

The establishment of the NASA-CORE at NCA&TSU bring lots of excitement to the minority student body on campus. Many students are interested in research work involved in the center. We tried to accommodate as many students as possible within the budget limit. To ensure the quality of our research programs, we carefully selected students with two criteria: (1) minority undergraduate students interested in graduate study in Aerospace Engineering with GPA higher than 3.0, and (2) minority graduate students who would like to pursue Aerospace Engineering research as his/her professional career. At this stage, the center was able to attract 6 graduate students and 14 undergraduate students. All twenty (20) students are U.S. citizens. Among them, eighteen (18) students are African-Americans. The detailed information of student data can be found in Table 6. In terms of student recruitment we are doing better than what was proposed - 5 graduate students and 10 undergraduate students, as given in Table 7, for the first year. For the second year, more minority graduate stdents are recruited to the Center. These include:

Table 6 - Student Involvement in the NASA-CORE Programs

Group/Dept.	Student Name	Grade	G.P.A.	Ethnic Preference
Center (School)	Darryl Bowe	M.S./2	3.50	African-American
	Monica Smith	Junior	3.34	African-American
	Jerry Hoggard	Senior	3.15	African-American
Structures (A.E.)	James Cox	Senior/5	3.60	African-American
	Raymond Dobbins	Senior/5	3.52	African-American
	Eddie Fitts	Senior/5	3.11	African-American
	Jerome Redmond	Senior/5	3.43	African-American
Controls (E.E.)	Ed McCormick	M.S.(8/92)	3.80	American (born)
	Kevin Barnhart	M.S./1	3.50	African-American
	John Hogans	M.S./2	4.00	African-American
	Christen Williams	Junior	3.21	African-American
	Lamark Chance	Junior	3.08	African-American
	Nikki Smith	Senior	3.60	African-American
C.F.D. (M.E.)	Cheryl Sellers	M.S.(8/92)	3.50	African-American
	Michael Gray	Senior/4	3.10	American (born)
M.M.I. (I.E.)	Woodrow Winchester	Senior	3.15	African-American
	Christopher Geiger	Senior	3.05	African-American
	Erika Mansfield	M.S./1	3.25	African-American
Education (M.E.)	Shiryl White	Sophomore	3.20	African-American
	Kimberly Musgrave	Junior	3.40	African-American

Table 7 - Proposed Personnel Involvement

Group Name		1st Year	2nd Year	3rd Year	4th Year	5th Year	GROUP- SUBTOTAL (man-year)
STRU Group	-Faculty	3	4	5	5	5	22
	-Grad. Students	1	2	2	3	3	11
	-Undergrad. Students	2	3	4	5	6	20
CFD Group	-Faculty	4	4	5	5	5	23
	-Grad. Students	1	2	3	3	3	12
	-Undergrad. Students	2	3	4	5	6	20
C&G Group	-Faculty	3	4	4	5	5	21
	-Grad. Students	1	2	3	3	3	12
	-Undergrad. Students	2	3	4	5	6	20
MMI Group	-Faculty	4	4	4	5	5	22
	-Grad. Students	1	2	3	3	3	12
	-Undergrad. Students	2	3	4	5	6	20
CNTR Personnel	-Faculty	1	2	3	3	3	12
	-Grad. Students	1	2	2	3	3	11
	-Undergrad. Students	2	3	4	5	6	20
YEARLY SUBTOTAL	-Faculty	15	18	21	23	23	100
	-Grad. Student	5	10	13	15	15	58
	-Undergrad. Student	10	15	20	25	30	100

1. Minority African-American students are mentored and encouraged in the senior undergraduate year to consider graduate study at NCA&TSU. Two I.E. students will be join the Human Engineering System group. Another two M.E. students will join the CFD group beginning Spring 1993.
2. More African-American students have been admitted to graduate program in IE, M.E., and E.E. department beginning Spring 1993.
3. As a part of our pipeline recruitment process, several senior students will join the research team in January of 1993.

6. University Commitment

Mr. Kenneth Jones was hired as a new faculty member in support of the Educational Component. He has many years experience working in the aerospace area and is currently completing the requirements for the Ph.D. in aerospace engineering from North Carolina State University. His research work is in CFD and experimental hypersonic flow and his expertise will be an important complement to the CFD efforts currently underway as part of the center and also in helping to develop new laboratories in Propulsion and Aerodynamics. Dr. Jones will teach the Aerodynamics course during Spring '92. Dr. Jones' position is given to the NASA-CORE by the University as part of university commitment to the Center.

The University has also rented a huge office space for the Center housed in the Woodson Building. At this time, we have three research associates working in the offices in that building. We also hold our regular meetings over there. The center is in the process of hiring a full-time secretary to sit in the office. By the end of 1992, we should have every room occupied. The office should be functioning, effective and productive soon.

7. Center's Budget Summary

The budget allotment and current levels of spending are listed in Table 8. The levels of budget spending vary from group to group. The average of overall spending for the whole center is approximately 95%. This number reflects the fact that the project is moving well in the first year of its five-year performance period.

To ensure the continued growth and vitality of the Center, we developed the following planned actions to ensure self supporting status:

1. A full time associate director position will be added beginning the second year to act as an extension specialist with government and industry.
2. An Industrial advisory committee and affiliation group will be formed to allow the participation from the Aerospace industry community. This allows the industrial experts to: (a) serve on the Industrial Advisory Committee to the center, (b) participate as an Industrial Affiliate to the center, (c) participate in setting the direction of the center, (d) establish aerospace research of mutual interest.

3. The center investigators have begun seeking additional funding in support of the center's research goals. The structures group is developing proposals to work with the Guidance and Control branch in LaRC. The controls group is working with the Marshall Space Flight Center for additional funding. Dr. Chandra in the CFD area also submitted a proposal to the U.S. Air Force. The Human Engineering group is working on proposals to establish external funding with the DOD and other government funding agencies.
4. The center investigators travelled in the summer to government laboratories to ensure integration of the center's research with that of the cooperating laboratories. The visits included trips to NASA Headquarters, NASA Langley Research Center, Goddard Space Flight Center, Marshall Space Flight Center, and NASA Lewis Research Center.

Table 8 - Budget Report Summary

Group	Budget Allotment	Budget Spent	Levels of Spending
Center	$146,086	$147,721	101.12%
Structures	$125,008	$106,151	84.92%
Controls	$125,012	$133,737	103.99%
C.F.D.	$125,031	$115,476	92.36%
M.M.I.	$125,093	$ 99,516	80.00%
Education	$125,019	$126,855	101.47%
NCSU Subcontract	$ 37,154	$ 37,153	100.00%
Total	$808,403	$766,609	94.83%

STRUCTURES RESEARCH

ANNUAL REPORT

Prepared for

NASA CENTER OF RESEARCH EXCELLENCE
SCHOOL OF ENGINEERING
NORTH CAROLINA A&T STATE UNIVERSITY

by

Elias Abu-Saba
Williams McGinley
Ji-Yao Shen

Structures Group
School of Engineering
North Carolina A&T State University
Greensboro, NC 27411

December, 1992

A. AREA SUMMARY

The main objective of the structures group is to provide quality aerospace research within the Center for Aerospace Research- A NASA Center of Excellence at North Carolina Agricultural and Technical State University. The group includes dedicated faculty and students who have a proven record in the area of structures, in particular space structures. The four students who are currently in the program have distinguished themselves academically in addition to being leaders in various student organizations.

The participating faculty in the structures group have had several years of experience working with the Guidance and Control Division at NASA Langley Research Center. They developed accurate mathematical models and effective computational algorithms to characterize the flexibility parameters of joint dominated beam-truss structures. Both experimental and theoretical modelling has been applied to the dynamic mode shapes and mode frequencies for a large truss system.

During the past few months, the above procedure has been applied to the hypersonic transport plane model. The plane structure has been modeled as a lumped mass system by Doctor Abu-Saba while Doctor Shen applied the transfer matrix method with a piecewise continuous Timoshenko tapered beam model. Results from both procedures compare favorably with those obtained using the finite element method. These two methods are more compact and require less computer time than the finite element method. The group intends to perform experiments on structural systems including the hypersonic plane model to verify the results from the theoretical models.

Focus

Space technology has been going on a fast track. NASA has committed itself to remain globally competitive in this field. The NASA Center for Research Excellence at North Carolina A & T State University is aimed at providing NASA with the needed expertise to achieve its goal of staying ahead in space technology.

The goal of the structures group is to develop procedures that can accurately predict the dynamic behavior of a variety of structural systems which can be used as components of space as well as sub-orbital structures. The evaluation of the accuracy of the predictions will be verified by experimental methods.

Long Range Objectives

1. Establish the geometric parameters for an hypersonic plane that is capable of operating at mach four and higher.
2. Specify the size and material for the various components for the hypersonic plane.
3. Apply thermal forces and forces due to fluid dynamics to structural systems and verify their effects.

4. Establish an analytical model for the hypersonic plane and determine its dynamic characteristics.
5. Provide the dynamic characteristics to the guidance and control group.
6. Establish test procedures and perform tests to verify theoretical results.
7. Train graduate and undergraduate students to perform specific tasks in the development of the above.
8. Build up the structural laboratory to a level that enables the structures group to provide governmental and private clients with appropriate expertise in the area of aircraft structures.

B. AREA RESEARCH PROJECTS

Project No. 1:

Dynamic Analysis of the Joint dominated Beam, Elias G. Abu-Saba, $20,000, NASA, continuation of an on-going project. This project began in 1986 and will end on December 31, 1993.

Publications Resulting from this Project:

1. "Dynamics of the Joint Dominated Beam", Elias G. Abu-Saba, Archibald N. Sherbourne and Raymond C. Montgomery; Engineering, Construction and Operations in Space, ASCE Conference, Albuquerque, NM, August 29-31, P. 495-505.
2. "Design of the Scole Boom Based on the Dynamic Analysis of the Joint dominated Beam", Elias G. Abu-Saba, Raymond C. Montgomery and William M. McGinley, Conference sponsored by NASA Langley Flight Research Center and Flight Systems Research Laboratory of UCLA, Lake Arrohead, CA, October 31- November 1,1988
3. "Mini-Mast Dynamic analysis Using the Truss-Beam Model", Elias G. Abu-Saba, William M. McGinley and Raymond C. Montgomery, Third Annual Conference on Aerospace computational control", Oxnard, CA., August 28-30, 1989
4. "Simplified Truss-Beam and Space Technology", Elias G. Abu-Saba, William M. McGinley and Raymond c. Montgomery, Workshop on Computational Techniques in Identification and Control of Flexible Flight Structures, Lake Arrowhead, CA., November 1-2, 1989
5. "The Truss-Beam and Space Technology", Elias G. Abu-Saba, William M. McGinley and Raymond C. Montgomery, Engineering, construction and Operation in Space, Space II., ASCE Conference, Albuquerque, NM., April 22-26, 1990, Vol2, P. 1112-1121.
6. "Dynamic analysis of the Truss-Beam System", Abu-Saba, McGinley and Montgomery, Journal of Aerospace Engineering, ASCE, New York, VOL. 4 NO. 4 October, 1991, P. 347- 354

Project No. 2

Distributed Parameter Modeling of Large Flexible Space Structures, Shen, J. Y., NAG - 1 - 1436 , 1-1- 1992 to 12-31- 1994, $380,000.

Publications Resulting from this Project:

1. "Likelihood Estimation for Distributed Parameter Models of Large Beam-Like Structures", J.Y.Shen, J.K. Huang and L.W. Taylor, Jr. Journal of sound and Vibration (1992), 155(3), pp. 467-480.
2. "Damping Models for Distributed Parameter Estimation of Large Beam-Like Structures", J.Y. Shen, J.K. Huang and L.W. Taylor, Jr, Pacific- Rim International conference on Modelling, Simulation and Identification, Vancouver, Canada, August 4-6, 1992.
3. "Application fo Transfer Matrix Method to Estimate the Model Characteristics of the NASA Mini-Mast Truss", NASA Workshop on Distributed Parameter Modelling and Control of Flexible Aerospace Systems, Williamsburg, VA., June 8-10, 1992.

C. AREA PROGRAM ACTIVITIES

The structures group began its activity in the Center on May 16, 1992. Dr. Abu-Saba put only five weeks during the summer of 1992 while Dr. McGinley worked for two months. Four undergraduate students were employed by the structures group only for the summer. Another set of undergraduate students were employed effective August 15, 1992.

Faculty:

Name:	Elias G. Abu-Saba
Classification:	Coordinator
Citizenship:	US
Research Activity:	Provides analytical support to the structural group such as mathematical modeling for the hypersonic plane
Telephone:	(919) 334-7575 Room 455, McNair Hall North Carolina A & T State University Greensboro, NC 27411

Name:	William M. McGinley
Classification:	Co-coordinator
Citizenship:	Canadian (Permanent Resident)
Research Activity:	Provides experimental support and consults on finite element modelling of structures
Telephone:	(919) 334-7575 Room 454, McNair Hall North Carolina A & T State University

Greensboro, NC 27411

Name:	**Ji-Yao shen**
Classification:	**Associate Researcher**
Citizenship:	**China (Labor Permit, Applying for Permanent Residency)**
Research Activity:	**Uses transform functions as an application to hypersonic plane to determine the eigen values and the mode shapes of the mathematical model.**
Telephone:	**(919) 334-7575**
	Room 456, McNair Hall
	North Carolina A & T State University
	Greensboro, NC 27411

Students:

Name:	**James Cox, II**
Citizenship:	**US**
GPA:	**3.597**
Research Advisor:	**Abu-Saba**

Name:	**Raymond Dobbins**
Citizenship:	**US**
GPA:	**3.110**
Research Advisor:	**Abu-Saba**

Name:	**Eddie Fitts**
Citizenship:	**US**
GPA:	**3.426**
Research Advisor:	**Abu-Saba**

Name:	**Jerome Redmond**
Citizenship:	**US**
GPA:	**3.520**
Research Advisor:	**Abu-Saba**

The four students listed above are being trained in aerospace structures research. They began participation in the center activities in August, 1992 and have been assigned a number of specific tasks to accomplish. These tasks include the determination of the weight of the hypersonic transport plane, its surface area, its overall density, its moment of inertia, and the masses for the mathematical model. The Structures group coordinator has been holding weekly seminars with the students and the co-investigators to discuss the approach and the development of the mathematical model. Dr. Abu-Saba is the academic advisor to these students.

D. FACULTY AND STUDENTS PARTICIPATION

Dr. Abu-Saba provided the theoretical background for the lump mass modelling for dynamic analysis of the truss-beam. The truss-beam system is widely used in the construction of space structures and aircraft frames. Theoretical understanding of this system is basic to any effort in the area of structural design of aircraft, space vehicles and space structures. In addition to this contribution, Dr. Abu-Saba provided the management requirements for the structural group.

Dr. McGinley has been responsible for the experimental component of the structures group effort. He has devised the testing procedure, outlined the testing requirement and acquired the necessary equipments to perform the testing of the truss-beam specimen. He was also responsible for training and supervising the students in experimental procedures. Dr. McGinley has also provided assistance in the finite element modelling.

Several tasks have been conducted by the structures group. These tasks have been primarily performed by the four students listed in the budget report above under the supervision of Dr. McGinley. The various tasks that have been performed are:

1. Each student was required to read the project proposal and familiarize themselves with the ultimate goals of the project.
2. The students were involved in general lab familiarization tasks which included small demonstration tests, lab facility and equipment maintenance.
3. Strain gauging of the truss-beam specimens was completed and the resistance of each gauge was verified and recorded. This had to be replaced a number of times due student inexperience.
4. The support apparatus for the vertical test configuration was fabricated.
5. The static load application apparatus for the vertical configuration was fabricated.
6. The air pad supports are being modified to attempt to reduce some of the apparent flutter.
7. The air compressor was torn down and inspected. The air compressor pump was malfunctioning and was replaced.
8. The computer analysis program was being modified to incorporate a more efficient numerical solver and to allow easier modification of the program for the future analysis of more complex systems.
9. The acquisition and experimental analysis program is under development.

Short term goals of the group's effort are outlined below.

1. Evaluate the accuracy of the plane truss-beam model.
2. Modify the plane truss-beam model to improve the accuracy of prediction.
3. To expand the analytical model to three dimensions.
4. Modify the computer program to incorporate the expanded model.
5. Provide the guidance and control group with a rough analytical model for the hypersonic plane including the stiffness and mass matrices.
6. Write two articles and submit them for publication and present one conference

technical report on the testing procedure for the truss-beam.

Work Schedule:

Abu-Saba

1. May 16, 1992 - June 6,1992
   Provided analytical model to McGinley for use in experimental procedure and assisted McGinley and the students in understanding the theoretical basis for the model.

2. July 20, 1992 - August 13, 1992
   Review activities of McGinley and students and investigate transfer of information learned previously into aircraft frame application.

3. August 24, 1992- December 18, 1992
   a. Evaluate the accuracy of the plane truss-beam model.
   b. Modify the plane truss-beam model to improve the accuracy of prediction.
   c. To expand the analytical model to include three dimensions.
   d. Modify the computer program to incorporate the expanded model.
   e. Develop equations of motion for a rough analytical model of the hypersonic plane.

McGinley

1. May 16, 1992 - June 16, 1992
   Introduced students to the project, familiarized the students with the lab facilities and supervised the strain gauging of the truss beam specimen.

2. July 15, 1992 - August 13, 1992
   Reviewed with students computer program for predicting dynamic behavior of the truss-beam, modified existing program. Completed the gauging and calibrated these strain gauges.

3. August 24, 1992- December 18, 1992
   a. Replace malfunctioning compressor pump.
   b. Perform static testing on truss-beam
   c. Perform dynamic testing on truss-beam.
   d. Assist Dr. Shen and Dr. Abu-Saba in finite element modelling of the hypersonic transport plane.

Shen

1. August 24, 1992- December 18, 1992
   Assist Dr. Abu-Saba in the development of the theoretical model for the hypersonic plane and prepare computer packages for the solution of the equations

of motion.

Students

1. May 23, 1992- June 19, 1992
   a. Became familiar with the goals of the project.
   b. Became familiar with the lab facilities
   c. Performed some checks on the equipment in readiness to perform test on the specimens.

2. June 20, 1992-July 17, 1992
   a. Continued strain gauging of specimen.
   b. Modified existing computer program.
   c. General lab familiarization and training in testing through demonstration.

3. August 24, 1992- December 18, 1992
   Students will assist both faculty members in completing the tasks listed for the appropriate period.

Publications

1. "Piecwise Continuous Timoshenko Beam Model for the Dynamic Analysis of Tapered Beam-Like Structures", J. Y. Shen, E. G. Abu-Saba, W. M. McGinley, L. Sharpe and L. W. Taylor, Jr., Submitted to the 1st SES-ASME-ASCE Joint Meeting, University of Virginia, Charlottesville, Virginia, June 6-9, 1993.
2. Lumped Mass Modelling for the Dynamic Analysis of Aircraft Structures", E. G. Abu-Saba, J. Y. Shen and W. M. McGinley, Submitted to the 1st SES-ASME-ASCE Joint Meeting, University of Virginia, Charlottesville, Virginia, June 6-9, 1993.
3. "Likelihood Estimation for distributed Parameter Models of Large Beam-Like Structures", J. Y Shen, J. K. Huang and L. W. Taylor, Jr. Journal of sound and Vibration (1992), 155(3), pp. 467-480.
4. "Damping Models for Distributed Parameter Estimation of Large Beam-Like Structures", J. Y. Shen, J. K. Huang and L. W. Taylor, Jr, Pacific- Rim International conference on Modelling, Simulation and Identification, Vancouver, Canada, August 4-6, 1992.
5. "Application of Transfer Matrix Method to Estimate the Model Characteristics of the NASA Mini-Mast Truss", NASA Workshop on Distributed Parameter Modelling and Control of Flexible Aerospace Systems, Williamsburg, VA., June 8-10, 1992.

E. AREA FINANCIAL REPORT

Line Items	Allotment	Expenditure
Faculty Salary Fringe (24%) and Indirect Cost (55%)	$70,000	$59,290
Student Salary Student Stipend Indirect Cost (55%)	$26,500	$19,522
Travel	$ 4,000	$ 3,435
Scientific Equipment	$20,000	$19,405
Direct Cost Office Supplies Subscriptions Books/Journals	$ 4,500	$ 4,500
TOTAL	$125,000	$106,152

Equipment Purchased

1. Vendor: Measurement Group Cost: $447.48
   Items : Bridge Completion Modules and wire
   Purpose: To expand the strain gauge monitoring capacity of the Structures Lab so that the gauges connected to the truss specimens can be individually monitored.

2. Vendor: Newark Electronics Cost: $299.05
   Items : Pots, etc. for strain gauge monitor circuits
   Purpose: To expand the strain gauge monitoring capacity of the Structures Lab so that the gauges connected to the truss specimens can be individually monitored.

3. Vendor: National Instruments Cost: $3,199.72
   Items : Signal Conditioning Modules and Circuits
   Purpose: To expand the strain gauge monitoring capacity of the Structures Lab so that the gauges connected to the truss specimens can be individually monitored. This expansion will also allow for future more complex testing to be performed.

4. Vendor: Southern Calibration and Service Cost: $708.10
   Items : Repair and Calibration of Material Tester
   Purpose: The tension actuators on the Forney Material Tester are broken and need repair before they may be used for testing the joint specimens for the Truss Beam model evaluation.

5. Vendor: W. W. Grainger Cost: $1,419.92
Items : Air compressor Pump and Welder Accessories.
Purpose: The air compressor pump is malfunctioning and must be replaced so that the air pad supports can be used for the testing of Truss Beam specimens. The welding accessories are required for fabrication of the various apparatus.

6. Vendor: Ensco Cost: $1,741.00
Items : Electric hydraulic pump and accessories
Purpose: To expand the loading capability of the Structures Lab to facilitate future testing of structural frame systems.

7. Vendor: Strain SERT Cost: $1,590.00
Items : Load cell
Purpose: To expand the load monitoring capability of the Structures Lab to facilitate future testing of structural frame systems.

8. Vendor: National Instruments Cost: $6,500
Items : Signal Conditioning Modules and Circuits, Upgrade on A/D Board
Purpose: To expand the monitoring capacity of the Structures Lab so that the sensors connected to the truss specimens can be individually monitored. This expansion will also allow for future more complex testing to be performed.

9. Vendor: Schaevitz Engineering Cost: $100,000.00
Items : Velocity, large displacement and acceleration sensors
Purpose: To expand the sensor capabilities of the structures lab to allow more complex monitoring of scale models of the HST structural systems

10. Vendor: Bibey Machine Cost: $8,000
Items : HST Model for dynamic characteristic testing
Purpose: This will be for the fabrication of the model of the HST structural system that will be tested to confirm and evaluate both the structural analytical models and, ultimately some of the control strategies

11. Vendor: Strain SERT Cost: $4,0000
Items : Load cells
Purpose: To expand the low load monitoring capability of the Structures Lab to facilitate future testing of structural frame systems.

CONTROLS AND GUIDANCE RESEARCH

ANNUAL REPORT

Prepared for

NASA CENTER OF RESEARCH EXCELLENCE
SCHOOL OF ENGINEERING
NORTH CAROLINA A&T STATE UNIVERSITY

by

Abdollah Homaifar
DeRome Dunn
Yong-Duan Song
Steven H.-Y. Lai

Controls and Guidance Group
School of Engineering
North Carolina A&T State University
Greensboro, NC 27411

December, 1992

A. AREA SUMMARY

The objectives of the control group are concentrated on research and education. The control problem of the Hypersonic Space Vehicle represents an important and challenging issue in aerospace engineering. The work described in this report is part of our effort in developing advanced control strategies for such a system. In order to achieve the objectives stated in the NASA-CORE proposal, the tasks were divided among the group based upon their educational expertise. Within the educational component we are offering a Linear Systems and Control course for students in Electrical and Mechanical engineering. Also, we are proposing a new course in Digital Control Systems with a corresponding laboratory.

Organization

In this research, attention is focused on the development of control strategies for the hypersonic vehicles based on adaptive control, robust control and (improved) inverse dynamics control (see Figure 1), and variable structure control. New control schemes are under-way for the vehicle under consideration.

This area annual report is organized as follows.

Research Task 1 - Development of optimal trajectory
Research Task 2 - (NASA Langley): Investigation on Mathematic modeling and Advanced Control of Hypersonic Vehicle
Research Task 3 - Design of Fuzzy Controllers for Autonomous docking and rendezvous
Research Task 4 - Calculate Flight Dynamics of hypersonic vehicle
Research Task 5 - Vibration Modeling/ Smart structure
Educational Component
Budget
Publications

Area Focus

The goal of the control and guidance group is to develop control strategies based on conventional and adaptive control methodologies. The control strategies are based on linear and nonlinear system dynamics. In considering hypersonic vehicle performance, subjects such as: model uncertainties, trajectory, vibration, manuverablity, fuel consumption, computer expert guidance, and others performance may be improved by using control.

Immediate and Long Range Objectives

1. Development of adaptive control strategies for the hypersonic vehicle
2. Development of robust control strategies for the hypersonic vehicle

3. Development of control laws for take, normal flight and landing flight for the hypersonic vehicle
4. Study the feasibility of fuzzy controller for hypersonic vehicle
5. Computer simulation of controlling hypersonic vehicle dynamics and vibration
6. Optimal Trajectories for hypersonic vehicle control simulation
7. Development of control Laboratory
8. Development of MEEN 652 Aero Vehicle Stability and Control
9. Experimental verification of control models
10. Experimental verification of vibration and dynamic models
11. Experimental verification of computer simulation of selected hypersonic vehicle subassemblies in combination with the control system.
12. Development of adaptive guidance for hypersonic vehicle

B. AREA RESEARCH PROJECTS

The specific tasks of the members for the control and guidance group along with publications are listed. Also, the tasks done by the undergraduate students and the travel made by the faculties/students to the international conferences and different NASA centers are presented. We are pleased to announce that Mr. Ed McCormick defended his MSEE through the corporate fund (Honeywell/Alliant Tech) and NASA-CORE in August of 1992.

Research Task 1 (NASA Langley): (Dr. Song)

One of the objectives of the control group is the development of optimal trajectories and guidance for a hypersonic vehicle. The work described in this section is part of our effort in developing advanced control strategies for such system. The fuel-optimal ascent of a single-stage-to-orbit vehicle using air breathing propulsion is the focus of research in advance control and guidance. Due to the high degree of complexity of the problem, we are attempting to investigate the applicability of the many state-of-the-art optimization techniques. Specifically, we will study the validity of the control laws based on the direct, indirect, inverse dynamic, and numerically motivated methods based on evolution strategy during take-off and landing. Difficulty arises in the solution of the two-point-boundary-value problem (TPBVP) resulting from the application of the necessary conditions. During the initial phase, the vehicle is a bench mark wing-cone configuration reported in the literature. As the research progresses, we will also concentrate on development of advanced control strategies and contact verifications.

Next, we consider the application of the methods presented earlier to the design of adaptive controllers. Our interest in adaptive control arises from possible parameter uncertainty in the rigid body dynamic equations of motion. Throughout the life of the spacecraft, its dominant rigid body dynamics may change due to loss of mass or changes in mass distribution, configuration, etc. These changes have the effect of modifying the system inertia. The motivation for the design of the adaptive controller is to provide

compensation for structural model uncertainty.

Research Task 2 (NASA Langley) - Dr. Song
Mathematic Modeling and Advanced Control of Hypersonic Vehicle

The control problem of the Hypersonic Space Vehicle represents an important and challenging issue in aerospace engineering. The work described in this report is part of our effort in developing advanced control strategies for such a system.

As we understand, hypersonic vehicle is a highly nonlinear and strongly coupled system. Its dynamic behavior is fast time varying. Furthermore, due to the fact that there always exist uncertain system parameters and external disturbances as well as structural flexibility, the overall system dynamics is uncertain. As a result, precise model of such system is not available, which calls for the control strategies that are not based on the exact system model.

In this research, attention is focused on the development of adaptive control, robust control and (improved) inverse dynamics control (see Figure 1). Motivated by our earlier work on nonlinear robotics systems [6-8], new control schemes for aircraft systems are proposed which achieve stable trajectory tracking and vibration suppression. It is shown that these strategies guarantee satisfactory operational performance in the face of modeling uncertainties and external disturbances.

This report is organized as follows. The work on nonlinear robotics systems, which is the direct motivation of the control strategies for aircraft systems, is presented first. This include paper 1, paper 2 and pacer 3. Secondly, we report the new robust control scheme for a class of nonlinear dynamic systems with application to hypersonic vehicle modeled by lumped mass approach. In this work, instead of assuming that the mass matrix M and the stiffness matrix K are exactly known, we consider the case where uncertain parts are involved in these matrices. Such consideration is of importance in practice. Finally, a new approach to controller design for aerodynamic systems is presented. Fundamentally, this is the so-called inverse dynamics. However, the essential difference is that our approach is an improved version, because an extra compensation is introduced, which make the over system either adaptive, or robust.

The work on nonlinear robotics systems, which is the direct motivation of the control strategies for aircraft systems, is presented first. This include paper 1, paper 2 and pacer 3. Secondly, we report the new robust control scheme for a class of nonlinear dynamic systems with application to hypersonic vehicle modeled by lumped mass approach. In this work, instead of assuming that the mass matrix M and the stiffness matrix K are exactly known, we consider the case where uncertain parts are involved in these matrices. Such consideration is of importance in practice. Finally, a new approach to controller design for aerodynamic systems is presented. Fundamentally, this is the so-called inverse dynamics. However, the essential difference is that our approach is an improved version, because an

extra compensation is introduced, which make the over system either adaptive, or robust.

Research Task 3 (Marshall Space Center) - Dr. Homaifar

This work examines the implementation of a fuzzy logic six degree-of-freedom controller for a general purpose spacecraft. This controller will provide autonomous docking capabilities for the spacecraft based on radar or other ranging data.

The six degree-of-freedom controller actually consists of six one degree-of-freedom controllers, one each for roll, pitch, yaw, range, elevation, and azimuth. Development of the controller began with the inclusion of code to determine translation information from the radar subroutine. Rotation information (roll, pitch, and yaw) was already provided for use in the proportional derivative autopilot controller which the fuzzy controller replaces. Work was then done fuzzifying the appropriate input angles, distances, and rates for use by the controller. Fuzzification encompasses the partitioning of the input spaces into membership functions which consist of separate but overlapping fuzzy sets. After fuzzification, the input data is passed through the rule set and the output is determined by matching the appropriate rules with the data. The output of the controller are three separate forces for range, azimuth, and elevation and three torques for roll, pitch, and yaw. The specific goals here can be stated as:

1. Improvement of control system and guidance
2. Reduction of overall computational burden

Research Task 4 (NASA-Langley) - Dr. Lai
Calculate flight dynamics of hypersonic vehicle

The combination of collocation with non-linear programming has resulted in a method of rapidly generating optimal trajectories. This method has been embodied in the Optimal Trajectories by Implicit Simulation (OTIS) program. The solution of optimal control problems by direct transcription using collocation and non-linear programming will be used to support hypersonic aerospace vehicle design studies. Applications of solutions to hypersonic cruise, constrained fly-outs, and optimal approach to landing will be studied. The flight dynamics optimization is a multi-disciplinary research area for conceptual and preliminary design and evaluation of advanced aircraft concepts. It consists of primary research subjects:
1) weights, 2) aerodynamics, 3) engine cycle analysis, 4) mission performance, 5) takeoff an landing.

The weights estimation will use statistical/empirical equations to predict the weight of each item in a group weight statement. We will incorporate a analytical wing weight estimation capability available for use with more complex wing platforms. Centers of gravity and moments of inertia will be calculated for multiple fuel conditions. The aerodynamics estimation will use the EDET (Empirical Drag Estimation Technique) to provide drag polars for performance calculations. Modifications include smoothing of the

drag polars, more accurate Reynolds number calculations, and the inclusion of the Sommer and Short T method for skin friction calculations. Alternatively, drag polars may be input and then scaled with variations in wing area and engine (nacelle) size. The engine cycle analysis will be based on the QNEP. It provides the capability to internally generate an engine deck consisting of thrust and fuel flow rate at a variety of Mach-altitude conditions. Engine cycle definition decks will be provided for turbojets turboprops, mixed flow turbofans, separate flow turbofans, and turbine bypass engines. The mission performance estimation will use the calculated weight, aerodynamics, and propulsion system data to calculate performance.

Based on energy considerations, optimum climb profiles will be flown to start of cruise conditions. The cruise segments may be flown at the optimum altitude and/or Mach number for maximum range or endurance, at the long range cruise Mach number, or at a constant lift coefficient. Descent may be flown at the optimum lift-drag ratio. In addition, acceleration, turn, refueling, payload release, and hold segments may be specified in any reasonable order. Reserve calculations can include flight to an alternate airport and a specified hold segment. The takeoff and landing analysis included the computation of the all-engine takeoff field length, the balanced field length including one-engine-out takeoff and aborted takeoff, and the landing field length. The approach speed will also be calculated, and the second segment climb gradient and the missed approach climb gradient criteria will be evaluated. The system will have the capability to generate a detailed take off and climb out profile for use in calculating noise footprints.

The study will include the analysis of a point design, parametrically varying certain design variables, (for minimum gross weight, minimum fuel burned, maximum range) using nonlinear programming techniques. The Fiacco-McCormick penalty function may be used with the Davidson-Fletcher-Powell (DFP) or the Broyden-Fletcher-Goldfarb-Shano (BFGS) algorithm. The configuration design variables are wing area, wing sweep, wing aspect ratio, wing taper ratio, wing thickness-chord ratio, gross weight, and thrust (size of engine). The performance design variables are cruise Mach number and maximum cruise altitude. The engine cycle design variables are the design point turbine entry temperature, the maximum turbine entry temperature, the fan pressure ratio, the overall pressure ratio, and the bypass ratio for turbofan and turbine bypass engines.

Research task 5 (NASA-Langley) - Dr. Dunn
Vibration and Smart Structures

A literature search was performed for reported investigations on prior National Aerospace Developments (NASP) and the experimental version of the X-30. The objective of this search was to obtain a list of various topics related to NASP research so that future work would parallel and have possible applications to NASP development. Pertinent information related specifically to integral systems engineering and programmatic development was sought so as to pick topics that could be integrated into A&T's CORE

disciplines of computational fluids, controls, structures, and human factors/tele-operations. Also, a topic was sought that would broaden my own area of expertise while also providing an additional area of expertise at A&T.

Smart (active and instrumented) structures and materials is another component investigated within the control and guidance group. The focal points of this study are: 1) structure flexibility and vibration issues due to the constraint of reduced weight, 2) controlling the contour of aerodynamic surfaces due to loading and temperature, and 3) controlling the contour of surfaces inside a Hyper-sonic jet engine to enhance propulsion. These materials could provide utility as integral sensors throughout NASP to monitor vehicular performance and to announce trouble.

Significant smart materials work is underway, as reported in the literature, in the area of composite materials which are combinations of traditional composites and piezoelectric materials where the piezoelectric material provides the active actuation and passive sensing element. An alternative area of prime interest is the development of composite structures and laminates with internal pressurization to provide the active actuation component to control the structures load and deformation response. By venturing away from composites with lay-ups which try to approach characteristics of isotropic materials, structures might be developed that would respond to loads advantageously and allow internal pressure to control the displacement of the structure and adverse stresses as needed. The working fluid used for internal pressurization may possibly be used to combine systems. One possibility is that this fluid space could be used for fuel storage. Another is that this fluid could also be utilized in cooling. Such combinations of functions for the working fluid could have possible advantages.

C. AREA PROGRAM ACTIVITIES

The control and structure group began its activities in the Center on January 4, 1992. Drs. Homaifar and Lai had released time for both fall and spring semester, while Dr. Dunn had released time during fall 1992. Also, Dr. Homaifar put two and half months during summer of 1992. Dr. Song joined the group as of August 10, 1992, where he is doing research full time.

Educational Component

The control group offered Linear Systems and Control(ELEN 410) during the Fall 1992. This course will be offered again on the spring of 1993. The course is open for seniors in Mechanical, Industrial and Electrical Engineering. The course includes: control system modeling and representation, features of feedback control system, state space representation, time domain analysis, root locus, and design compensation. This course is being offered to students in Electrical and Mechanical Engineering. The course syllabus and requirement is given in Appendix A. Also, ELEN 668 (Advanced Automatic Control course is listed as an option for the students specialized in Aerospace discipline as an

option in Mechanical engineering. Also, a new course MEEN 652 Aero Vehicle Stability and Control will be developed as an option for the students specialized in Aerospace discipline as an option in Mechanical engineering.

Computer System and Software Purchases

In order to familiarize the student in ELEN 410, with different compensators and to provide a thorough understanding of the different characteristics of the compensators, the following computer packages are acquired:

Personal Computers: 3 (486 DX/50Mhz)
Visual Solutions' software package for PC (2 units)
MATHLAB for workstation: Control System Toolbox
Robust-Control Toolbox

The designs of the compensators are interactive, thus the students can visualize the changes made in the coefficients of the compensators.

Laboratory Development (Target date August 93)

The analog control systems laboratory will have (as a goal) to teach the student the practical aspects of continuous-time dynamical system modeling, analysis, design and simulation, and will consist of the following experiments:

- Scaling instrumentation variables and programming differential equations on analog computers.
- Determination of transfer function of dynamical systems using frequency response methods.
- Transient response of dynamical systems via analog computer simulation.
- Stability analysis of dynamical systems modeled by differential equations.
- Open-loop and closed-loop velocity control using analog computer models.
- Position control using conventional cascade compensators (lag, lead, and lag-lead).
- Minor feedback loop compensation techniques.
- Implementation of elementary state variable observers.
- Laboratory design project; e.g., analog computer simulation of a compensated physical system which takes into account nonlinear effects such as back lash, saturation, dead zones, etc.

Travel

1. HBCU Orientation Conference (Steven Lai, A. Homaifar)
2. Marshal Space Flight Center (Steven Lai, A. Homaifar)
3. Attend workshop on Distributed Parameters (Steven Lai, A. Homaifar)
4. Attend and Present Paper at International Symposium (SPIE) in Mathematical

Engineering (Homaifar, McCormick)

5. Attend and Present Paper at Second International Conference on Automation Technology (Steven Lai)
6. Attended workshop on Thermal Protection Systems (TPS) at NASA-Langley (DeRome Dunn)
7. Travel to NASA-Lewis for ten weeks as NASA-ASEE summer faculty fellow located within the structures division in the fatigue and fracture branch (DeRome Dunn)

Date:	May 9-11, 1992
From:	Greensboro, NC
Destination(s):	Marshal Space Center, Huntsville, AL
Purpose:	To visit facilities at site
Cost:	$ 472.00

Date:	March 24-27, 1992
Destination(s):	Washington, DC and Hampton, VA
Purpose:	To participate in HBCU-NASA conference
Cost:	$ 414.09

Date:	June 9-11, 1992
Destination(s):	Williamsburg, VA
Purpose:	To attend workshop
Cost:	$ 364.50

Date:	May 28-29, 1992
Destination(s):	Hampton, VA and Washington, DC
Purpose:	To discuss project with technical monitor
Cost:	$ 340.77

Date:	December 14-20, 1992
Destination(s):	Tuscon, AZ
Purpose:	31st IEEE Conference on Decision and Control, and attend a workshop
Cost: (Estimated)	$1624.80

Date:	November 17-19, 1992 (Professor Wei-Bing Gao)
From:	Beijing, China
Destination(s):	Greensboro, NC
Purpose:	To give seminar in control and guidance of hypersonic vehicles
Cost:	$1010.00

D. FACULTY AND STUDENT PARTICIPATION

Faculty Participants

Name:	Abbie Homaifar (Electrical Engineering)
Classification:	Coordinator
Citizenship:	Iran
Research Activity:	Work on application of Adaptive control, Fuzzy controller strategies related to hypersonic plane
Telephone:	(919)-334-7760 Room 537, McNair Hall North Carolina A & T State University Greensboro, NC 27411

Name:	DeRome Dunn (Mechanical Engineering)
Classification:	Group member
Citizenship:	US
Research Activity:	Development of computational methods for Vibration of smart material
Telephone:	(919)-334-7620 Room 636, McNair Hall North Carolina A & T State University Greensboro, NC 27411

Name:	Steven Lai (Mechanical Engineering)
Classification:	Group member
Citizenship:	US
Research Activity:	Flight dynamics of hypersonic vehicle, and smart materials
Telephone:	(919)-334-7620 Room 623, McNair Hall North Carolina A & T State University Greensboro, NC 27411

Name:	Yong-Duan Song (Electrical Engineering)
Classification:	Research Associate
Citizenship:	China
Research Activity:	Work on adaptive control, nonlinear control theory, robust control and their applications to hypersonic vehicle
Telephone:	(919)-334-7255 Center Office, Woodson Building North Carolina A & T State University Greensboro, NC 27411

Student Participants

SUMMER, 1992

Undergraduate students:

Name:	Christen Bonita Williams (Junior, Electrical Engineering)
Citizenship:	US
GPA:	3.21
Research Advisor:	Dr. Homaifar, and Dunn

Name:	Lamark Chance(Junior)
Citizenship:	US
GPA:	3.08
Research Advisor:	Drs. Homaifar, and Lai

Name:	Robert Lynn Dismuke (Senior, Electrical Engineering)
Citizenship:	US
GPA:	3.60
Research Advisor:	Dr. Homaifar

FALL, 1992

Name:	Christen Bonita Williams (Junior, Electrical Engineering)
Citizenship:	US
GPA:	3.21
Research Advisor:	Dr. Homaifar, and Dunn

Name:	Lamark Chance(Junior)
Citizenship:	US
GPA:	3.08
Research Advisor:	Drs. Lai, Song

Name:	Nikki Smith (Senior, Electrical Engineering)
Citizenship:	US
GPA:	3.60
Research Advisor:	Dr. Homaifar

Graduate students

FALL, 1992

Name:	Kevin Barnhart (Electrical Engineering)
Citizenship:	US
Classification:	First semester
Research Advisor:	Dr. Lai

Name:	**John Hogans (Electrical Engineering)**
Citizenship:	**US**
Classification:	**Third semester-GEM Fellow**
Research Advisor:	**Dr. Homaifar**

Name:	**Nadeem Bowe (Electrical Engineering**
Citizenship:	**US**
Classification:	**Third semester-GEM Fellow**
Research Advisor:	**Dr. Homaifar**

Summary of Student Involvement

Each student was assigned several separate jobs that contributed to the overall research activities. The tasks which were split among the students included:

1. Research on the dynamics and background of control systems and several documents from the Marshall Space Program.
2. Analysis of the FORTRAN computer program which accompanied the aforementioned documents.
3. Assistance for graduate students in their theses. One involves the design of fuzzy controllers using genetic algorithms (GAs), and the other involves non-linear constrained optimization by GAs and its comparison with other existing methods of solution. Within this task, the undergraduate students were exposed to the use of the C programming language.
4. Introduction to VisSim software, a package that involves creating block diagrams and simulation with the use of advanced engineering graphics
5. Exposure to writing and preparing papers for publication.

John E Hogans IV

1. Development of real time adaptive fuzzy controllers. The research will include a study of large population GA and Evolution strategies. ES will be used for the adaptive control law development. Currently, he is reading background materials on fuzzy controllers.
2. MRI Brain Scan images using Genetic Algorithms for Bowman Gray School of Medicine. The amount of grey matter, white matter, and cerebral spinal fluid (CSF) contained in the image was to be quantified automatically using a histogram of the MRI image.

Kevin Barnhart

Mr. Barnhart is working on the development of flight dynamic models. He is currently involved in a literature survey of articles related to the guidance and control of aircraft. In addition, he is studying the basic principles involved with rigid body dynamics and aerodynamics.

Nadeem Bowe

Mr. Bowe is working on the subject entitled "System Identification Via Evolution Strategy Employing Group Method Data Handling Techniques." The central problem in system control and prediction is the formation of a suitable mathematical model given some small amount of noisy system measurements. In addition, an unknown system may be potentially nonlinear and thereby difficult to describe by deterministic methods. It is with this in mind that the attempt to employ the Group Method Data Handling (GMDH) approach with Evolution Strategy (ES) is motivated. Two such systems to be explored are, the Glass-Mackey Equation:

$$\frac{dx}{dt} = \frac{ax(t-\tau)}{1+x^{10}(t-\tau)} - bx(t) \qquad (1)$$

and the Logistic Equation:

$$x(t+1) = \lambda x(t)(1-x(t))$$

Both of these functions generate chaotic data and would be difficult to characterize given a small number of data points.

Taking cues from Kargupta and Smith's paper,"System Identification with Evolving Polynomial Networks," the author will attempt to demonstrate that the GMDH/ES combination is a more robust method than either GMDH or Genetic Algorithms alone in deriving a suitable model for system prediction and identification.

E. PROGRAM IMPACT AND FINANCIAL REPORT

Drs. Homaifar, Lai and Dunn were the supervisors to all of the students who participated in the research. They provided the background and documents to begin working on the required tasks assigned by NASA and made all the necessary arrangements for the students to work in the laboratory both on and off the computer. Dr. Homaifar instructed the students, advised them, and gave the appropriate tasks to them. This program provide the students good understanding of control theory and technology in application to aerospace engineering research. Many publications resulting from this research program are listed below.

Publications

1. A. Homaifar, and E. McCormick, " Full Design of Fuzzy Controllers Using Genetic Algorithms", Proceedings of the Neural and Stochastic Methods in Image and Signal Processing at the International Society of Optical Applied Science and Engineering. July 18-24, 1992.
2. A. Homaifar, E. McCormick, " A New Approach for the Design and Implementation

of Fuzzy Controllers", The IEEE Proceedings of the Southeastern Symposium on System Theory, and Third Annual symposium on CSA, Greensboro, NC 1992.

3. H.Y. Lai and A. Homaifar, 1992, "Design of Fuzzy Controllers Using Genetic Algorithms," The Second International Conference on Automation Technology, July 4-6, 1992.
4. A. Homaifar, H.Y. Lai, and Ed McCormick, 1992, "Design Optimization of Turbofan Engines Using Genetic Algorithms," (Submitted).
5. A. Homaifar, H.Y. Lai, and X. Qi, " Constrained Optimization Via Genetic Algorithms", (Submitted).
6. Y. D. Song, J. N. Anderson, A. Homaifar and H. Y. Lai, Robust Motion Tracking Control of Robotics Arms Based on the Generalized Energy Accumulation Principle, to appear in IEEE *Int. Conf. on Decision and Control*, December 1992, Tucson, Arizona.
7. Y. D. Song, J. N. Anderson, A. Homaifar and H. Y. Lai, System Stability and Performance Analysis Based on Generalized Energy Accumulation: Part II - Applications, to appear in IEEE *Int. Conf. on Decision and Control*, December 1992, Tucson, Arizona.
8. Y. D. Song, J. N. Anderson, A. Homaifar and H. Y. Lai, Nonlinear Robust Controller Design for Multi-Robotics Systems with Unknown Payloads, *The Fourth NASA Conf. on Muli-Robot Systems*, New York, November, 1992.

Area Financial Report

1. Faculty	**Spring(@25%)**	**Fall(@25%)**	**Summer(2.5 months**
Abbie Homaifar	**$5,142.00**	**$5,194.00**	**$11,427.00**
DeRome Dunn	**$4,654.00**	**-**	**-**
Steven Lai	**$5,656.00**	**$5,713.00**	**-**
Y.D. Song		**$2,760.00**	**$12,420.00(@100%)**
Total Release Time =			**$ 52,967.00**
2. Research Assistant (Two Graduate)			**$ 8,100.00**
3. Fringe Benefit (24% of 1)			**$12,712.00**
4. Social Security (7.65% of 2)			**$ 620.00**
5. Indirect Cost (55% of 1)			**$29,131.00**
6. Other Direct Cost			
Undergraduate Stipend			**$ 7,442.00**
Tuition			**$ 1,310.00**
Lab Setup			**$15,984.00**
Printing			**$ 500.00**
Office Supply			**$ 272.00**
Travel			**$ 4,699.00**
TOTAL			**$133,737.00**

Equipment Purchased

Vendor 1:	**Digitz**
Items:	**Texas Instruments Microlaser Turbo (Part #2559821-4501)**
	Texas Instruments Toner (Part #2550770-0001)
	1 MB RAM Third Party Equivalent to Part#2555739-0001
Cost:	**$1,982.06**

Vendor 2:	**MGA**
Items:	**ACSL/PC 3.5 inch diskettes**
Cost:	**$1010.00**

Vendor 3:	**United Office & Business Concept**
Items:	**3 Deluxe Desk Dispensers**
	1 dozen Uniball Pens
	3 Scotch Brand Magic Tape Dispensers
	1 box white Envelopes
	3 boxes Kraft Envelopes
	2 boxes brown Kraft Clasps
	2 boxes brown Kraft Envelopes
Cost:	**$ 271.66**

Vendor 4:	**North Carolina A & T State University**
Items:	**3 Copier Cards for Literature Research**
Cost:	**$500.00**

Vendor 5:	**Tri-Star Computer Corporation**
Items:	**3 TRI*CAD YZ-250 VESA Local Bus Systems**
Cost:	**$12,992.30**

COMPUTATIONAL FLUID DYNAMICS RESEARCH

ANNUAL REPORT

Prepared for

NASA CENTER OF RESEARCH EXCELLENCE
SCHOOL OF ENGINEERING
NORTH CAROLINA A&T STATE UNIVERSITY

by

Suresh Chandra
Kenneth Jones
and
Hassan Hassan
David Scott McRae

Computational Fluid Dynamics Group
School of Engineering
North Carolina A&T State University
Greensboro, NC 27411

December, 1992

A. AREA SUMMARY

The focus of research in the CFD area is two-fold:

1. Develop new approaches for turbulence modeling so that high speed compressible flows can be studied for applications to entry and re-entry flows,
2. Perform research to improve CFD algorithm accuracy and efficiency for high speed flows.

Short-Range Plans

(1) Continued recruitment efforts with the objective of enticing two graduate students and two undergraduate students in Spring, 1993.

(2) Offering an advanced course in CFD at NCA&TSU in Fall 1993 if the enrollment is adequate. If only one or two students and faculty members are interested, efforts will be made to enroll in NCSU courses.

(3) Modeling of the pressure dilatation term as well as the compressible dissipation term and using the SPARK code to predict useful parameters such as the shear layer growth rate for compressible high speed turbulent flows.

(4) Development of efficient numerical algorithms for high speed flow fields. It is hoped that a new research associate can be hired in early 1993 to initiate research in this vital area.

(5) Continued association with the Theoretical Flow Physics Branch at the NASA Langley Research Center (LaRC). It is anticipated that Dr. Chandra and/or one faculty member and two students will spend most of 1993 summer at LaRC. Such an association enables faculty and students to (a) use the LaRC technical library; (b) interact with faculty and students from NCSU and other universities; and (c) interact with NASA and ICASE researchers and facilities on a daily basis.

(6) Development of algorithms for two-dimensional, three-dimensional, and axisymmetric radiation heat transfer for chemically reacting hypersonic flows.

B. AREA RESEARCH PROJECTS

Project Title:	Turbulence Modeling for High Speed Compressible Flows
Principal Investigator:	Dr. Suresh Chandra
Funding Amount:	$25,000
Funding Source:	NASA Langley Research Center
Duration:	May 16, 1991 - December 31, 1992

C. AREA PROGRAM ACTIVITIES

During 1992, Dr. Chandra supervised the M.S. thesis work of one graduate student (Cheryl Sellers). Both Dr. Chandra and Ms. Sellers spent the bulk of the summer in 1991

and 1992 at NASA Langley Research Center (Theoretical Flow Physics Branch). Ms. Sellers focussed on studying compressibility effects in modeling turbulent high speed mixing layers. The accomplishments to date are:

(1) Incorporation of the extension of the compressibility dissipation model of Sarkar et al. of ICASE in the SPARK code using two-equation turbulence modeling.

(2) An extensive literature review to delineate work done or being done in the study of compressibility effects in turbulent shears flows.

(3) Comparison of results in (1) with the results of a large number of experimental and analytical studies.

(4) Presentation of a paper entitled "Study of Compressibility Effects in Turbulent Shear Flows" at the ASME Fluids Engineering Conference, June 22-23, 1992.

(5) Ms. Sellers defended her M.S. thesis on August 10, 1992. She has been admitted to the Ph.D. program in ME at the University of Illinois and has begun her doctoral studies this fall.

Additional Personnel

(1) For the period through October 1992, Dr. Chandra has been the only faculty member involved in CFD research. We have hired a full-time research associate beginning October 15. Dr. Gregory Elbert completed his Ph.D studies at Mississippi State University in early October and will initiate our effort in the areas of radiation heat transfer for hypersonic chemically reacting flows, thus complementing the turbulence modeling work for high speed flows.

(2) Mr. Kenneth Jones joined the ME Department in the of fall of 1992 as a tenure-track faculty member. He completed his Ph.D. studies at NCSU in late October. He is an asset to the CFD area in CORE by virtue of his experimental/analytical background in CFD research. Mr. Jones plans to apply for participation in one of the NASA/ASEE summer institutes in 1993 with the objective of becoming closely associated with appropriate NASA facilities and personnel. Dr. Chandra, Mr. Jones, and Dr. Elbert will work closely with Drs. Hassan and McRae of NCSU in accordance with the attached subcontract, which delineates the long-range research plan for the CFD area.

Educational Effort

1. A course in computational fluid dynamics is being offered by Dr. Chandra this fall. This course has a mix of undergraduate ME Seniors and graduate students.
2. Dr. Hassan A. Hassan will offer an advanced course in combustion and reacting flows at NCSU in spring. Some faculty members and graduate students in the CFD area at NCA&TSU will enroll in this course if their schedules permit.

Travel

1. NASA Orientation Conference - Washington, D. C.; March 24-25, 1992 (S. Chandra)
2. NASA Langley Research Center - Hampton, VA; April 21-24, 1992 (S. Chandra)

3. ASME - Fluids Engineering Conference, Los Angeles; June 20, 1992 (S. Chandra)
4. NASA Langley Research Center, Hampton, VA; November 16-19, 1992 (S. Chandra)

D. FACULTY AND STUDENT PARTICIPATION

Faculty Involved

Name & Title	Depart.	Ethic Background	Starting Date	Nature of Participation
S. Chandra Research Prof.	ME	Asian (U.S. citizen)	April 1992	CFD Group Coordinator Student Research Advisor
K. Jones Asst. Prof.	ME	White (U.S. citizen)	November 1992	Core Research Leader Student Research Advisor
G. Elbert Research Assoc.	ME	White (U.S. citizen)	October 1992	Core Research Leader Student Research Advisor
H. Hassan Prof. (NCSU)	Mech.&Aero.	Middle Eastern (U.S. citizen)	April 1992	Subcontractor (NCSU)
S. McRae Assoc. Prof. (NCSU)	Mech. & Aero.	White (U.S. citizen)	April 1992	Subcontractor (NCSU)

Student Involved

Name of Student	Classification/Major	Advisor	Graduation Date
Cheryl Sellers*	Graduate/M.E.	Chandra	August, 1992
Rafael Jones**	Undergraduate/M.E.	Elbert/ Chandra	December, 1992
Michael Gray**	Undergraduate/M.E.	Elbert/ Chandra	May, 1993
Stapleton Tabb	Undergraduate/M.E.	Chandra	December, 1993

* Currently a Ph.D.student in M.E.at the University of Illinois.
** Scheduled to begin graduate study in CFD at NCA&TSU upon graduation.

E. PROGRAM IMPACT AND FINANCIAL REPORT

Publications

1. Chandra, S., 1992, "Study of Compressibility Effects in Turbulent Shear Layers", ASME Fluids Engineering Conference, Los Angles, CA, June 21-23, Abstract published in "Fluids Engineering 1992 - Abstracts, FED-Vol. 133, ASME/Fluids Engineering Division, 1992".
2. Jones, K.M., DeJarnette, F. R., Griffith, W.C., and Yanta, W. J., 1992, "Boundary Layer Study on Nozzle Wall at Hypersonic Velocities", AIAA Paper No. 92-4013, presented at the AIAA 17th Aerospace Ground Testing Conference, Nashville, TN, July 6-8, 1992.
3. Sellers, C. and Chandra, S., "Compressibility Effects in Modeling Turbulent High Speed Mixing Layers", Accepted for Presentation at the 1993 ASME Forum on Turbulent Flows, Washington, DC, June 1993.
4. Elbert, G. J. and Cinnella, P., "Truly Two-Dimensional Algorithms for Radiative Non-equilibrium Flows", 13th International Conference on Numerical Methods in fluid Dynamics, Rome, Italy, July 1992.
5. Elbert, G. J. and Cinnella, P., "Axisymmetric Radiative Heat Transfer Calculations for Flows in Chemical Non-equilibrium", AIAA Paper 93-0139, 31st Aerospace Sciences Meeting, Reno, Nevada, January 1993.
6. Sellers, C., "Compressibility Effects in Modeling High Speed Turbulent Mixing Layers", M. S. Thesis, Department of Mechanical Engineering, North Carolina A&T State University, 1992.

Area Financial Report

Line Items	Allotments	Expenditure
1. Faculty Salaries (Chandra: 2.5 months) (Elbert: 2.5 months)	$31,375	$31,375
2. Student Wages	$ 6,000	$ 1,000
3. Fringe Benefits (24% of 1)	$ 7,530	$ 7,530
4. Indirect Costs (59% of 1 & 2)	$ 20,556	$ 17,806
5. Travel	$ 3,000	$ 2,962
6. Scientific Equipment	$ 52,519	$ 52,102
7. Contract Services	$ 2,000	$ 1,590
8. Subscriptions/Memberships	$ 600	$ 90
9. Books/Journals	$ 1,420	$ 990
10.Subcontract to NCSU	$ 37,153	$ 37,153
TOTAL	$162,153	$152,598

Equipment Purchased

The following equipment will be purchased in November 1992:

Vendor:	**Silicon Graphics, Inc.**
Items:	**3 IRIS INDIGO Model #W-RPC50**
Unit Cost:	**$11,314.00**
Totl Cost:	**$33,942.00**
Vendor:	**Silicon Graphics, Inc.**
Items:	**CD-ROM Update Media #M05-CD**
Unit Cost:	**$ 1,967.89**
Totl Cost:	**$ 1,967.89**
Vendor:	**Parity Systems, Inc.**
Items:	**1 1.2 GB Inetrnal HD for the SGI R4000**
	1 2.0 GB External DAT Drive for SGI R4000
Totl Cost:	**$10,399.66**
Vendor:	**AMTEC Engineering, Inc.**
Items:	**3 Tecplot Release 5**
Unit Cost:	**$ 530.00**
Totl Cost:	**$ 1590.00**
Vendor:	**DATAPRINT Inc.**
Items:	**1 HP Laserject IVm Model #C2021A**
Totl Cost:	**$ 1759.00**

F. SUBCONTRACT RESEARCH WORK AT NCSU UNDER GRANT NAGW-2924

1. Develop a New Approach for Turbulence Modeling

When employing a two-equation turbulence model, there is general agreement that one of the equations must be the equation governing the turbulent kinetic energy. The most popular second equation is based on the rate of turbulent kinetic energy dissipation or the characteristic turbulent frequency. Unfortunately, such equations do not account for certain mechanisms that are present when one examines the vorticity equation, namely, the effects of vortex stretching, which is a three-dimensional effect, and the production of vorticity term which is important when compressibility effects are important.

Because both TKE dissipation and turbulent frequency equations ignore the existence of above important effects, there has been general dissatisfaction with one equation or the other. There is one equation which governs the mean vorticity fluctuation, which is referred to as entropy, which can serve as a basis for the second equation in two-equation models. This equation has all the physics that exists in the vorticity equation and thus, may be an attractive alternative. Our goal is to pursue this approach.

2. Perform Research to Improve Computational Algorithm Accuracy and Efficiency

(a) Develop efficient numerical algorithms for high speed internal flow fields. This project involves the development of an efficient iteration strategy for solution of the Navier-Stokes equations. In three-dimensions, the governing equations are written in Newton's form and the Jacobian is partitioned and updated such that a Gauss-Seidel like iterative sequence is performed with forward and backward sweeps to approximately invert the Jacbian. Residual updating will be used to increase information transfer and quasi-Newton acceleration techniques will be applied. The resulting code will be applied to supersonic internal flows.

(b) Develop dynamic 3-D solution mesh algorithms. This task will involve the further development of a solution adaptive algorithm to include adaption of block grid interfaces and interiors. The algorithm presently only works for single block grids. The resulting code will be used to compute unsteady flows over complex aircraft shapes.

Other tasks will be performed in support of the effort at NCA&TSU at the direction of Dr. Suresh Chandra, CFD Coordinator.

FLIGHT SIMULATOR FOR HYPERSONIC VEHICLE AND A STUDY OF NASP HANDLING QUALITIES

ANNUAL REPORT

Prepared for

NASA CENTER OF RESEARCH EXCELLENCE
SCHOOL OF ENGINEERING
NORTH CAROLINA A&T STATE UNIVERSITY

by

Celestine A. Ntuen, Ph.D.
Eui H. Park, Ph.D.
Joseph M. Deeb, Ph.D.
Jung H. Kim, Ph.D.

Human-Machine Systems Engineering Group
School of Engineering
North Carolina A&T State University
Greensboro, NC 27411

December, 1992

A. AREA SUMMARY

The research goal of the Human-Machine Systems Engineering Group was to study the existing handling quality studies in aircrafts with sonic to supersonic speeds and power in order to understand information requirements needed for a hypersonic vehicle flight simulator. This goal falls within the NASA task statements:

1. **Develop Flight Simulator for Hypersonic Vehicle**
2. **Study NASP Handling Qualities**
3. **Study Effects of Flexibility on Handling Qualities and on Control System Performance**

Following the above statement of work, the group has developed three research strategies. These are:

1. To study existing handling quality studies and the associated aircrafts and develop flight simulation data characterization.
2. To develop a profile for flight simulation data acquisition based on objective statement #1 above.
3. To develop a simulator and an embedded expert system platform which can be used in handling quality experiments for hypersonic aircraft/flight simulation training.

B. AREA RESAERCH PROJECTS

Title: Investigation of Human Response Error In A Flight Simulation Domain
PI: Celestine A. Ntuen

Title: Investigation of A Model To Analyze Pilot/Vehicle Interaction In A Hypersonic Flight Simulator
PI: Joseph M. Deeb

Title: A Robust Methodology For Visual Reconstruction and Surface Rendering For a NASP Cockpit Environment.
PI: Jung H. Kim and Eui H. Park

C. PROGRAM ACTIVITIES

To achieve objective #1, extensive data is being collected from various sources including NASA handling quality source data, U.S. Air Force handling quality handbooks, and MIT's Center For Man-Machine Flight Simulation Reports. The research outcome for this objective is in progress and is to be published under the title: "Development of Flight Database Using Handling Quality Studies". Data in this category are:

- Type of aircraft.
- Aircraft categories (e.g; sonic, hypersonic, etc.).
- Aircraft aerodynamic parameters.

- Human (pilot) characteristics.
- Environment in which handling quality are derived.
- Controllable and non-controllable variables in the flight simulation studies.
- The performance data (dependent variables) of interest.

Data collection for handling quality (HQ) was accelerated by documents made available to the group by Dr. L. Taylor of NASA Langley Research Center. While the group continues to develop conceptual models for synthetic flight simulation for hypersonic vehicle, the following drawbacks were encountered:

- It is difficult to develop the simulator from scratch. It would be better if an unused flight simulator could become available for the NASA-CORE project by NASA. This can be through surplus equipment identification from any of the NASA research centers.
- The group also needs a technical monitor from NASA. The person should have a background in developing flight training simulators and/or human factors with bias in human-machine interaction. In all meetings related to the project, the Human-Machine Group is always left out when discussions on future directions and research accomplishments are discussed. We need a collaborator to consult with in matters related to the group.

The original proposal to develop a prototype simulation model is behind by about four months due to lateness in equipment delivery. However, there is no loss time since the investigators are developing concepts and theories related to the Research program.

D. FACULTY AND STUDENT PARTICIPATION

Faculty participants

Faculty	Department Affiliation	Ethnic Backg.	Teaching Interest	Research Interest	CORE Responsibility	No. of Students Advised
Celestine A. Ntuen	Industrial Engineering	Black	Human-Machine Interaction Systems Design Methodology	Human-Machine Systems, Artificial Intelligence and Reliability	Team Leader	2
Eui H. Park	Industrial Engineering	Asian	Simulation, Quality Control Manufacturing	Manufacturing Systems, Robotics & Quality Control	Team Member	-
Joseph M. Deeb	Industrial Engineering	White	Human Factors, Ergonomics and Manual Material Handling	Human Factors & Ergonomics	Team Member	1
Jung H. Kim	Electrical Engineering	Asian	Computer Vision & Signal Processing	Signal Processing and Expert Systems	Team Member	-

NASA-CORE (HUMAN-MACHINE SYSTEMS GROUP)
Student Participant's Profile

Research Assistant	Citizenship/ Ethnic Group	Address	Major	Classification	GPA	Advisor
Woodrow Winchester	U.S.A. (Black)	912 Fairgreen Road Greensboro, NC 27410	Industrial Engineering	Senior*	3.15	J. Deeb
Christopher Geiger	U.S.A. (Black)	408-C Savannah Street Greensboro, NC 27406	Industrial Engineering	Senior*	3.05	C. Ntuen
Erika Mansfield	U.S.A. (Black)	2920-B Cottage Place Greensboro, NC 27455	Industrial Engineering	First Semester Graduate Student	3.5 in UG	C. Ntuen

The three students work as a team on a project entitled: "The Development of Flight Simulation Database Using Handling Quality Studies". An object-oriented database using functional nets is used as an investigative tool. The paper has been submitted for conference presented by the students.

E. PROGRAM IMPACT AND FINANCIAL REPORT

Project Impact Statement

1. Two African-American students mentored and encouraged in the senior undergraduate year to consider graduate school. All two students will be full time graduate students in Industrial Engineering beginning Spring 1993.
2. Two African-American students have been admitted to graduate program in Industrial Engineering beginning Spring 1993 (one female and one male).
3. As a part of our pipeline recruitment process, two senior Industrial Engineering students will join the research team in January of 1993.
4. There are 146 undergraduate students in the Department of Industrial Engineering of which 124 students (or 85%) are African-American. The graduate program has 40 students, of which 36 students (or 90%) are African-American.
5. Enrollment prediction for the next five years in Industrial Engineering

Year	Undergraduate	Graduate	Total
1993	146	40 (MSIE)	186
1994	150	40 (MSIE)	190
1995	155	45 (MSIE)	200
1996	155	50 (MSIE + PH.D)	205
1997	160	50 (MSIE + PH.D)	220

With this growth prediction, it is expected that five full time faculty (teaching and research) and at least one research faculty will be needed.

Publications

1. Kim, J.H., Yoon, S.H., Park, E.H. and Ntuen, C.A., Recognition of Partially Occluded Threat Objects Using the Annealed Hopfield Network, Proc. of SPIE OE/Technology Conference, Boston, Massachusetts: 15-20 Nov., 1992.
2. Brooks, T.D., and Kim, J.H., An Approach to Three-Dimensional Object Recognition Using A Hybrid Hopfield Network, Submitted, IEEE Southeastcon '93, Charlotte, N.C.
3. Knight, D.D. and Kim, J.H., Object Identification Using a Reconstructed Surface of Concealed Object, Submitted, IEEE Southeastcon '93, Charlotte, N.C.
4. Ntuen, C.A., Information Theoretic Models of Human-Machine Interaction, Submitted, International Journal for Information Sciences.
5. Ntuen, C.A., Park, E.H., Deeb, J.M., Geiger, C., Mansfield, E. and Winchester, W. The Development of Flight Simulation, Database Using Handling Quality Studies, Submitted, 15th Annual Conference on Computers and Industrial Engineering, Cocoa Beach, FL, March 8-10, 1993.
6. Ntuen, C.A., A New Approach To Modeling Human Response Errors In Synthetic Flight Simulator Domain, Submitted, 15th Annual Conference on Computers and Industrial Engineering, Cocoa Beach, FL, March 8-10, 1993.
7. Johnson, A.R., Ntuen, C.A. and Park, E.H., An Experimental Study of Human Interpretation of Computer Generated Image Data, Submitted, 15th Intl. Conference on Human-Computer Interaction/9th Japanese Symposium on Human Interface, Orlando, FL, August 8-13, 1993.

Area Financial Report

BUDGET FOR THE FIRST YEAR

ITEMS	ALLOCATION	ACTUAL EXPENSES	%OF SPENDING
1. Investigators' Salaries[1]	$ 40,500	$ 34,309	85 %
2. Secretary Salary	$ 1,500	$ 0	0 %
3. Student Assistanship[2]	$ 7,500	$ 4,473	60 %
4. Fringe Benefits[3]	$ 10,800	$ 9,308	86%
5. Indirect Costs[4]	$ 27,225	$ 21,330	78%
6. Direct Costs	$ 37,288	$ 30,362	81 %
- Scientific Equipment[5]	$ 24,688	$ 22,193	95 %
- Lab/Office Supplies	$ 2,000	$ 852	43 %
- Contracted Services[6]	$ 500	$ 500	100 %
- Other Supplies	$ 1,000	$ 0	0 %
- Travel Expenses[7]	$ 6,000	$ 4,104	68 %
- Printing[8]	$ 400	$ 0	0 %
- Postage	$ 200	$ 0	0 %
- Books/Journals[9]	$ 1,500	$ 903	60 %
- Tuition/Scholarships[10]	$ 2,000	$ 1,090	55 %
TOTAL	$ 125,093	$ 99,516	80 %

NOTE:

1. Investigators' release times for this project are as follows:
   - Dr. Celestine Ntuen (1 man-month)
   - Dr. Joseph Deeb (3.625 man-months)
   - Dr. Eui Park (0.45 man-month)
   - Dr. Jung Kim (1 man-month)
2. This project successfully motivated three African-American students to pursue their advanced degrees in Industrial Engineering. Ms. Erika Mansfield started her graduate study in Fall of 1992. Both Mr. Woodrow Winchester and Mr. Christopher Geiger are senior students and will join the Industrial Engineering graduate program in Spring of 1993.
3. 24 % of Items 1 and 3, and 7.65% of Item 3.
4. 55 % of Items 1, 2 and 3.
5. Four equipment are purchased as follows to implement this project.
   - DT Image Grabber
   - MATRIX$_x$ Simulation Software

- SUN SPARCstation 10
- HP LaserJet IIIP

6. This was used to build a pilot seat simulator.
7. All investigators visited NASA-Langley Research Center to discuss our research direction and to collect research materials in May 1992. Drs. Ntuen and Deeb attended a workshop in June on "Fundamentals of Flight Simulation" organized by MIT.
8. Library copy cards were purchased for necessary materials to be copied.
9. Necessary books to implement this project were purchased.
10. These funds were used to support tuition fees for Mr. Winchester and Mr. Geiger.

Student Support and Equipment Purchased

STUDENT SUPPORT

Name	SUMMER 1992	FALL 1992
Woodrow Winchester	20 hrs/wk	15 hrs/wk
Christopher Geiger	10 hrs/wk	15 hrs/wk
Erika Mansfield	------	20 hrs/wk

EQUIPMENT PURCHASED

EQUIPMENT	PRICE	DELIVERY STATUS
DT Precision Frame Grabber	$ 2,661.00	June 1992
$MATRIX_x$	$ 1,054.70	not yet
SUN SPARCstation 10	$ 19,197.66	not yet
HP LaserJet IIIP/DeskJet	$ 1,534.00	not yet
TOTAL	$ 24,447.36	

Students and Faculty Profiles

Research Assistants' Profile

Research Assistant	Citizenship	Address	Major	Classification	GPA	Advisor
Woodrow Winchester	U.S.A.	912 Fairgreen Rd. Greensboro, NC 27410	Industrial Engineering	Senior*	3.15	J. Deeb
Christopher Geiger	U.S.A.	408-C Savannah St. Greensboro, NC 27406	Industrial Engineering	Senior*	3.05	C. Ntuen
Erika Mansfield	U.S.A.	2920-B Cottage Place Greensboro, NC 27455	Industrial Engineering	Graduate Student	3.25 in UG	C. Ntuen

Investigators' Profile

Investigator	Citizenship	Address	Research Interests
Dr. Celestine Ntuen	Nigeria (Permanent Resident in U.S.A.)	3101 Paddington Street Greensboro, NC 27406	Human-Machine Systems, Artificial Intelligence, & Reliability
Dr. Eui Park	U.S.A.	1623 Helmwood Dr. Greensboro, NC 27411	Manufacturing Systems, Robotics, & Quality Control
Dr. Joseph deeb	U.S.A.	1715 Swannanoa Dr. Greensboro, NC 27410	Human Factor/Ergonomics, & Manual Material Handling
Dr. Jung Kim	U.S.A.	2711 New garden Rd. Greensboro, NC 27408	Signal Processing, & Expert Systems

NOTE: * They will be in the IE Graduate Program from the Spring semester of 1993.

AEROSPACE ENGINEERING EDUCATIONAL PROGRAM

ANNUAL REPORT

Prepared for

NASA CENTER OF RESEARCH EXCELLENCE
SCHOOL OF ENGINEERING
NORTH CAROLINA A&T STATE UNIVERSITY

by

William Craft
David Klett
Steven Lai

Mechanical Engineering Department
School of Engineering
North Carolina A&T State University
Greensboro, NC 27411

December, 1992

A. AREA SUMMARY

The principle goal of the educational component of NASA CORE is the creation of Aerospace Engineering options in the Mechanical Engineering program at both the undergraduate and graduate levels. To accomplish this goal, a concerted effort during the past year has resulted in detailed plans for the initiation of Aerospace options in both the BSME and MSME programs in the fall of 1993.

All proposed new courses and the BSME Aerospace option curriculum must undergo a lengthy approval process involving two curriculum oversight committees (School of Engineering and University level) and three levels of general faculty approval. Assuming approval is obtained from all levels, the options will officially take effect in Fall '93. In anticipation of this, certain courses in the proposed curriculum are being offered during the current academic year under special topics headings so that current junior level students may graduate in May '94 under the BSME Aerospace option. The proposed undergraduate aerospace option curriculum (along with the regular mechanical engineering curriculum for reference) is attached at the end of this report, and course outlines for the new courses are included in the appendix.

One new permanent faculty member with an aerospace background was added in Fall 1992 to assist with teaching aerospace courses and developing laboratories.
Three existing faculty members, Drs. Craft, Klett and Lai, have participated in developing the aerospace option plans and two undergraduate students have been supported this year under the auspices of the educational component.

B. PROGRAM DEVELOPMENT

Student Tracking Method

The aerospace options in the BSME and MSME programs are currently under development and must pass a lengthy university approval process during the Spring '93 semester, as explained below, before being officially offered beginning in Fall '93.
Tracking of students in the aerospace options will begin at that time.

Strategies to Recruit Underrepresented Minority Students

The majority of our undergraduate students are African Americans. We are recruiting our current undergraduate mechanical engineering students to enter the aerospace option through announcements about the program in classes and on bulletin boards. Certain aerospace courses have been offered under special topic headings for the current Fall '92 semester, and about six undergraduate students have enrolled in these courses. When the program option receives university approval and can be officially advertised, a brochure will be printed descrawing the aerospace engineering option and it will be included in the Mechanical Engineering Undergraduate Handbook and the

University Bulletin. The brochure, in particular, can be used as a recruiting tool at university days, etc.

Equipment Purchased to Develop Teaching Laboratories

The following equipment, software, video tapes and reference texts have been purchased from the first year budget in support of the development of teaching laboratories.

Qty	Description	Cost
3	486 PC for Controls Lab	$ 9,823
4	486 PC for Aero Des Lab	$12,910
1	486 PC for Wind Tunnel Lab	$ 4,030
2	486 PC for Center Support	$ 8,060
5	Laser Printers	$ 8,252
2	Workstations for Aero Design Lab	$29,910
1	Smoke gen for wind tunnel	$ 2,600
2	Adv Aircraft Analysis Software	$ 3,045
2	AIAA aerospace Video courses	$ 4,771
3	Physics of Spaceflight Video tapes	$ 150
6	AIAA aerospace reference books	$ 374
	Total	$83,925

C. CURRICULUM ACTIVITIES

The development of educational programs to support the research activities proposed under the NASA Center of Research Excellence is considered to be vital to the overall success of the center. Work on the educational component began in earnest in May '92 when funds for release time first became available to the group. This report covers the period of activity through November 30, 1992.

During the summer months, undergraduate and graduate curriculums for aerospace options were developed as part of the proposal requirement. During August and September, the proposed curriculum structure was reviewed both internally and by Mr. Larry Taylor of NASA-LRC. As a result, the undergraduate curriculum was updated slightly to include additional emphasis in the controls area. During October and November, the undergraduate aerospace option was further modified to incorporate proposed changes to the existing mechanical engineering curriculum which itself is currently undergoing significant revision. Also during the current Fall '92 semester we have begun a phase-in of the undergraduate aerospace option.

The undergraduate and graduate curricula and the phase-in plan are described in the following sections.

Undergraduate Aerospace Option

The development of the undergraduate aerospace option presented particular difficulties since, at least in the near term, it must exist as an option within the mechanical engineering program and must meet all of the accreditation criteria for mechanical engineering programs as specified by the Accreditation Board for Engineering and Technology (ABET). We have attempted to construct an aerospace program option that: 1) meshes well with the existing mechanical engineering curriculum; 2) meets the required ABET criteria and; 3) provides sufficient background in aerospace engineering to allow a graduate to work in the aerospace field while retaining sufficient fundamental mechanical engineering training to permit a graduate to function well as a mechanical engineer if he/she, for some reason, does not enter the aerospace field.

Toward this end, the attached aerospace option curriculum has been developed. Where possible, existing courses have been replaced by similar courses with an emphasis on aerospace applications. These course substitutions include the following:

Existing ME Curriculum Course	Aerospace Option Substitution
ELEN 442 Survey of Elec Engr	ELEN 410 Linear Sys and Contrl
MEEN 416 Fluid Mechanics	MEEN 415 Aerodynamics
MEEN 442 Appl'd Thermodynamics	MEEN 576 Propulsion
MEEN 500 Mech Engr Lab III	MEEN 577 Aero & Propulsion Lab
MEEN 564 Machine Design II	MEEN 422 Aero Veh Structures I
MEEN 566 Design of Thermal Sys	MEEN 578 Flight Veh Performance
MEEN 574 Mechanical Sys Design	MEEN 580 Aero Veh Design

In addition, the two technical electives in the program will be restricted to the following group of courses.

Aerospace Technical Electives

MEEN 651 Aero Vehicle Structures II
MEEN 652 Aero Vehicle Stability and Control
MEEN 653 Aero Vehicle Flight Dynamics
MEEN 654 Advanced Propulsion
MEEN 655 Computational Fluid Dynamics
MEEN 656 Boundary Layer Theory
ELEN 668 Automatic Control Theory

Course outlines in the standard ABET format for all of the above courses are included in an appendix at the end of this report.

Under this plan, students will take a total of nine courses that are unique to the aerospace option. These courses will provide a reasonably broad background in aerospace engineering, but are similar enough in basic content to the courses they replace so as not to impair the student's fundamental mechanical engineering training. Aerospace related courses begin in the second semester of the junior year while the first five semesters remain unchanged from the existing ME program. A copy of the recently revised mechanical engineering curriculum (effective fall '93) is also included at the end of this report for comparison.

One of the most critical ABET accreditation criteria is the requirement that all engineering programs must include a minimum of 16 credit hours of engineering design content including a capstone design course in the senior year. The proposed aerospace option curriculum outline presented below indicates design content credit hours in parentheses beside the course credit hour column. With some difficulty, 16 credits of design content were maintained in the program.

Phase-In Plan

It is important to note that the undergraduate aerospace option is still in the proposal stage. Both the curriculum outline and the new courses proposed for the option must go through a lengthy approval process involving the Department of Mechanical Engineering, the School of Engineering, the University Faculty Senate and the University Faculty Forum. This process, which normally requires an entire academic year, must be completed before information on the option can be included in the University Bulletin. Nevertheless, a phase-in plan has been implemented beginning with the current Fall '92 semester. This is possible since one of the courses currently exists (ELEN 410 Linear Systems and Control) and others can be offered on a temporary basis under a Special Topics course number. The phase-in time table is shown below.

Fall '92	Spring '93
ELEN 410 Linear Sys & Control	MEEN 544 Spec Top: Aerodynamics
MEEN 660 Spec Top: Comp Fluid Dyn	MEEN 544 Spec Top: Aero Veh Struc I
	ELEN 410 Linear Systems & Contrl
Fall '93	**Spring '94**
MEEN 576 Propulsion	MEEN 415 Aerodynamics
MEEN 578 Flight Veh Performance	MEEN 422 Aero Veh Structures I
MEEN 652 Aero Veh Stabil & Contrl	MEEN 577 Aero & Propulsion Lab
ELEN 668 Automatic Contrl Theory	MEEN 580 Aero Vehicle Design
	MEEN 651 Aero Veh Structures II
	MEEN 653 Aero Veh Flight Dyn

Under this plan, current first semester juniors can begin the option in Fall '92 and graduate under the option in May '94, assuming that the plan gains eventual approval from all requisite university committees.

There are currently two ME students enrolled in ELEN 410 -Linear Systems and Controls and 9 students enrolled in MEEN 660 Spec Topics: Computational Fluid Dynamics, including four undergraduates. The number of students who enter the option should increase significantly next year when it can be officially advertised and promoted through the University Bulletin and the Mechanical Engineering Undergraduate Handbook and new brochures to be created for this purpose.

Graduate Aerospace Option

Creation of an aerospace option under the Master of Science in Mechanical Engineering program is significantly less complicated than the undergraduate option since ABET accreditation issues are not involved.

The Mechanical Engineering Department currently offers a Master of Science degree program with specializations in the areas of 1) Energy and Thermo/Fluids, 2) Mechanics and Materials and 3) Design and Manufacturing. With the advent of the NASA Center of Research Excellence, we plan to add Aerospace as a fourth specialization. Five MEEN 600 level aerospace courses are being added to the curriculum offerings along with ELEN 668 - Automatic Control Theory. These courses will be open to both undergraduate and graduate students. Undergraduates can take them as technical electives (two required) and graduate students can take them as part of the eight courses required under the MSME thesis option. Graduate students will round out their programs with existing 600 and 700 level courses as listed later. The five new 600 level courses are the following:

MEEN 651 Aero Vehicle Structures II
MEEN 652 Aero Vehicle Stability and Control
MEEN 653 Aero Vehicle Flight Dynamics
MEEN 654 Advanced Propulsion
MEEN 655 Computational Fluid Dynamics

Existing graduate courses that complement the aerospace option are:

ELEN 668 Automatic Control Theory
MEEN 604 Intermediate Dynamics
MEEN 612 Modern Composite Materials
MEEN 616 Design by Finite Element Methods
MEEN 618 Numerical Analysis for Engineers
MEEN 626 Advanced Fluid Dynamics
MEEN 650 Mechanical Properties and Structure of Solids
MEEN 656 Boundary Layer Theory (currently MEEN 710)

MEEN 702 Continuum Mechanics
MEEN 704 Advanced Dynamics
MEEN 731 Conduction Heat Transfer
MEEN 732 Convection Heat Transfer
MEEN 733 Radiation Heat Transfer
MEEN 720 Advanced Classical Thermodynamics
MEEN 724 Irreversible Thermodynamics
MEEN 777 Thesis
MEEN 788 Research
MATH 651 Methods in Applied Mathematics I
MATH 652 Methods in Applied Mathematics II

The thesis option MSME degree requires 24 credit hours of course work (8 courses) and 6 credit hours of thesis. Students are required to include 6 hours of mathematics in their program which can be chosen from MEEN 618 and MATH 651 and 652. Two typical MS programs with an aerospace specialization might contain the following courses.

Typical Program of Study I	Typical Program of Study II
MATH 651 Meth in Appl Math I	MATH 651 Meth in Appl Math I
MEEN 618 Num Anal for Engrs	MATH 652 Meth in Appl Math II
MEEN 626 Advanced Fluid Dynamics	MEEN 604 Intermediate Dynamics
MEEN 656 Boundary Layer Theory	MEEN 612 Modern Composite Mater
MEEN 655 Computational Fluid Dyn	MEEN 652 Aero Veh Stabil & Contr
MEEN 654 Advanced Propulsion	MEEN 653 Aero Veh Flight Dyn
MEEN 732 Convec Heat Transfer	ELEN 668 Automatic Control Theory
MEEN 733 Radiat Heat Transfer	MEEN 704 Advanced Dynamics
MEEN 777 Thesis	MEEN 777 Thesis

The undergraduate aerospace option will provide a firm foundation for continuing study with aerospace specialization at the MS level. The graduate students in this option should be actively involved with the ongoing research of the center.

D. FACULTY AND STUDENT PARTICIPATION

Student Involvement

Two undergraduate students are currently supported under the educational component of NASA-CORE. These are Miss Shiryl White and Miss Kimberly Musgrave, both mechanical engineering juniors. Both students work 10 hours per week under the supervision of Dr. Craft. Miss White's efforts are split about equally between clerical and research activities. Her research work involves investigating possible finite element models

for orthotropic braids used in composite materials for aircraft and spacecraft applications. The purpose of the research is to develop better modeling techniques to determine global material properties.

Miss Musgrave is also doing both clerical and research work. Her research involves running a finite element computer model of a composite sandwich shell for varying cases of skin and core thickness to find a minimum weight composite structure with adequate strength characteristics for possible application as an aerobrake.

Two additional undergraduate students are currently supported by the Center to help develop laboratory tools. These two students are Miss Monica Smith and Mr. Jerry Hoggard. Miss Monica Smith is working with Dr. Lai to develop computer programs for NASP simulation. This includes the development of NASP plane model and the computation of flight dynamics. Mr. Hoggard's effort is to compute the optimal trajectory using the NASP plane model.

Organization and Staffing

Dr. William Craft, Chairman of Mechanical Engineering, heads the educational component of the Center. Other faculty involved with the educational component include Dr. David Klett, Undergraduate Program coordinator, and Dr. Hsin-Yi Lai, Center Director.

Mr. Kenneth Jones was hired as a new faculty member in support of the Educational Component. He has many years experience working in the aerospace area and is currently completing the requirements for the PhD in aerospace engineering from North Carolina State University. His research work is in CFD and experimental hypersonic flow and his expertise will be an important complement to the CFD efforts currently underway as part of the center and also in helping to develop new laboratories in Propulsion and Aerodynamics. Dr. Jones will teach the Aerodynamics course during Spring '92.

Other faculty involved in teaching aerospace courses this academic year include:

1. Dr. Suresh Chandra, Prof. of Mech. Engr. - Teaching Computational Fluid Dynamics, Fall '92
2. Dr. Abdollah Homaifar, Assoc. Prof. of Elec. Engr. - Teaching Linear Systems and Controls, Fall '92 and Spring '93
3. Dr. Shen, Adjunct Asst. Prof. of Mech. Engr. - Teaching Aero Vehicle Structures I, Spring '93

E. FINANCIAL REPORT AND DETAILED COURSE OUTLINES

Financial Report of the Educational Component

1110	Faculty Release Time:		
	D.E. Klett	July 23, 1992 - August 6, 1992	$4,653
		August 14, 1992 - December 31, 1992	$3,489
1450	Undergraduate Assistants:		
	Shiryl White	July 1, 1992 - August 14, 1992	$ 315
		August 15, 1992 - December 31, 1992	$ 630
	Kimberly Musgrave	September 3, 1992 - December 31, 1992	$ 525
1800	Fringes (July 23, 1992 - December 31, 1992)		$1,985
2302	Laboratory Supplies		$ 0
2601	Office Supplies		$ 300
2902	Other Supplies		$ 0
3100	Travel Expenses		
	(Trip to NASA Headquarters March, 1992 - W. J. Craft		$ 655
	(Trip to Anaheim, CA November 8 - 12, 1992 - D. E. Klett		$1,239
4801	Indirect Cost		$5,287
5302	Scientific Equipment		
	3 pc's		$9,320
	1 printer		$ 890
	3 tape backup units		$1,440
	1 Wind tunnel instrumentation unit		$87,400
	(drag, lift, velocity, 3 planes of moment measurements)		
Total Budget for 1992			$120,828

Detailed Course Outline

Course outlines in the standard ABET format for all of the aerospace courses are included in the next few pages of this report.

AEROSPACE OPTION IN MECHANICAL ENGINEERING (Effective Fall'93)

FALL SEMESTER Course	cr	SPRING SEMESTER Course	cr
		FRESHMAN YEAR	
ENGL 100 Ideas & Expres I	3	ENGL 101 Ideas & Expres II	3
HIST Elec	3	MATH 132 Calculus II	4
MATH 131 Calculus I	4	GEEN 102 Comp Prog for Engrs	2
GEEN 100 Intro. to Engineering	2	CHEM 101 Gen. Chem. I	3
GEEN 101 Intro. Engr Graphics	2	CHEM 111 Gen. Chem. I Lab	1
SOC SCI Elec	3	HISTORY Elective	3
		HEALTH/PE Elective	1
Total	17	Total	17
		SOPHOMORE YEAR	
PHYS 241 Gen. Phys. I	4	MEEN 210 Num Methods in ME	2
PHYS 251 Gen. Phys. I Lab	1	PHYS 242 Gen. Physics II	4
MATH 231 Calculus III	4	PHYS 252 Gen. Physics II Lab	1
ECON 300 Prin of Economics	3	MATH 331 Appl. Engr. Math I	3
MEEN 226 Manuf. Processes	2	MEEN 335 Statics	3
HUMANITIES Elective	1	MEEN 360 Materials Science	2
Total	17	MEEN 300 Mech Engr Lab I	2
		Total	17
		JUNIOR YEAR	
MATH 332 Appl. Engr. Math II	3	*ELEN 410 Linear Sys & Contrl	3
ELEN 200 Elec. Circuit Anal.	3	MEEN 440 Mechanism Des & Anal	3 (1.5)
ELEN 206 Circuits Lab	1	*MEEN 415 Aerodynamics	3 (0.5)
MEEN 336 Strength of Matrl.	3	*MEEN 422 Aero Veh Structures I	3 (1)
MEEN 337 Dynamics	3	MEEN 474 Engineering Design	3 (2)
MEEN 441 Thermodynamics I	3	MEEN 400 Mech Engr Lab II	1
HEALTH/PE ELECTIVE	1	Total	16
Total	17		
		SENIOR YEAR	
MEEN 560 Mod. Engr. Materials	3 (1)	MEEN 562 Heat Transfer	3 (1)
MEEN 565 Machine Design	3 (2)	MEEN 581 Mechanical Vibration	3 (1)
* MEEN 576 Propulsion	3 (1)	* MEEN 580 Aero Veh. Design	3 (3)
* MEEN 577 Aero & Propulsion Lab	1	* AEROSPACE Elective	3 (1)
* MEEN 578 Flight Veh. Perform.	3 (1)	HUMANITIES Elective	3
* AEROSPACE Elective	3	Total	15
Total	16	(Numbers in Parentheses Indicate Design Credits)	

TECHNICAL ELECTIVES

* MEEN 651 Aero. Veh. Structures II	3 (1)
* MEEN 652 Aero. Veh. Stab. & Cont.	3 (1)
* MEEN 653 Aero. Veh. Flight Dyn.	3
* MEEN 654 Advanced Propulsion	3 (1)
* MEEN 655 Computation Fluid Dyn.	3
MEEN 656 Boundary Layer Theory	3
ELEN 668 Automatic Control Theory	3

CONTENT

Engineering Design:	16
Engineering Science:	52
Math. and Basic Sci:	35
Humanities & Soc Sci:	18
Other:	11
Total Credit Hours:	132

ELEN 410 Linear Systems and Controls

Catalog Data: This course is designed to provide the student with techniques used in analyzing control systems. Introduction to control theory. This includes: control system modeling and representation, features of feedback control system, state space representation, time domain analysis, root locus, and design compensation.

Textbook: Automatic Control Systems by B. Kuo, Prentice-Hall, 6th Edition.

References: Analysis and Synthesis of Linear Control Systems, C.T. Chen, and Feedback Control of Dynamic Systems, Gene F. Franklin, J. David Powell, and Abbas Emami-Naeini.

Coordinator: Abdollah Homaifar

Prerequisite: MATH 331 and ELEN 200.

Topics:

1. Laplace Transforms
2. Mathematical modeling of physical systems
3. Block diagram and signal flow graphs
4. State space characterization of systems
5. Time domain analysis
6. Stability of systems
7. Root locus techniques
8. Frequency domain analysis (Bode)
9. Control system design and performance prediction.
10. Applications: Airplane attitude control, satellite control, and antenna tracking.

Computer usage: The course uses the CC computer package to solve the state space problem, draw the root locus as well as Bode diagrams, and design the compensator.

ABET category content as estimated by faculty member who prepared this course description:

Engineering Science: 3 credits or 100%

MEEN 415 Aerodynamics

Catalog Data: The course begins with the fundamentals of fluid statics and dynamics followed by an introduction to inviscid flow theory with applications to incompressible flows over airfoils, wings and flight vehicle configurations.

Textbook: J.D. Anderson, Fundamentals of Aerodynamics, McGraw-Hill, 1984.

Coordinator: S. Chandra

Goals: The objectives are to provide fundamental knowledge of the equations of fluid flow and of incompressible flow aerodynamics. This knowledge should include the application of inviscid flow theory to obtain forces and moments on elementary lifting surfaces (airfoils and finite wings).

Prerequisites: MATH 231, MEEN 337

Prerequisite by Topic:

1. Differential Equations
2. Dynamics

Topics:

1. Fluid Properties
2. Concepts of Fluid Statics
3. Concepts of Fluid Dynamics
4. Flow Similarity
5. Introduction to Viscous Flow Concepts
6. Introduction to Inviscid Flow Theory
7. Thin Airfoil Theory
6. Circulation

ABET category content as estimated by faculty member who prepared this course description:

Engineering Science: 3 credit or 100%

MEEN 422 Aero Vehicle Structures

Catalog Data: This course covers the determination of typical flight and landing loads and methods of analysis and design of aircraft structures to be able to withstand expected loads.

Textbook: Introduction to Aerospace Structural Analysis, Allen/Cole, 1985

Coordinator: A. Kelkar

Goals: The purpose of this course is to develop the student's ability to determine typical flight loads, to select acceptable analysis methods, and to apply these methods to the analysis of flight structures.

Prerequisites: MEEN 336, MEEN 337, MATH 331

Prerequisites by Topic:

Dynamics
Strength of Materials
Vector Analysis

Topics:

1. Flight and landing loads
2. Review of solid mechanics
3. Advanced beam theory
4. Design considerations
5. Design Project

ABET category content as estimated by faculty member who prepared this course description:

Engineering Science:	1.5 credits or 50%
Engineering Design:	1.5 credits or 50%

MEEN 576 Propulsion

Catalog Data: This introductory course to aero propulsion systems includes coverage of one-dimensional internal flow of compressible fluids, normal shock, flow with friction, and simple heat addition. The basic concepts are applied to air-breathing aircraft ropulsion systems.

Textbook: High and Peterson, Mechanics and Thermodynamics, Addison Wesley, 1965

Coordinator: D. E. Klett

Goals: The objective of this course is to provide the student with the concepts and tools necessary for the analysis and design of modern air-breathing propulsion systems. Analysis of the various system components as well as the overall Propulsion system are stressed.

Prerequisites: MEEN 415 and MEEN 441

Prerequisites by Topic:

Differential Equations
Thermodynamics
Aerodynamics

Topics:

1. Gas Mixtures
2. Isentropic Flow
3. Flow with Heat Addition
4. Flow with Friction
5. Gas Generator Systems
6. Turbo Jets
7. Turbo Fans
8. Ram Jets

ABET category content as estimated by faculty member who prepared this course description:

Engineering Science: 2 credit or 66 2/3%
Engineering Design: 1 credit or 33 1/3%

MEEN 577 Aerodynamics and Propulsion Laboratory

Catalog Data: This is a laboratory course to provide experimental verification of concepts learned in MEEN 415 and MEEN 576. Experiments are performed that reinforce the concepts from the lecture courses including wind tunnel experiments and performance of a gas turbine engine.

Textbook: Class handouts

Coordinator: K. Jones

Goals: To provide hands-on experience associated with the concepts and laboratory tools of aircraft aerodynamics and propulsion systems. The characteristics of one-dimensional flow with friction and/or heat addition are determined. The effects of operating conditions on the performance of a simple gas turbine are studied.

Corequisite: MEEN 576

Prerequisites by Topic: Aerodynamics
Thermodynamics

Topics:

1. Temperature, pressure, velocity and mass flow measurements
2. Introduction to wind tunnel and data acquisition system
3. Measurement of turbulence factor
4. Measurement of pressure distribution over a circular cylinder
5. Measurement of pressure distribution over an airfoil
6. Measurement of lift, drag, and pitching moment on a wing
7. Unchoked isentropic flow
8. Choked isentropic flow
9. Supersonic flow and shock waves
10. One-dimensional flow with friction
11. One-dimensional flow with heat
12. Performance of a single shaft gas turbine

ABET category content as estimated by faculty member who prepared this course description:

Engineering Science: 1 credit or 100%

MEEN 578 Flight Vehicle Performance

Catalog Data: This course provides an introduction to the performance analysis of aircraft. Aircraft performance in gliding, climbing, level, and turning flight are analyzed as well as calculation of vehicle take-off and landing distance, range and endurance.

Textbook: F.J. Hale, Introduction to Aircraft Performance, Selection, and Design, John Wiley & Sons, 1984

Coordinator: H. Y. Lai

Goals: The objective of this course is to familiarize the student with the basic concepts of aircraft performance.

Prerequisites: MATH 231, MEEN 337

Prerequisite by Topic:

Calculus
Differential Equations
Dynamics

Topics:

1. Aerodynamic Forces
2. Propulsion Systems
3. Propeller Theory
4. Gliding Performance
5. Climbing Perfomance
6. Level Flight
7. Turning Flight
8. Take Off and Landing

ABET category content as estimated by faculty member who prepared this course description:

Engineering Science: 2 credits or 66 2/3%
Engineering Design: 1 credit or 33 1/3%

MEEN 580 Aerospace Vehicle Design

Catalog Data: This is the capstone design course for the Aerospace option. This course requires the synthesis of knowledge acquired in previous courses and the application of this knowledge to the design of a practical aerospace vehicle system.

Textbook: D. Stinton, The Design of the Airplane, Van Nostrand, 1983.

Coordinator: H. Y. Lai

Goals: The objective of this course is to provide aerospace option students with the opportunity to apply previously acquired knowledge, with the aid of modern software, to the design of an aerospace vehicle system.

Prerequisites: MEEN 415, MEEN 422, MEEN 474, MEEN 576, MEEN 578, ELEN 410

Prerequisite by Topic:

Aerodynamics
Flight Vehicle Performance
Controls
Engineering Design
Flight Vehicle Structural Analysis
Propulsion

Topics:

1. Weight and Balance
2. Power Plant Selection and Performance
3. Determination of Aerodynamic Loads
4. Vehicle Performance
5. Analysis of Static and Dynamic Stability and Control
6. System Synthesis
7. Construction and Components
8. Cost Analysis
9. Performance Testing

ABET category content as estimated by faculty member who prepared this course description:

Engineering Design 4 credits or 100%

MEEN 651 Aero Vehicle Structures II

Catalog Data: This course covers deflection of structures, indeterminate structures, fatigue analysis, and minimum weight design. Finite element methods and software are utilized.

Textbook: Introduction to Aerospace Structural Analysis, Allen/Cole, 1985

Coordinator: A. Kelkar

Goals: The purpose of this course is to develop the student's ability to perform structural analysis using finite element methods and software packages and to apply these methods to the design and analysis of flight structures.

Prerequisites: MEEN 422

Prerequisites by Topic:

Strength of Materials
Introductory Structural Analysis

Topics:

1. Work and energy principles
2. Deformation and force analysis
3. Fatigue analysis
4. Finite element methods
5. Finite element software
6. Design for minimum weight
7. Design project

ABET category content as estimated by faculty member who prepared this course description:

Engineering Science: 2 credits or 66 2/3%
Engineering Design: 1 credit or 33 1/3%

MEEN 652 Aero Vehicle Stability and Control

Catalog Data: This course covers longitudal, directional and lateral static stability and control of aerospace vehicles. It also covers linearized dynamic analysis of the motion of a six degree-of-freedom flight vehicle in response to control inputs and disturbance through use of the transfer function concept, plus control of static and dynamic behavior by vehicle design (stability derivatives) and/or flight control systems.

Textbook: None (Instructor's Notes)

Coordinator: A. Homaifar

Goals: The objective of this course is to extend the student's basic concept regarding vehicle stability and control to the more difficult problems in this area, and to introduce the mathematical tools and techniques necessary for the analysis of vehicle stability and control.

Prerequisites: ELEN 410

Corequisites: MEEN 415, MEEN 422

Prerequisite by Topic:

Aerodynamics
Flight Dynamics
Control Theory

Topics:

1. Static Stability
2. Equations of motion for a rigid aircraft
3. Linearization of equations of motion
4. Linear system analysis
5. Longitudal dynamics
6. Lateral dynamics

ABET category content as estimated by faculty member who prepared this course description:

Engineering Science: 2 credits or 66 2/3%
Engineering Design: 1 credit or 33 1/3%

MEEN 653 Aero Vehicle Flight Dynamics

Catalog Data: This course covers the basic dynamics of aerospace flight vehicles including orbital mechanics, interplanetary and ballistic trajectories, powered flight maneuvers and spacecraft stabilization.

Textbook: None (Instructor's notes and handouts)

Coordinator: H. Y. Lai

Goals: The objective of this course is to familiarize the student with the fundamental dynamic problems associated with space flight.

Prerequisites: MATH 332, MEEN 337, MEEN 422

Prerequisite by Topic:

Partial Differential Equations
Dynamics
Flight Vehicle Performance

Topics:

1. Two-body Orbital Mechanics
2. Interplanetary Trajectories
3. Ballistic Trajectories
4. Optimal Trajectory Shaping
5. Powered Flight Maneuvers
6. Atmospheric Entry
7. Spacecraft Stabilization

ABET category content as estimated by faculty member who prepared this course description:

Engineering Science: 3 credits or 100%

MEEN 654 Advanced Propulsion

Catalog Data: This technical elective is a second course in propulsion. It covers the analysis and design of individual components and complete air-breathing propulsion systems including turbo fans, turbo jets, ram jets and chemical rockets.

Textbook: High and Peterson, Mechanics and Thermodynamics, Addison Wesley, 1965

Coordinator: H. Y. Lai

Goals: To provide the student with the concepts and tools necessary for the analysis and design of modern air-breathing systems. Analysis of the various system components as well as the overall propulsion system will be stressed.

Prerequisites: MEEN 576

Prerequisite by Topic:

Aerodynamics
Thermodynamics
Basic Propulsion

Topics:

1. Subsonic and supersonic burners
2. Combustion and afterburners
3. Compressors
4. Turbines
5. Propellors
6. Engine design and component matching
7. Chemical rockets

ABET category content as estimated by faculty member who prepared this course description:

Engineering Science: 2 credit or 66 2/3%
Engineering Design: 1 credit or 33 1/3%

MEEN 655 Computational Fluid Dynamics

Catalog Data: This course provides an introduction to numerical methods for solving the exact equations of fluid dynamics. Finite difference methods are emphasized as applied to viscous and inviscid flows over bodies. Students are introduced to a modern CFD computer code.

Textbook: Computational Fluid Mechanics and Heat Transfer, Anderson, Tannehill and Pletcher, Hemishphere

Coordinator: S. Chandra

Goals: The objective of this course is to familiarize the student with modern numerical methods for solving the governing equations of fluid flow.

Prerequisites: MATH 332, MEEN 415 or 416

Prerequisite by Topic:

Partial Differential Equations
Fluid Mechanics or Aerodynamics

Topics:

1. Governing Equations
2. Finite difference representation
3. Stability Analysis
4. Boundary Conditions
5. Applications

ABET category content as estimated by faculty member who prepared this course description:

Engineering Science: 3 credits or 100%

MEEN 656 Boundary Layer Theory

Catalog Data: This course covers the fundamentals of internal and external boundary layer flows. Exact solutions of the Navier-Stokes equations are developed for a few specialized cases. The approximate boundary layer methods are developed and applied to a variety of problems. Turbulent boundary layer flows are introduced.

Textbook: Boundary Layers, A.D. Young, AIAA

Coordinator: K. Jones

Goals: The objective of this course is to familiarize the student with the fundamentals of viscous laminar and turbulent boundary layer flows.

Prerequisites: MATH 332, MEEN 415 or 416

Prerequisite by Topic:
Partial Differential Equations
Fluid Mechanics or Aerodynamics

Topics:

1. Governing equations and theoretical foundations
2. Some basic solutions of steady laminar 2-D flows
3. Approximate methods of solution of steady 2-D laminar flows
4. Transition
5. Structure of attached turbulent boundary layers
6. Integral methods of drag prediction
7. Turbulence modeling

ABET category content as estimated by faculty member who prepared this course description:

Engineering Science: 3 credits or 100%

ELEN 668 Automatic Control Theory

Catalog Data: The automatic control problem icludes the development of mathematical descriptions of a system, the specification of schemes to control the system, the prediction of system performance by analysis or simulation, and the possible iteration or repeating of these sequential steps until satisfactory actual system performance is predicted.

Textbook: Linear System Theory and Design, Chi-T Chen, Holt, Rinehart and Winston

Coordinator: Abdollah Homaifar

Prerequisite: ELEN-410 or equivalent.

Topics:

Study of state variable approach to control system analysis and design:

1. Control System Realization
2. Controllability
3. Observability
4. State Estimation
5. Stability
6. Controller Design
7. State Function approach to linear system synthesis.
8. Presentation of Linear Algebra tools required for above.

ABET category content as estimated by faculty member who prepared this course description:

Engineering Science: 3 credits or 100%

AD-Vol. 31

SPACE EXPLORATION SCIENCE AND TECHNOLOGIES RESEARCH

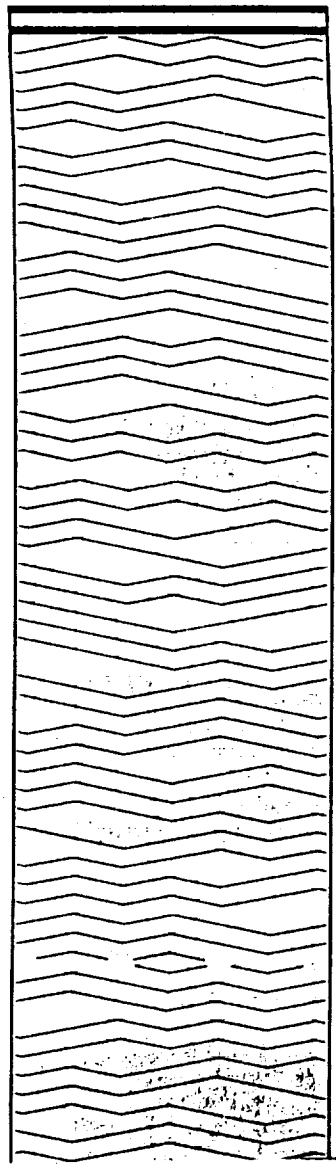

ISBN 0-7918-1106-9

9 780791 811061

BOOK NO. G00750

edited by
W. J. CRAFT
D. M. ACHGILL

AD-Vol. 31, Space Exploration Science and Technologies Research
ASME 1992

DYNAMIC CHARACTERIZATION, MONITORING AND CONTROL OF ROTATING FLEXIBLE BEAM-MASS STRUCTURES VIA PIEZO-EMBEDDED TECHNIQUES

Steven H.-Y. Lai
Controls and Guidance Group
NASA CORE for Aerospace Research
North Carolina A&T State University
Greensboro, North Carolina

ABSTRACT

A variational principle and a finite element discretization technique were used to derive the dynamic equations for a high speed rotating flexible beam-mass system embedded with piezo-electric materials. The dynamic equation thus obtained allows the development of finite element models which accommodate both of the original structural element and the piezoelectric element. The solutions of finite element models provide system dynamics needed to design a sensing system. The characterization of gyroscopic effect and damping capacity of smart rotating devices are addressed. Several simulation examples are presented to validate the analytical solution.

INTRODUCTION

Structural monitoring and control using smart sensing materials has become of importance in recent years due to the rapid development of large flexible structures and flexible mechanical systems. These materials and structures have their own sensing, actuating, tuning, controlling and computational abilities (Gandhi and Thomas, 1989). Typically, smart materials and structures are distributed-parameter systems operating under a variety of service conditions and having a theoretically infinite number of vibration modes. Current design practice is to model the system with a finite number of modes and to design a sensing system using lumped parameter approach. "Truncating" the model may lead to performance trade-off when designing a control system for distributed parameter systems. Lumped parameter approach is generally acceptable for sensing applications due to its nature of simplicity and ease of implementation. Although significant progress has been made in the recent past in the development of smart materials and structures featuring piezo-electric materials (Bailey and Hubbard, 1985; Plump et.al, 1987, Crawley, 19887), shape memory alloys (Miwa, 1985; Yaeger, 1984; Rogers and Robertshaw, 1988), electro-rheological fluids (Gandhi et al, 1989; Choi et al, 1989; Gandhi et al, 1989), and optical fibers (Morikawa, 1985; Rogowski, 1988), very few work have been done to characterize the dynamic behaviors of these devices, especially when it is used for high-speed applications.

Emphasis is placed on the accurate modeling and characterization of structural parameters of sensing devices for flexible structures. The analysis of a beam attached to a rotating base is a subject of interest to many researchers because numerous structural configurations such as spinning satellites (Laurenson, 1976; Kane et al., 1987) and flexible robots (Cannon and Schmitz, 1984; Mitchell and Bruch, 1988; Yang and Donath, 1988) fall into this category. The analysis of these rotating dynamic structures with payloads is quite different from those of stationary structures due to the inertia of gyroscopic effect at high rotating speeds.

Piezoelectric materials are media which develop mechanical strain when subjected to an electrical field, or conversely, they develop an electrical field when subjected to mechanical deformation. Their inherent high power-to-weight ratio makes them ideal candidates for embedding piezoelectric materials in traditional structures for vibration sensing and control. Crawley and de Luis (1987) studied the effect of a beam with bonded piezoelectric sensors. Plump et al. (1987) used a piezoelectric film to enhance the damping ratio of a cantilever beam. Tzou applied a piezoelectric film as an active vibration in a flexible structure (1987) and an active vibration isolator and exciter (1989). This paper focuses on the development of analytical models for dynamic characterization of a high-speed rotating flexible beam-mass system with embedded sensing system. The design of such a sensing system featuring piezoelectric materials is addressed. Several simulation examples are presented to validate the analytical solutions.

DESIGN AND ANALYSIS

Basic Assumptions and Coordinate Systems

To derive a simple yet effective sensing model for the physical system of interest, several assumptions are imposed here, namely:

(1) Large Overall Rigid-Body Displacements with Small Elastic Deformations: This assumption is valid for a mechanical system rotating at speeds less than one thousand revolutions per minute with low payload.

(2) Negligible Gravity Effect: For high-speed rotating space structure, the gravity effect can be ignored.

(3) Negligible Geometric Stiffening Effect: When rotating in plane, the magnitude of the axial displacement is much smaller than that of the transverse displacement. The effect of geometric stiffening is negligible.

(4) Plane Stress Condition: Since the beam is thin, the stress variation through the thickness is negligible.

(5) Average Material Properties: The average material properties of smart beams is used. Since the piezoelectric film is relatively thin, the isotropic aluminum beam plays a dominant role in contributing to the overall beam deflection. For structural monitoring, this assumption is valid.

$$\rho_{eq} = \frac{\rho_1 A_1 + \rho_2 A_2}{A}$$
$$E_{eq} = \frac{E_1 I_1 + E_2 I_2}{I} \qquad (1)$$

where A_1 is the cross sectional area of AL layer, A_2 is the cross sectional area of PVF_2 layer, I_1 is the moment of inertia of Aluminum layer about z axis, $I_1=b_1h_1^3/12$, and I_2 is the moment of inertia of PVF_2 layer about z axis, $I_2=b_2h_2^3/12$. The Euler-Bernoulli beam theory is used for dynamic formulation.

Two coordinate systems, one being the global X-Y and the other local x-y, are introduced to describe the dynamic system. The local coordinate system moves with the rigid body configuration of the link. Figures 1 and 2 show the schematic of the deflected

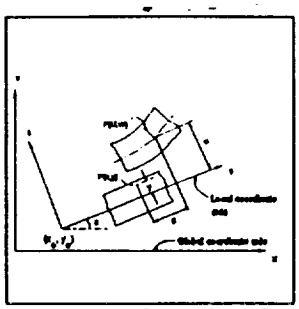

Figure 1: Schematic of a deflected beam element in local and global coordinate axes.

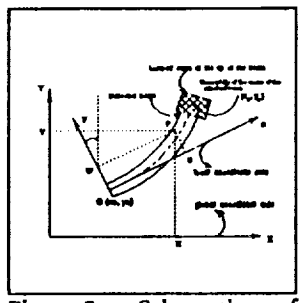

Figure 2: Schematic of rotating beam-mass system showing local and global coordinate axes

beam in both local and global coordinates. In classical small deflection beam theory, the displacements of an arbitrary point P(U, W) on a beam can be expressed in terms of homogenous coordinates as

$$\begin{Bmatrix} W \\ U \\ 1 \end{Bmatrix} = \begin{bmatrix} 1 & 0 & 0 & y \\ 0 & -y & 1 & x \\ 0 & 0 & 0 & 1 \end{bmatrix} \begin{Bmatrix} w \\ w' \\ u \\ 1 \end{Bmatrix} = B\{g\} \tag{2}$$

where x and y are the local coordinates of point P in the undeformed state. U and W are the local coordinates of point P after deformation. u, w, and w' are the axial, transverse and tangential displacements of point P, respectively. {g} is the displacement vector of point P in homogenous coordinates. The displacement vector, {g}, can be expressed in terms of nodal displacement vector {p} as $\{g\} = N\{p\}$, where $\{p\} = [\{q\}^T \mid 1]^T$, $\{q\} = [w_i\ w_i'\ u_i\ w_j\ w_j'\ u_j]^T$, and N, the shape function matrix, is given as

$$N = \begin{bmatrix} N_1 & N_2 & 0 & N_3 & N_4 & 0 & 0 \\ N_1' & N_2' & 0 & N_3' & N_4' & 0 & 0 \\ 0 & 0 & N_5 & 0 & 0 & N_6 & 0 \\ 0 & 0 & 0 & 0 & 0 & 0 & 1 \end{bmatrix} \tag{3}$$

where the shape functions, N_1, N_2, N_3, N_4, are the Hermite polynomials used for a beam element. N_5 and N_6 are the shape functions for a bar element in axial loading [24]. Note that $N_i' = dN_i/dx$. These shape functions are reported as

$$N_1 = 1-3(\frac{x}{L})^2+2(\frac{x}{L})^3; \quad N_2 = x(\frac{x}{L}-1)^2; \quad N_3 = (\frac{x}{L})^2(3-2\frac{x}{L})$$
$$N_4 = \frac{x^2}{L}(\frac{x}{L}-1); \quad N_5 = \frac{(L-x)}{L}; \quad N_6 = (\frac{x}{L}) \tag{4}$$

Substitute the expression of {g} into equation (2) to get

$$[W\ \ U\ \ 1]^T = B\,N\{p\} \tag{5}$$

and describe point P in terms of the global coordinates as

$$[X\ \ Y\ \ 1]^T = R\,B\,N\{p\} \tag{6}$$

where R is the transformation matrix that relates the local and global coordinate systems.

The expression for R is

$$R = \begin{bmatrix} -\sin\theta & \cos\theta & x_o \\ \cos\theta & \sin\theta & y_o \\ 0 & 0 & 1 \end{bmatrix} \tag{7}$$

where (x_0, y_0) are the coordinates of the origin of the local coordinate axis and θ is the angle between the local and global coordinate axes.

Elemental Equation of Motion

The variational principle (Washizu, 1968) for a dynamic system and the Lagrange equation are used to derive the element matrices. The first step in the finite element formulation is to discretize the domain of interest. The Lagrangian of a system is the sum of the Lagrangian of its constituting elements. In terms of the kinetic and potential energy, the Lagrange equation can be presented as

$$\begin{aligned} \sum_e Q_{(q)} &- \sum_e \left[\frac{d}{dt}\left(\frac{\partial T_e}{\partial \{\dot{q}\}}\right) - \frac{\partial T_e}{\partial \{q\}} + \frac{\partial U_e}{\partial \{q\}} \right] \\ &- \sum_e \left[\frac{d}{dt}\left(\frac{\partial T_b + T_m}{\partial \{\dot{q}\}}\right) - \frac{\partial T_b + T_m}{\partial \{q\}} + \frac{\partial U_e}{\partial \{q\}} \right] \\ &- \sum_e \left[(M_{2b} + M_{2m})\ddot{q} + (M_{1b} + M_{1m})\dot{q} + (M_{0b} + M_{0m})q + K_b q \right] \end{aligned} \tag{8}$$

where T_e and U_e are the kinetic and potential energy of a beam element. Note, that for the element connected to the payload block, $T_e = T_b + T_m$, T_b and T_m being the kinetic energies of the rotating beam and the tip mass attached at the end, respectively. U is the potential energy of the beam element, $\{q\}$ and $\{Q_q\}$ are the generalized coordinates and forces, respectively. The expressions of M_{2b}, M_{1b}, M_{0b}, K_b, M_{2m}, M_{1m}, M_{0m}, and Q are given below. The detailed derivation of these matrices are reported in Lai et al. (1992).

$$M_{2b} = \rho \begin{bmatrix} \frac{13}{35}AL + \frac{6I}{5L} & \frac{11}{210}AL^2 + \frac{I}{10} & 0 & \frac{9}{70}AL - \frac{6I}{5L} & -\frac{13}{420}AL^2 + \frac{I}{10} & 0 \\ & \frac{AL^3}{105} + \frac{2}{15}IL & 0 & \frac{13}{420}AL^2 - \frac{I}{10} & -\frac{AL^3}{140} - \frac{IL}{30} & 0 \\ & & \frac{AL}{3} & 0 & 0 & \frac{AL}{6} \\ & \text{symmetric} & & \frac{13}{35}AL + \frac{6I}{5L} & -\frac{11}{210}AL^2 - \frac{I}{10} & 0 \\ & & & & \frac{AL^3}{105} + \frac{2}{15}IL & 0 \\ & & & & & \frac{AL}{3} \end{bmatrix} \tag{9}$$

$$M_{1b} = \rho AL\dot{\theta} \begin{bmatrix} 0 & 0 & \frac{7}{10} & 0 & 0 & \frac{3}{10} \\ & 0 & \frac{L}{10} & 0 & 0 & \frac{L}{15} \\ & & 0 & -\frac{3}{10} & \frac{L}{15} & 0 \\ & \text{antisymmetric} & & 0 & 0 & \frac{7}{10} \\ & & & & 0 & -\frac{L}{10} \\ & & & & & 0 \end{bmatrix} \tag{10}$$

$$M_{0b} = \rho \begin{bmatrix} -(\frac{13AL}{35} + \frac{6I}{5L})\dot{\theta}^2 & -(\frac{11AL^2}{210} + \frac{I}{10})\dot{\theta}^2 & \frac{7AL}{20}\ddot{\theta} & (-\frac{9AL}{70} + \frac{6I}{5L})\dot{\theta}^2 & (\frac{13AL^2}{420} - \frac{I}{10})\dot{\theta}^2 & \frac{3AL}{20}\ddot{\theta} \\ -(\frac{11AL^2}{210} + \frac{I}{10})\dot{\theta}^2 & -(\frac{AL^3}{105} + \frac{2IL}{15})\dot{\theta}^2 & \frac{AL^2}{20}\ddot{\theta} & (-\frac{13AL^2}{420} + \frac{I}{10})\dot{\theta}^2 & (\frac{AL^3}{140} + \frac{IL}{30})\dot{\theta}^2 & \frac{AL^2}{30}\ddot{\theta} \\ -\frac{7AL}{20}\ddot{\theta} & -\frac{AL^2}{20}\ddot{\theta} & -\frac{AL}{3}\dot{\theta}^2 & (-\frac{3AL}{20})\ddot{\theta} & \frac{AL^2}{30}\ddot{\theta} & -\frac{AL}{6}\dot{\theta}^2 \\ (-\frac{9AL}{70} + \frac{6I}{5L})\dot{\theta}^2 & (-\frac{13AL^2}{420} - \frac{I}{10})\dot{\theta}^2 & (\frac{3AL}{20})\ddot{\theta} & -(\frac{13AL}{35} + \frac{6I}{5L})\dot{\theta}^2 & (\frac{11AL^2}{210} + \frac{I}{10})\dot{\theta}^2 & \frac{7AL}{20}\ddot{\theta} \\ (\frac{13AL^2}{420} - \frac{I}{10})\dot{\theta}^2 & (\frac{AL^3}{140} + \frac{IL}{30})\dot{\theta}^2 & -\frac{AL^2}{30}\ddot{\theta} & (\frac{11AL^2}{210} + \frac{I}{10})\dot{\theta}^2 & -(\frac{AL^3}{105} + \frac{2IL}{15})\dot{\theta}^2 & (-\frac{AL^2}{20})\ddot{\theta} \\ -\frac{3AL}{20}\ddot{\theta} & -\frac{AL^2}{30}\ddot{\theta} & -\frac{AL}{6}\dot{\theta}^2 & -\frac{7AL}{20}\ddot{\theta} & (\frac{AL^2}{20})\ddot{\theta} & -\frac{AL}{3}\dot{\theta}^2 \end{bmatrix} \tag{11}$$

$$M_{0b} = -\dot{\theta}^2 M_{2b} + \frac{\ddot{\theta}}{2} M_{1b} \tag{12}$$

$$Q_{0b} = \rho \begin{bmatrix} \frac{AL}{2}\{y_c\cos(\theta) - z_c\sin(\theta)\} - \{J - \frac{3AL^2}{20}\}\theta \\ \frac{AL^2}{12}\{y_c\cos(\theta) - z_c\sin(\theta)\} + \frac{AL^2}{30}\ddot{\theta} \\ \frac{AL}{2}\{y_c\sin(\theta) + z_c\cos(\theta)\} - \frac{AL^2}{6}\dot{\theta}^2 \\ \frac{AL}{2}\{y_c\cos(\theta) - z_c\sin(\theta)\} + \{J + \frac{7AL^2}{20}\}\theta \\ \frac{AL^2}{12}\{-y_c\cos(\theta) + z_c\sin(\theta)\} - \frac{AL^2}{20}\ddot{\theta} \\ \frac{AL}{2}\{y_c\sin(\theta) + z_c\cos(\theta)\} - \frac{AL^2}{3}\dot{\theta}^2 \end{bmatrix} \tag{13}$$

$$K_b = \begin{bmatrix} \frac{12EJ}{L^3} & \frac{6EJ}{L^2} & 0 & -\frac{12EJ}{L^3} & \frac{6EJ}{L^2} & 0 \\ & \frac{4EJ}{L} & 0 & -\frac{6EJ}{L^2} & \frac{2EJ}{L} & 0 \\ & & \frac{EA}{L} & 0 & 0 & -\frac{EA}{L} \\ & \text{symmetric} & & \frac{12EJ}{L^3} & -\frac{6EJ}{L^2} & 0 \\ & & & & \frac{4EJ}{L} & 0 \\ & & & & & \frac{EA}{L} \end{bmatrix} \tag{14}$$

where I and A represent the moment of inertia and the cross section area of the beam, respectively. The nonzero terms of M_{2m}, M_{1m}, M_{0m} and Q_{1m} matrices are given as

$$\begin{aligned}
[M_{2m}]_{4,4} &= M_m[1 - (y_c\sin w' - z_c\cos w')] \\
[M_{2m}]_{5,5} &= M_m[(c+1)(x_c^2+y_c^2) - (y_c+z_c)\sin w' - (y_c-z_c)\cos w'] \\
[M_{2m}]_{6,6} &= M_m[1 - (y_c\cos w' + z_c\sin w')] \\
[M_{1m}]_{4,4} &= 2M_m\dot{\theta}[(y_c\cos w' + z_c\sin w') - 1] \\
[M_{1m}]_{5,5} &= M_m(\dot{\theta} + \dot{w}')[(y_c - z_c)\sin w' - (y_c + z_c)\cos w'] \\
[M_{1m}]_{6,6} &= 2M_m\dot{\theta}[1 - (y_c\sin w' - z_c\cos w')] \\
[M_{0m}]_{4,4} &= -M_m\dot{\theta}^2[1 - (y_c\sin w' - z_c\cos w')] - M_m\ddot{\theta}[1 - (y_c\cos w' + z_c\sin w')] \\
[M_{0m}]_{6,6} &= M_m\ddot{\theta}[1 - (y_c\sin w' - z_c\cos w')] - M_m\dot{\theta}^2[1 - (y_c\cos w' + z_c\sin w')] \\
[Q_{1m}]_{4,1} &= M_m\ddot{\theta}[L - (y_c\sin w' - z_c\cos w')] - M_m\dot{\theta}^2(y_c\cos w' + z_c\sin w') \\
[Q_{1m}]_{5,1} &= M_m\ddot{\theta}[(x_c^2+y_c^2)(c+1) - L(y_c\sin w' - z_c\cos w')] + M_m\dot{\theta}^2 L(y_c\cos w' + z_c\sin w') \\
[Q_{1m}]_{6,1} &= -M_m\ddot{\theta}(y_c\cos w' + z_c\sin w') - M_m\dot{\theta}^2[L - (y_c\sin w' - z_c\cos w')]
\end{aligned} \tag{15}$$

Note that the system mass matrix is the sum of the mass matrices of the tip mass and the beam element, i.e., $M_2 = M_{2b} + M_{2m}$, and so on.

System Equations and FEM Solution

The system governing equation is obtained in a two-stage procedure. In the first stage, the elemental equations of motion are generated. In the second stage, the elemental equations are assembled into a system equation. The detailed assembly procedure was presented by Fallahi and Lai (1992). The displacement is obtained by the integration of the system equation. The secondary information, such as the strain, stress, and induced electric voltage, are calculated using the result of finite element solutions.

Stress-Strain Relationship

The longitudinal strain ϵ_x is given as

$$\epsilon_x = \frac{\partial U}{\partial x} = u' - yw'' = [0 \; -y \; 1 \; 0] \begin{bmatrix} 0 & 0 & 0 & 0 & 0 & 0 \\ (-\frac{6}{L^2}+\frac{12x}{L^3}) & (\frac{6x}{L^2}-\frac{4}{L}) & 0 & (\frac{6}{L^2}-\frac{12x}{L^3}) & (\frac{6x}{L^2}-\frac{2}{L}) & 0 \\ 0 & 0 & -\frac{1}{L} & 0 & 0 & \frac{1}{L} \\ 0 & 0 & 0 & 0 & 0 & 0 \end{bmatrix} \begin{bmatrix} w_1 \\ w_1' \\ u_1 \\ w_2 \\ w_2' \\ u_2 \end{bmatrix} \tag{16}$$

C-2

Stress at the same point can be obtained by using

$$\sigma_z = E\,\epsilon_z \tag{17}$$

Dynamic Monitoring System

From these equations, strain and stress at any arbitrary point, p(x, y), on the beam element are computed. The voltage, V(x,t), generated by the piezo strain is calculated by

$$V(x,t) = e_p(x,t).(h_2/d_{31}) \tag{18}$$

where E is the modulus of elasticity, h is the thickness of the layers, V is the strain induced voltage, h_2 is the thickness of the PVF_2 layer, and d_{31} is the appropriate piezoelectric constant, and

$$e_p(x) = -\frac{E_1h_1 + E_2h_2}{E_2h_2}\,e_i(x) \tag{19}$$

The sensor configuration used in this study is a layer of PVF_2, polyvinylidene fluoride, bonded to one side of the rotating beam. Fig. 3 shows the cross sectional view of the beam with PVF_2 layer. PVF_2 is a polymer that can be polarized or made piezoelectrically active through appropriate processing during manufacture (Bailey and Hubbard, 1985). In its nonpolarized form, PVF_2 is a common electrical insulator. In it's polarized form PVF_2 is essentially a tough, flexible piezoelectric crystal. Polarized PVF_2 is commercially available as thin polymeric film having a layer of nickel or aluminum deposited on each face to conduct a voltage or applied across its faces in y-direction which results in a longitudinal strain in x-direction. This is the d_{31} component of the piezoelectric activity. If PVF_2 is polarized biaxially that would strain in both the x and the z directions. For this study we consider uniaxial PVF_2 only.

Fig. 4 shows the smart beam configuration. The longitudinal strain, ϵ_l, is obtained by force equilibrium in axial direction by finite element formulation. The strain, ϵ_p, in the PVF_2 layer introduce a corresponding piezo voltage to the PVF_2. The combined dynamic effect of gyroscopic, coriolis and other inertia are recorded by the piezo voltage. This voltage can be used as an monitoring index. When the index value exceeds the imposed constraints or material's natural constraints, the control action, i.e. the direct piezoelectric effect, can be triggered to take place.

Control Algorithm

The piezoelectric strain creates the net force in each layer acting as the moment arm from the midplane of the layer to the neutral axis of the beam, producing a bending moment

$$T(x,t) = E_1h_1be_l\,[(h_1/2)-D] + E_2h_2b(e_p+e_l)\,[(h_2/2)+h_1-D] \tag{20}$$

where b is the width of the beam, and D is the location of the neutral axis of the composite beam given by

$$D = \frac{E_1h_1^2 + E_2h_2^2 + 2h_1h_2E_2}{2(E_1h_1+E_2h_2)} \tag{21}$$

Performing some algebraic manipulations to yield

$$T(x,t) = -V(x,t).d_{31}\left(\frac{h_1+h_2}{2}\right)\frac{E_1h_1E_2b}{(E_1h_1+E_2h_2)} - V(x,t).c \tag{22}$$

where c is constant for a given beam material and geometry expressing the bending moment per volt. If the material property and geometry of the composite beam change along its length, c is a function of x.

Combining the above equation with a conventional Euler-Bernoulli beam yields the equations of motion for transverse vibrations, w(x,t), of the composite beam. The governing equation becomes

$$\frac{\partial^2}{\partial x^2}[EI\frac{\partial^2 w}{\partial x^2} - c.V(x,t)] + \rho A\frac{\partial^2 w}{\partial t^2} = 0; \qquad for\ 0<x<L \tag{23}$$

and the boundary conditions are

$$\begin{aligned} w|_0 &= \frac{\partial w}{\partial x}|_0 = 0 \\ EI\frac{\partial^2 w}{\partial x^2}|_L &= -I_t\frac{\partial^3 w}{\partial t^2 \partial x}|_L + c.V(x,t) \\ EI\frac{\partial^3 w}{\partial x^3}|_L &= M_t\frac{\partial^2 w}{\partial x^2}|_L + c.\frac{\partial V(x,t)}{\partial x} \end{aligned} \tag{24}$$

where $EI = E_1I_1 + E_2I_2$, I is the area moment of inertia of the layer about the z axis, $\rho A = \rho A_1 + \rho A_2$, ρ is the density of the layer, A is the cross sectional area of the layer, and M_t and I_t the tip mass and tip inertia.

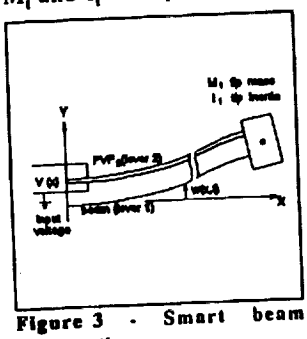

Figure 3 - Smart beam configuration

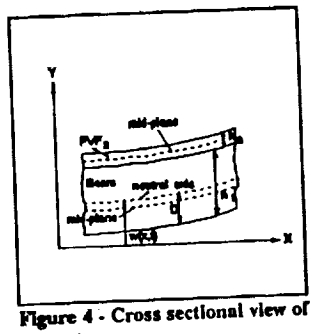

Figure 4 - Cross sectional view of smart beam

Since our PVF_2 has uniform geometry and a spatially uniform voltage applied along its length, the derivatives for the input voltage of the system becomes zero. The voltage that appears in the boundary condition can be used to control the bending moment. The functional of the system is formed by the squares of the curvature and the velocity as

$$I(w) = \frac{1}{2}\int_0^L [(\frac{\partial^2 w}{\partial t^2} + (\frac{\partial w}{\partial t})^2]dx \tag{25}$$

Applying the first variational principle we obtain the Euler-Lagrangian equation of motion, and both the essential and natural boundary conditions. Carrying out integration by parts of the first variation of the functional gives

$$\frac{\partial I}{\partial t} = \int_0^L (1-\frac{EI}{\rho A}).\frac{\partial^3 w}{\partial t \partial x^2}.\frac{\partial^2 w}{\partial x^2}dx - \frac{M_t}{\rho A}.\frac{\partial^2 w}{\partial t^2}.\frac{\partial w}{\partial t}|_L - \frac{I_t}{\rho A}.\frac{\partial^3 w}{\partial t^2 \partial x}.\frac{\partial^2 w}{\partial t \partial x}|_L + \frac{cV(t)}{\rho A}.\frac{\partial^2 w}{\partial t \partial x}|_L \tag{26}$$

The voltage appears only in one term. To extremize the functional, the voltage is chosen such that it appears as negative as

$$V = -sgn(c.\frac{\partial^2 w}{\partial x \partial t}|_L).V_{max} \tag{27}$$

where $\frac{\partial^2 w}{\partial t \partial x}|_L$ is the angular velocity at the tip of the beam. The control voltage is chosen to generate a bending moment that opposes the angular motion at the tip of the beam. The geometry of the piezoelectric layer can be tailored to obtain the necessary control function.

NUMERICAL EXPERIMENTS

Several numerical simulations are conducted to illustrate the effectiveness of the full beam formulation of the beam-mass system. A beam-mass system made of rectangular aluminum materials with an embedded PVF_2 layer is used for the study. The dimensions and material properties of the beam are given in Table 1. The beam is subjected to a spin-up maneuver (Kane, 1985) prescribed by

$$\theta = \begin{cases} \frac{\dot{\theta}_0}{T}[\frac{t^2}{2} + (\frac{T}{2\pi})^2(\cos\frac{2\pi t}{T} - 1)] ; & 0 \le t \le T \\ \dot{\theta}_0[t - \frac{T}{2}] ; & t > T \end{cases} \tag{29}$$

where $\dot{\theta}_0$ is the steady state angular velocity. In order to characterize the dynamic behavior of the system at different rotating speeds, we set the steady state speeds to 300, 500 and 700 rpm, and time constant, T, is 1 seconds. The simulation is carried out for a period of 5 seconds.

Table 1 - Geometric parameters and material properties of the smart beam

	Aluminum	PVF_2	Composite Beam
Length (L)	20	20	20
Thickness (h; in)	.9989	.0011	1
Width (w; in)	.25	.25	.25
Density (ρ; lb s^2/in^4)	2.45×10^{-4}	1.68×10^{-4}	2.45×10^{-4}
Young's Modulus (E; psi)	1×10^7	2.9×10^5	1×10^7
Static Piezo-electric Constant (d_{31};in/V)		8.66×10^{-10}	

Figures 5 and 6 show the transverse displacement, w, of the piezo-aluminum beam-mass system rotating at three different speeds. The transverse tip displacement of the beam is computed and recorded for both formulation with and without payload mass inertia. Both of the maximum transient tip displacement and the steady-state tip deflection are proportional to the size of the mass attachment. The contribution of gyroscopic terms is computed and recorded in Table 2. A maximum 4.35% contribution of gyroscopic inertia is observed at a speed of 700 rpm. The contribution becomes significant when the mass attachment is increased. The contribution of gyroscopic inertia becomes more pronounced when the speed is increased.

When 10% of a equivalent beam mass is attached to the tip of the rotating beam, the tip strain is increased at least two times. Figures 7 and 8 show the longitudinal tip strain at three different speeds. The corresponding longitudinal stresses are presented in Figures 9 and 10. These plots are similar to those of Figures 7 and 8 with an amplification in magnitude by the factor of an equivalent modulus of elasticity. The tip strain induced voltage of the piezoelectric layer at three speeds are presented in Figures 11 and 12. It is observed that the piezo voltage introduced by tip strain of no payload is in the range of 50 to 170 volts. The piezo voltage induced by the tip strain with a 10% tip mass attachment is in the range of 120 to 530 volts. The contribution of tip masses and speeds are

experimented to allow control voltage to be adjusted to the design range. The geometric parameters of both aluminum beams and piezoelectric layers are design variables to be tailored to satisfy the design need.

Table 2 - Contribution of gyroscopic terms at different speeds (*)

	Tip Mass Attached to Beam	Angular Velocity		
		300 rpm	500 rpm	700 rpm
Aluminum beam-mass system	0%	0.52%	1.02%	2.08%
	10%	0.67%	1.47%	3.20%
Piezo-aluminum beam-mass system	0%	0.69%	1.36%	2.80%
	10%	0.90%	2.08%	4.35%

(*) Percentage difference in steady-state solution at different speeds for M_0 and M_1

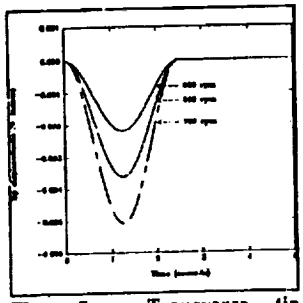

Figure 5 - Transverse tip displacements, w, of piezo-aluminum beam rotating at 300, 500 and 700 rpm

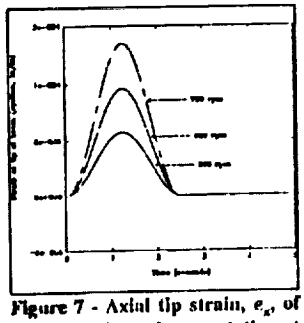

Figure 7 - Axial tip strain, e_x, of piezo-aluminum beam rotating at 300, 500, and 700 rpm

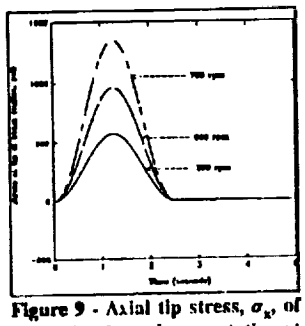

Figure 9 - Axial tip stress, σ_x, of piezo-aluminum beam rotating at speeds of 300, 500, and 700 rpm

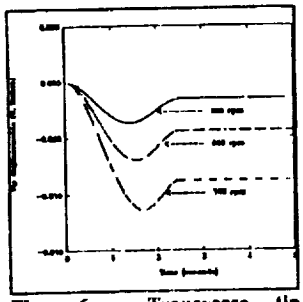

Figure 6 - Transverse tip displacements, w, of the piezo-aluminum beam-mass(10%) system rotating at 300, 500, and 700 rpm

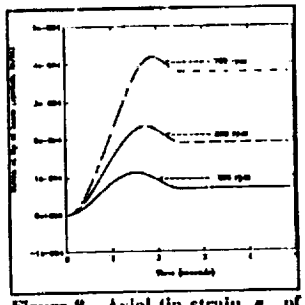

Figure 8 - Axial tip strain, e_x, of piezo-aluminumbeam-mass(10%) system rotating at 300, 500, and 700 rpm

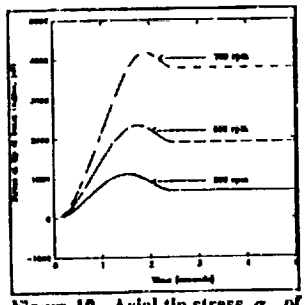

Figure 10 - Axial tip stress, σ_x, of piezo-aluminumbeam-mass(10%) system rotating at 300, 500, and 700 rpm

CONCLUSION

A systematic finite element based design method is presented in the paper. The method allows the a high-speed rotating dynamic structure with embedded piezoelectric films to be designed and monitored. The gyroscopic effect introduced by different payload at various speeds can be taken into consideration in the early design. The result of numerical simulations indicates that current approach can be used for application in the sensing and monitoring of high-speed spinning space structures and flexible mechanical systems. The finite element based method is simple and systematic. The dynamic characteristics of high speed rotating structures and machinery can be observed and used in distributed parameter models for control of such systems.

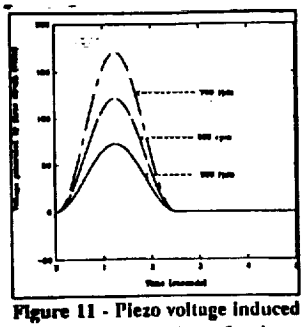

Figure 11 - Piezo voltage induced by the tip strain of piezo-aluminum beam rotating at 300, 500, and 700 rpm

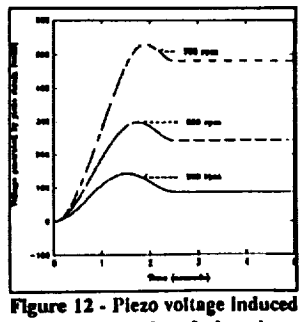

Figure 12 - Piezo voltage induced by the tip strain of the piezo-aluminum beam-mass (10%) system rotating at 300, 500, and 700 rpm

ACKNOWLEDGEMENT

The authors gratefully acknowledge the support provided by the United States Army Strategic Defense Command and the NASA Center for Aerospace Research at A&T.

REFERENCES

Bailey, T. and Hubbard Jr., J.E., 1985, Distributed Piezo-electric-Polymer Active Vibration Control of A Cantilever Beam, Journal of Guidance, Control and Dynamics, Vol. 8, No. 5, pp. 605-611, 1985.

Choi, S.B., Gandhi, M.V., and Thompson, B.S., 1989, An Active Vibration Tuning for Smart Flexible Structures Incorporating Electro-Rheological Fluids: A Proof-of-Concept Investigation, Proceedings of 1989 American Control Conference.

Crawley, E.F. and deLuis, J., 1987, Use of Piezoelectric Actuators as Elements of Intelligent Structures, AIAA Journal, Vol. 25, No. 10, pp. 1373-1385.

Fallahi, B., Lai, H.Y. and C. Venkat, 1992, A Comparative Study of the Finite Element Assembly Procedures Using Conventional and Modified Lagrange Equations, Canadian Society of Mechanical Engineering Forum 92.

Gandhi, M.V. and Thompson, B.S., 1989, Smart Materials and Structures Technologies: The Impending Revolution, Technomic Publishing Company, Inc., Lancaster, PA.

Gandhi, M.V., Thompson, B.S., and Choi, S.B., 1989, A New Generation of Innovative Ultra-Advanced Intelligent Composite Materials Featuring Electro-rheological Fluids: An Experimental Investigation, Journal of Composite Materials.

Gandhi, M.V., Thompson, B.S., Choi, S.B. and Shakir, S., 1989, Electro-Rheological-Fluid-Based Articulating Robotics Systems, ASME Journal of Mechanisms, Transmissions and Automation in Design.

Kane, T.R., Ryan, R.R., Banerjee, A.K., 1985, Dynamics of a Beam Attached to a Moving Base, AAS/AIAA Astrodynamics Specialist Conference, Paper AAS 85-390, Vail, Colorado.

Lai, H.Y., Fallahi, B. and R. Gupta, 1992, Full Beam Formulation of a Rotating Laminated Beam-Mass System, to appear in Composite Journal, Paper No. COMP/91/1008KK.

Morikawa, T., 1985, Optical Actuators, Japanese Journal of Society Instrumentation and Control Engineering, Vol. 24, No. 9, pp. 827-831.

Miwa, Y., 1985, Shape Memory Alloys Application for Sequential Operation Control, System and Control (Japan), Vol. 29, No. 5, pp. 303-310, 1985.

Plump, J.M., Hubbard Jr., J.E. and Bailey, T., 1987, Nonlinear Control of A Distributed System: Simulation and Experimental Results, ASME Journal of Dynamics, Measurement, and Control, Vol. 109, pp. 133-139.

Rogers, C.A. and Robertshaw, H.H., 1988, Shape Memory Alloy Reinforced Composites, Engineering Science Reprint 25, ESP25.88027, Society of Engineering Sciences Inc..

Rogowski, R.S., Heyman, J.S., and Claus, R.O., 1988, The Evolution of Smart Composite Materials, NASA Tech Briefs, Vol. 12, No. 10, pp. 20-22.

Tzou, H.S. and Tseng, C.I., 1990, Distributed Modal Identification and Vibration Control of Continua, Journal of Sound and Vibration, Vol. 138, No. 1, pp. 17-34.

Yaeger, J.R., 1984, A Practical Shape-Memory Electro-mechanical Actuator, ISATA 84 Proceedings, International Symposium on Automotive Technology and Automation, Milan, Italy, Vol. 1, pp. 633-642.

A Piecewise Continuous Timoshenko Beam Model for the Dynamic Analysis of Tapered Beam-like Structures

Ji Yao Shen, Elias G. Abu-Saba
and
William M. McGinley, Lonnie Sharpe, Jr.

Center for Aerospace Research
School of Engineering
North Carolina A&T State University
Greensboro, North Carolina 27411

Lawrence W. Taylor, Jr.

Control & Guidance Division
Langley Research Center
Hampton, Virginia 23665

Submitted to
The Journal of Aerospace Engineering
Aerospace Division, American Society of Civil Engineering

ABSTRACT

Distributed parameter modeling is being seen to offer a viable alternative to finite element approach for modeling large flexible space structures. The introduction of the transfer matrix method into the continuum modeling process provides a very useful tool to facilitate the distributed parameter model applied to some more complex configurations. A uniform Timoshenko beam model for the estimation of the dynamic properties of beam-like structures has given comparable

results. But many aeronautical and aerospace structures are of the non-uniform sections or sectional properties, such as aircraft wing, satellite antenna.

This paper proposes a piecewise continuous Timoshenko beam model which is used for the dynamic analysis of tapered beam-like structures. A tapered beam is divided into several segments of uniform beam elements. Instead of arbitrarily assumed shape functions used in finite element analysis, the closed-form solution of the Timoshenko beam equation has been used. Application of transfer matrix method relates all the elements as a whole. By corresponding boundary conditions and compatible conditions a characteristic equation for the global tapered beam has been yielded, from which natural frequencies can be derived. A computer simulation is shown in this paper, and compared with the results obtained from the finite element analysis. While piecewise continuous Timoshenko beam model decreases the number of elements significantly, comparable results to the finite element method are obtained.

SYMBOLS

A	sectional area, or characteristic matrix
a	parameter in the Timoshenko beam equation, $a^2 = EI/m$
C_1, C_2, C_3, C_4	mode shape coefficients
Det [A]	characteristic determinant
E	modulus of elasticity
G	shear modulus
I	second moment of area of the beam section
k	bending stiffness, $k = EI$
L_j	length of the jth beam segment
M	bending moment
m	mass per unit length of the beam
Q	shear force
r	radius of gyration of the beam section, $r^2 = I/A$
T	time function
t	time
x, y, z	Cartesian coordinates
y(z,t)	lateral deflection
$\bar{z}$	dimensionless z-coordinate, $\bar{z} = z/L$
Y(z)	spatial lateral deflection function
α, γ	dimensionless parameters
β	eigenvalue coefficient, $\beta^4 = \omega^2 / a^2$

ε	Timoshenko shear coefficient
ψ	slope of lateral deflection
ω	circular natural frequency
$[\Phi]$	transfer matrix for the global beam
$[\Phi]_j$	transfer matrix for the jth beam segment
Φ_{ki}	elements of the global transfer matrix
$\phi_{ki}^{(j)}$	elements of the jth beam transfer matrix

1. INTRODUCTION

Distributed parameter modeling is being seen to offer a viable alternative to finite element approach for modeling large flexible space structures. Continuum models have been made of several flexible space structures, which include the Spacecraft Control Laboratory (SCOLE) [1], Solar Array Flight Experiment [2], NASA Mini-Mast Truss [3], the Space Station Freedom [4]. Especially, the introduction of the transfer matrix method into the continuum modeling process provides a very useful tool to facilitate the distributed parameter model applied to some more complex configurations [5,6]. A uniform Timoshenko beam model for the estimation of the dynamic properties of beam-like structures has given comparable results [7]. But many aeronautical and aerospace structures are of the non-uniform sections or sectional properties, such as aircraft wing, satellite antenna.

This paper proposes a piecewise continuous Timoshenko beam model which is used for the dynamic analysis of tapered beam-like structures. A tapered beam is divided into several segments of uniform beam elements. Instead of arbitrarily assumed shape functions used in finite element analysis, the closed-form solution of the Timoshenko beam equation has been used. Application of transfer matrix method relates all the elements as a whole. By corresponding boundary conditions and compatible conditions a characteristic equation for the global tapered beam has been yielded, from which natural frequencies can be derived. A computer simulation is shown in this paper, and compared with the results obtained from the finite element analysis. While piecewise continuous Timoshenko beam model decreases the number of elements significantly, comparable results to the finite element method are obtained.

2. TRANSFER MATRIX OF A TIMOSHENKO BEAM

Timoshenko beam model accounts for both rotary inertia and shear deformation of the beam. Usually, Timoshenko beam model produces more accurate estimation of the modal natural frequencies compared with the Bernoulli-Euler beam equation, especially for the range of higher frequencies [8]. In this section, a transfer matrix for Timoshenko beam model has been derived. The Timoshenko beam is represented by the equation,

$$\frac{\partial^4 y}{\partial z^4} + \frac{m}{EI}\frac{\partial^2 y}{\partial t^2} - \frac{m}{EA}\left(1 + \frac{E}{\varepsilon G}\right)\frac{\partial^4 y}{\partial z^2 \partial t^2} + \frac{m^2}{\varepsilon EGA^2}\frac{\partial^4 y}{\partial t^4} = 0 \qquad (2.1)$$

For harmonic motion, y(x,t) can be expressed as

$$y(x,t) = Y(x)\, e^{j\omega t}$$

then, Eq.(2.1) will become

$$Y'''' + \frac{m}{EA}\left(1 + \frac{E}{\varepsilon G}\right)\omega^2 Y'' + \left(\frac{m^2\omega^2}{\varepsilon EGA^2} - \frac{m}{EI}\right)\omega^2 Y = 0 \qquad (2.2)$$

Defining $\beta^4=\omega^2/a^2$, where $a^2=EI/m$, Eq.(2.2) becomes

$$Y'''' + \beta^4 r^2\left(1 + \frac{E}{\varepsilon G}\right)Y'' + \beta^4\left[\beta^4 r^4\left(\frac{E}{\varepsilon G}\right) - 1\right]Y = 0 \qquad (2.3)$$

where, $r^2=I/A$, the radius of gyration of the section. If we use the following dimensionless parameters,

$$\bar{z} = \frac{z}{L}, \qquad \alpha = \frac{1}{\varepsilon}\left(\frac{r^2}{L^2}\right)\frac{E}{G}, \qquad \gamma = \frac{r^2}{L^2}$$

the Timoshenko equation may finally be written as

$$Y'''' + (\beta L)^4(\alpha + \gamma)Y'' + (\beta L)^4\left[(\beta L)^4\alpha\gamma - 1\right]Y = 0 \qquad (2.4)$$

Assuming that the solution is

$$Y(\bar{z}) = A\, e^{(BL)\bar{z}}$$

which, when substituted into Eq.(2.4), leads to

$$(BL)^4 + (\beta L)^4 (\alpha + \gamma)(BL)^2 + (\beta L)^4 [(\beta L)^4 \alpha\gamma - 1] = 0 \qquad (2.5)$$

The solution to the Eq.(2.5) is as follows.

$$\begin{cases} (BL)_{1,2} = \pm(\eta L) = \pm\frac{\sqrt{2}}{2}\left[-(\beta L)^4(\alpha+\gamma) + \sqrt{(\beta L)^8(\alpha-\gamma)^2 + 4(\beta L)^4}\right]^{1/2} \\ (BL)_{3,4} = \pm j(\theta L) = \pm j\frac{\sqrt{2}}{2}\left[(\beta L)^4(\alpha+\gamma) + \sqrt{(\beta L)^8(\alpha-\gamma)^2 + 4(\beta L)^4}\right]^{1/2} \end{cases}$$

Then, the solution to the Eq.(2.4) can be expressed as

$$Y(\bar{z}) = C_1 \sin(\theta L\bar{z}) + C_2 \cos(\theta L\bar{z}) + C_3 \sinh(\eta L\bar{z}) + C_4 \cosh(\eta L\bar{z}) \qquad (2.6)$$

Similarly, for the bending slope ψ the differential equation has the same form as the Eq.(2.4),

$$\Psi'''' + (\beta L)^4 (\alpha + \gamma)\Psi'' + (\beta L)^4 [(\beta L)^4 \alpha\gamma - 1]\Psi = 0 \qquad (2.7)$$

The solution to Eq.(2.7) will be

$$\Psi(\bar{z}) = \sigma_1 C_1 \cos(\theta L\bar{z}) - \sigma_1 C_2 \sin(\theta L\bar{z}) + \sigma_2 C_3 \cosh(\eta L\bar{z}) + \sigma_2 C_4 \sinh(\eta L\bar{z}) \qquad (2.8)$$

where,

$$\sigma_1 = \frac{1}{L}\left[(\theta L) - \frac{\alpha}{(\theta L)}(\beta L)^4\right] \quad \text{and} \quad \sigma_2 = \frac{1}{L}\left[(\eta L) + \frac{\alpha}{(\eta L)}(\beta L)^4\right]$$

For the Timoshenko beam model, the shear force is

$$Q(z,t) = k\frac{\partial^3 y}{\partial z^3} - k\frac{m}{\varepsilon GA}\frac{\partial^3 y}{\partial z \partial t^2} - J\frac{\partial^2 \psi}{\partial t^2} \qquad (2.9)$$

or, equivalently,

$$Q(z) = k\,Y''' + k\frac{m\omega^2}{\varepsilon GA}\,Y' + J\omega^2\psi \qquad (2.10)$$

And the bending moment is

$$M(z,t) = k\frac{\partial^2 y}{\partial z^2} - k\frac{m}{\varepsilon GA}\frac{\partial^2 y}{\partial t^2} \qquad (2.11)$$

or, equivalently,

$$M(z) = k\,Y'' + k\,\frac{m\omega^2}{\varepsilon GA}\,Y \tag{2.12}$$

Eqs. (2.10) and (2.12) can be written in dimensionless format as,

$$Q(\bar{z}) = \frac{k}{L^3}Y''' + \frac{k}{L^3}\alpha(\beta L)^4 Y' + \frac{k}{L^2}\gamma(\beta L)^4\psi \tag{2.13}$$

$$M(\bar{z}) = \frac{k}{L^2}Y'' + \frac{k}{L^2}\alpha(\beta L)^4 Y \tag{2.14}$$

Substituting the solutions of Y(z)(Eq.2.6) and Ψ(z)(Eq.2.8) into Eqs.(2.13) and (2.14), we derive

$$Q(\bar{z})=-k\sigma_{11}C_1\cos\theta L\bar{z}+k\sigma_{11}C_2\sin\theta L\bar{z}+k\sigma_{21}C_3\cosh\eta L\bar{z}+k\sigma_{21}C_4\sinh\eta L\bar{z} \tag{2.15}$$

$$M(\bar{z})=-k\sigma_{12}C_1\sin\theta L\bar{z}-k\sigma_{12}C_2\cos\theta L\bar{z}+k\sigma_{22}C_3\sinh\eta L\bar{z}+k\sigma_{22}C_4\cosh\eta L\bar{z} \tag{2.16}$$

where,

$$\sigma_{11} = \theta^3 - \alpha L^2\beta^4\theta - \gamma L^2\beta^4\sigma_1, \qquad \sigma_{12} = \theta^2 - \alpha L^2\beta^4$$

$$\sigma_{21} = \eta^3 + \alpha L^2\beta^4\eta + \gamma L^2\beta^4\sigma_2, \qquad \sigma_{22} = \eta^2 + \alpha L^2\beta^4$$

For the jth beam element, the displacement Y(0), slope Ψ(0), shear Q(0), and the bending moment M(0) at the end of z=0 can then be written in matrix form as,

$$\begin{Bmatrix} Y_0 \\ \Psi_0 \\ Q_0 \\ M_0 \end{Bmatrix}_j = \begin{bmatrix} 0 & 1 & 0 & 1 \\ \sigma_1 & 0 & \sigma_2 & 0 \\ -k\sigma_{11} & 0 & k\sigma_{21} & 0 \\ 0 & -k\sigma_{12} & 0 & k\sigma_{22} \end{bmatrix}_j \begin{Bmatrix} C_1 \\ C_2 \\ C_3 \\ C_4 \end{Bmatrix}_j \tag{2.17}$$

Thus,

$$\begin{Bmatrix} C_1 \\ C_2 \\ C_3 \\ C_4 \end{Bmatrix}_j = [\lambda]_j \begin{Bmatrix} Y_0 \\ \Psi_0 \\ Q_0 \\ M_0 \end{Bmatrix}_j \tag{2.18}$$

where,

$$[\lambda]_j=\begin{bmatrix} 0 & 1 & 0 & 1 \\ \sigma_1 & 0 & \sigma_2 & 0 \\ -k\sigma_{11} & 0 & k\sigma_{21} & 0 \\ 0 & -k\sigma_{12} & 0 & k\sigma_{22} \end{bmatrix}_j^{-1}=\begin{bmatrix} 0 & \frac{\sigma_{21}}{\sigma_1\sigma_{21}+\sigma_2\sigma_{11}} & -\frac{\sigma_2}{k(\sigma_1\sigma_{21}+\sigma_2\sigma_{11})} & 0 \\ \frac{\sigma_{22}}{\sigma_{12}+\sigma_{22}} & 0 & 0 & -\frac{1}{k(\sigma_{12}+\sigma_{22})} \\ 0 & \frac{\sigma_{11}}{\sigma_1\sigma_{21}+\sigma_2\sigma_{11}} & \frac{\sigma_1}{k(\sigma_1\sigma_{21}+\sigma_2\sigma_{11})} & 0 \\ \frac{\sigma_{12}}{\sigma_{12}+\sigma_{22}} & 0 & 0 & \frac{1}{k(\sigma_{12}+\sigma_{22})} \end{bmatrix}_j$$

Similarly, at the end of z=L, the corresponding quantities are, if written in matrix form,

$$\begin{Bmatrix} Y \\ \Psi \\ Q \\ M \end{Bmatrix}_j^L = [\zeta]_j \begin{Bmatrix} C_1 \\ C_2 \\ C_3 \\ C_4 \end{Bmatrix}_j \tag{2.19}$$

where,

$$[\zeta]_j = \begin{bmatrix} \sin\theta L & \cos\theta L & \sinh\eta L & \cosh\eta L \\ \sigma_1\cos\theta L & -\sigma_1\sin\theta L & \sigma_2\cosh\eta L & \sigma_2\sinh\eta L \\ -k\sigma_{11}\cos\theta L & k\sigma_{11}\sin\theta L & k\sigma_{21}\cosh\eta L & k\sigma_{21}\sinh\eta L \\ -k\sigma_{12}\sin\theta L & -k\sigma_{12}\cos\theta L & k\sigma_{22}\sinh\eta L & k\sigma_{22}\cosh\eta L \end{bmatrix}_j$$

Substituting Eq.(2.18) into Eq.(2.19) we obtain

$$\begin{Bmatrix} Y_L \\ \Psi_L \\ Q_L \\ M_L \end{Bmatrix}_j = [\Phi]_j \begin{Bmatrix} Y_0 \\ \Psi_0 \\ Q_0 \\ M_0 \end{Bmatrix}_j \tag{2.20}$$

where, $[\Phi]_j$ is the transfer matrix of the Timoshenko beam,

$$[\Phi]_j = [\zeta]_j [\lambda]_j \tag{2.21}$$

and the elements of the transfer matrix $[\Phi]_j$ are as follows.

$$\varphi_{11} = \frac{1}{\sigma_{12}+\sigma_{22}}(\sigma_{22}\cos\theta L + \sigma_{12}\cosh\eta L)$$
$$\varphi_{12} = \frac{1}{\sigma_1\sigma_{21}+\sigma_2\sigma_{11}}(\sigma_{21}\sin\theta L + \sigma_{11}\sinh\eta L)$$

$$\varphi_{13} = \frac{1}{k(\sigma_1\sigma_{21}+\sigma_2\sigma_{11})}(-\sigma_2\sin\theta L + \sigma_1\sinh\eta L)$$
$$\varphi_{14} = \frac{1}{k(\sigma_{12}+\sigma_{22})}(-\cos\theta L + \cosh\eta L)$$

$$\varphi_{21} = -\frac{1}{\sigma_{12}+\sigma_{22}}(\sigma_1\sigma_{22}\sin\theta L - \sigma_2\sigma_{12}\sinh\eta L)$$
$$\varphi_{22} = \frac{1}{\sigma_1\sigma_{21}+\sigma_2\sigma_{11}}(\sigma_1\sigma_{21}\cos\theta L + \sigma_2\sigma_{11}\cosh\eta L)$$
$$\varphi_{23} = \frac{\sigma_1\sigma_2}{k(\sigma_1\sigma_{21}+\sigma_2\sigma_{11})}(-\cos\theta L + \cosh\eta L)$$
$$\varphi_{24} = \frac{1}{k(\sigma_{12}+\sigma_{22})}(\sigma_1\sin\theta L + \sigma_2\sinh\eta L)$$

$$\varphi_{31} = \frac{k}{\sigma_{12}+\sigma_{22}}(\sigma_{11}\sigma_{22}\sin\theta L + \sigma_{12}\sigma_{21}\sinh\eta L)$$
$$\varphi_{32} = -\frac{k\sigma_{11}\sigma_{21}}{\sigma_1\sigma_{21}+\sigma_2\sigma_{11}}(\cos\theta L - \cosh\eta L)$$
$$\varphi_{33} = \frac{1}{\sigma_1\sigma_{21}+\sigma_2\sigma_{11}}(\sigma_2\sigma_{11}\cos\theta L + \sigma_1\sigma_{21}\cosh\eta L)$$
$$\varphi_{34} = \frac{1}{\sigma_{12}+\sigma_{22}}(-\sigma_{11}\sin\theta L + \sigma_{21}\sinh\eta L)$$

$$\varphi_{41} = -\frac{k\sigma_{12}\sigma_{22}}{\sigma_{12}+\sigma_{22}}(\cos\theta L - \cosh\eta L)$$
$$\varphi_{42} = -\frac{k}{\sigma_1\sigma_{21}+\sigma_2\sigma_{11}}(\sigma_{12}\sigma_{21}\sin\theta L - \sigma_{11}\sigma_{22}\sinh\eta L)$$
$$\varphi_{43} = \frac{1}{\sigma_1\sigma_{21}+\sigma_2\sigma_{11}}(\sigma_2\sigma_{12}\sin\theta L + \sigma_1\sigma_{22}\sinh\eta L)$$
$$\varphi_{44} = \frac{1}{\sigma_{12}+\sigma_{22}}(\sigma_{12}\cos\theta L + \sigma_{22}\cosh\eta L)$$

3. PIECEWISE CONTINUOUS MODEL FOR A TAPERED BEAM

A tapered beam can be considered as a piecewise continuous step beam consisting of N uniform beam elements as shown in the figure. Using the transform matrix (Eq.2.21) to describe

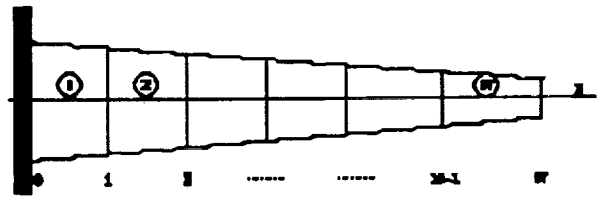

each beam element, then the state vectors at the two ends of the global beam will be related by the global transfer matrix [Φ], that is,

$$\begin{Bmatrix} Y \\ \Psi \\ Q \\ M \end{Bmatrix}_N = [\Phi] \begin{Bmatrix} Y \\ \Psi \\ Q \\ M \end{Bmatrix}_0 \tag{3.1}$$

where, the global transfer matrix

$$[\Phi] = \prod_{j=N}^{1} [\Phi]_j$$

Without loss of generality, let us consider the case of N=3. As N=3, the global transfer matrix will be

$$[\Phi] = \begin{bmatrix} \sum_{i=1}^{4}\left(\sum_{k=1}^{4}\phi_{1k}^{(3)}\phi_{ki}^{(2)}\right)\phi_{i1}^{(1)} & \sum_{i=1}^{4}\left(\sum_{k=1}^{4}\phi_{1k}^{(3)}\phi_{ki}^{(2)}\right)\phi_{i2}^{(1)} & \sum_{i=1}^{4}\left(\sum_{k=1}^{4}\phi_{1k}^{(3)}\phi_{ki}^{(2)}\right)\phi_{i3}^{(1)} & \sum_{i=1}^{4}\left(\sum_{k=1}^{4}\phi_{1k}^{(3)}\phi_{ki}^{(2)}\right)\phi_{i4}^{(1)} \\ \sum_{i=1}^{4}\left(\sum_{k=1}^{4}\phi_{2k}^{(3)}\phi_{ki}^{(2)}\right)\phi_{i1}^{(1)} & \sum_{i=1}^{4}\left(\sum_{k=1}^{4}\phi_{2k}^{(3)}\phi_{ki}^{(2)}\right)\phi_{i2}^{(1)} & \sum_{i=1}^{4}\left(\sum_{k=1}^{4}\phi_{2k}^{(3)}\phi_{ki}^{(2)}\right)\phi_{i3}^{(1)} & \sum_{i=1}^{4}\left(\sum_{k=1}^{4}\phi_{2k}^{(3)}\phi_{ki}^{(2)}\right)\phi_{i4}^{(1)} \\ \sum_{i=1}^{4}\left(\sum_{k=1}^{4}\phi_{3k}^{(3)}\phi_{ki}^{(2)}\right)\phi_{i1}^{(1)} & \sum_{i=1}^{4}\left(\sum_{k=1}^{4}\phi_{3k}^{(3)}\phi_{ki}^{(2)}\right)\phi_{i2}^{(1)} & \sum_{i=1}^{4}\left(\sum_{k=1}^{4}\phi_{3k}^{(3)}\phi_{ki}^{(2)}\right)\phi_{i3}^{(1)} & \sum_{i=1}^{4}\left(\sum_{k=1}^{4}\phi_{3k}^{(3)}\phi_{ki}^{(2)}\right)\phi_{i4}^{(1)} \\ \sum_{i=1}^{4}\left(\sum_{k=1}^{4}\phi_{4k}^{(3)}\phi_{ki}^{(2)}\right)\phi_{i1}^{(1)} & \sum_{i=1}^{4}\left(\sum_{k=1}^{4}\phi_{4k}^{(3)}\phi_{ki}^{(2)}\right)\phi_{i2}^{(1)} & \sum_{i=1}^{4}\left(\sum_{k=1}^{4}\phi_{4k}^{(3)}\phi_{ki}^{(2)}\right)\phi_{i3}^{(1)} & \sum_{i=1}^{4}\left(\sum_{k=1}^{4}\phi_{4k}^{(3)}\phi_{ki}^{(2)}\right)\phi_{i4}^{(1)} \end{bmatrix} \tag{3.2}$$

where, the superscripts (j) represent the jth beam, and $\phi_{ki}^{(j)}$ is the elements of the transfer matrix for the jth beam.

If we consider a cantilevered beam fixed at the end of z=0, we have the following boundary conditions: at the fixed end: Y(0)=0 and ψ(0)=0; at the free end: Q(L)=0 and M(L)=0. Applying the boundary conditions to the global equation (3.1), we will have

$$\begin{Bmatrix} Y \\ \Psi \\ 0 \\ 0 \end{Bmatrix}_3 = [\Phi] \begin{Bmatrix} 0 \\ 0 \\ Q \\ M \end{Bmatrix}_0 \tag{3.3}$$

Rearranging the state vector, Eq.(3.3) can be written as

$$[A]\begin{Bmatrix} Y_3 \\ \Psi_3 \\ Q_0 \\ M_0 \end{Bmatrix} = [0] \tag{3.4}$$

where, the coefficient matrix

$$[A] = \begin{bmatrix} -1 & 0 & \Phi_{13} & \Phi_{14} \\ 0 & -1 & \Phi_{23} & \Phi_{24} \\ 0 & 0 & \Phi_{33} & \Phi_{34} \\ 0 & 0 & \Phi_{43} & \Phi_{44} \end{bmatrix}$$

and Φ_{ij}'s are the elements of the global transfer matrix. The condition for Eq.(3.4) to have a non-trivial solution is that the determinant of the coefficient matrix equals zero, that is

$$\mathrm{Det}[A] = \mathrm{Det}\begin{bmatrix} -1 & 0 & \Phi_{13} & \Phi_{14} \\ 0 & -1 & \Phi_{23} & \Phi_{24} \\ 0 & 0 & \Phi_{33} & \Phi_{34} \\ 0 & 0 & \Phi_{43} & \Phi_{44} \end{bmatrix} = 0 \tag{3.5}$$

Eq.(3.5) is the so-called characteristic equation. Solving for the roots of the characteristic equation, we obtain the natural frequencies ω's. Expanding the determinant in Eq.(3.5) we can simplify the characteristic equation as

$$\Phi_{33}\,\Phi_{44} - \Phi_{34}\,\Phi_{43} = 0 \tag{3.6}$$

or, expressing Eq.(3.6) in terms of the elements of each sub-transfer matrices, we have

$$\left[\sum_{i=1}^{4}\left(\sum_{k=1}^{4}\phi_{3k}^{(3)}\phi_{ki}^{(2)}\right)\phi_{i3}^{(1)}\right]\left[\sum_{i=1}^{4}\left(\sum_{k=1}^{4}\phi_{4k}^{(3)}\phi_{ki}^{(2)}\right)\phi_{i4}^{(1)}\right] - \left[\sum_{i=1}^{4}\left(\sum_{k=1}^{4}\phi_{3k}^{(3)}\phi_{ki}^{(2)}\right)\phi_{i4}^{(1)}\right]\left[\sum_{i=1}^{4}\left(\sum_{k=1}^{4}\phi_{4k}^{(3)}\phi_{ki}^{(2)}\right)\phi_{i3}^{(1)}\right] = 0 \tag{3.7}$$

If we consider a free-free beam, then the boundary conditions will become as $Q_0=M_0=0$ and $Q_3=M_3=0$ at the both ends. Thus the characteristic equation (Eq.3.5) should be

$$\mathrm{Det}[A] = \mathrm{Det}\begin{bmatrix} \Phi_{31} & \Phi_{32} & 0 & 0 \\ \Phi_{41} & \Phi_{42} & 0 & 0 \\ \Phi_{11} & \Phi_{12} & -1 & 0 \\ \Phi_{21} & \Phi_{22} & 0 & -1 \end{bmatrix} = 0 \tag{3.8}$$

or,

$$\Phi_{31}\,\Phi_{42} - \Phi_{32}\,\Phi_{41} = 0 \qquad (3.9)$$

Expressing Eq.(3.9) in terms of the elements of each sub-transfer matrices, we have

$$\left[\sum_{i=1}^{4}\left(\sum_{k=1}^{4}\phi_{3k}^{(3)}\phi_{ki}^{(2)}\right)\phi_{i1}^{(1)}\right]\left[\sum_{i=1}^{4}\left(\sum_{k=1}^{4}\phi_{4k}^{(3)}\phi_{ki}^{(2)}\right)\phi_{i2}^{(1)}\right] - \left[\sum_{i=1}^{4}\left(\sum_{k=1}^{4}\phi_{3k}^{(3)}\phi_{ki}^{(2)}\right)\phi_{i2}^{(1)}\right]\left[\sum_{i=1}^{4}\left(\sum_{k=1}^{4}\phi_{4k}^{(3)}\phi_{ki}^{(2)}\right)\phi_{i1}^{(1)}\right] = 0 \quad (3.10)$$

4. COMPUTER SIMULATION

The computer simulation is designed to analyze the natural frequency for a tapered beam with 15-meter length (Fig.4.1). The modulus of elasticity is assumed to be $E=200*10^9$ N/m^2. To

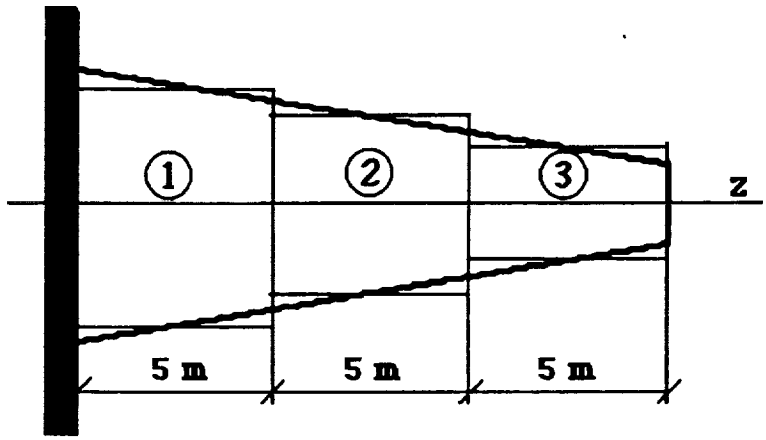

Fig.4.1 A Tapered Beam

simplify the calculation, the change of the sectional foil is specified by the changes of the second moment of area of the beam section and the mass of the beam segments along the longitudinal axis z, that is, assuming

$$I = (0.02z^2-0.6z+5.375)*10^{-6}\ (m^4) \qquad (4.1)$$

and

$$m = 0.0112z^2-0.495z+7.708\ (kg.) \qquad (4.2)$$

In so doing, we may readily determine the sectional parameters necessary for the element stiffness and mass matrices when we divide the beam as any desired number of segments. For example, if we use three uniform beam elements to represent the global tapered beam, then we use $z_1=2.5$, $z_2=7.5$ and $z_3=12.5$ to calculate the I_i and m_i for each beam element according to Eqs.(4.1) and (4.2). They are

$I_1=4*10^{-6}$, $I_2=2*10^{-6}$, $I_3=1*10^{-6}$ (m^4) and $m_1=6.54$, $m_2=4.03$, $m_3=3.27$ (kg)

In the computer simulation, three-segment piecewise continuous Timosenko beam model has been applied. For finite element analysis, the commonly used two-node and four-degree-of-freedom plane beam element has been selected. Table 4.1 exhibit the comparison of the frequency results calculated by both the piecewise continuous Timosenko beam model and the finite element model. The results show that at least ten beam elements are needed for the finite element analysis to achieve the comparable frequency values while the piecewise continuous Timosenko beam model uses only three beam segments. The advantage is clear in decreasing the number of elements by using the piecewise continuous Timosenko beam model to analyze large flexible tapered beam-like structures.

Table 4.1 The comparison of the results obtained from Finite Element Method & Piecewise Continuous Timoshenko Beam Model

(Circular Natural Frequency, rad/sec)

Order of Mode		1	2	3	4	5
Finite Element Analysis	Number of Elements N = 3	15.274	70.066	179.455	415.646	775.990
	4	13.364	61.444	159.541	305.038	577.351
	5	12.210	55.790	143.917	278.314	455.985
	6	11.208	51.205	131.761	253.865	419.438
	7	10.411	47.566	122.267	234.973	387.374
	8	9.760	44.592	114.562	219.847	362.437
	9	9.223	42.108	108.144	207.421	340.663
	10	8.748	39.989	102.689	198.878	323.080
Piecewise Continuous Model (N=3)		8.776	39.993	101.758	204.243	329.268

5. CONCLUDING REMARKS

This paper proposed a piecewise continuous Timoshenko beam model which is to be used for the dynamic analysis of large flexible tapered beam-like structures. The procedure for establishing natural frequency has been described in detail. A tapered beam is divided into several

segments of uniform beam elements. Instead of arbitrarily assumed shape functions used in finite element analysis,-the elosed-form solution of the Timoshenko beam equation has been used. Application of transfer matrix method relates all the elements as a whole. By corresponding boundary conditions and compatible conditions a characteristic equation for the global tapered beam has been yielded. Through the root-searching process to the characteristic equation the natural frequencies have been derived. A computer simulation is shown in this paper, and compared with the results obtained from the finite element analysis. While the comparable results is obtained, piecewise continuous Timoshenko beam model decreases the number of elements significantly.

REFERENCE

1. Balakrishnan, A.V.,"**A Mathematical Formulation of the SCOLE Problem, Part1**", NASA CR 172581, May 1985

2. Taylor, L.W., Jr. and Williams, J.,"**Maximum Likelihood Estimation for Distributed Parameter Models of Flexible Spacecraft**", IFAC/IFORS Symposium on Identification and Parameter Estimation, Beijing, China, 1988

3. Shen, J.Y., Huang, J.K. and Taylor, L.W., Jr.,"**Likelihood Estimation for Distributed Parameter Models of Large Beam-like Structures**", Journal of Sound and Vibration (1992) 155(3), pp467-480

4. Thomas, S.,"**A Continuum Model for Dynamic Analysis of the Space Station**", the 40th IAF International Astronautical Congress, Malaga, Spain, Oct.7-13,1989

5. Shen, J.Y. and Taylor, L.W., Jr.,"**Application of Transfer Matrix Method to Estimate the Modal Characteristics of the NASA Mini-Mast Truss**", NASA Workshop on Distributed Parameter Modeling and Control of Flexible Aerospace Systems, Williamsburg, VA. June 8-10,1992

6. Shen, J.Y. and Sharpe, Lonnie,"**Applying Transfer Matrix Method to Formulate a Distributed Parameter Model for the LACE Satellite Model**", accepted as NASA Contractor Report, 1992

7. Shen, J.Y., Huang, J.K. and Taylor, L.W., Jr.,"**Damping Models for Distributed Parameter Estimation of Large Beam-like Structures**", the Pacific-Rim International Conference on Modelling, Simulation and Identification, Vancouver, Canada, Aug.4-6, 1992

8. Shen, J.Y.,"**Maximum Likelihood Estimation for Distributed Parameter Models of Large Beam-like Structures**", Ph.D. Dissertation, Dept. of Mechanical Engineering & Mechanics, Old Dominion University, Norfolk, VA. Aug. 1991

Lumped Mass Modelling For the Dynamic Analysis of Aircraft Structures

Elias G. Abu-Saba, Ji Yao shen, and William M. Mcginley

Center for Aerospace Research
School of Engineering
North Carolina A & T State University
Greensboro, North carolina 27411

Raymond C. Montgomery
Aerospace Technologist
NASA-Langley Research Center
Hampton, Virginia 23665

Submitted to
The Journal of Aerospace Engineering
Aerospace division, American Society of Civil Engineering

ABSTRACT

Aircraft sctructures may be modelled by lumping the masses at particular strategic points and the flexibility or stiffness of the structure is obtained with reference to these points. Equivalent moments of inertia for the section at these positions are determined. The lumped masses are calculated based on the assumption that each point will represent the mass spread on one half of the space on each side. Then these parameters are used in the diferential equation of motion and the eigen characteristics are determined. A comparison will be made with results obtained by other established methods.

The lumped mass approach in the dynamic analysis of complicated structures provides an easier means of predicting the dynamic characteristics of these structures. It involves less computor time and avoids computational errors that are inherent to the numerical solution of complicated systems.

INTRODUCTION

The mass of the hypersonic plane is continuously distributed over the entire structure. Consequently, the real structure has an infinite number of degrees of freedom as far as the dynamic behavior is concerned. However, in the dynamic analysis of structures, it is possible to replace the real structure with an ideal one consisting of a number of lumped masses. These are assumed to be connected to one another through elastic massless elements which, to a certain extant , retain the actual behavior of the original structure. The method of idealizing actual structures bears significantly on the final results in any vibration analysis, and the selection of the method and the number of lumped masses for the system has to made while taking into consideration the various aspects of the structure under study. The skill and experience of the analyst are very helpful in obtaining the best ideal model for the structure.

In idealizing the hypersonic plane, there are certain assumptions which have to be made:

a. Idealization of real strucutres is limited to those structures which deflect in a linearly elastic manner. It is possible to extend the procedure to structures loaded in the plastic region, but the solution of such structures is more complex.

b. To be idealized, a structure must be stable under static loads. This condition applies for both determinate and indeterminate structures.

c. All structures demonstrate a certain amount of damping when they are subjected to dynamic loading conditions. Such damping in structures is controlled by structural hysteresis and by external friction. In the dynamic analysis of ordinary structures damping may be necglected in determining the natural frequencies, but it must be included in the evaluation of mode shapes under resonant conditions.

DEVELOPMENT OF THE METHOD

Consider that the frame of the hypersonic plane is fixed at the narrow end to act as a cantilever and that the masses are lumped as seen in Figure 2. In this study the shear and rotary inertia effects are ignored. the dynamic loading on the cantilever beam is the inertia of the moving bodies. The inertia force due to each body is expressed as

$$M_i Z_{im} = - M_i \omega_m^2 Z_{im} \qquad (1)$$

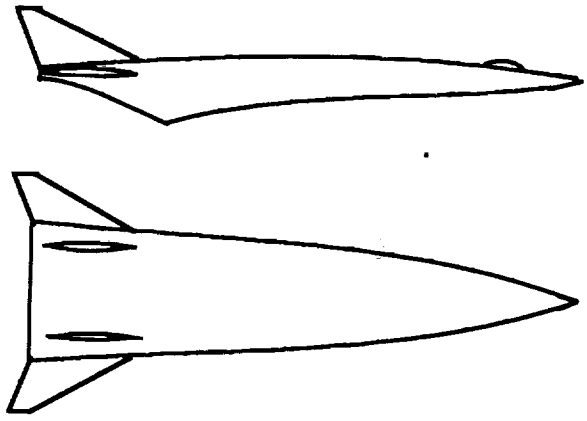

HYPERSONIC PLANE AT MACH 4

(a)

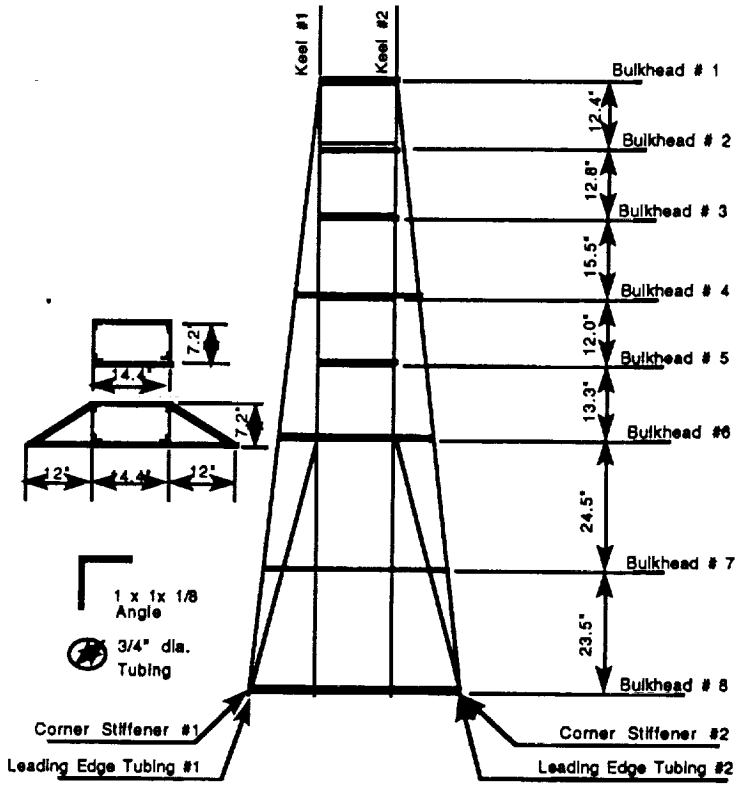

Stiffener Distribution
HYPERSONIC PLANE AT MACH 4

(b)

Figure 1

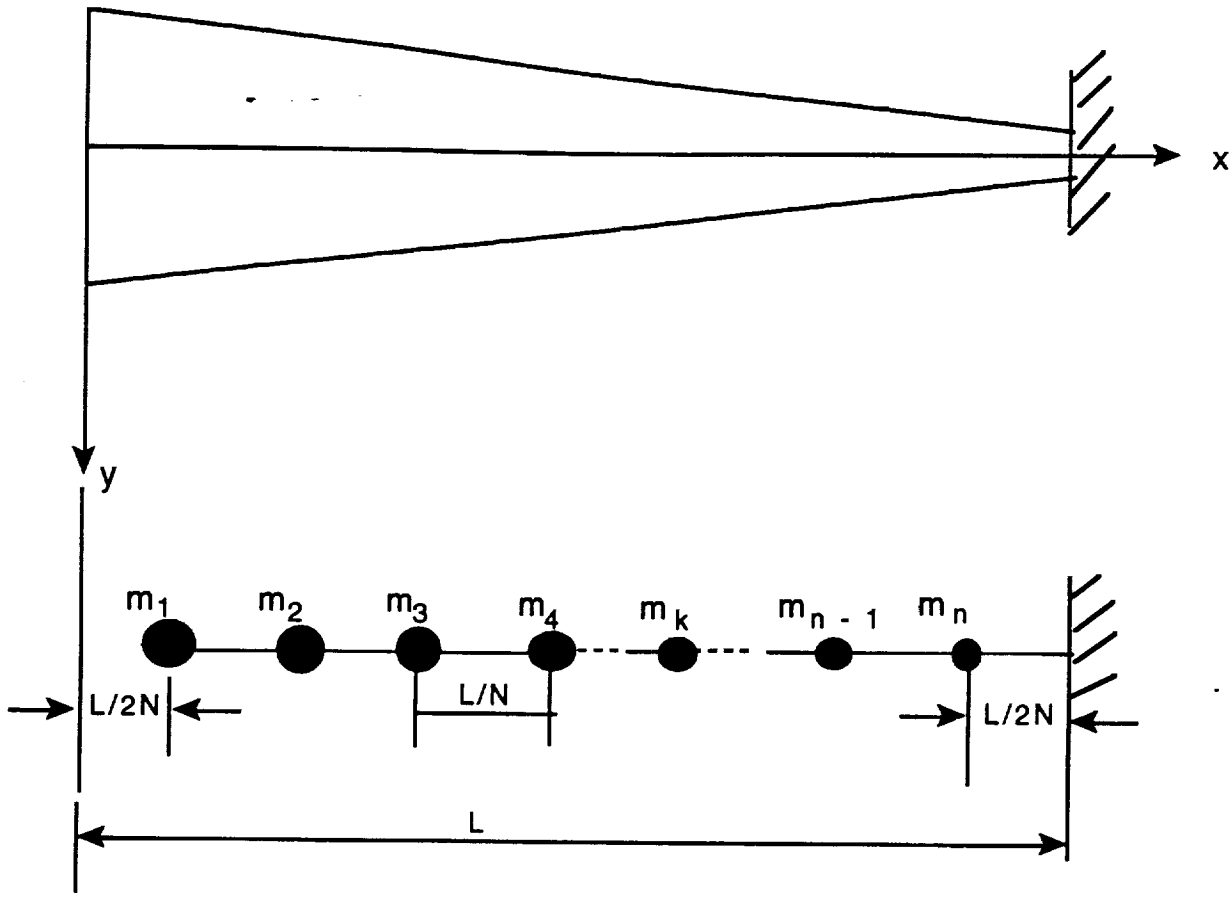

Figure 2

where:

M_i = the lumped mass at a point i

Z_{im} = the deflection of point i in the mth mode

Z_{im} = the acceleration of point i in the mth mode

ω = the circular frequency of the system vibrating in the mth mode

The deflection equation for the structure under dynamic loading due to inertial forces is expressed in the following form:

$$\{Z_m\} = \omega_m^2 [A] [M] \{Z_m\} \qquad (2)$$

where

$\{Z_m\}$ = a column matrix of the displacement of the structure in the mth mode.

$[A]$ = a square matrix of the flexibility coefficients of the structure

$[M]$ = a diagonal matrix of the mass of the structure.

Equation (2) can be expressed in the alternate form as in

$$0 = [D] \{Z_m\} \qquad (3)$$

where

$$[D_{\cdot}] = [[I] - \omega_m^2 [A][M] \quad (4)$$

To obtain a non-trivial solution for Equation (3), the determinant of matrix [D] must be identical to zero.

$$0 = |D| \quad (5)$$

The expansion of Equation (4) yields the characteristic equation for the stucture which is a polynomial. The nth degree of the characteristic equation is equal to the rank of the matrix [D]. The roots of this equation represent the eigen values of the structure.

DEVELOPMENT OF THE FLEXIBILITY MATRIX [A]

The model as shown in Figure 2 has displacement in one plane only. The displacements are considered to be lateral and rotational ones. The shear displacements are neglected in this model. The orientation of the model displacements is shown in Figure 3.

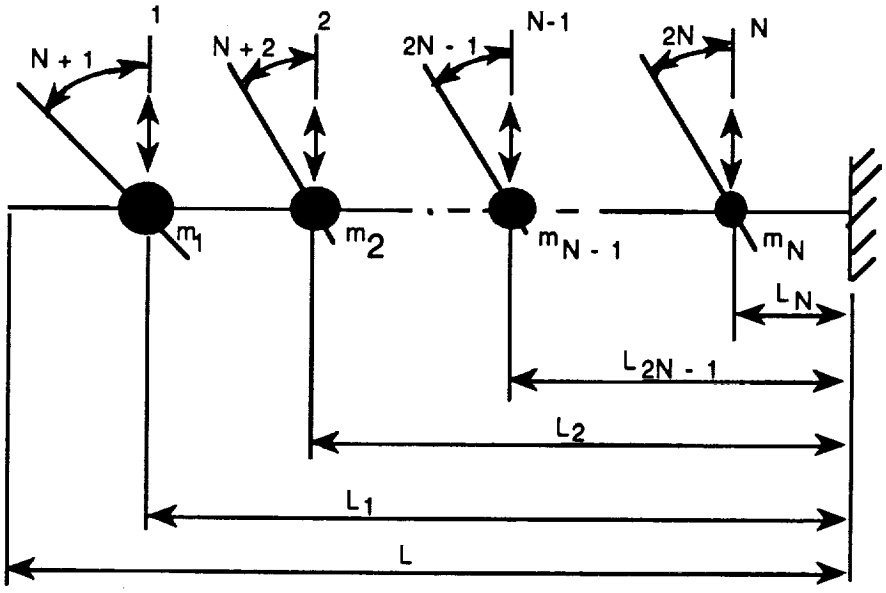

Figure 3

SYMBOLES

N = Number of lumped masses

L = Length of beam

I = Moment of inertia

E = Young's modulus of elasticity

m_i = ith mass of the beam/mass moment of inertia

ρ = Density of the beam per unit length

Considering that the beam is divided into equal segments along the longitudinal axis, the length of each segment is given by

$$\Delta = \frac{L}{N} \qquad (6)$$

The mass of a segment of the beam at any point i is

$$m_{ii} = \frac{2.788}{Ng} \left[14.4 + \frac{24}{114} (114 - x_i) \right] , i = 1, N \qquad (7a)$$

The function for x_i is given by the following:

$$x_1 = \frac{L}{2N} \qquad (7b)$$

$$x_i = x_{i-1} + \frac{L}{N} , \qquad i = 2, N \qquad (7c)$$

The mass moment of inertia is assumed to be that of a bar with a uniform mass over the length of the segment. It is given by the expression

$$mm_{ii} = m_{ii} \frac{l^2}{12} , i = N + 1 , 2N \qquad (8)$$

where $l = \frac{L}{N}$, mij = mji = 0 and mmij = mmji = 0

The flexibility matrix [A] in Equation 2 is expressed as follows:

$$[A] = \begin{matrix} A_{11} & A_{12} \\ A_{21} & A_{22} \end{matrix} \qquad (9)$$

where

[A_{11}] = is NxN matrix that represents the translational diasplacements due to unit lateral forces.

[A_{12}] = is NxN matrix that represents the rotational displacements due to unit lateral forces.

[A_{21}] = is NxN matrix that represents the translational displacements due to unit rotanational forces.

[A_{22}] = is NxN matrix that represents the rotational displacements due to unit rotational forces.

The matrix [A_{11}] is generated from the following equation:

$$a_{ij} = \frac{L^3}{6EI} \times \frac{1}{4N^3} [(2N + 1 - 2i)^3 - 3(2N + 1 - 2i)^2 (j-i) + 4 (j-i)^3] \qquad (10)$$

$$a_{ji} = a_{ij} \qquad (11)$$

for i = 1, N and j = i, N.

Matrix [A_{12}] is obtained by taking the derivative of Equation (9).

$$b_{ij} = - \frac{L^2}{2EI} (\frac{1}{4N^2})[(2N + 1 - 2i)^2 - 4(j -i)^2] \qquad (12)$$

for i = 1, N and j = i , N.

$$b_{ji} = b_{ii}, \quad i = 1, N \text{ and } j = 1, i \qquad (13)$$

The development of the matrix [A_{21}] follows from the application of unit moments at the position of the lumped masses on the beam and finding the lateral displacements that ensue from these actions. These displacements are given by

$$c_{ij} = \frac{L^2}{2EI}\left(\frac{1}{4N^2}\right)[(2N + 1 - 2i) - 2(j - i)]^2 \qquad (14)$$

for i = 1, N and j = i, N.

$$c_{ji} = c_{ii} + (i - j)\frac{L}{N} d_{ii} \qquad (15)$$

for i = 1, N and j = i, i - 1

The roatational displacements matrix [A_{22}] due to rotational forces is expressed as

$$d_{ij} = \frac{L}{EI}\left(\frac{1}{2N}\right)[(2N + 1 - 2i) - 2(j-i)] \qquad (16)$$

for i = 1, N and j = i, N.

$$d_{ji} = d_{ij}, \quad i = 1, N \text{ and } j = 1, i. \qquad (17)$$

Equations (10) through (17) define the flexibilty matrix for the entire structure. Having determined matrices [A] and [M], substitute them in Equation 4 and solve for the eigen values.

EXAMPLE

Consider that the hypersonic plane model is subdivided into three parts. The [A] and [M] matrices are given below.

$$[A] = \begin{matrix} A_{11} & A_{12} \\ A_{21} & A_{22} \end{matrix}$$

$$[A_{11}] = \frac{L^3}{648EI}\begin{matrix} 125 & 54 & 7 \\ 54 & 27 & 4 \\ 7 & 4 & 1 \end{matrix}$$

$$[A_{12}] = -\frac{L^2}{72EI}\begin{matrix} 25 & 21 & 9 \\ 9 & 9 & 5 \\ 1 & 1 & 1 \end{matrix}$$

$$[A_{21}] = \frac{L^2}{72EI}\begin{matrix} 25 & 9 & 1 \\ 21 & 9 & 1 \\ 9 & 5 & 1 \end{matrix}$$

$$[A_{22}] = \frac{L}{6EI}\begin{matrix} 5 & 3 & 1 \\ 3 & 3 & 1 \\ 1 & 1 & 1 \end{matrix}$$

$$[M] = \begin{matrix} M1 & 0 \\ 0 & M2 \end{matrix}$$

where

$$[M_1] = \frac{1}{386.4} \begin{matrix} 33.0 & 0.0 & 0.0 \\ 0.0 & 25.3 & 0.0 \\ 0.0 & 0.0 & 17.7 \end{matrix}$$

and

$$[M_2] = \frac{1083}{386.4} \begin{matrix} 33.0 & 0.0 & 0.0 \\ 0.0 & 25.3 & 0.0 \\ 0.0 & 0.0 & 17.7 \end{matrix}$$

The modulus of elasticity $E = 10^7$ psi. The equivalent average moment of inertia $I = 42.5$ in^4. The length of the beam $L = 114$ in. With the values of the matrices [A] and [M] known, the solution of Equation (5) provides the following frequency results.

The natural frequencies ensuing from the model with three lumped masses are given in the first row for the first six modes. Values in subsequent rows correspond to models of 4, 5, 6, and 7 lumped masses.

Natural Frequency in Hz for a Lumped Mass system

Number of Elements	Number of Modes					
	1	2	3	4	5	6
3	19.54	146.08	396.08	560.60	1329.9	2125.6
4	19.21	138.15	411.18	454.22	1041.8	1492.6
5	19.08	134.70	399.10	509.07	779.19	1661.1
6	19.00	132.87	391.36	558.29	778.32	1247.7
7	18.95	131.78	386.46	603.53	770.65	1273.1

Natural Frequency in Hz for a Finite Element Model

Number of Elements	Number of Modes					
	1	2	3	4	5	6
3	18.11	132.15	385.01	874.00	1656.55	3108.26

CONCLUSION

A lumped mass model for the hypersonic transport airplane has been established. Algorithms for the determination of the flexibility matrix [A] and the mass and mass moment of inertia matrix [M] have been found. The natural frequencies for a 3-lumped mass system have been determined using the lumped mass method and the finite element method. The results from the two methods converge in the lower three modes and diverge in the upper three ones. The lumped mass system requires less computer time than the finite element model. For models with a large number of elements, the lumped mass system is more efficient. Results from both models need to be verified experimentally.

Full design of fuzzy controllers using genetic algorithms

Abdollah Homaifar
Ed McCormick

NASA Center of Research Excellence / Controls and Guidance Group
North Carolina A&T State University, Dept. of Electrical Engineering
McNair Building, Greensboro, North Carolina 27411

ABSTRACT

This paper examines the applicability of genetic algorithms in the complete design of fuzzy logic controllers. While GA has been used before in the development of rule sets or high performance membership functions, the interdependence between these two components dictates that they should be designed together simultaneously. GA is fully capable of creating complete fuzzy controllers given the equations of motion of the system, eliminating the need for human input in the design loop. We show the application of this new method to the development of a cart controller.

1.INTRODUCTION

Genetic algorithms (GA) are powerful search procedures based on the mechanics of natural selection. They use operations found in natural genetics to guide them through the paths in the search space. They provide a means to search poorly understood, irregular spaces. Because of its robustness, GA has been successfully applied to a variety of function optimizations, self-adaptive control systems, and learning systems.

Fuzzy systems arose from the desire to describe complex systems with simple tools. In contrast to boolean systems where an item either has a membership of {1} or {0} in a set, fuzzy systems allow for degrees of membership over the range {0-1}. This imitates the linguistic approach to describing conditions (i.e. cold, very warm) used in everyday life.

Interest in fuzzy controllers has recently been gaining in popularity across a broad array of disciplines and with good reason. Fuzzy controllers allow for a simpler, more human approach to control design and do not demand the mathematical modelling knowledge of more conventional control design methods. As systems become more complex, the ability to describe them mathematically becomes more difficult. For this reason, fuzzy controllers provide reasonable, effective alternatives to classical or state-space controllers.

By using a linguistic approach, it is easy to see that fuzzy theory can be integrated into control theory using rules of the form *IF*{condition} *THEN*{action}. Using these rules, one can create a functional controller. The problem with this method comes from determining the appropriate rules and determining the shape of the membership functions.

This work sought to use genetic algorithms in the design and implementation of fuzzy logic controllers. Previously, generation of membership functions had been a task mainly done either iteratively, by trial-and-error, or by human expert. A task such as this was a natural candidate for GA since GA will attempt to create membership functions that will cause the controller to perform optimally. In much the same manner, GA could be used to generate the rules which use these membership functions. Work had been done using GA to do each of these tasks separately, but since the two are co-dependent, using a hand-designed rule set with GA designed membership functions or hand-designed membership functions with a GA designed rule set does not use GA to its full advantage. Thus, the use of GA to determine both simultaneously and determine an optimal or near-optimal controller was the main objective of this work.

The problem used to check the effectiveness of this method was centering and stopping a cart located on a one-dimensional track as described by Thrift[1]. Given an initial velocity and location on the track, the objective was to determine a controller which will bring the cart to zero velocity and zero location in minimum time. Different controllers were designed for this problem by dividing the input and output spaces into different partition sizes.

2. GENETIC ALGORITHMS AND FUZZY CONTROLLERS

2.1 Genetic Algorithms

Genetic Algorithms are general purpose optimization algorithms with a probabilistic component. They provide a means to search poorly understood, irregular spaces. John Holland originally developed GA and provided its theoretical

foundation in his book, Adaptation in Natural and Artificial Systems[2]. Holland developed GA to simulate some of the processes observed in natural evolution. Evolution is a process that operates on chromosomes (organic devices for encoding the structure of living beings) rather than on living beings. Natural selection links chromosomes with the performance of their decoded structure. The processes of natural selection cause those chromosomes that encode successful structures to reproduce more often than those that do not. Recombination processes create different chromosomes in children by combining material from the chromosomes of the two parents. Mutation may cause the chromosomes of children to be different from those of their parents.

GA appropriately incorporates these features of natural evolution in computer algorithms to solve difficult problems in the way that nature has done -- through evolution. GA requires the problem to be maximized (or minimized) to be stated in the form of a cost (objective) function. In GA, a set of variables for a given problem is encoded into a string (or other coding structure), analogous to a chromosome in nature. These strings are converted to a numerical value and then linearly mapped over the range allowed for the variable. This value is then used to evaluate the cost function, yielding a "fitness." GA selects parents from a pool of strings (population) according to the basic criteria of "survival of the fittest." It reproduces new strings by recombining parts of the selected parents in a random manner. Although GA is a stochastic method, it is not a simple random walk. It exploits historical information to guide the search with improved performance.

The repopulation of the next generation is done using three methods: reproduction, crossover, and mutation. Reproduction means simply that strings with high fitnesses should receive multiple copies in the next generation while the strings with low fitnesses receive fewer copies or even none at all. Crossover refers to taking a fit string, splitting it into two parts at a randomly generated crossover point and recombining it with another string which has also been split at the same crossover point. This procedure serves to promote changes in the best strings which will give them even higher fitnesses. Mutation is the random alteration of a bit in the string. This will assist in keeping diversity in the population.

In explaining the inner workings of GA, let us initially make a few definitions[3]. Since we are dealing with binary strings, a notation must be developed to denote similarity subsets (*schemata*). A schema is a similarity subset which contains strings that have similarities at some bit positions. We can expand this thinking even further with the introduction of a wild card character, *, in addition to the binary set {0,1}. For example, the set {0001,0101,0011} can be described by the *similarity template* 0**1. Using this notation, we can now define a schema's *order* and *defining length*. For a given schema, h, its order o(h) is defined as the number of fixed bit positions within that schema. The defining length of a schema, δ(h), is the distance between the outermost defining positions of a schema. As an example, the schema 01****0 has order 3 and defining length 5.

With these definitions we can now present the fundamental theorem of genetic algorithms, the *schema theorem*[4]. The schema theorem enables us to calculate a lower bound on the expected number of a particular schema, h, following reproduction, crossover, and mutation[2,3]. The theorem is stated as:

$$\lambda(h,t+1) \geq \lambda(h,t)\frac{f(h)}{f}\left[1 - p_c\frac{\delta(h)}{l-1} - p_m o(h)\right] \qquad (1)$$

where λ is the expected number of schemata, t is the generation index, l is the overall string length, f(h) is the average fitness of those strings representing the subset h, f is the average fitness of the entire population, p_c and p_m are, respectively, the crossover and mutation probabilities. Examining the schema theorem, we see that it states that a schema will grow when it is short, has low order, and has above average fitness.

Given a history of genetic algorithms, one might ask what advantages does it have over other methods. GA's primary advantage over other methods is its robustness. GA works through function evaluation, not through differentiation or other such means. Because of this trait, GA does not care what type of problem it is asked to maximize, only that it be properly coded. Thus GA is able to solve a wide range of problems: linear, nonlinear, discontinuous, discrete, etc.

2.2 Fuzzy Controllers

Fuzzy theory extends from the inability to describe some physical phenomena with the exact mathematical models dictated by more conventional, boolean models. Fuzziness describes event ambiguity. It measures the degree to which an event occurs, not whether it occurs[5]. The fact that fuzziness is lacking in precision has led to its dismissal by some researchers. Others, however, see fuzzy theory as a powerful tool in the exploration of complex problems because of its ability to determine outputs for a given set of inputs without using a mathematical model. As Jain noted[6], the basic motivation behind fuzzy set theory was the fact that the conventional methods had become so complex that researchers trying to apply

them had to make a choice between a complex system and a complex tool.

Fuzzy theory owes a great deal to human language. As explained by Leung[7], daily languages cannot be precisely characterized on either the syntactic or semantic level. When we speak of temperature in terms such as "hot" or "cold" instead of in physical units such as degrees Fahrenheit or Celsius, we can see language becomes a fuzzy variable whose spatial denotation is imprecise. In this sense, fuzzy theory becomes easily understood because it can be made to resemble a high level language instead of a mathematical language. As an example, consider the fuzzy variable TEMPERATURE. The fuzzy set describing TEMPERATURE can be categorized as five fuzzy-set values {very cold (VC), cold (C), medium (M), hot (H), very hot(VH)}. Figure 1 shows one possible set of the membership functions of the fuzzy-set values VC, C, M, H, and VH for the range of TEMPERATURE 0°-130° F. Note that every value of temperature has a membership in every fuzzy-value set although in most cases this membership is 0.

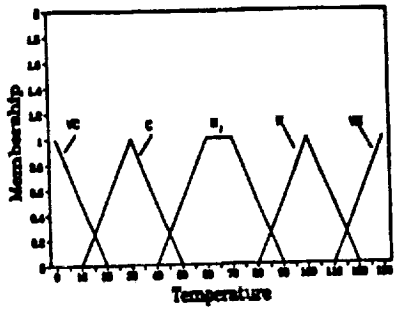

Figure 1 Fuzzy-Set Variables for the Fuzzy Variable TEMPERATURE

Also, some values of TEMPERATURE overlap into two fuzzy-value sets. For example a temperature of 47° has membership in both "cold" and "medium" although the membership in "medium" is larger than the membership in "cold." This example shows how membership functions play the role of discretizing the linguistic terminology to values a computer can use. Of course in most respects these membership functions are subjective in nature. What determines the ranges for these fuzzy-set values or the shape of these membership functions? In most cases, membership functions are designed by experts with a knowledge of the system being analyzed. However, human experts cannot be expected to provide optimal membership functions for a given system. Often, these functions are modified iteratively while trying to obtain optimality.

How are these membership functions used in fuzzy controllers? In its simplest form a fuzzy logic controller is simply a set of rules describing a set of actions to be taken for a given set of inputs. It is easiest to think of these rules as if-then statements of the form *IF*{set of inputs} *THEN*{outputs}. For the example above, a fuzzy controller can be used for a thermostat. One rule might be *IF*{very cold} *THEN*{turn furnace on for x minutes}. Another may be *IF*{hot} *THEN*{turn air conditioner on for y minutes}. Since "very cold" applies to a range of temperatures which also may belong to another fuzzy-set variable (i.e. "cold") which has rules of its own, the output which results from "defuzzification" of the application of these rules must take into account how much each rule applies before determining how much output must be applied. Usually a centroid method is used to account for the influence of each rule on the output.

2.3 Applicability of GA to Fuzzy Controllers

The application of genetic algorithms to fuzzy logic controllers holds a great deal of promise. Previous work has been done mainly in two areas: learning the fuzzy rules used in a controller and learning membership functions. These two areas are the most time consuming of fuzzy controller design and are for the most part done by trial-and-error. This methodology is lacking in two main respects: it may take too much time to get a satisfactory rule set or set of membership functions and there is little chance that these sets will be optimal. Genetic algorithms has the ability to improve both of these shortcomings. GA's robustness enables it to cover a complex search space in a relatively short period of time while ensuring an optimal or near-optimal solution. Because of this capability, GA is a natural match for fuzzy controllers.

Thrift's paper[1] examined the feasibility of using GA to find fuzzy rules. In this paper, fuzzy control synthesis was done in decision table form. The problem examined was centering a cart of mass m on a one dimensional track. The objective is to move the cart from a given initial position and velocity to zero position and velocity in minimum time. This is done through the application of a force F from the controller. For 100 runs with random starting points, the average number of time steps for the hand-designed fuzzy controller to bring the cart to zero position and velocity was 164. I

comparison, a GA designed controller using the same starting points had an average of 143 time steps. As Thrift noted, while the GA based fuzzy rules performed reasonably well, work could be done to further improve its performance, such as letting GA determine the endpoints of the membership functions.

Karr[8] examined using GA to find high-performance membership functions for a controller for the a pole-cart system. The task for the controller is as follows:

> A wheeled cart has a rigid pole hinged to its top. The cart is free to move right or left along a straight bounded track and the pole is free to move within the vertical plane parallel to the track. The cart is to be kept within the predefined limits of the track and the pole should be prevented from falling beyond a predefined vertical angle by applying a force of fixed magnitude to the left or right of the base of the cart.

The objective is to bring the cart to rest at the center of the track with the pole balanced, much the same as in Thrift's paper. Also, he examined the use of micro-GA, a small population GA developed by Krishnakumar[9], to determine an adaptive real-time controller for the same problem where system parameters may be time varying. In determining the membership functions, GA was used to determine the anchor points for each of the linguistic variables used. For the non-adaptive problem, the GA designed fuzzy logic controller consistently outperformed the hand-designed controller. For the adaptive controller, the performance was even better: the non-adaptive author designed controller always became unstable, while the non-adaptive GA controller and the micro-GA designed adaptive controller were always able to complete the task. The difference between the two GA designed controllers was in their convergence times; the micro-GA controller consistently balanced the system faster than the non-adaptive GA controller.

Previous work done with optimizing fuzzy controllers has dealt with optimizing membership functions or rule sets. For example, Mamdani and Procyk[10] iteratively designed membership functions, Thrift[1] used GA to design rule sets, and Karr used GA to design membership functions[11]. These methodologies have a major limitation; how can an optimal design be obtained when one of the two main components is designed in a non-optimal method. Logically, to obtain an optimal rule set and set of membership functions, the two must be designed together so the links between them can be fully exploited. By using GA to design both simultaneously, the two elements of fuzzy controllers can be fully integrated to deliver a more finely tuned, high performance controller.

3. PROBLEM DESCRIPTION AND METHODOLOGY

3.1 Cart-Centering Problem

A common problem used in literature is the centering of a cart of mass m, on a one-dimensional track. The input variables for this problem are the cart's location on the track, x, and the cart's velocity, v. The objective was to find a controller which could provide a force F which would bring the cart to x=0 and v=0 from an arbitrary initial condition (x_0 and v_0) in minimum time. The equations of motion for the cart are:

$$x(t+\tau) = x(t) + \tau\, v(t)$$
$$v(t+\tau) = v(t) + \tau \frac{F(t)}{m} \qquad (2)$$

where τ is the time step. The values for the constants and the range of values of the variables are given in Table I.

Three controllers were developed for the cart-centering problem. They will be referred to by the number of fuzzy sets that partition the x-location, velocity, and output. For example, the controller which had the velocity divided into 5 fuzzy sets, the x-location divided into 5 fuzzy sets, and the output divided into 5 fuzzy sets was called the 555 controller. While GA was allowed to determine the location of the triangle bases for the input variables, the output fuzzy set locations were fixed. The different output fuzzy membership functions are shown in Figures 2-4.

Table I Constants and Ranges for Cart Problem

Variable or Constant	Value
m	20 kg
τ	.02 sec
x	-2 to +2 m
v	-2 to +2 m/s
F	-150 to +150 N

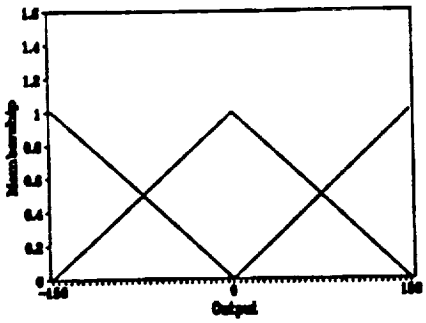

Figure 2 Output Divided Into 3 Fuzzy Sets

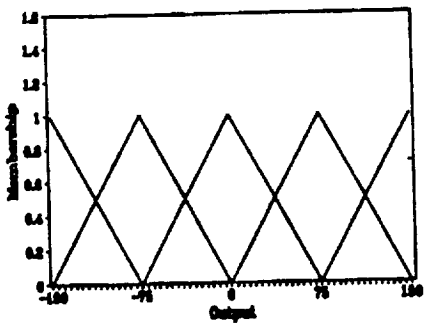

Figure 3 Output Divided Into 5 Fuzzy Sets

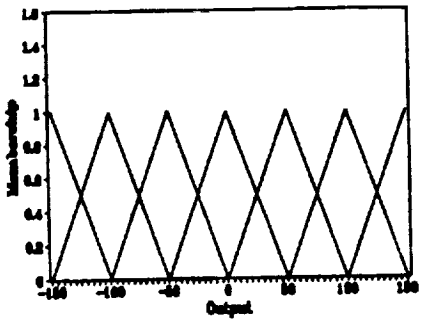

Figure 4 Output Divided Into 7 Fuzzy Sets

3.2 Software and Modifications

The basis for the software used in this paper is the Simple Genetic Algorithm (SGA) program developed by Goldberg[3]. The program was run on a 25 MHz 80386 computer with a 80387 math coprocessor. The SGA program allows the user to define the values for population size, maximum number of generations, probability of crossover, and probability of mutation. The values used for these parameters are given in Table II. Since run time became extremely long, population size was kept at a relatively small number, 100. This did lead to difficulties when larger string sizes were used and will be discussed in the following chapter.

3.3 Modification of String Structure

The Simple Genetic Algorithm uses binary strings to encode the parameters which are to be optimized. While this method could also be used in the determination of the fuzzy controller design, a more representative method was chosen.

First, the number of alleles was determined from the size of the rule set plus the number of fuzzy sets used to partition the

Table II Parameters Used in SGA Program

Parameter	Value
Population Size	100
Max. No. of Generations	100
P_c	0.7
P_m	0.03

spaces of the input variables. For the cart centering problem, the shapes of the triangles which formed the output space were fixed, while the input variables, x-location and velocity, were each partitioned using five triangles: negative medium (NM), negative small (NS), zero (ZE), positive small (PS), and positive medium (PM). The rule set, then, contained twenty-five (5 x 5) rules to account for every possible combination of input fuzzy sets. The rules are of the form, *IF*(x is {NM, NS, ZE, PS, or PM}) and (v is {NM, NS, ZE, PS, or PM}) *THEN* {*output*}, where *output* is one of the fuzzy sets used to partition the output space. The two input spaces use a total of ten triangles, so the string to represent a given rule set and membership function combination would have thirty-five alleles (25 + 10). Note that the term alleles is used instead of bits, because the value of each allele contains either the output fuzzy set to be used (for the first twenty-five alleles where NM=1, NS=2, etc.) or the value which will be converted to the length of the base of the triangles which make up the input spaces (the last ten alleles). The calculation of the triangle bases from the allele values (1-5) were done as follows:

1. Subtract 1 from the allele value (making the range now 0-4).
2. Subtract this value from 1 (which is the distance between the peaks of each triangle).
3. Double this value and divide by 10, giving the base length for each particular triangle. This value can be anywhere from 1.2m to 2.0m.

Thus we are able to incorporate the two main ingredients of a fuzzy controller, the rule set and the membership functions, into a single string which GA will seek to optimize. This is shown in the following example.

```
String: 14321524321245143122113454525234124
String: |14321524321245143122113454| 45252 | 34124 |
        |        rule set           | x-location | velocity |
        |                           | locations  | locations |
```

x-location

velocity	NM	NS	ZE	PS	PM
NM	1	4	3	2	1
NS	5	2	4	3	2
ZE	1	2	4	5	1
PS	4	3	1	2	2
PM	1	1	3	4	5

Rule Set

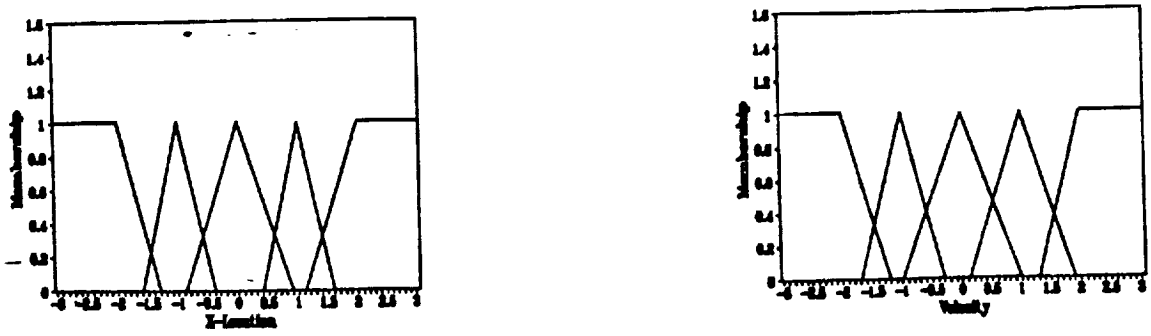

Figure 5 Example of String-Fuzzy Controller Conversion

4. SIMULATION RESULTS

4.1 Initial Conditions

To find a satisfactory controller, the controller must be able to operate over the entire range of the input spaces. For GA to properly design fuzzy controllers, this fact must be integrated into the function evaluation. This was done by using multiple initial conditions in the evaluation of each member of the population. If a single initial condition were used, for example $x_0 = 0.7$m and $v_0 = -0.5$m/s, then GA would find a controller which would work well around that particular point but may fail elsewhere. This makes the choice of initial conditions an important consideration. The points must be chosen to sufficiently cover the input spaces, but at the same time, the more initial conditions used, the more time the program takes to run. These initial conditions are listed in Table III.

4.2 Fitness Function

The fitness function proved to be the most challenging aspect of applying GA to fuzzy controller design. As stated earlier, the process finally was divided into two stages, an evolution stage and a refinement stage. In the evolution stage, GA was used to find satisfactory controllers, while in the refinement stage, GA used the previously developed controllers and attempted to minimize the amount of time needed to bring both x-location and velocity to zero.

Table III Initial Conditions

Controller	Initial Conditions (x_0, v_0)
333	(-2,-2) (-2,2) (0,0) (2,-2) (2,2)
5557	(-2,-2) (-2,2) (-1,-1) (-1,1) (0,0) (1,-1) (1,1) (2,-2) (2,2)
777	(-2,-2) (-2,0) (-2,2) (-4/3,-4/3) (-4/3,4/3) (-2/3,-2/3) (-2/3,2/3) (0,0) (2/3,-2/3) (2/3,2/3) (4/3,-4/3) (4/3,4/3) (2,-2) (2,0) (2,2)

For the first stage, which lasted through generation 30, the fitness function rewarded a member of the population according to how well it came to the tolerance value, ± 0.5 for both x-location and velocity. If the controller succeeded in bringing x and v within the tolerance, it was given a fitness relative to the time it took. If the controller "timed out," it was either slightly punished with a negative fitness or slightly rewarded depending on x-location and velocity. If the controller diverged, the fitness was given a larger negative value. The first fitness function is shown below.

```
if (|x| < 0.5) and (|velocity| < 0.5) then
   fitness = 8 * 175 / time
else if (time = 175) then
   if (|x| < 1.0) and (|velocity| < 1.0) then
      fitness = 3.5 / sqrt( x² + velocity² )
   else
      fitness = -1
else
   fitness = -7
```

The total fitness was then given by the sum of the fitnesses determined for each initial condition. Through the use of this reinforcement/reward scheme, GA was able to develop controllers which could solve all the initial conditions.

The second stage, from generation 31 to generation 100, was based almost completely on time. If the controller reached the tolerance values it was rewarded according to how short a time it took. If the controller "timed out," it was punished according to how much it missed the tolerance values, and if the controller diverged, it was given a very large negative fitness which would probably ensure its failure to continue on to the next generation. This fitness function was given as:

```
if (|x| < 0.5) and (|velocity| < 0.5) then
   fitness = 3 * (175 - time)
else if (time = 175) then
   fitness = -42 * sqrt( x² + velocity² )
else
   fitness = -300
```

4.3 333 Controller

The 333 controller was the simplest controller to design. It consisted of only 9 rules, and the number of triangle base locations to be determined was 6, yielding a total string length of 15. The controller determined by GA is shown in Figure 6.

velocity \ x	N	ZE	P
N	3	3	1
ZE	3	2	1
P	3	1	1

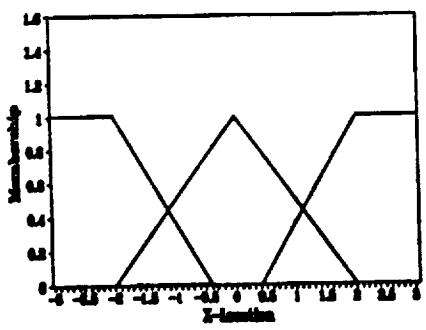

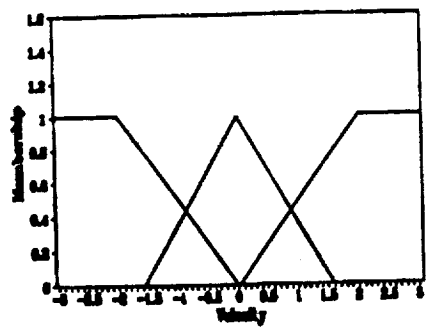

Figure 6 333 Controller

4.4 555 Controller

The 555 controller used 25 rules and needed 10 alleles to determine the location of the bases of the fuzzy sets covering the input spaces. With a total string length of 35, the first indication that better performance could be obtained with larger population sizes became apparent. Considering that each allele could have a value between 1 and 5, this meant that if a binary string had been used, 3 bits would be necessary to represent the same information. This would yield a string length of 105. A population of 100 cannot begin with enough diversity to ensure that the search space will be sufficiently covered to enable GA to find the optimal solution. Even with a relatively small population size, the run time took between two and one-half to three hours. However, the performance of the controller did indicate that GA was finding a near-optimal controller. Figure 7 shows the resultant best controller determined by GA.

velocity \ x	NM	NS	ZE	PS	PM
NM	5	4	4	4	2
NS	5	5	5	1	1
ZE	5	5	3	1	1
PS	5	5	1	1	1
PM	4	2	2	2	1

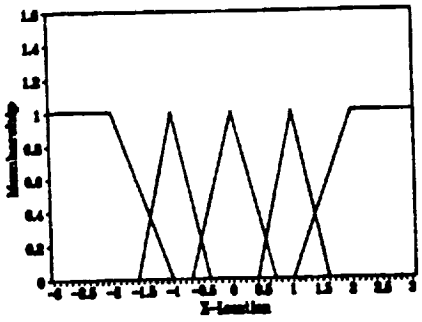

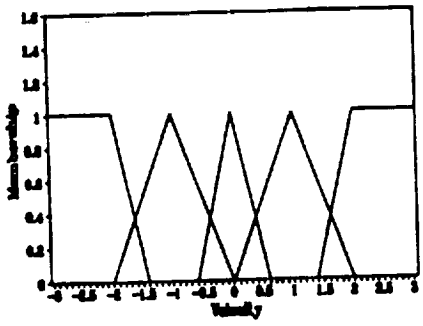

Figure 7 555 Controller

4.5 777 Controller

The final controller designed was the 777 controller. This controller took the most computer time to design because of the long string length (63 alleles) and the large number of initial conditions (17). Run times took between seven and eight hours. The best performing controller designed by GA is shown in Figure 8.

4.6 Comparison of Cart Controllers

Once GA had been used to determine the different controllers, a study was made to determine their performance and stability. Because there is no accepted method to determine stability for fuzzy controllers as there is for classical and state-space controllers, a "brute force" method was adopted. To examine the controllers, the input space of each variable was divided into 40 points. Then each point was examined, one by one, to determine if the controller diverged anywhere in the input space. For 40 points in the x-location space and 40 points in the velocity space, this yields a total of 1600 points. While the ability of a controller to satisfy all these points does not necessarily guarantee its stability (since it only takes one point to make a controller unstable), this did ensure some measure of confidence in the procedure. While examining each point, it was a simple task to also count the number of time steps used to bring all these points within the tolerance values and these numbers are given in Table IV. Also shown in Table IV is an additional 555 controller designed with th

membership functions fixed. GA was used to design only a rule set, with the membership function being done by hand. This controller, shown in Figure 9, was created for comparison purposes to illustrate the importance of membership function selection. As Table IV shows all the controllers were able to successfully bring the system within the tolerance values.

velocity \ x	NL	NM	NS	ZE	PS	PM	PL
NL	7	5	3	7	7	1	2
NM	7	6	6	7	3	2	1
NS	7	6	7	7	1	1	1
ZE	7	5	7	5	1	2	2
PS	6	6	6	1	1	4	1
PM	6	6	6	1	1	6	1
PL	6	5	1	1	5	2	1

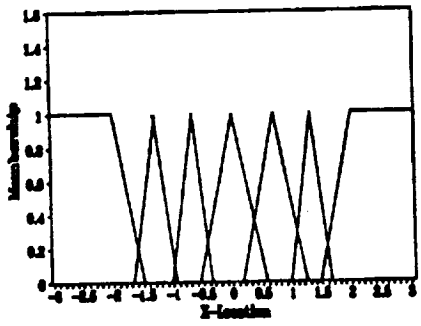

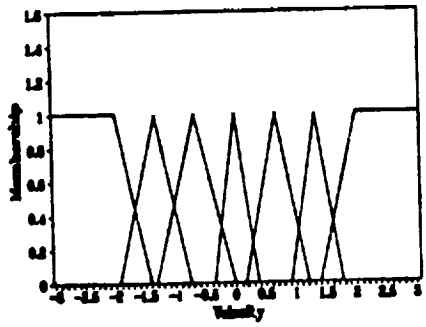

Figure 8 777 Controller

Table IV Comparison of Cart Controllers

	333	555	777	555 fixed
No. of Initial Conditions	1600	1600	1600	—
Time Steps Required	82380	68208	78958	90156
Avg. No. of Time Steps	51.49	42.63	49.35	56.35
% Difference w/555 Controller	20.8%	—	14.8%	32.2%
No. of Failures	0	0	0	0

Table IV shows that the best performance, on average, came from the 555 controller. The 333 controller, while being the simplest, did not have the flexibility to produce fast response times. On the other hand the 777 controller had too much flexibility and became bogged down in the number of rule evaluations required for each force calculation. Finally, note that while the 555 controller with the fixed membership function was able to bring the cart to equilibrium for all points, its performance was clearly inferior, needing almost 1/3 longer than the GA designed rule set and membership function combination, indicating the importance of proper membership function design.

velocity \ x	NM	NS	ZE	PS	PM
NM	5	5	5	3	2
NS	5	5	5	1	1
ZE	5	5	3	1	1
PS	5	5	1	1	1
PM	5	1	4	2	1

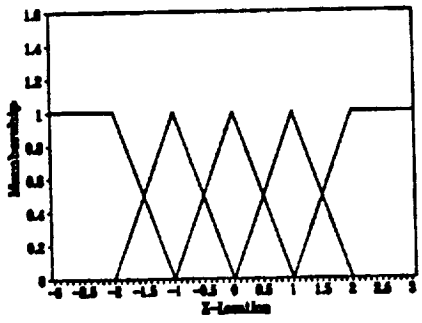

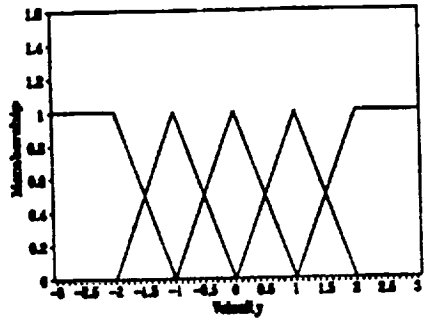

Figure 9 555 Controller w/ Fixed Membership Functions

5. CONCLUSION

This paper clearly shows the potential for using genetic algorithms to solve optimization problems. The ability of fuzzy logic controllers to provide control where more conventional methods become too complex has also been shown by researchers. This work has shown these two, fairly new, methods can be used to together to form controllers without the previously needed human expert. This methodology allows the complete design of both major components of fuzzy controllers, the rule sets and membership functions, leading to high performing controllers which are completely computer designed. We have shown three different controllers for the cart problem, each of which was able to bring the cart to equilibrium over the entire ranges of the input spaces. While these results are encouraging, more work must be done on refining the process. First, more powerful and faster computers will allow the use of larger population sizes, and, therefore, greater diversity. Work will be done to examine the development of a robust controller, where the parameters in the equations of motion are nc longer fixed to a specific value, but can instead be a range of values. Also, the need to ensure the performance of the controller when faults occur in the rule set should be investigated to see if this would alter the configuration of the rule set. Finally, controllers for other problems should be developed to show the effectiveness of this method.

6. ACKNOWLEDGMENTS

This work is supported by grants from Honeywell Inc. under grant number 48057 and the NASA Center for Research Excellence at N.C. A&T State University under grant number NAGW-2924. The authors wish to thank them for their

financial support which made this work possible.

7. REFERENCES

1. Thrift, P., "Fuzzy Logic Synthesis with Genetic Algorithms," Proceedings of the Fourth International Conference on Genetic Algorithms, Morgan Kaufmann Publishers, Inc., San Mateo, CA, 1991, pp.509-513.
2. Holland, J.H., Adaptation in Natural and Artificial Systems, The University of Michigan, Ann Arbor, MI, 1975.
3. Goldberg, D.E., Genetic Algorithms in Search, Optimization and Machine Learning, Addison-Wesley, MA, 1989.
4. Holland, J.H., "Schemata and intrinsically Parallel Adaptation," Proceedings of the NSF Workshop on Learning System Theory and Application, Gainsville, FL, University of Florida Press, 1975, pp.43-46.
5. Kosko, B., Neural Networks and Fuzzy Systems: A Dynamical Systems Approach to Machine Intelligence, Prentice Hall, Englewood Cliffs, NJ, 1992.
6. Jain, R., "Fuzzyism and Real World Problems," Fuzzy Sets: Theory and Applications to Policy Analysis and Information Systems, Wang, P.P, and Chang, S.K. (Eds.), Plenum Press, New York, NY, 1980.
7. Leung, Y., Spatial Analysis and Planning Under Imprecision, Elsevier Science Publishers B.V., New York, NY, 1988.
8. Karr, C.L., "Design of an Adaptive Fuzzy Logic Controller Using a Genetic Algorithm," Proceedings of the Fourth International Conference on Genetic Algorithms, Morgan Kaufmann Publishers, Inc., San Mateo, CA, 1991, pp.450-457.
9. Krishnakumar, K., "Microgenetic Algorithms for Stationary and Nonstationary Function Optimization," SPIE Proceedings on Intelligent Control and Adaptive Systems, Vol. 1196, pp.289-296, November, 1989.
10. Procyk, T.J., and Mamdani, E.H., "A Linguistic Self-Organizing Process Controller," Automatica, Vol. 15, No.1, pp.15-30, 1979.
11. Karr, C., "Genetic Algorithms for Fuzzy Controllers,", AI Expert, February 1991, PP.26-33.

Nonlinear Robust Controller Design for Multi-Robot Systems with Unknown Payloads

Y. D. Song J. N. Anderson* A. Homaifar H. Y. Lai

NASA Center for Aerospace Research
North Carolina A&T State University, Greensboro, NC 27411

* Center for Manufacturing Research
Tennessee Technological University, Cookeville, TN 38505

Abstract

This work is concerned with the control problem of a multi-robot system handling a payload with unknown mass properties. Force constraints at the grasp points are considered. Robust control schemes are proposed that cope with the model uncertainty and achieve asymptotic path tracking. To deal with the force constraints, a strategy for optimally sharing the task is suggested. This strategy basically consists of two steps. The first detects the robots that need help and the second arranges that help. It is shown that the overall system is not only robust to uncertain payload parameters, but also satisfies the force constraints.

Keywords: Multi-robot systems, unknown payloads, robust control, adaptive control, force constraints.

1 INTRODUCTION

The range of tasks that require anthropomorphic manipulation motivates the use of multi-robot systems. In particular, tasks that require manipulation of a single heavy load or a cumbersome object could exceed the force and work envelope limits of a single arm. One of the major issues involved in a multi-robot system is to coordinate all the robots so that they perform a given task in a cooperative manner. More specifically, the control problem includes dynamic behavior modeling, trajectory tracking control, internal force control and task distribution among the robots.

Although still in its early stages of development, there has been significant progress in this area, and a great deal of work has been reported in recent years. In the area of modeling, the work by Luh and Zheng [14] is among the earliest research dealing with the kinematic and dynamic constraints imposed on such a system. This was also studied for a two-arm system by Suh and Shin [28].

The dynamics model of a multi-robot system is required for the development of control algorithms. As has been reported in the literature, the dynamics model of a multi-robot system exhibits its own inherent properties. Hayati [9] investigated a dynamic model for a closed-chain system. This issue, together with the control problem, has also been studied by Tarn, Bejczy and Yun [29], Furuta, et al [8], Özgüner, Yurkovich and Al-Abbass [18], Yun [35] and Li, Hsu and Sastry [13].

The work by Cole, Hause and Sastry [6] considered the case of a multifingered hand in rolling contact with an object and both the kinematics and control issues were investigated. Alford and Belyeu [2] studied a two-arm system and proposed a leader-follower control strategy, which was generalized to a multi-arm system by Arimoto, Miyazaki and Kawamura [4]. A position and force control scheme for a multi-robot system was proposed by Nakamura, Nagai and Yoshikawa [16].

Issues related to force distribution in closed kinematic chains were discussed by Orin and Oh [17]. Alberts and Soloway [1] suggested a control law which distributes force among the manipulators by using a weighting function. In the work by Salisbury and Craig [21], Yoshikawa and Nagai [34] and Nakamura, Nagai and Yoshikawa [16], the force exerted on the object is distributed based on an object-related criterion. Zheng and Luh [36] developed load distribution schemes for two-manipulator systems which were based on minimizing either the system energy or the force imparted to the object. In those schemes, the manipulator's dynamics are explicitly considered. Anderson and Pittelkau [3] proposed a load sharing force controller that apportions control forces between two manipulators. An adaptive algorithm that uses a joint torque-based criterion to determine the optimum load sharing was suggested in that work.

By considering the effect of loading on the dynam-

ics constraints, Walker, Marcus and Freeman [32] presented an approach for load distribution. The reaction forces created by a given arm's input loading was considered in Unseren and Koivo [30]. Carignan and Akin [5] derived the torques for two planar cooperating arms. A coordinated control law for a multi-manipulator system performing parts-matching tasks was proposed by Hsu [10] and a decentralized structure for the control strategy was suggested. In a recent work by Walker, Freeman and Marcus [31], the motion and internal loads induced on an object grasped by two or more robotic manipulators were analyzed and the load distribution problem was formulated by using the non-squeezing pseudoinverse.

In the context of controller design, two approaches are generally used. In the first, the problem is simplified by implicitly assuming that the payload information is known exactly and can be precisely modelled. In the second approach uncertain payload effects are compensated by the use of a wrist force sensor (see references [3], [9], [19] and [29]). In general precise information about the payload is not available for many applications, and the force sensor method depends heavily on the precision of the force measurement, as has been shown in [3]. These facts motivate the study of adaptive control schemes for multi-robot systems.

Mo and Bayoumi [15] proposed an adaptive control method for a multi-arm robotic system by using a method similar to that in Craig, Hsu and Sastry [7]. Walker, Kim and Dionise [33] reported an adaptive control strategy that accounts for payload effects. Hu and Goldenberg [11] also investigated the case of uncertain parameters in a multi-arm system. However, in most of these strategies the force constraint problem is not considered.

In a recent work by Song and Anderson [23], a new adaptive control law with a colleague-like strategy for task distribution was reported in which the force constraints are explicitly considered. As an extension of and a complement to that work, this paper is devoted to the robust controller design for multi-robot systems with both unknown payload dynamics and force constraints. First, following a modeling procedure similar to that in [6], a combined dynamic model which accounts for payload effects is derived. This model is slightly different in structure from the one obtained in [6] as a result of considering the forces *and* the moments exerted on the object. New robust control algorithms that explicitly deal with unknown payload parameters are developed. By using the generalized energy accumulation method, it is shown that the control strategy guarantees asymptotically stable path tracking of the payload's mass center. A strategy for task distribution is suggested which considers the dual contributions of the control torques. That is, it not only produces the control torques required for path tracking, but also satisfies the force constriants, a necessary condition for fine manipulation of the workpiece.

The main uncertainty in practice is due to the payload, not the robots themselves. Thus the attention in this paper is focused on the uncertain payload — the most significant effect on system performance (Leahy [12]). However, the technique presented herein can be readily extended to the case where uncertain parameters exist in both the robot and payload models.

The remainder of this paper is organized as follows. Section 2 presents a derivation of the combined multi-robot/payload dynamics model based on the fundamental equations presented in the first part of the section. The structural properties of this model are investigated, and are utilized in Section 3 to develop robust control strategies. Tracking stability is analyzed in Section 4, and a new robust control which does not rely on norm bounds is proposed in Section 5. Task distribution among the robots is discussed in Section 6 and a strategy for optimal sharing of the task is proposed. The application of the strategy is illustrated in Section 7 by means of a three-robot example. Comments and conclusions are given in Section 8.

2 MODELING

A dynamic model for a multi-robot system handling a workpiece was developed in [23]. However, due to limited space, many important details were omitted. For completeness, the modeling process of [23] is expanded in the following.

2.1 Kinematics

The multi-robot system illustrated in Figure 1 represents several robots handling a common payload. For simplicity, it is assumed that each robot has six degrees-of-freedom. The first joint of each robot is attached to a fixed base and the i^{th} robot is grasping the payload at the contact point C_i. Rigid grasping is assumed such that there is no relative motion at the contact points and there is perfect force transmission between the robots and the payload. Also each contact point is fixed and has a known location on the payload. Each robot applies a force f_{c_i} and a moment n_{c_i} through the contact point C_i to the payload. There are totally d ($d \geq 2$) robots handling the payload, and the payload lies within the combined loading capacity of the robots.

The Cartesian coordinate frames shown in Figure 2 are defined as follows:

$\{F_f\}$ is the inertial reference frame.

$\{F_p\}$ is the frame fixed at the payload's center-of-mass.

Figure 1: A Multi-Robot System

$\{F_{b_i}\}$ is the frame fixed to the base of the i^{th} robot.
$\{F_{c_i}\}$ is the frame attached to the i^{th} end-effector at the contact point C_i.

According to Chasle's theorem [22] from elementary mechanics, the motion of a rigid body in world space can decomposed into a translation plus a rotation. This is referred to as a rigid motion by Spong and Vidyasagar [27]. Six parameters are required to describe the position and orientation of the rigid body.

At the contact point C_i (see Figure 2),

$$x_{c_i} = x_0 + R_p^f c_i + d_i \tag{1}$$

and

$$\omega_{c_i} = \omega_0, \tag{2}$$

where

d_i is the vector that locates the origin of $\{F_{b_i}\}$ relative to $\{F_f\}$,
c_i is the vector that locates the origin of $\{F_{c_i}\}$ relative to $\{F_p\}$,
$x_0 = [x_{0x}, x_{0y}, x_{0z}]^T$ is a vector in $\{F_f\}$ locating the mass-center of the payload,
$\omega_0 = [\omega_{0y}, \omega_{0p}, \omega_{0r}]^T$ is the angular velocity vector of $\{F_p\}$ in terms of the yaw, pitch and roll rates,
ω_{c_i} is the angular velocity of $\{F_{c_i}\}$, and
R_p^f is the rotation matrix which maps c_i, measured in frame $\{F_p\}$, to the reference frame $\{F_f\}$.

In much of the literature, it is implicitly assumed that $R_p^f = E_3 \in R^{3\times 3}$, a unit matrix. This is true if

Figure 2: Coordinate Frames

the frames $\{F_p\}$ and $\{F_f\}$ have the same orientation. However, since R_p^f depends on $\phi_0 = [\phi_{0y}, \phi_{0p}, \phi_{0r}]^T$, the yaw, pitch and roll angles of frame $\{F_p\}$, respectively, it is generally not true that $R_p^f = E_3$ as the payload undergoes rotational motion. Hence, in the following, a time varying R_p^f is considered. To simplify notation, R is used to denote R_p^f in the following.

As can be verified, the matrix R has the property [27]

$$\dot{R} = \omega_0 \times R, \tag{3}$$

where

$$\omega_0 \times = \begin{bmatrix} 0 & -\omega_{0p} & \omega_{0r} \\ \omega_{0p} & 0 & -\omega_{0y} \\ -\omega_{0r} & \omega_{0y} & 0 \end{bmatrix}.$$

Differentiating (1) and noting that d_i and c_i are constant yields

$$\begin{aligned} \dot{x}_{c_i} &= \dot{x}_0 + \dot{R}c_i \\ &= \dot{x}_0 + \omega_0 \times Rc_i. \end{aligned} \tag{4}$$

Since $\omega_0 \times Rc_i = -(Rc_i)\times\omega_0$, (2) and (4) can be written as

$$\begin{aligned} \begin{bmatrix} \dot{x}_{c_i} \\ \omega_{c_i} \end{bmatrix} &= \begin{bmatrix} E_3 & -(Rc_i)\times \\ 0 & E_3 \end{bmatrix} \begin{bmatrix} \dot{x}_0 \\ \omega_0 \end{bmatrix} \\ &\triangleq S_i \begin{bmatrix} \dot{x}_0 \\ \omega_0 \end{bmatrix}, \end{aligned} \tag{5}$$

where

$$S_i = \begin{bmatrix} E_3 & -(Rc_i)\times \\ 0 & E_3 \end{bmatrix}. \quad (6)$$

In the task space, the position and orientation of the i^{th} end-effector can be represented as

$$\begin{aligned} P_i &= [x_{c_i}^T, \phi_{c_i}^T]^T \\ &= [x_{cix}, x_{ciy}, x_{ciz}, \phi_{ciy}, \phi_{cip}, \phi_{cir}]^T \end{aligned} \quad (7)$$

where ϕ_{ci} is composed of the yaw, pitch and roll angles representing the orientation of the i^{th} end-effector with respect to $\{F_f\}$. In joint space P_i can be expressed as

$$P_i = P_i(q_i), \quad (8)$$

where $q_i \in R^6$ is the generalized joint displacement of the i^{th} robot and $P_i(.)$: $R^6 \rightarrow R^6$ represents its forward kinematics. Therefore,

$$\begin{aligned} \dot{P}_i &= [\dot{x}_{c_i}^T, \dot{\phi}_{ci}^T]^T \\ &= \frac{\partial P_i(q_i)}{\partial q_i}\dot{q}_i. \end{aligned} \quad (9)$$

Since

$$\omega_{c_i} = T_{c_i}(\phi_{ciy}, \phi_{cip}, \phi_{cir}) \begin{bmatrix} \dot{\phi}_{ciy} \\ \dot{\phi}_{cip} \\ \dot{\phi}_{cir} \end{bmatrix}, \quad (10)$$

where

$$T_{c_i}(.) = \begin{bmatrix} 0 & -\sin\phi_{ciy} & \cos\phi_{cip}\cos\phi_{ciy} \\ 0 & \cos\phi_{ciy} & \cos\phi_{cip}\sin\phi_{ciy} \\ 1 & 0 & -\sin\phi_{cip} \end{bmatrix}, \quad (11)$$

then using (5), (9) and (10) yields

$$S_i \begin{bmatrix} \dot{x}_0 \\ \omega_0 \end{bmatrix} = J_i \dot{q}_i, \quad (12)$$

where

$$J_i = \begin{bmatrix} E_3 & 0 \\ 0 & T_{c_i}(\phi_{ciy}, \phi_{cip}, \phi_{cir}) \end{bmatrix} \frac{\partial P_i(q_i)}{\partial q_i} \quad (13)$$

is the generalized Jacobian matrix of robot i. It is assumed in the following that each robot works in a nonsingular region. Thus the inverse of J_i exists.

Considering all the robots that act on the payload, (12) can be expressed compactly as

$$\mathbf{J}\dot{\mathbf{q}} = \mathbf{S} \begin{bmatrix} \dot{x}_0 \\ \omega_0 \end{bmatrix}, \quad (14)$$

where

$$\begin{aligned} \mathbf{J} &\triangleq \text{blockdiag}\{J_1, J_2, \ldots, J_d\} \in R^{6d\times 6d}, \\ \mathbf{S} &\triangleq [S_1^T\ S_2^T \ldots S_d^T]^T \in R^{6d\times 6}, \end{aligned}$$

and

$$\mathbf{q} \triangleq [q_1^T\ q_2^T \ldots q_d^T]^T \in R^{6d}.$$

Since the forces $\{f_{c1}, f_{c2}, \ldots, f_{cd}\}$ and moments $\{n_{c1}, n_{c2}, \ldots, n_{cd}\}$ act on the load, the equivalent force and moment applied at the mass-center are

$$f_0 = f_{c_1} + f_{c_2} + \ldots + f_{c_d} \quad (15)$$

and

$$\begin{aligned} n_0 &= n_{c_1} + n_{c_2} + \ldots + n_{c_d} + (Rc_1)\times f_{c_1} \\ &\quad + (Rc_2)\times f_{c_2} + \ldots + (Rc_d)\times f_{c_d}, \end{aligned} \quad (16)$$

respectively. In matrix form, (15) and (16) become

$$\begin{aligned} \begin{bmatrix} f_0 \\ n_0 \end{bmatrix} &= \begin{bmatrix} E_3 & 0 \\ (Rc_1)\times & E_3 \end{bmatrix} F_1 + \begin{bmatrix} E_3 & 0 \\ (Rc_2)\times & E_3 \end{bmatrix} F_2 \\ &\quad + \ldots + \begin{bmatrix} E_3 & 0 \\ (Rc_d)\times & E_3 \end{bmatrix} F_d \\ &= W_1F_1 + W_2F_2 + \ldots + W_dF_d \\ &\triangleq \mathbf{WF}, \end{aligned} \quad (17)$$

where

$$\begin{aligned} F_i &\triangleq \begin{bmatrix} f_{c_i} \\ n_{c_i} \end{bmatrix}, \qquad W_i \triangleq \begin{bmatrix} E_3 & 0 \\ (Rc_i)\times & E_3 \end{bmatrix}, \\ \mathbf{W} &\triangleq [W_1\ W_2 \ldots W_d] \in R^{6\times 6d}, \end{aligned}$$

and

$$\mathbf{F} \triangleq [F_1^T\ F_2^T \ldots F_d^T]^T \in R^{6d}.$$

Concerning the matrices $\mathbf{W}$ and $\mathbf{S}$, the following properties hold.

Property 2.1

(1) $\mathbf{S}$ and $\mathbf{W}$ are full rank, i.e., $\text{rank}(\mathbf{W}) = \text{rank}(\mathbf{S}) = 6$.
(2) Both S_i and W_i are nonsingular, $i = 1, 2, \ldots, d$.
(3) $\mathbf{S}^T = \mathbf{W}$.

The proof is similar to that given by Song and Anderson [24].

2.2 Motion Equation

Suppose that the mass and the inertia of the payload is m and I_0, respectively. With the action of f_0 and n_0, the payload undergoes a rigid motion in the world space as described by

$$f_0 = m\ddot{x}_0 + mg \quad (18)$$

and

$$n_0 = RI_0R^T\dot{\omega}_0 + \omega_0 \times RI_0R^T\omega_0, \quad (19)$$

where $g \in R^3$ is the gravity vector. In view of (17)–(19),

$$\mathbf{WF} = \mathcal{D}_1 \begin{bmatrix} \ddot{x}_0 \\ \dot{\omega}_0 \end{bmatrix} + \mathcal{D}_2 \begin{bmatrix} \dot{x}_0 \\ \omega_0 \end{bmatrix} + \mathcal{D}_3,$$

where

$$\mathcal{D}_1 = \begin{bmatrix} mE_3 & 0 \\ \vec{0} & \dot{R}I_0R^T \end{bmatrix}, \quad (20)$$

$$\mathcal{D}_2 = \begin{bmatrix} 0 & 0 \\ 0 & \omega_0 \times RI_0R^T \end{bmatrix} \quad (21)$$

and

$$\mathcal{D}_3 = \begin{bmatrix} mg \\ 0 \end{bmatrix}. \quad (22)$$

The reactive forces and moments of the payload appearing at the i^{th} end-effector are represented as F_{react_i}. Under the assumption of rigid grasping at the contact point,

$$F_{react_i} = -F_i, \quad (23)$$

which causes the joint reaction torques

$$\begin{aligned} \tau_{F_{react_i}} &= J_i^T(q)F_{react_i} \\ &= -J_i^T(q_i)F_i. \end{aligned} \quad (24)$$

So for each robot it follows that

$$\begin{aligned} H_i\ddot{q}_i + C_i\dot{q}_i + G_i &= \tau_i + \tau_{F_{react_i}} number \quad (25) \\ &= \tau_i - J_i^T F_i, \quad i = 1, 2, \ldots, d, \quad (26) \end{aligned}$$

where, for the i^{th} robot, H_i is the inertia matrix, $C_i\dot{q}_i$ is the vector of centrifugal and Corolis forces, G_i is the vector of gravitational forces and τ_i is the vector of control torques. Defining

$$\begin{aligned} \mathbf{H} &\triangleq \text{block diag}\{H_1, H_2, \ldots H_d\} \in R^{6d\times 6d}, \\ \mathbf{C} &\triangleq \text{block diag}\{C_1, C_2, \ldots C_d\} \in R^{6d\times 6d}, \\ \mathbf{G} &\triangleq [G_1^T\ G_1^T \ldots G_d^T]^T \in R^{6d}, \end{aligned}$$

and

$$\mathbf{T} \triangleq [\tau_1^T\ \tau_2^T \ldots \tau_d^T]^T \in R^{6d},$$

the combined form of (25) is

$$\mathbf{T} = \mathbf{H}\ddot{\mathbf{q}} + \mathbf{C}\dot{\mathbf{q}} + \mathbf{G} + \mathbf{J}^T\mathbf{F}. \quad (27)$$

This model can easily be transformed to the task space. From (14)

$$\dot{\mathbf{q}} = \mathbf{J}^{-1}\mathbf{S}\begin{bmatrix} \dot{x}_0 \\ \omega_0 \end{bmatrix}. \quad (28)$$

Noting that

$$\begin{aligned} \omega_0 &= T_0(\phi_{0y}, \phi_{0p}, \phi_{0r})\begin{bmatrix} \dot{\phi}_{0y} \\ \dot{\phi}_{0p} \\ \dot{\phi}_{0r} \end{bmatrix} \\ &\triangleq T_0\dot{\phi}_0, \end{aligned} \quad (29)$$

where

$$T_0(.) = \begin{bmatrix} 0 & -\sin\phi_{0y} & \cos\phi_{0p}\cos\phi_{0y} \\ 0 & \cos\phi_{0y} & \cos\phi_{0p}\sin\phi_{0y} \\ 1 & 0 & -\sin\phi_{0p} \end{bmatrix},$$

it follows that

$$\begin{aligned} \begin{bmatrix} \dot{x}_0 \\ \omega_0 \end{bmatrix} &= \begin{bmatrix} E_3 & 0 \\ 0 & T_0 \end{bmatrix}\begin{bmatrix} \dot{x}_0 \\ \dot{\phi}_0 \end{bmatrix} \\ &\triangleq A\dot{X}_0, \end{aligned} \quad (30)$$

where

$$A = \begin{bmatrix} E_3 & 0 \\ 0 & T_0 \end{bmatrix} \in R^{6\times 6}$$

and

$$X_0 = \begin{bmatrix} x_0 \\ \phi_0 \end{bmatrix}.$$

Notice that $\det(T_0) = -\cos\phi_{0p}$. For small changes in the payload's orientation ($|\phi_{0p}| < \frac{\pi}{2}$), the matrix A is invertible. Now by (27) and (29),

$$\dot{\mathbf{q}} = \mathbf{J}^{-1}\mathbf{S}A\dot{X}_0 \quad (31)$$

such that

$$\ddot{\mathbf{q}} = \mathbf{J}^{-1}\mathbf{S}A\ddot{X}_0 + \frac{d}{dt}(\mathbf{J}^{-1}\mathbf{S}A)\dot{X}_0. \quad (32)$$

In view of (20)–(22), (26) and (29)–(31), the combined dynamics of the multi-robot system through the payload may be written as

$$\begin{aligned} \mathbf{W}\mathbf{J}^{-T}\mathbf{T} &= \left(\mathbf{W}\mathbf{J}^{-T}\mathbf{H}\mathbf{J}^{-1}\mathbf{S}A + \mathcal{D}_1A\right)\ddot{X}_0 \\ &\quad + \left(\mathbf{W}\mathbf{J}^{-T}\mathbf{H}\frac{d}{dt}(\mathbf{J}^{-1}\mathbf{S}A)\right. \\ &\quad \left. + \mathbf{W}\mathbf{J}^{-T}\mathbf{C}\mathbf{J}^{-1}\mathbf{S}A + \mathcal{D}_1\dot{A} + \mathcal{D}_2A\right)\dot{X}_0 \\ &\quad + \mathbf{W}\mathbf{J}^{-T}\mathbf{G} + \mathcal{D}_3. \end{aligned} \quad (33)$$

It turns out that the combined model is somewhat "irregular" in that the well-known properties applicable to general robot dynamics do not necessarily hold. That is;

1. the generalized inertia matrix $\mathbf{W}\mathbf{J}^{-T}\mathbf{H}\mathbf{J}^{-1}\mathbf{S}A + \mathcal{D}_1A$ is not symmetric, and
2. the property of skew-symmetry is not valid.

Remark 2.1

The fact that the generalized inertia matrix is not symmetric positive definite makes it difficult to directly use the Lyapunov method to verify stability. The passivity principle also cannot be directly

applied because the property of skew-symmetry does not hold. In the next section, a simple transformation is applied to "regularize" the combined model.

3 ROBUST CONTROL METHODS

3.1 Control Objective

As previously noted, it is generally difficult to know the payload's characteristics precisely. For this reason, it is assumed that the mass m and the inertia matrix I_0 of the payload are unknown. The desired path is given in terms of position and orientation as

$$X_0^d = \begin{bmatrix} x_0^d \\ \phi_0^d \end{bmatrix},$$

$$\dot{X}_0^d = \begin{bmatrix} \dot{x}_0^d \\ \dot{\phi}_0^d \end{bmatrix},$$

and

$$\ddot{X}_0^d = \begin{bmatrix} \ddot{x}_0^d \\ \ddot{\phi}_0^d \end{bmatrix}.$$

The tracking error is expressed as

$$\begin{aligned} \varepsilon &= X_0 - X_0^d \\ &= \begin{bmatrix} x_0 - x_0^d \\ \phi_0 - \phi_0^d \end{bmatrix} \triangleq \begin{bmatrix} \varepsilon_1 \\ \varepsilon_2 \end{bmatrix}. \end{aligned}$$

The motion control problem is stated as:

Design the control torque $\mathbf{T}$ *such that the actual path of the payload's mass center* (X_0) *asymptotically tracks the desired path* (X_0^d) *in the face of unknown payload parameters.*

3.2 Model Transformation

Due to the "irregularity" of the model (32), direct solution to this problem is complicated. In the following, a simple transformation is introduced. By observing the structure of the combined model (32), it is seen that if both sides are premultiplied by A^T, the transformed generalized inertia matrix is symmetric positive definite. Moreover, this mutiplication also leads to the property of skew-symmetry. After the transformation, (32) becomes

$$[\mathcal{H}_0 + \mathcal{H}_p]\ddot{X}_0 + [\mathcal{C}_0 + \mathcal{C}_p]\dot{X}_0 + [\mathcal{G}_0 + \mathcal{G}_p] = \mathcal{F}, \quad (34)$$

where

$$\mathcal{F} \triangleq A^T\mathbf{W}\mathbf{J}^{-T}\mathbf{T}, \quad (35)$$

$$\mathcal{H}_0 \triangleq A^T\mathbf{W}\mathbf{J}^{-T}\mathbf{H}\mathbf{J}^{-1}\mathbf{S}A, \quad (36)$$

$$\begin{aligned} \mathcal{H}_p &\triangleq A^T\mathcal{D}_1 A \\ &= \begin{bmatrix} mE_3 & 0 \\ 0 & T_0^T R I_0 R^T T_0 \end{bmatrix}, \end{aligned} \quad (37)$$

$$\begin{aligned} \mathcal{C}_0 &= A^T\mathbf{W}\mathbf{J}^{-T}\mathbf{H}(\dot{\mathbf{J}}^{-1}\mathbf{S}A + \mathbf{J}^{-1}\dot{\mathbf{S}}A + \mathbf{J}^{-1}\mathbf{S}\dot{A}) \\ &\quad + A^T\mathbf{W}\mathbf{J}^{-T}\mathbf{C}\mathbf{J}^{-1}\mathbf{S}A, \end{aligned} \quad (38)$$

$$\begin{aligned} \mathcal{C}_p &\triangleq A^T\mathcal{D}_1\dot{A} + A^T\mathcal{D}_2 A \\ &= \begin{bmatrix} 0 & 0 \\ 0 & T_0^T\omega_0 \times R I_0 R^T T_0 + T_0^T R I_0 R^T \dot{T}_0 \end{bmatrix}, \end{aligned} \quad (39)$$

$$\mathcal{G}_0 \triangleq A^T\mathbf{W}\mathbf{J}^{-T}\mathbf{G} \quad (40)$$

and

$$\mathcal{G}_p \triangleq A^T\mathcal{D}_3 = \begin{bmatrix} mg \\ 0 \end{bmatrix}. \quad (41)$$

For this model the following properties hold.

Theorem 3.1

The transformed model (33) is regular. That is;
(1) $\mathcal{H}_0 + \mathcal{H}_p$ is symmetric positive definite, and
(2) $[\dot{\mathcal{H}}_0 + \dot{\mathcal{H}}_p] - 2[\mathcal{C}_0 + \mathcal{C}_p]$ is skew-symmetric.

Proof:
(1) The first property can be shown easily by using the fact that

$$\mathbf{W}^T = \mathbf{S}.$$

(2) By the definitions of $\mathcal{H}_0, \mathcal{H}_p, \mathcal{C}_0$ and $\mathcal{C}_p$, it follows that

$$\begin{aligned} &[\dot{\mathcal{H}}_0 + \dot{\mathcal{H}}_p] - 2[\mathcal{C}_p + \mathcal{C}_0] \\ &\quad = N_1 + N_2 + N_3 + N_4 + N_5, \end{aligned} \quad (42)$$

where

$$\begin{aligned} N_1 &= A^T\mathbf{W}\mathbf{J}^{-T}(\dot{\mathbf{H}} - 2\mathbf{C})\mathbf{J}^{-1}\mathbf{S}A, \\ N_2 &= A^T\mathbf{W}\dot{\mathbf{J}}^{-T}\mathbf{H}\mathbf{J}^{-1}\mathbf{S}A - A^T\mathbf{W}\mathbf{J}^{-T}\mathbf{H}\dot{\mathbf{J}}^{-1}\mathbf{S}A, \\ N_3 &= A^T\dot{\mathbf{W}}\mathbf{J}^{-T}\mathbf{H}\mathbf{J}^{-1}\mathbf{S}A - A^T\mathbf{W}\mathbf{J}^{-T}\mathbf{H}\mathbf{J}^{-1}\dot{\mathbf{S}}A, \\ N_4 &= \dot{A}^T\mathbf{W}\mathbf{J}^{-1}\mathbf{H}\mathbf{J}^{-1}\mathbf{S}A - A^T\mathbf{W}\mathbf{J}^{-T}\mathbf{H}\mathbf{J}^{-1}\mathbf{S}\dot{A}, \end{aligned}$$

and

$$N_5 = \begin{bmatrix} 0 & 0 \\ 0 & \mathcal{N} \end{bmatrix},$$

where

$$\begin{aligned} \mathcal{N} &= \frac{d}{dt}(T_0^T R I_0 R^T T_0) \\ &\quad - 2T_0^T\omega_0 \times R I_0 R^T T_0 - 2T_0^T R I_0 R^T \dot{T}_0. \end{aligned}$$

Property 2.1 ensures that the N_i $(i = 1, 2, 3, 4)$ are skew-symmetric. Furthermore it can be shown that N_5 is also skew-symmetric (see Appendix). Thus the result follows.

3.3 Controller Design

Instead of designing control torque $\mathbf{T}$ directly, the transformed input $\mathcal{F}$ is specified first. This approach allows the use of the regularized model and its properties, as stated in Theorem 3.1. Section 6 introduces a method to calculate $\mathbf{T}$ from $\mathcal{F}$.

Robust Control I

To develop the first robust strategy, the decomposition of the transformed model is performed first, so that the payload parameters are isolated from the dynamics. To this end, the following matrices are introduced:

$$E_{xx} = R\begin{bmatrix}1&0&0\\0&0&0\\0&0&0\end{bmatrix}R^T,$$

$$E_{xy} = R\begin{bmatrix}0&1&0\\1&0&0\\0&0&0\end{bmatrix}R^T,$$

$$E_{xz} = R\begin{bmatrix}0&0&1\\0&0&0\\1&0&0\end{bmatrix}R^T,$$

$$E_{yy} = R\begin{bmatrix}0&0&0\\0&1&0\\0&0&0\end{bmatrix}R^T,$$

$$E_{zz} = R\begin{bmatrix}0&0&0\\0&0&0\\0&0&1\end{bmatrix}R^T$$

and

$$E_{yz} = R\begin{bmatrix}0&0&0\\0&0&1\\0&1&0\end{bmatrix}R^T.$$

Therefore the matrix RI_0R^T can be written as

$$\begin{aligned}RI_0R^T &= R\begin{bmatrix}I_{0xx}&I_{0xy}&I_{0xz}\\I_{0yx}&I_{0yy}&I_{0yz}\\I_{0zx}&I_{0zy}&I_{0zz}\end{bmatrix}R^T\\ &= \sum_{i=x}^{z}\sum_{j=i}^{z} I_{0ij}E_{ij},\end{aligned}$$

due to the symmetry of I_0. The transformed model (33) can now be decomposed as

$$\begin{aligned}\mathcal{F} &= \mathcal{H}_0\ddot{X}_0 + \mathcal{C}_0\dot{X}_0 + \mathcal{G}_0\\ &\quad + \begin{bmatrix} m(\ddot{x}_0+g)\\ \sum_{i=x}^{z}\sum_{j=i}^{z}\mathcal{M}_{ij}\end{bmatrix},\end{aligned} \tag{43}$$

where

$$\begin{aligned}\mathcal{M}_{ij} &= I_{0ij}T_0^T[E_{ij}T_0\ddot{\phi}_0\\ &\quad + (\omega_0\times E_{ij}T_0 + E_{ij}\dot{T}_0)\dot{\phi}_0].\end{aligned} \tag{44}$$

Based on this model, a robust path tracking control scheme is developed.

The control input ($\mathcal{F}$) is designed as

$$\begin{aligned}\mathcal{F} &= \mathcal{H}_0[\ddot{X}_0^d - (\lambda+\beta)\dot{\varepsilon} - \lambda\beta\varepsilon] + \mathcal{C}_0[\dot{X}_0^d - \beta\varepsilon]\\ &\quad + \mathcal{G}_0 + \begin{bmatrix}\hat{m}\Psi_m\\ \sum_{i=x}^{z}\sum_{j=i}^{z}\hat{I}_{0ij}\Psi_{ij}\end{bmatrix} - K\Phi,\end{aligned} \tag{45}$$

where $\beta > 0$, $\lambda > 0$, and $K = K^T > 0$ are design parameters (affecting stability, speed of response and disturbance rejection properties) and $\hat{m}$ and $\hat{I}_0$ are computed by

$$\hat{I}_0 = \begin{bmatrix}\hat{I}_{0xx}&\hat{I}_{0xy}&\hat{I}_{0xz}\\ \hat{I}_{0xy}&\hat{I}_{0yy}&\hat{I}_{0yz}\\ \hat{I}_{0xz}&\hat{I}_{0yz}&\hat{I}_{0zz}\end{bmatrix}, \tag{46}$$

$$\hat{m} = -\frac{\Phi_1^T\Psi_m\bar{m}^2}{|\Phi_1^T\Psi_m|\bar{m}+\nu}, \tag{47}$$

$$\hat{I}_{0xx} = -\frac{\Phi_2^T\Psi_{xx}\bar{I}_{0xx}^2}{|\Phi_2^T\Psi_{xx}|\bar{I}_{0xx}+\nu}, \tag{48}$$

$$\hat{I}_{0xy} = -\frac{\Phi_2^T\Psi_{xy}\bar{I}_{0xy}^2}{|\Phi_2^T\Psi_{xy}|\bar{I}_{0xy}+\nu}, \tag{49}$$

$$\hat{I}_{0xz} = -\frac{\Phi_2^T\Psi_{xz}\bar{I}_{0xz}^2}{|\Phi_2^T\Psi_{xz}|\bar{I}_{0xz}+\nu}, \tag{50}$$

$$\hat{I}_{0yy} = -\frac{\Phi_2^T\Psi_{yy}\bar{I}_{0yy}^2}{|\Phi_2^T\Psi_{yy}|\bar{I}_{0yy}+\nu}, \tag{51}$$

$$\hat{I}_{0yz} = -\frac{\Phi_2^T\Psi_{yz}\bar{I}_{0yz}^2}{|\Phi_2^T\Psi_{yz}|\bar{I}_{0yz}+\nu} \tag{52}$$

and

$$\hat{I}_{0zz} = -\frac{\Phi_2^T\Psi_{zz}\bar{I}_{0zz}^2}{|\Phi_2^T\Psi_{zz}|\bar{I}_{0zz}+\nu}. \tag{53}$$

In (44)–(52), $\bar{m}$ and $\bar{I}_{0ij}$ are the upper bounds of m and I_{0ij}, respectively,

$$\Psi_m = \ddot{x}_0^d - (\lambda+\beta)\dot{\varepsilon}_1 - \lambda\beta\varepsilon_1 + g \tag{54}$$

$$\begin{aligned}\Psi_{ij} &= T_0^T\Big\{E_{ij}T_0[\ddot{\phi}_0^d - (\lambda+\beta)\dot{\varepsilon}_2 - \lambda\beta\varepsilon_2]\\ &\quad + [\omega_0\times E_{ij}T_0 + E_{ij}\dot{T}_0](\dot{\phi}_0^d - \lambda\varepsilon_2)\Big\}\end{aligned} \tag{55}$$

$$\Phi_i = \dot{\varepsilon}_i + \beta\varepsilon_i, \quad i = 1,2, \tag{56}$$

$$\Phi = [\Phi_1^T, \Phi_2^T]^T \tag{57}$$

and $\nu \geq 0$ is a design variable that satisfies

$$\int_0^t \nu(\tau)d\tau \leq C_{02}^2 < \infty. \tag{58}$$

Robust Control II

For brevity, let

$$\begin{aligned} \mathcal{Z}_1 &= \ddot{X}_0^d - (\lambda+\beta)\dot{\varepsilon} - \lambda\beta\varepsilon, \\ \mathcal{Z}_2 &= \dot{X}_0^d - \beta\varepsilon \end{aligned}$$

and

$$L = \mathcal{H}_p\mathcal{Z}_1 + \mathcal{C}_p\mathcal{Z}_2 + \mathcal{G}_p.$$

The control torque is specified by

$$\mathcal{F} = \mathcal{H}_0\mathcal{Z}_1 + \mathcal{C}_0\mathcal{Z}_2 + \mathcal{G}_0 - K\Phi + U_a \qquad (59)$$

and

$$U_a = -\frac{\Phi\eta^2}{\|\Phi\|\eta + \nu}, \qquad (60)$$

where η is defined by

$$\begin{aligned} &\|\mathcal{H}_p\|\|\mathcal{Z}_1\| + \|\mathcal{C}_p\|\|\mathcal{Z}_2\| + \|\mathcal{G}_p\| \\ &\quad\leq \alpha_1\|\mathcal{Z}\| + \alpha_2\|\dot{X}_0\|\|\mathcal{Z}_2\| + \alpha_3 \\ &\quad\triangleq \eta. \end{aligned} \qquad (61)$$

In (61), the α_i represent upper bounds on the model norms.

The proposed control strategies lead to the following results.

Theorem 3.2

Consider the multi-robot dynamics (33) in which the payload parameters m and I_0 are unknown a priori. If the control input $\mathcal{F}$ is designed as in (44)–(57), the payload then asymptotically tracks the given position and orientation, i.e., $X_0 \to X_0^d$ and $\dot{X}_0 \to \dot{X}_0^d$ as $t \to \infty$.

Theorem 3.3

Given the conditions stated in Theorem 3.2, if the control input $\mathcal{F}$ is specified as in (58) and (59), then stable path tracking of payload is ensured.

4 STABILITY

Stability can be proven by the following result (see [25] for more detail). Consider a dynamical system $\Sigma(\xi, \dot{\xi})$ with $\xi \in R^n$ being the system state. Defining the generalized energy function of the system as

$$E(\xi) = \xi^T K \xi, \qquad (62)$$

where $K \in R^{n\times n}$ is a symmetric positive definite matrix, leads to the following result.

Theorem 4.1

Let J_A be the integration of the generalized energy function $E(\xi)$ over the time interval $[0,t]$, i.e., $J_A = \int_0^t E(\xi)d\tau$. Suppose ξ is uniformly continuous. If $J_A \leq C_0^2 < \infty$ for all $t \in [0,\infty)$, then the system is asymptotically stable, i.e., $\xi \to 0$ as $t \to \infty$.

This result can be shown by using Barbalat's Lemma [20] (see [25] for details).

The interpretation of the above theorem is that the system must be stable if the accumulation of the system's energy over a time interval of infinite length is finite. One advantage to this approach is that it is fairly easy to choose a suitable energy function. (Another advantage is discussed later.) In the following, this result is used to prove the tracking stability of the proposed strategies.

Proof of Theorem 3.2:

Note that if the control input in (33) is designed as in (44), the closed-loop system dynamics is given by

$$\begin{aligned} K\Phi &= -(\mathcal{H}_0 + \mathcal{H}_p)(\dot{\Phi} + \lambda\Phi) - (\mathcal{C}_0 + \mathcal{C}_p)\Phi \\ &\quad + \begin{bmatrix} (\hat{m} - m)\Psi_m \\ \sum_{i=x}^{z}\sum_{j=i}^{z}(\hat{I}_{0ij} - I_{0ij})\Psi_{ij} \end{bmatrix}. \end{aligned}$$

To simplify notation in the following, let $H^* = \mathcal{H}_0 + \mathcal{H}_p$ and $C^* = \mathcal{C}_0 + \mathcal{C}_p$. As can be seen, there exist several generalized energy functions for this problem. For example

$$\begin{aligned} E_1(\Phi) &= \Phi^T K \Phi, \\ E_2(\lambda, \Phi) &= \lambda\Phi^T H^* \Phi \quad (\forall\lambda > 0) \end{aligned}$$

or

$$E_3(\lambda, \Phi) = \Phi^T K \Phi + \lambda\Phi^T H^* \Phi \quad (\forall\lambda > 0).$$

In the following only $E_1(\Phi)$ is considered. Clearly

$$\begin{aligned} J_A &= \int_0^t E_1(\Phi)d\tau \\ &= \int_0^t \Phi^T K \Phi d\tau \\ &= -\int_0^t \Phi^T H^*(\dot{\Phi} + \lambda\Phi)d\tau - \int_0^t \Phi^T C^* \Phi d\tau \\ &\quad + \int_0^t (\hat{m} - m)\Phi_1^T \Psi_m d\tau \\ &\quad + \sum_{i=x}^{z}\sum_{j=i}^{z}\int_0^t (\hat{I}_{0ij} - I_{0ij})\Phi_2^T \Psi_{ij} d\tau. \end{aligned}$$

Noting that H^* is symmetric positive definite, it can be shown that

$$\lambda\int_0^t \Phi^T H^* \Phi d\tau > 0 \quad (\forall\lambda > 0)$$

and

$$\int_0^t \Phi^T H^* \dot{\Phi} d\tau \geq -\frac{1}{2}\Phi^T H^* \Phi \mid_{t=0} - \frac{1}{2}\int_0^t \Phi^T \dot{H}^* \Phi d\tau.$$

Using these relations yields the inequality

$$\begin{aligned} J_A \leq\ & C_{01}^2 + \int_0^t (\hat{m} - m)\Phi_1^T \Psi_m d\tau \\ & + \sum_{i=x}^{z}\sum_{j=i}^{z} \int_0^t (\hat{I}_{0ij} - I_{0ij})\Phi_2^T \Psi_{ij} d\tau \\ & + \frac{1}{2}\int_0^t \Phi^T (\dot{H}^* - 2C^*)\Phi d\tau. \end{aligned} \tag{63}$$

where $C_{01}^2 = \frac{1}{2}\Phi^T H^* \Phi \mid_{t=0}$. Due to the property of skew-symmetry, $\int_0^t \Phi^T (\dot{H}^* - 2C^*)\Phi d\tau = 0$. Employing this and the bounds on m and I_0, (63) becomes

$$\begin{aligned} J_A \leq\ & C_{01}^2 + \int_0^t (\hat{m} - m)\Phi_1^T \Psi_m d\tau \\ & + \sum_{i=x}^{z}\sum_{j=i}^{z} \int_0^t (\hat{I}_{0ij} - I_{0ij})\Phi_2^T \Psi_{ij} d\tau \\ \leq\ & C_{01}^2 + \int_0^t \hat{m}\Phi_1^T \Psi_m d\tau + \int_0^t \bar{m}|\Phi_1^T \Psi_m| d\tau \\ & + \sum_{i=x}^{z}\sum_{j=i}^{z} \int_0^t \hat{I}_{0ij}\Phi_2^T \Psi_{ij} d\tau \\ & + \sum_{i=x}^{z}\sum_{j=i}^{z} \int_0^t \bar{I}_{0ij}|\Phi_2^T \Psi_{ij}| d\tau. \end{aligned} \tag{64}$$

Inserting the algorithms (46)-(52) into (63) and conducting a little manipulation yields

$$\begin{aligned} J_A \leq\ & C_{01}^2 + \int_0^t \frac{|\Phi_1^T \Psi_m|\bar{m}\nu}{|\Phi_1^T \Psi_m|\bar{m} + \nu} d\tau \\ & + \sum_{i=x}^{z}\sum_{j=i}^{z} \int_0^t \frac{|\Phi_2^T \Psi_{ij}|\bar{I}_{0ij}\nu}{|\Phi_2^T \Psi_{ij}|\bar{I}_{0ij} + \nu} d\tau \\ \leq\ & C_{01}^2 + \int_0^t \nu d\tau + \sum_{i=x}^{z}\sum_{j=i}^{z} \int_0^t \nu d\tau. \end{aligned}$$

Since ν satisfies (57),

$$J_A \leq C_{01}^2 + 7C_{02}^2 < \infty,$$

which implies that $\Phi \in L_2$. Furthermore, by making use of the same argument as in Song and Middleton [26], it can be shown that $\Phi \in L_\infty$ and $\dot{\Phi} \in L_\infty$. Hence Φ is uniformly continuous. By Theorem 4.1, $\Phi \to 0$ as $t \to \infty$. Since $\Phi = \dot{\varepsilon} + \lambda\varepsilon$, the result stated in Theorem 3.2 is obtained.

Proof of Theorem 3.3

In this case, the control law (58)-(60) yields the closed-loop dynamics

$$(\mathcal{H}_0 + \mathcal{H}_p)(\dot{\Phi} + \lambda\Phi) + (\mathcal{C}_0 + \mathcal{C}_p)\Phi = -K\Phi + U_a - L,$$

where L is defined as before. Following the same procedure as in the proof of Theorem 3.2, it is seen that

$$\begin{aligned} J_A &= \int_0^t \Phi^T K \Phi d\tau \\ &\leq C_{01}^2 + \int_0^t \Phi^T [U_a - L] d\tau \\ &\leq C_{01}^2 + \int_0^t \Phi^T U_a d\tau + \int_0^t \|\Phi\| \|L\| d\tau. \end{aligned}$$

Substituting for U_a from (59) and noting that $\|L\| \leq \eta$ (see (60)), yields

$$\begin{aligned} J_A &\leq C_{01}^2 - \int_0^t \frac{\|\Phi\|^2 \eta^2}{\|\Phi\|\eta + \nu} d\tau + \int_0^t \|\Phi\|\eta d\tau \\ &= C_{01}^2 + \int_0^t \frac{\|\Phi\|\eta\nu}{\|\Phi\|\eta + \nu} d\tau \\ &\leq C_{01}^2 + \int_0^t \nu d\tau. \end{aligned}$$

Since ν satisfies (57), J_A is bounded and the result follows from Theorem 4.1.

Remark 4.1

It is seen that the design variable ν plays an important role in the above control strategies. It is required in both that ν be integrable. As can be verified,

$$\nu = \frac{1}{2}v_1(1 + t^m)^\rho e^{-v_2 t^n},$$

where $v_1 \geq 0$ and $v_2 \geq 0$, satisfies such a requirement if m, ρ and n are chosen properly.

Remark 4.2

It is worth mentioning that, in addition to proving stability, J_A also provides a relative measure of the tracking performance in terms of transient and steady-state errors. This is because Φ is a filtered tracking error, and the quantity $\Phi^T K \Phi$ is a weighted version of the squared error. Its integral over $[t_0, t]$ represents the accumulation of the weighted, squared tracking error within the interval. The smaller this integral, the better the tracking performance. (See [25] for a thorough investigation of this point.)

5 SIMPLIFIED STRATEGY

In strategy II, the quantity η has to be determined. This is accomplished by estimating α_1, α_2 and α_3. Knowing the bounds on m and I_0 and the formulations of $\mathcal{H}_p$, $\mathcal{C}_p$ and $\mathcal{G}_p$ makes it possible to obtain these quantities. To eliminate this tedious procedure, an alternate control strategy is proposed.

Theorem 5.1

Let the control input be defined as

$$\mathcal{F} = \mathcal{H}_0 \mathcal{Z}_1 + \mathcal{C}_0 \mathcal{Z}_2 + \mathcal{G}_0 - K\Phi + U_a, \qquad (65)$$

with $\mathcal{Z}_1$ and $\mathcal{Z}_2$ defined as before and

$$U_a = -\frac{\Phi\hat{\eta}}{\|\Phi\|}, \qquad (66)$$

where

$$\hat{\eta} = \hat{\alpha}_1\|\mathcal{Z}_1\| + \hat{\alpha}_2\|\dot{X}_0\|\|\mathcal{Z}_2\| + \hat{\alpha}_3. \qquad (67)$$

If the $\hat{\alpha}_i$ are estimated on-line via

$$\hat{\alpha}_1 = \hat{\alpha}_1(0) + c_1\int_0^t \|\Phi\|\|\mathcal{Z}_1\|d\tau,$$

$$\hat{\alpha}_2 = \hat{\alpha}_2(0) + c_2\int_0^t \|\Phi\|\|\dot{X}_0\|\|\mathcal{Z}_2\|d\tau,$$

and

$$\hat{\alpha}_3 = \hat{\alpha}_3(0) + c_3\int_0^t \|\Phi\|d\tau,$$

where $\hat{\alpha}_i(0)$ is the initial value of $\hat{\alpha}_i$ and the c_i are positive constants, then stable path tracking is achieved.

Proof:

Applying this strategy to (33) leads to the following.

$$\begin{aligned} J_A &= \int_0^t \Phi^T K\Phi d\tau \\ &\le C_{01}^2 + \int_0^t \|\Phi\|(\eta - \hat{\eta})d\tau \\ &= C_{01}^2 + \int_0^t (\alpha_1 - \hat{\alpha}_1)\|\Phi\|\|\mathcal{Z}_1\|d\tau \\ &\quad + \int_0^t (\alpha_2 - \hat{\alpha}_2)\|\Phi\|\|\dot{X}_0\|\|\mathcal{Z}_2\|d\tau \\ &\quad + \int_0^t (\alpha_3 - \hat{\alpha}_3)\|\Phi\|d\tau. \end{aligned} \qquad (68)$$

To show the boundedness of J_A, the following relation is needed,

$$\int_0^t \int_0^\tau f(\gamma)d\gamma f(\tau)d\tau = \frac{1}{2}\left(\int_0^t f(\tau)d\tau\right)^2.$$

Substituting for the $\hat{\alpha}_i$ in (67) and using the above relation yields

$$\begin{aligned} J_A \le\ & C_{01}^2 + (\alpha_1 - \hat{\alpha}_1(0))\int_0^t \|\Phi\|\|\mathcal{Z}_1\|d\tau \\ & - \frac{c_1}{2}\left[\int_0^t \|\Phi\|\|\mathcal{Z}_1\|d\tau\right]^2 \\ & + (\alpha_2 - \hat{\alpha}_2(0))\int_0^t \|\Phi\|\|\dot{X}_0\|\|\mathcal{Z}_2\|d\tau \\ & - \frac{c_2}{2}\left[\int_0^t \|\Phi\|\|\dot{X}_0\|\|\mathcal{Z}_2\|d\tau\right]^2 \\ & + (\alpha_3 - \hat{\alpha}_3(0))\int_0^t \|\Phi\|d\tau \\ & - \frac{c_3}{2}\left[\int_0^t \|\Phi\|d\tau\right]^2. \end{aligned}$$

By completing the square,

$$\begin{aligned} J_A \le\ & C_{01}^2 + \frac{(\alpha_1 - \hat{\alpha}_1(0))^2}{2c_1} + \frac{(\alpha_2 - \hat{\alpha}_2(0))^2}{2c_2} \\ & + \frac{(\alpha_3 - \hat{\alpha}_3(0))^2}{2c_3} \triangleq C_0^2 < \infty. \end{aligned}$$

The result follows using the same argument as before.

Remark 5.1

The primary advantage of this strategy is that one does not need to calculate the design parameters α_1, α_2, and α_3. Instead, these variables are updated on-line using simple algorithms.

6 TASK DISTRIBUTION

What is actually needed to guarantee the path tracking of the multi-robot/payload system is the vector of control torques for each robot (the elements of $\mathbf{T}$). Fortunately, since $\mathbf{W}$ is full rank (Property 2.1), there exists a matrix,

$$\mathbf{W}^+ = \mathbf{W}^T(\mathbf{W}\mathbf{W}^T)^{-1} \in R^{6d\times 6},$$

such that the total control torque $\mathbf{T}$ becomes

$$\mathbf{T} = \mathbf{J}^T\mathbf{F}_{end}, \qquad (69)$$

where

$$\begin{aligned} \mathbf{F}_{end} &= \mathbf{W}^+A^{-T}\mathcal{F} + \mathbf{F}_I \\ &\triangleq \mathbf{F}_P + \mathbf{F}_I. \end{aligned}$$

In these equations, $\mathbf{F}_P$ is the force causing the motion of the payload ($\mathcal{F}$ is computed by (44), (58) and (59),

or (64)–(66)) and $\mathbf{F}_I \in$ Null Space($\mathbf{W}$) represents an internal force vector. A well known formulation for $\mathbf{F}_I$,

$$\mathbf{F}_I = (E_{6d} - \mathbf{W}^{\sharp}\mathbf{W})\bar{\mu} \quad \forall \mu \in R^{6d}, \tag{70}$$

has been the basis for much work dealing with load distribution. However, it is noted in [34] that, although $\mathbf{F}_I$ in (69) satisfies $\mathbf{W}\mathbf{F}_I = 0$, it is an inadequate definition for internal force from a physical point of view. A recent work [31] also pointed out that (69) does not completely define the internal loading.

Furthermore, in practical applications force constraints are generally imposed on the manipulating forces/moments at the grasp points due to the limited control energy, i.e.,

$$\begin{aligned} |F_{end_j}(i)| &= |F_{P_j}(i) + F_{I_j}(i)| \le \mu_j(i), \\ & j = 1, \ldots, d, \quad i = 1, \ldots, 6, \end{aligned} \tag{71}$$

where $F_{end_j}(i)$, $F_{P_j}(i)$ and $F_{I_j}(i)$ are the i^{th} elements of the j^{th} partitions of $\mathbf{F}_{end}$, $\mathbf{F}_P$ and $\mathbf{F}_I$, respectively, and $\mu_j(i)$ are given positive numbers. Such constraints are also necessary to achieve fine manipulation.

So an interesting problem is how to distribute the task among the robots such that the force constraints (70) and $\mathbf{W}\mathbf{F}_I = 0$ are satisfied. The following strategy provides a solution to this problem.

First let

$\Omega_1 \triangleq$ {the set of robots working on the task}

$\Omega_2 \triangleq$ {the set of robots needing help}, and

$\Omega_3 \triangleq$ {the set of robots with spare capacity.}

Assume $\Omega_1 = \Omega_2 \bigoplus \Omega_3$ and $\Omega_2 \neq \{\emptyset\}$ and $\Omega_3 \neq \{\emptyset\}$. This implies that each robot either needs help or has spare capacity, at least one robot needs help and at least one robot can provide help. It is further assumed that the number of the robots with spare capacity is r and those robots are able to provide the required forces.

The strategy basically consists of two steps. Step 1 checks which robots need help and step 2 arranges the help. The first step uses $F_{P_j}(i)$ as a criterion. That is,

- *STEP 1a: If $|F_{P_j}(i)| \ge \mu_j(i)$, then $j \in \Omega_2$.*

- *STEP 1b: The F_{I_j} are adjusted so as to guarantee the force constraints (70). This is achieved by choosing F_{I_j} as*

$$\begin{aligned} F_{I_j}(i) &\triangleq F^*_{I_j}(i) \\ &= \begin{cases} \mu_j(i) - F_{P_j}(i), & \text{if } F_{P_j}(i) \ge \mu_j(i); \\ -\mu_j(i) - F_{P_j}(i), & \text{if } F_{P_j}(i) \le -\mu_j(i). \end{cases} \end{aligned} \tag{72}$$

The second step is motivated by the following observations. First it is noted that in order to make the payload asymptotically track the desired path, the total control force $\mathcal{F}$ must be equivalently generated by the total joint torque. Thus $\mathbf{T}$ should satisfy,

$$A^T\mathbf{W}\mathbf{J}^{-T}\mathbf{T} = A^T\mathbf{W}\mathbf{F}_{end} = \mathcal{F}. \tag{73}$$

With F_{I_j} specified as in (71), the condition (72) may not be satisfied. Furthermore, (71) may also cause the null space property of $\mathbf{F}_I$ to be violated. Hence we need to seek help from the other robots. Clearly such help should completely compensate the load that the robot j ($j \in \Omega_2$) cannot supply. This is ensured if the payload lies within the loading capacity of the robots (otherwise, more robots should be assigned to the task). Once F_{I_j} ($j \in \Omega_2$) is specified according to (71), F_{I_k} ($k \in \Omega_3$) must be chosen such that the null space condition holds. This is ensured if F_{I_k} is determined by

$$\sum_{k=k_1}^{k_r} W_k F_{I_k} = -\sum_{\text{all } j \in \Omega_2} W_j F^*_{I_j}, \tag{74}$$

where $F^*_{I_j}$ is given by (71).

In helping robot j ($j \in \Omega_2$), there is no constraint on how much effort each robot in Ω_3 should provide. Hence one generally has infinite choices for F_{I_k}, as long as the resultant $\mathbf{F}_I$ lies in the null space of $\mathbf{W}$. But what we are interested in is an "optimal" choice for the F_{I_k}. This brings us to step 2.

- *STEP 2: Determine the $F_{I_k}(i)$, $i = 1, \ldots, 6$, $k \in \Omega_3$, such that, under the constraints (70) and (73), the cost function,*

$$J_c(F_{I_k}) = \frac{1}{2}\sum_{k=k_1}^{k_r}\sum_{i=1}^{6} \rho_k(i) F^2_{I_k}(i) = \frac{1}{2}\chi^T P \chi, \tag{75}$$

is minimized. In this equation, $\rho_k(i) > 0$ is a weighting parameter, $\chi = [F^T_{I_{k_1}}\ F^T_{I_{k_2}} \ldots F^T_{I_{k_r}}]^T \in R^{6r}$ and $P = \text{diag}[\rho_k(i)] \in R^{6r \times 6r}$ is a symmetric, positive-definite matrix.

By denoting

$$\Gamma = -\sum_{\text{all } j \in \Omega_2} W_j F^*_{I_j} \in R^6,$$

the constraints (73) can be rewritten as

$$Q\chi = \Gamma, \tag{76}$$

where $Q = [W_{k_1}\ W_{k_2} \ldots W_{k_r}] \in R^{6 \times 6r}$. Therefore, the optimal task distribution problem under force constraints becomes

$$\begin{aligned} &\text{minimize:} && J_c(\chi) = \frac{1}{2}\chi^T P \chi \\ &\text{subject to:} && Q\chi = \Gamma. \end{aligned}$$

The Lagrangian multiplier method is used to solve this problem. Using ν_i, $i = 1, \ldots, 6$ as the Lagrange multipliers, the Lagrangian function is

$$\begin{aligned} L(\chi, \nu) &= J_c(\chi) + \sum_{i=1}^{6} \nu_i [(Q\chi)_i - \Gamma_i] \\ &= \frac{1}{2}\chi^T P \chi + \nu^T [Q\chi - \Gamma]. \end{aligned}$$

The necessary conditions for the optimal solution can be found from

$$\begin{aligned} \frac{\partial L(\chi, \nu)}{\partial \chi} &= \frac{\partial \left[\frac{1}{2}\chi^T P \chi\right]}{\partial \chi} + \frac{\partial \left[\nu^T Q \chi\right]}{\partial \chi} \\ &= P\chi + Q^T \nu = 0 \end{aligned}$$

and

$$\frac{\partial L(\chi, \nu)}{\partial \nu} = Q\chi - \Gamma = 0.$$

Thus

$$\nu^* = -\left[QP^{-1}Q^T\right]^{-1} \Gamma \tag{77}$$

and

$$\chi^* = P^{-1}Q^T \left[QP^{-1}Q^T\right]^{-1} \Gamma. \tag{78}$$

Correspondingly the minimium cost function is

$$J_{c_{optimal}} = L(\chi^*, \nu^*) = \frac{1}{2}\Gamma^T \left[QP^{-1}Q^T\right]^{-1} \Gamma. \tag{79}$$

Notice that the inverse of the matrix $[QP^{-1}Q^T]$ should exist in order to obtain (76), (77) and (78). Since this is an important issue concerning the existence of the optimal solution, a rigorous proof of the invertibility of the matrix $QP^{-1}Q^T$ is worth investigating. For simplicity, let $P = E_{6r}$, a unit matrix. In view of the definition of Q, it is seen that

$$QQ^T = W_{k_1} W_{k_1}^T + W_{k_2} W_{k_2}^T + \cdots + W_{k_r} W_{k_r}^T. \tag{80}$$

Since

$$W_i = \begin{bmatrix} E_3 & 0 \\ B_i & E_3 \end{bmatrix},$$

where

$$B_i = (Rc_i)\times,$$

then

$$W_{k_i} W_{k_i}^T = \begin{bmatrix} E_3 & B_{k_i}^T \\ B_{k_i} & E_3 + B_{k_i} B_{k_i}^T \end{bmatrix}.$$

Therefore

$$QQ^T = \begin{bmatrix} rE_3 & \sum_{i=k_1}^{k_r} B_i^T \\ \sum_{i=k_1}^{k_r} B_i & rE_3 + \sum_{i=k_1}^{k_r} B_i B_i^T \end{bmatrix}.$$

The Schur formula,

$$\det \begin{bmatrix} A & B \\ C & D \end{bmatrix} = \det(A)\det(D - CA^{-1}B)$$

gives

$$\det(QQ^T) = r\det[rE_3 + \Lambda],$$

where

$$\Lambda = \sum_{i=k_1}^{k_r} B_i B_i^T - \frac{1}{r}\left[\sum_{i=k_1}^{k_r} B_i\right]\left[\sum_{i=k_1}^{k_r} B_i^T\right].$$

With a little manipulation, it can be shown that

$$\begin{aligned} \left[\sum_{i=k_1}^{k_r} B_i\right]\left[\sum_{i=k_1}^{k_r} B_i^T\right] &= \sum_{i=k_1}^{k_r} B_i B_i^T \\ &\quad + \sum_{i=k_1}^{k_{r-1}} \sum_{j=i+1}^{k_r} (B_i B_j^T + B_j B_i^T). \end{aligned}$$

This relation reduces Λ to

$$\begin{aligned} \Lambda &= \frac{(r-1)}{r} \sum_{i=k_1}^{k_r} B_i B_i^T \\ &\quad - \frac{1}{r} \sum_{i=k_1}^{k_{r-1}} \sum_{j=i+1}^{k_r} (B_i B_j^T + B_j B_i^T). \end{aligned}$$

Also noting that

$$(r-1) \sum_{i=k_1}^{k_r} B_i B_i^T = \sum_{i=k_1}^{k_{r-1}} \sum_{j=i+1}^{k_r} (B_i B_i^T + B_j B_j^T)$$

$\forall r \geq 1$, it can be shown that

$$\Lambda = \frac{1}{r} \sum_{i=k_1}^{k_{r-1}} \sum_{j=i+1}^{k_r} (B_i - B_j)(B_i - B_j)^T,$$

which shows that Λ is at least positive semi-definite. Therefore $rE_3 + \Lambda$ is positive definite and QQ^T is invertible. The same conclusion can be drawn for a general diagonal P with more effort. Based on this discussion, following results can be claimed.

Theorem 6.1

If $\mathbf{T}$ is generated by

$$\mathbf{T} = \mathbf{J}^T \mathbf{W}^+ A^{-T} \mathcal{F} + \mathbf{J}^T \mathbf{F}_I, \tag{81}$$

where $\mathcal{F}$ is from (44), (58) and (59), or (64)–(66), F_{I_j} $(j \in \Omega_2)$ is specified by (71) and F_{I_k} $(k \in \Omega_3)$ is computed by (77), then;

(1) asymptotically stable path tracking is ensured,
(2) internal forces are non-zero at the contact points,
(3) force constraints are guaranteed and
(4) optimal sharing of the task is achieved.

Result 1 is true because such a $\mathbf{T}$ leads to the equivalent control force $\mathcal{F}$. Results 2, 3 and 4 hold because the choice for $\mathbf{F}_I$ satisfies (71), (73) and (77). The property of non-zero internal force is of particular interest in many advanced applications where no slippage and effective manipulation are required. It is seen that with this strategy, whenever $|F_{P_j}| > \mu_j(i)$, help from other robots is provided. Thus the given task is shared in a colleague-like manner in the sense that robots help each other when necessary. Furthermore, with F_{I_k} $(k \in \Omega_3)$ determined by (77), the task is shared among the robots in Ω_3 optimally in that the cost function (74) is minimized.

7 DESIGN EXAMPLE

The case of three robots (each with three joints) transfering a point-mass payload is used to demonstrated the application of the strategy. Note that no rotations are involved in this case. Assume that the force constraints at the grasp point for robot i $(i = 1,2,3)$ in the x, y and z directions are given in Newtons as

$$\begin{aligned} |F_{end_i}(x)| &\leq 120, \\ |F_{end_i}(y)| &\leq 150 \end{aligned}$$

and

$$|F_{end_i}(z)| \leq 150.$$

Since the payload is a point-mass with no rotation, $A = E_3$ and $\mathbf{W} = [E_3\ E_3\ E_3]$. Hence

$$W^+ = \frac{1}{3}\begin{bmatrix} E_3 \\ E_3 \\ E_3 \end{bmatrix}, \quad \mathbf{F}_P = \frac{1}{3}\begin{bmatrix} \mathcal{F} \\ \mathcal{F} \\ \mathcal{F} \end{bmatrix},$$

where $\mathcal{F} \in R^3$ is computed by (44), (58) and (59), or (64)–(66).

Suppose that at time t_1,

$$\begin{aligned} |F_{P_1}(x)(t_1)| &\geq 120, \\ |F_{P_1}(y)(t_1)| &\geq 150 \end{aligned}$$

and

$$|F_{P_1}(z)(t_1)| \geq 150.$$

Then robot 1 needs help and the $F_{I_1}(x/y/z)$ are specified as

$$F^*_{I_1}(x) = \begin{cases} 120 - \frac{1}{3}\mathcal{F}(x) & \text{if } \frac{1}{3}\mathcal{F}(x) \geq 120; \\ -120 - \frac{1}{3}\mathcal{F}(x) & \text{if } \frac{1}{3}\mathcal{F}(x) \leq -120, \end{cases}$$

$$F^*_{I_1}(y) = \begin{cases} 150 - \frac{1}{3}\mathcal{F}(y) & \text{if } \frac{1}{3}\mathcal{F}(y) \geq 150; \\ -150 - \frac{1}{3}\mathcal{F}(y) & \text{if } \frac{1}{3}\mathcal{F}(y) \leq -150 \end{cases}$$

and

$$F^*_{I_1}(z) = \begin{cases} 150 - \frac{1}{3}\mathcal{F}(z) & \text{if } \frac{1}{3}\mathcal{F}(z) \geq 150; \\ -150 - \frac{1}{3}\mathcal{F}(z) & \text{if } \frac{1}{3}\mathcal{F}(z) \leq -150. \end{cases}$$

To optimally help robot 1, choose $P = \frac{1}{4}E_6$. By (77) the task can be optimally shared if

$$F^*_{I_2} = -\frac{1}{2}F^*_{I_1} \quad \text{and} \quad F^*_{I_3} = -\frac{1}{2}F^*_{I_1},$$

and the minmium cost function is

$$J_{c_{optimal}} = \frac{1}{16}F^{*T}_{I_1}F^*_{I_1}.$$

It can be verified that;
(1) the force constraints are satisfied,
(2) the null space property holds,

$$\begin{aligned} \mathbf{W}\mathbf{F}_I &= F_{I_1} + F_{I_2} + F_{I_3} \\ &= F^*_{I_1} - \frac{1}{2}F^*_{I_1} - \frac{1}{2}F^*_{I_1} \\ &= 0 \end{aligned}$$

and
(3) the equivalent control force $\mathcal{F}$ is guaranteed since

$$\begin{aligned} A^T\mathbf{W}(\mathbf{F}_P + \mathbf{F}_I) &= E_3^T[E_3E_3E_3]\begin{bmatrix} F_{P_1} + F_{I_1} \\ F_{P_2} + F_{I_2} \\ F_{P_3} + F_{I_3} \end{bmatrix} \\ &= (F_{P_1} + F_{P_2} + F_{P_3}) \\ &\quad + (F_{I_1} + F_{I_2} + F_{I_3}) \\ &= (\frac{1}{3}\mathcal{F} + \frac{1}{3}\mathcal{F} + \frac{1}{3}\mathcal{F}) + 0 \\ &= \mathcal{F}. \end{aligned}$$

8 CONCLUSIONS

The path tracking control problem of a multi-robot system handling an unknown rigid payload is studied. Based on the combined dynamic model which reflects payload effects, three robust path tracking control algorithms are constructed. The payload can be of any shape as long as its center-of-mass is known. As can be seen, the strategies do not require wrist force sensors, but the quantity $\{(x_0, \phi_0), (\dot{x}_0, \dot{\phi}_0)\}$ is required. Also the matrix S_i, which depends on the location and orientation of the i^{th} end-effector, is needed. A vision system would be appropriate to obtain this information.

Notice that in this work the manipulation force and moment constraints are explicitly considered. In some applications, it is desirable to limit the stress in the

object while manipulating it. This imposes a constraint on the internal forces of the form,

$$F_{I_j}(i) \in \Delta_j(i), \tag{82}$$

where $\Delta_j(i)$ describes the region in which the i^{th} element of the internal force at contact point j should lie. This region is specified as

$$\Delta_j(i) = [\eta_j^-(i), \eta_j^+(i)]$$

where $\eta_j^-(i)$ and $\eta_j^+(i)$ are given constants.

A similar strategy can be developed to satisfy this requirement. It is natural to ask if one can choose a value for $F_{I_j}(i)$ $(j \in \Omega_2)$ such that both (70) and (81) are satisfied. The answer to this question is positive if the constraints imposed in (70) and (81) do not lead to conflicting choices for $F_{I_j}(i)$. Otherwise, the answer is negative.

In developing the control strategy, it is assumed that each robot firmly grasps the payload through the contact point. For some advanced applications, flexible grasping may be required. Hence extension of the results to the soft grasp case would be an interesting future research topic. Another issue worth investigating is the effects of load-transitions during "pick-up" and "drop-off" phases.

APPENDIX

Skew Symmetry of N_5

It is sufficient to show that $\mathcal{N}$ is skew-symmetric. In fact since

$$\omega_0 \times R = \dot{R},$$

it follows that

$$\begin{aligned}\mathcal{N} &= \frac{d}{dt}(T_0^T R I_0 R^T T_0) - 2T_0^T \omega_0 \times R I_0 R^T T_0 \\ &\quad - 2T_0^T R I_0 R^T \dot{T}_0 \\ &= (\dot{T}_0^T R I_0 R^T T_0 - T_0 R I_0 R^T \dot{T}_0) \\ &\quad + (T_0^T R I_0 \dot{R}^T T_0 - T_0^T \dot{R} I_0 R^T T_0).\end{aligned}$$

It can be verified that

$$\mathcal{N} + \mathcal{N}^T = 0,$$

which implies the skew-symmetry of N_5.

ACKNOWLEDGEMENT

This work was partially supported by the Center for Manufacturing Research at Tennessee Technological University and by NASA grant NAGW-2924.

References

[1] Alberts, T. E., and D. I. Soloway, "Force Control of a Multi-Arm Robot System," *Proc. of the 1988 IEEE Int. Conf. on Robotics and Automation*, Philadephia, PA, April 1988, pp. 1490–1496.

[2] Alford, C. O., and S. M. Belyeu, "Coordinated Control of Two Robots Arms," *Proc. of the 1984 IEEE Int. Conf. on Robotics and Automation*, Atlanta, GA, 1984.

[3] Anderson, J. N., and M. E. Pittelkau, "Reflex-Action Position Control and Two-Arm Load-Sharing Force Control for Robotic Manipulators," Tech. Report No. MCTR-1-88-1, Center for Manufacturing Research, Tennessee Technological University, January 1988.

[4] Arimoto, S., F. Miyazaki and S. Kawamura, "Cooperative Motion Control of Multiple Robot Arms or Fingers," *Proc. of the 1989 IEEE Int. Conf. on Robotics and Automation*, Raleigh, NC, March 1987, pp. 1407–1412.

[5] Carignan, C. R., and D. L. Akin,"Optimal Force Distribution for Payload Positioning Using a Planar Dual-Robot," Jour. of Dynamic Systems, Measurement and Control, Vol. 111, 1989, pp. 205–210.

[6] Cole, A., J. Hause and S. Sastry, "Kinematics and Control of Multifingered Hands with Rolling Contact," *Proc. of the 1988 IEEE Int. Conference on Robotics and Automation*, Philadephia, PA, April 1988, pp. 228–233.

[7] Craig, J. J., P. Hsu and S. Sastry, "Adaptive Control of Robotic Manipulators," Int. Jour. of Robotics Research, Vol. 6 (6), 1987.

[8] Furuta, K., K. Kosuge, Y. Shiote and H. Hatano, "Master-Slave Manipulator Based on Internal Model-Following Control Concept," *Proc. the 1987 IEEE Int. Conf. on Robotics and Automation*, Raleigh, NC, March 1987, pp. 567–572.

[9] Hayati, S., "Position and Force Control of Coordinated Multiple Arms," IEEE Trans. on Aerospace and Electronic Systems, Vol. 24, No. 5, September 1988, pp. 584–590.

[10] Hsu, P., "Control of Multi-Manipulator Systems — Trajectory Tracking, Load Distribution, Internal Force Control and Decentralized Architecture," *Proc. of the 1989 IEEE Int. Conf. on Robotics and Automation*, Scottsdale, AZ, May 1989, pp. 1234–1239.

[11] Hu, Y. R., and A. A. Goldenberg, "An Adaptive Approach to Motion and Force Control of Multiple Coordinated Robot Arms," *Proc. of the 1989 IEEE Int. Conf. on Robotics and Automation*, Scottsdale, AZ, May 1989, pp. 1091–1096.

[12] Leahy, Jr., M. B., "Compensation of Industrial Manipulator Dynamics in the Presence of Variable Payloads," Int. Jour. of Robotics Research, Vol. 9 (4), 1990, pp. 86–98.

[13] Li, Z., P. Hsu and S. Sastry, "Dynamic Coordination of a Multi-Robot System with Point Contact," *Proc. of the 1988 American Control Conference*, 1988, pp. 505–510.

[14] Luh, J. Y. S., and Y.-F. Zheng, "Constrained Relations Between Two Coordinated Industrial Robots for Motion Control," Int. Jour. of Robotics Research, Vol. 6 (3), 1987, pp. 60–70.

[15] Mo, L., and M. M. Bayoumi, "Adaptive Control of the Multi-arm Robotic System" *Proc. of the 28th IEEE Int. Conf. on Decision and Control*, Tampa, FL, December 1989, pp. 1962–1963.

[16] Nakamura, Y., K. Nagai and T. Yoshikawa, "Mechanics of Coordinative Manipulation By Multiple Robotic Mechanisms," *Proc. of the 1987 IEEE Int. Conf. on Robotics and Automation*, Raleigh, NC, March 1987, pp. 991–998.

[17] Orin, D. E., and S. Y. Oh, "Control of Force Distribution in Robotic Mechanisms Containing Closed Kinematic Chains," ASME Jour. of Dynamic Systems, Measurement, and Control, Vol. 102, 1981, pp. 134–141.

[18] Özgüner, Ü., S. Yurkovich and F. Al-Abbass, "Decentralized Variable Structure Control of a Two-Arm Robotic System," *Proc. of the 1987 IEEE Int. Conf. on Robotics and Automation*, Raleigh, NC, March 1987, pp. 1248–1254.

[19] Pittelkau, M. E., "Adaptive Load-Sharing Force Controller for Two-Arm Manipulators," *Proc. of the 1988 IEEE Int. Control on Robotics and Automation*, Philadephia, PA, April 1988, pp. 498–505.

[20] Popov, V. M., *Hyperstability of Control Systems*, Acdemic Press, New York, 1973.

[21] Salisbury, J. K., and J. J. Craig, "Articulated Hands: Force Control and Kinematics Issues," Int. Jour. Robotics and Research, Vol. 1, 1982, pp. 4–17.

[22] Shames, J., *Engineering Mechanics: Dynamics*, Prentice-Hall, Englewood Cliffs, NJ, 1960.

[23] Song, Y.-D., and J. N. Anderson, "Adaptive Control of a Colleague-Like Multi-Robot System Handling a Common Unknown Object," *Proc. of the 30th IEEE Conf. on Decision and Control*, Brighton, England, December, 1991.

[24] Song, Y.-D., and J. N. Anderson, "Adaptive Path Tracking Control of Robot Manipulators with Uncertain Payload Dynamics," Systems and Control Letters, Vol. 17, 1991, pp. 59–70.

[25] Song, Y.-D., and J. N. Anderson, "System Stability and Performance Analysis Based on the Generalized System Energy Accumulation: Part I — Criteria Development," *Proc. of 1st IEEE Int. Conf. on Control Applications*, September, 1992.

[26] Song, Y.-D., and R. H. Middleton, "Dealing with the Impassive Parameter Variation Problem of Robot Manipulators Performing Path Tracking Tasks," IEEE Trans. on Automatic Control, 1992 (to appear).

[27] Spong, M. W., and M. Vidyasagar, *Robot Dynamics and Control*, Wiley, New York, 1989.

[28] Suh, I. H., and K. G. Shin, "Coordination of Dual Robot Arms Using Kinematic Redundancy," *Proc. of the 1988 IEEE Int. Conf. on Robotics and Automation*, Philadephia, PA, April 1988, pp. 504–509.

[29] Tarn, T. J., A. K. Bejczy and X. Yun, "Nonlinear Control Algorithms for Multiple Robot Arms," IEEE Trans. on Aerospace and Electronic Systems, Vol. 24, No. 5, 1988, pp. 571–583.

[30] Unseren, M. A., and A. J. Koivo, "Kinematic Relations and Dynamic Modeling for Two Cooperating Manipulators in Assembly," *Proc. IEEE Conf. on Systems, Man, and Cybernetics*, 1987, pp. 789–802.

[31] Walker, I. D., R. A. Freeman and S. I. Marcus, "Analysis of Motion and Internal Loading of Objects Grasped by Multiple Coorperating Manipulators," Int. Jour. of Robotics Research, Vol 10(4), 1991, pp. 396–409.

[32] Walker, I. D., S. I. Marcus and R. A. Freeman, "Distribution of Dynamic Loads for Multiple Cooperating Robot Manipulators," Jour. of Robotics Systems, Vol. 6 (1), 1989, pp. 35–47.

[33] Walker, M. M., D. Kim and J. Dionise, "Adaptive Coordinated Motion Control of Two Manipualtor Arms," *Proc. of the 1989 IEEE Int. Conf. on Robotics and Automation*, Scottsdale, AZ, May 1989, pp. 1084–1090.

[34] Yoshikawa, T., and K. Nagai, "Manipulating and Grasping Force in Manipulation by Multifingered Robot Hands," IEEE Trans. Robotics and Automation, Vol. 7, No. 1, 1991, pp. 67–77.

[35] Yun, X., "Nonlinear Feedback Control of Two Manipulators in the Presence of Environmental Constraints," *Proc. of the 1989 IEEE Int. Conf. on Robotics and Automation*, Scottsdale, AZ, 1989, May 1989, pp. 1252–1259.

[36] Zheng, Y.-F., and J. Y. S. Luh, "Optimal Load Distribution for Two Industrial Robots Handling a Single Object," *Proc. of the 1988 IEEE Int. Conf. on Robotics and Automation*, Philadephia, PA, April 1988, pp. 344–349.

S11-37

N93-19463

Robust Motion Tracking Control of Robotic Arms Based on the Generalized Energy Accumulation Principle

Y. D. Song J. N. Anderson ⋆ A. Homaifar H. Y. Lai

NASA Center for Aerospace Research
North Carolina A&T State University, Greensboro, NC 27411

⋆ Center for Manufacturing Research
Tennessee Technological University, Cookeville, TN 38505

1. Objective

Consider a rigid-link robot with the dynamic model

$$\tau = H(q;p)\ddot{q} + C(q,\dot{q};p)\dot{q} + G(q;p) + \mathcal{N}(t)$$

where $\mathcal{N}(.)$ denotes a bounded external disturbance (definitions of other terms and variables can be found in the literature). The objective addressed herein is to find a control strategy that exhibits the following features: (1) simple to implement, (2) easy to code for program and (3) robust to possible time-varying uncertainties

2. Results

Define tracking error ϵ as $\epsilon = q - q^*$, where q^* denotes the desired trajectory. Also let $W = \dot{\epsilon} + D\epsilon$, $y_s = \dot{q}^* - D\epsilon$, and $x_s = \ddot{q}^* - D\dot{\epsilon} - \dot{\kappa}\kappa^{-1}W$, where $D = D^T > 0$ and $\kappa(t)$ is one of the rate functions which is introduced to adjust rate-of-convergence (ROC) (see [4]).

Definition 1

Let $\nu(t)$ be defined on $[t_0,\infty)$. $\nu(t)$ is in the class $\mathcal{V}_I$ if $\nu(t)$ is nonnegative constant or in $\mathcal{V}_{II}$ if $\nu(t)$ is bounded, positive, and decreasing for all $t \in [t_0,\infty)$.

The robust control law is given by

$$\tau = H_s(q^*;p^*)x_s + C_s(q^*,\dot{q}^*;p^*)y_s + G_s(q^*;p^*) - KW + U_a, \quad (1)$$

where $K = K^T > 0$, and $H_s(.)$, $C_s(.)$, and $G_s(.)$ are simplified versions of H, C, and G, respectively. U_a is an auxiliary control defined by

$$U_a = -\frac{W\eta^2}{\|W\|\eta + \nu(t)}, \quad (2)$$

where $\nu(t) \in \mathcal{V}_I$ or $\mathcal{V}_{II}$ and η is a nonnegative scalar nonlinear function defined as

$$\begin{aligned}\|H_s - H\|\|x_s\| \;+\; &\|C_s - C\|\|y_s\| + \|G_s - G - \mathcal{N}\| \\ \le\; &\alpha_0\|x_s\| + \alpha_1\|\dot{q}\|\|y_s\| + \alpha_2 \triangleq \eta.\end{aligned}$$

In this equation, α_i are constants representing bounds on the modelling errors. There are many possible choices for $\nu(t)$ in U_a, and different choices leads to different tracking properties. The $\nu(t)$ defined by

$$\nu(t) = \frac{1}{2}v_1(1+t^m)^\rho e^{-v_2 t^n} \quad (3)$$

are in $\mathcal{V}_I$ or $\mathcal{V}_{II}$ if m, n, and ρ are chosen properly (v_1 and v_2 are appropriate positive constants). Specifically, if $\rho = -1$, $m,n = 0$, one gets $\nu(t) = v_1 e^{-v_2} \triangleq \mu_0$, which gives, $U_a = -\frac{W\eta^2}{\|W\|\eta+\mu_0}$. This is called saturation (or boundary layer) controller [1] and has been widely used to achieve bounded stability. Another specific choice for $\nu(t)$ ($\rho = -1$, $m = 0$, $n = 1$) is $\nu(t) = v_1 e^{-v_2 t}$, which gives the strategy proposed by Dawson, et al. [2], $U_a = -\frac{W\eta^2}{\|W\|\eta + v_1 e^{-v_2 t}}$. An extreme case, $n \to \infty$, $m \to \infty$ and $\rho = -1$, gives $\nu(t) = 0$, which corresponds to the variable structure control [3], $U_a = -\frac{W}{\|W\|}\eta$. As is shown later, $\nu(t) = 0$ gives the fastest convergence, while $\nu(t) = \mu_0$ gives the slowest. However, due to physical limitations, "too fast" could lead to chattering. Hence, the choice of $\nu(t)$ depends on the requirements for ROC, transient response, and steady state performance.

Tracking stability results based on the so-called generalized energy accumulation principle [4] are given next.

Theorem 1: *Given (1) and (2), if $\nu(t)$ and $\kappa(t)$ are chosen such that*

$$\int_{t_0}^{t} \nu(\tau)\kappa^2(\tau)d\tau \le C_2^2 < \infty \qquad \forall t \in [t_0,\infty), \quad (4)$$

then stable path tracking is ensured and the rate-of-convergence is at least $\kappa^{-1}(t)$.

Proof (outline): The closed-loop model is governed by

$$\begin{aligned}H(q;p)(\dot{W} + \dot{\kappa}\kappa^{-1}W) + C(q,\dot{q};p)W &= -KW \\ +\; \delta H(q;p)x_s + \delta C(q,\dot{q};p)y_s + \delta\mathcal{G}(q,t;p) + U_a.\end{aligned}$$

where $\delta H(.) = H_s - H, \delta C(.) = C_s - C, \delta\mathcal{G}(.) = G_s - G - \mathcal{N}$. Introducing the transformation $\Psi = \kappa W$ gives

$$\begin{aligned}H(q;p)\dot{\Psi} \;+\; &C(q,\dot{q};p)\Psi = -K\Psi + \delta H(q;p)x_s\kappa \\ +\; &\delta C(q,\dot{q};p)y_s\kappa + \delta\mathcal{G}(q,t;p)\kappa + U_a\kappa.\end{aligned}$$

According to the criteria in [4], boundedness of the accumulated generalized energy, $\int_{t_0}^{t} \Psi^T K \Psi d\tau$, proves tracking stability. In fact,

$$\begin{aligned} J^c &= \int_{t_0}^{t} \Psi^T K \Psi d\tau \\ &= -\int_{t_0}^{t} \Psi^T H(q;p)\dot{\Psi} d\tau - \int_{t_0}^{t} \Psi^T C(q,\dot{q};p)\Psi d\tau \\ &+ \int_{t_0}^{t} \Psi^T \{\delta H(q;p)x_s\kappa + \delta C(q,\dot{q};p)y_s\kappa + \delta \mathcal{G}(q,t;p)\kappa\} \\ &+ \int_{t_0}^{t} \Psi^T U_a \kappa d\tau. \end{aligned}$$

The symmetric positive definite property of $H(.)$ and the skew-symmetric property of $\dot{H}(.) - 2C(.)$ yields,

$$J^c \le C_v^2 + \int_{t_0}^{t} \|\Psi\|\eta\kappa d\tau + \int_{t_0}^{t} \Psi^T U_a \kappa d\tau \qquad (5)$$

where $C_v^2 = \frac{1}{2} W^T H W \kappa^2|_{t=t_0}$. Inserting (2) into (5),

$$\begin{aligned} J^c &\le C_v^2 + \int_{t_0}^{t} \|\Psi\|\eta\kappa d\tau - \int_{t_0}^{t} \Psi^T \kappa \frac{W\eta^2}{\|W\|\eta + \nu(\tau)} d\tau \\ &= C_v^2 + \int_{t_0}^{t} \nu(\tau)\kappa^2 \frac{\|W\|\eta}{\|W\|\eta + \nu(\tau)} d\tau \\ &\le C_v^2 + \int_{t_0}^{t} \nu(\tau)\kappa^2(\tau) d\tau. \qquad (6) \end{aligned}$$

Condition (4) implies J^c is bounded. The result follows [4].

Theorem 2: *Given (1) and (2), if $\nu(t)$ and $\kappa(t)$ are chosen such that*

$$\limsup_{t\to\infty} \frac{1}{t-t_0} \int_{t_0}^{t} \nu(\tau)\kappa^2(\tau) d\tau \le C_2^2 < \infty \qquad \forall t \in [t_0, \infty),$$

then stable path tracking is also ensured.

Proof: The proof follows the approach used in [4].

Corollary *If $\kappa(t)$ and $\nu(t)$ are chosen such that*

$$\kappa^2(t)\nu(t) \le C_s^2 < \infty, \qquad (7)$$

then stable path tracking is ensured.

Proof: Under the condition of the Corollary, it is seen that $\int_{t_0}^{t} \nu(\tau)\kappa^2(\tau) d\tau \le C_s^2(t - t_0)$. Therefore, $\limsup_{t\to\infty} \frac{J^c}{t-t_0} = \limsup_{t\to\infty} \frac{C_s^2}{t-t_0} + C_s^2$.

Several observations are made. First H_s, C_s and G_s are not based on q, $\dot{q}$ and p, but on the desired path $\{q^*, \dot{q}^*\}$ and parameters p^* which can be precomputed off-line. Second, one does not need to re-organize the robotic dynamics (so as to isolate unknown parameters) before calculating the control torque. Also a simple way to get $H_s(.)$, $C_s(.)$, and $G_s(.)$ is to set, $H_s = 0$, $C_s = 0$, and $G_s = 0$, the control torque reduces to $\tau = -KW + U_a$. This gives the same structure as in [2]. However, since $\|U_a\| \le \eta$, $H_s = 0, C_s = 0$, and $G_s = 0$ leads to a larger U_a which could require more control energy.

3. Synthesis Examples

Example 1: (Natural Rate-of-Convergence)

Assume that a natural ROC is sufficient ($\kappa(t) = 1$). Then

$$J^c \le C_v^2 + \int_{t_0}^{t} \nu(\tau) d\tau.$$

Suppose that $\nu(t)$ is chosen such that $J^c \le C_v^2 + \int_{t_0}^{t} \nu(\tau) d\tau \le J^*$, where J^* is a design specification. If $\nu(t) = v_1 e^{-v_2 t}$, with $v_1 > 0, v_2 > 0$, then $J_A \le C_v^2 + \frac{v_1}{v_2} e^{-v_2 t_0}$. In order to meet the specification, v_1 and v_2 are determined such that $C_v^2 + \frac{v_1}{v_2} e^{-v_2 t_0} \le J^*$. Suppose $t_0 = 0$ and the initial condition is such that $C_v^2 = 10$. It the performance specification is $J^* = 12$, then $\frac{v_1}{v_2} \le 2$. So by choosing $v_2 > 0$ and $0 < v_1 \le 2v_2$, $J_A \le J^*$.

Example 2: (Variable Structure Control)

For any $\kappa(t)$, J^c is ensured to be less than or equal to C_v^2 (see (6)) by choosing $\nu(t) = 0$. This implies that the ROC can be arbitrarily fast and the accumulated tracking error is smaller than any other choice of ν. So one might conclude that variable structure control gives the best control performance and the greatest ROC. However, it is its fast speed that causes chattering. So from a practical point of view, one should not require too large a ROC over the entire period of operation. A piecewise ROC may be useful. This can be achieved by methods similar to those given in [4].

4. Comment

Clearly ν plays an interesting role in these robust control strategies. First, ν is related to the overall tracking performance in that the bound on J^c depends on the choice of ν. Second, ν specifies the boundary layer in the strategies. Since ν is time varying, the boundary layer is also varying. This property can be used to retain the merits of the VSC strategy and avoid the problem of chattering.

Acknowledgement

This work was partly supported by NASA grant NAGW-2924.

References

[1] J. J. Slotine and W. Li, Applied Nonlinear Control, 1991.

[2] D. Dawson, Z. Qu and S. Lim, "Re-thinking the Robust Control of Robot Manipulators," *Proc. of IEEE Conf. CDC 1991.*

[3] V. I. Utkin, Control System with Variable Structure, 1976.

[4] Y. D. Song and J. N. Anderson, "System Stability Analysis Based on Generalized Energy Accumulation: Part I — Criteria Development," *Proc. of IEEE Conf. Control Application*, 1992.

System Stability and Performance Analysis Based on Generalized Energy Accumulation: Part II — Applications

Y.D. Song J.N. Anderson ⋆ A. Homaifar H.Y. Lai

NASA Center for Aerospace Research
North Carolina A&T State University, Greensboro, NC 27411

⋆ Center for Manufacturing Research
Tennessee Technological University, Cookeville, TN 38505

Abstract

Based on the generalized energy accumulation principle, criteria for system stability and performance analysis are established in the first part of this work [8]. These criteria are of immediate use in many systems. The main purpose in this part of the work is to apply these criteria to robotic systems. Both adaptive and robust control are investigated.

1. Introduction

The concept of stability concerning a dynamic system is always important to system engineers. Motivated by the generalized energy accumulation principle, certain criteria for testing system stability are proposed in [8]. As a continuation to that work, this paper demonstrates the applications of the established criteria to a practical system — robotic system. Specifically, the path tracking control problem of robotic systems is considered. By introducing the concept of rate transformation, new adaptive and robust control strategies are developed which achieve stable path tracking and provide a priori information about how fast the tracking errors will converge. With these strategies, different rates-of-convergence (ROCs) can be obtained by simply choosing a different scalar rate function $\kappa(t)$ (to be defined later). It turns out that the conventional adaptive control scheme is a special case of the proposed strategies (i.e., with $\kappa(t) = 1$). Global exponential path tracking is easily achieved by simply setting $\kappa(t) = e^{\lambda t}$, where $\lambda > 0$. Moreover, one may obtain other types of path tracking than asymptotic and exponential tracking by choosing a proper κ.

2. Review of Stability Criteria

For convenience and continuity, stability criteria established in [8] are summarized first.

By introducing a rate function $\kappa(t)$ (see §3 for definition), stability criteria represented by integral inequalities in [8] can be unified as follows,

$$J^c = \int_{t_0}^{t} \kappa^2(\tau) G_c[x(\tau)] d\tau \leq C_A^2 < \infty,$$

where $G_c(.)$ is a generalized energy function of the s tem and C_A is a real number. To analyze system stabil and performance, one only needs to verify these equalit (see [8] for more details). It is seen that asymptotic s bility corresponds to $\kappa(t) = 1$, while exponential stabil corresponds to $\kappa(t) = e^{\lambda t}$.

3. A Useful Lemma [8]

The objective is to derive new adaptive and robust c trol strategies, which ensure stable path tracking and low adjustable ROCs. To this end, the concepts of r function and rate transformation are introduced.

Definition 3.1 Rate Function

A real function of time, $\kappa(t)$, is a rate function (deno by $\kappa(t) \in \mathcal{S}$), if it satisfies the following conditions:

(1) $\kappa(t)$ is positive for all $t \in [t_0, \infty)$,
(2) $\kappa(t_0)$ is bounded,
(3) $\kappa(t)$ is increasing, and
(4) $\dot{\kappa}(t)$ is well-defined for $t \in [t_0, \infty)$.

Note that under these conditions, such a $\kappa(t)$ is inverti and $\kappa^{-1}(t)$ is upper bounded and decreasing. Obvi examples for such a rate function include $\kappa = 1$, $\kappa = t$ $\kappa = e^{\lambda t}$, $(1 + t)e^{\lambda t}$, $(1+t)+e^{\lambda t}$ $(\lambda > 0)$ etc. (see [8] other types).

Definition 3.2 Rate Transformation

The rate transformation is defined as

$$\Psi = \kappa(t)\chi, \qquad (3.1)$$

where $\kappa(t)$ is a rate function as defined before.

The terminology "rate transformation" is motivate the fact that such a transformation affects the rat convergence of the system, as is shown in the followi

Consider a nonlinear system described by

$$\dot{\chi} = f(\chi; p), \qquad \chi(t_0) = \chi_0, \tag{3.2}$$

where $\chi \in R^n$ is the system state vector, $p \in R^s$ is the system parameter vector, and $f \in R^n$ is a nonlinear vector function of χ and p. Applying the rate transformation (3.1) to (3.2) leads to

$$\dot{\Psi} = \dot{\overline{\kappa(t)}}\kappa^{-1}\Psi + \kappa f(\Psi\kappa^{-1}; p) \triangleq F(\kappa, \dot{\kappa}, \Psi; p), \tag{3.3a}$$

$$\Psi(t_0) = \kappa(t_0)\chi(t_0) \tag{3.3b}$$

where $F(\kappa, \dot{\kappa}, \Psi, p)$ is a new nonlinear function. It should be noted that the transformed system (3.3) is not equivalent to the original system (3.2) in the sense that the stability of (3.2) does not necessarily guarantee the stability of (3.3). However the stability of (3.3) absolutely guarantees the stability of (3.2). This is specified by the following lemma.

Lemma 3.3

Let κ be a rate function as defined before. Consider the systems (3.2) and (3.3), related by (3.1). If system (3.3) is stable (bounded or asymptotically stable), the system (3.2) converges to its equilibrium point with a certain ROC.

Proof:

Noting that $\chi = \kappa^{-1}\Psi$ and κ^{-1} is decreasing, the result can be easily obtained. §

Based on this lemma, it is seen that if the transformed system (3.3) is at least bounded stable, then the original one exhibits enhanced stability. This result which is an extension of [6] (where a special choice for κ is utilized, i.e., $\kappa = e^{\lambda t}$) is used in the solution of the tracking problem. Note that since χ could either be tracking error, state estimation error, regulation error, or model following error, the idea behind this lemma could also be used in these cases. Investigation of this possibility, beyond the scope of this work, represents an interesting further research effort.

4. Application to Robotic Systems

The formulation for the dynamics of a serial-link robot with n joints is

$$H(q; p)\ddot{q} + C(q, \dot{q}; p)\dot{q} + G(q; p) = \tau, \tag{4.1}$$

where

$\tau \in R^n$	control torque,
$q, \dot{q}, \ddot{q} \in R^n$	joint positions/velocities/accelerations,
$p \in R^s$	equivalent system parameters,
$H(q; p) \in R^{n \times n}$	symmetric, positive, definite inertia matrix,
$C(q, \dot{q}; p)\dot{q} \in R^n$	joint torques and forces due to Coriolis and centrifugal effects, and
$G(q; p) \in R^n$	torques and forces due to gravity.

Concerning this model, the following structural property is useful.

Property 4.1

For a rigid robot with the dynamics (4.1) in which $C(q, \dot{q}; p)$ is defined as in [5], then

$$H(q; p)x + C(q, \dot{q}; p)y + G(q; p) = \Phi(q, \dot{q}, y, x)p \tag{4.2}$$

and

$$v^T \left\{ \frac{d}{dt}H(q; p) - 2C(q, \dot{q}; p) \right\} v = 0, \ \forall v \in R^n, \tag{4.3}$$

where $x \in R^n, y \in R^n, \Phi = [\Phi_1, \Phi_2, ..., \Phi_s]$ $R^{n \times s}$ and $\Phi_i \in R^n$. It is worth mentioning that in (4.2) $\dot{y} = x$ is not required. This restriction is typically assumed in the literature. Equation (4.3) represents the well-known skew-symmetric property.

Note that this equation represents a highly nonlinear and strongly coupled system. In general, not all the information concerning the system parameters is available a priori. Thus the path tracking control problem is stated as follows:

Given the desired path, $\{q^*, \dot{q}^*, \ddot{q}^*\}$, find a control torque, $\tau(q, \dot{q}, q^*, \dot{q}^*, \ddot{q}^*)$, which depends only on the joint positions and velocities, such that the actual path, $\{q, \dot{q}\}$, automatically tracks the desired path with a controllable ROC in the presence of uncertain system parameters represented by p.

Note that there is an essential difference between this problem statement and that which is typically seen in the literature. This problem statement not only requires convergence of the tracking errors, but also imposes the requirement of an adjustable ROC. This is of particular interest in many practical applications.

4.1 Adaptive Tracking with Adjustable ROC

The criteria proposed in Part I of this work are applied to synthesize new adaptive control algorithms for robotic systems that achieve stable path tracking with controllable ROCs. First let the tracking error be defined as

$$\epsilon \triangleq q - q^* \tag{4.4}$$

and let W represent an auxiliary variable defined by

$$W \triangleq \dot{\epsilon} + D\epsilon. \tag{4.5}$$

Also let

$$s_p \triangleq \ddot{q}^* - D\dot{\epsilon} - \dot{\kappa}(t)\kappa^{-1}(t)W \tag{4.6}$$

and

$$y_p \triangleq \dot{q}^* - D\epsilon, \tag{4.7}$$

where $D \in R^{n \times n}$ is a symmetric positive definite matrix and $\kappa(t)$ is a rate function. The controller structure for path tracking is given by

$$\tau = H(q; \hat{p})s_p + C(q, \dot{q}; \hat{p})y_p + G(q; \hat{p}) - KW, \tag{4.8}$$

where $K = K^T > 0$ is a controller gain matrix, and $\hat{p} \in R^s$ is the vector of parameter estimates as determined by the following algorithms.

Estimation Algorithm 1 (I-Estimate)

$$\hat{p}_i = -\alpha_i \int_{t_0}^{t} W^T \Phi_i(q, \dot{q}, y_s, x_s)\kappa^2(\tau)d\tau + \hat{p}_i(t_0), \quad i = 1, 2, ..., s, \tag{4.9}$$

where $\alpha_i > 0$ is an adaptation gain (design parameter), $\hat{p}_i(t_0)$ is the initial parameter estimate, and Φ_i is the i-th element of the vector Φ defined by Equation (4.2).

Estimation Algorithm 2 (PI-Estimate)

$$\hat{p}_i = \hat{p}_i(t_0) - \alpha_i \int_{t_0}^{t} W^T \Phi_i(q, \dot{q}, y_s, x_s)\kappa^2(\tau)d\tau - \beta_i W^T \Phi_i(q, \dot{q}, y_s, x_s)\kappa^2(t), \ i = 1, 2, ..., s, \tag{4.10}$$

where $\beta_i \geq 0$ is one other adaptation gain.

Theorem 4.1

Consider the robot dynamics (4.1) with the controller (4.8). If the parameters are estimated by (4.9) or (4.10), then stable path tracking control is ensured. The rate-of-convergence is specified by $\kappa^{-1}(t)$, which can be chosen by the designer.

Proof: Combining (4.1) and (4.8) yields the closed-loop system dynamics,

$$H(q;p)(\dot{W} + \dot{\kappa}\kappa^{-1}W) + C(q, \dot{q}; p)W = -KW + \sum_{i=1}^{s}(\hat{p}_i - p_i)\Phi_i(q, \dot{q}, y_s, x_s) \tag{4.11}$$

where Property 4.1 was used. Introducing the rate transformation, $\Psi = \kappa W$, (4.11) becomes

$$H(q;p)\dot{\Psi} + C(q, \dot{q}; p)\Psi = \sum_{i=1}^{s}(\hat{p}_i - p_i)\Phi_i(q, \dot{q}, y_s, x_s)\kappa - K\Psi.$$

According to the criteria in [8], it is only necessary to show the boundedness of the accumulated generalized energy $J^c = \int_{t_0}^{t} \Psi^T K \Psi d\tau$. Using the above equation, Property 4.1 and integration by parts, yields

$$\begin{aligned} J^c &= -\int_{t_0}^{t} \Psi^T H(q;p)\dot{\Psi}d\tau - \int_{t_0}^{t} \Psi^T C(q, \dot{q}; p)\Psi d\tau \\ &\quad + \sum_{i=1}^{s}\int_{t_0}^{t}(\hat{p}_i - p_i)W^T\Phi_i\kappa^2(\tau)d\tau \\ &\leq C_v^2 + \sum_{i=1}^{s}\int_{t_0}^{t}(\hat{p}_i - p_i)W^T\Phi_i\kappa^2(\tau)d\tau \end{aligned}$$

where $C_v^2 = \frac{1}{2}W^T H W \kappa^2|_{t=t_0}$. Inserting (4.9) and applying the following relation

$$\int_{t_0}^{t}\int_{t_0}^{\tau} \Phi(\tau)d\tau\Phi(\gamma)d\gamma = \frac{1}{2}\left[\int_{t_0}^{t}\Phi(\gamma)d\gamma\right]^2, \tag{4.12}$$

J^c reads

$$\begin{aligned} J^c &\leq C_v^2 - \sum_{i=1}^{s}\frac{\alpha_i}{2}\left[I_i - \frac{\hat{p}_i(t_0) - p_i}{\alpha_i}\right]^2 + \sum_{i=1}^{s}\frac{[p_i - \hat{p}_i(t_0)]^2}{2\alpha_i} \\ &\leq C_v^2 + \sum_{i=1}^{s}\frac{[p_i - \hat{p}_i(t_0)]^2}{2\alpha_i} < \infty, \end{aligned} \tag{4.}$$

where $I_i = \int_{t_0}^{t} W^T \Phi_i \kappa^2(\tau)d\tau$. The boundedness of implies that Ψ is at least L_2. Note that $W = \kappa^{-1}\Psi$, result follows. (The result for Estimation Algorithm can be shown in the same way.) §

4.2 Illustrative Examples

To make the foregoing concepts clear, three examp are presented in this section.

Example 1 Asymptotic Convergence

Suppose the control torque is of the same structure in (4.8). If $\kappa = 1$, then ϵ, y_s, W are defined as bef and

$$x_s = \ddot{q}^* - D\dot{\epsilon}.$$

Estimation Algorithm 1 becomes

$$\hat{p}_i = -\alpha_i \int_{t_0}^{t} W^T \Phi_i(q, \dot{q}, y_s, x_s)d\tau + \hat{p}_i(t_0), i = 1, 2, ...$$

Considering the proof of Theorem 4.1, convergence this case is asymptotic.

Example 2

Choosing $\kappa(t)$ as $\kappa(t) = 1 + t$ gives

$$x_s = \ddot{q}^* - D\dot{\epsilon} - \frac{1}{1+t}W,$$

and

$$W = \dot{\epsilon} + D\epsilon = \frac{\Psi}{1+t}.$$

Estimation Algorithm 2 is now

$$\begin{aligned} \hat{p}_i &= -\alpha_i \int_{t_0}^{t} W^T \Phi_i(q, \dot{q}, y_s, x_s)(1+\tau)^2 d\tau \\ &\quad - \beta_i W^T \Phi_i(q, \dot{q}, y_s, x_s)(1+t)^2 + \hat{p}_i(t_0), \end{aligned}$$

$i = 1, 2, ..., s$. In this case, convergence is stronger asymptotic due to the choice of κ.

Example 3 Exponential Convergence

Let $\kappa(t)$ be the exponential function $\kappa(t) = e^{\lambda t}$. In case

$$x_s = \ddot{q}^* - D\dot{\epsilon} - \lambda W$$

$$W = \dot{\epsilon} + D\epsilon = \Psi e^{-\lambda t}.$$

The parameter estimation algorithm is

$$\begin{aligned}\dot{\hat{p}}_i &= -\alpha_i \int_{t_0}^{t} W^T \Phi_i(q,\dot{q},y_s,x_s)e^{2\lambda\tau}d\tau \\ &- \beta_i W^T \Phi_i(q,\dot{q},y_s,x_s)e^{2\lambda t} + \dot{\hat{p}}_i(t_0), i = 1,2,...,s.\end{aligned}$$

This corresponds to the exponential tracking.

It is observed from the above examples that for different $\kappa(t)$, different ROCs for the filtered tracking errors are achieved. It is interesting to note that $\kappa(t) = 1$ corresponds to the conventional adaptive control [1-2][4-5]. Note that in this case, $W = \Psi$ and the ROC of W is not adjustable. As for the exponential tracking, one only needs to choose $\kappa(t) = e^{\lambda t}$, where $\lambda > 0$. Also it is possible to change the ROC over different time intervals. This can be done by the technique shown in [8].

4.3 Robust Tracking with Adjustable ROC

Robust control of robotic systems has been extensively investigated recently [1]. Most of the strategies are based on upper bounds of the uncertain model. Obtaining such bounds, however, is not trivial because H, C, and G are complicated matrices depending on $q, \dot{q}$ and p. Improper determination of such bounds may lead to instability. A strategy based on the maximum absolute value of each element of H, C, and G is suggested as follows.

Let $H_s(.)$, $C_s(.)$ and $G_s(.)$ represent simplified versions of $H(.)$, $C(.)$ and $G(.)$, respectively. Also let p^* represent the nominal system parameters and q^* and $\dot{q}^*$ represent the desired trajectory.

For the following development, let

$$\begin{aligned}\delta H = [\delta h_{ij}] &= H(q;p) - H_s(q^*;p^*), \\ \delta C = [\delta c_{ij}] &= C(q,\dot{q};p) - C_s(q^*,\dot{q}^*;p^*), \\ \delta G = [\delta g_i] &= G(q;p) - G_s(q^*;p^*).\end{aligned}$$

The robust control torque is given by

$$\tau = H_s(q^*;p^*)\dot{x}_s + C_s(q^*,\dot{q}^*;p^*)y_s + G_s(q^*;p^*) - KW + U_a, \quad (4.14a)$$

where $K = K^T > 0$ and U_a is an auxiliary control defined by

$$\begin{aligned}U_a &= \sum_{i=1}^{n}\sum_{j=1}^{n} s_{ij}^H U(i,j)x_s \\ &+ \sum_{i=1}^{n}\sum_{j=1}^{n} s_{ij}^C U(i,j)y_s + \sum_{i=1}^{n} s_i^G U(i), \quad (4.14b)\end{aligned}$$

In equation (4.14b), $U(i,j)$ are '$0-1$' matrices [9] and s_{ij}^H, s_{ij}^C and s_i^G are scalars to be defined later. The tracking stability of the system is now addressed by the following result.

Theorem 4.2

Let the control strategy be defined by (4.14). If

$$s_{ij}^H = -\frac{W_i x_{s_j} \bar{h}_{ij}^2}{|W_i x_{s_j}|\bar{h}_{ij} + \nu(t)},$$

$$s_{ij}^C = -\frac{W_i x_{s_j} \bar{c}_{ij}^2}{|W_i y_{s_j}|\bar{c}_{ij} + \nu(t)}$$

$$s_i^G = -\frac{W_i \bar{g}_i^2}{|W_i|\bar{g}_i + \nu(t)},$$

where $\bar{h}_{ij} = \max|\delta h_{ij}|$, $\bar{c}_{ij} = \max|\delta c_{ij}|$, $\bar{g}_i = \max|\delta g_i$ *and* κ *and* ν *satisfy*

$$\int_{t_0}^{t} \kappa^2 \nu d\tau \le C_{1s} < \infty \quad (4.15$$

or

$$\kappa^2 \nu \le C_{2s} < \infty \quad (4.1$$

then stable path tracking is achieved.

Proof (outline):

Note that with the control (4.14a), the closed-loo model becomes

$$\begin{aligned}&H(q;p)(\dot{W} + \dot{\kappa}\kappa^{-1}W) + C(q,\dot{q};p)W = -KW \\ &+ \delta H(q;p)\dot{x}_s + \delta C(q,\dot{q};p)y_s + \delta G(q;p) + U_a.\end{aligned}$$

Introducing the transformation $\Psi = \kappa W$ and using U_a (4.14b) gives

$$\begin{aligned}H(q;p)\dot{\Psi} &+ C(q,\dot{q};p)\Psi = -K\Psi \\ &+ \sum_{i=1}^{n}\sum_{j=1}^{n}[s_{ij}^H + \delta h_{ij}]U(i,j)\dot{x}_s\kappa \\ &+ \sum_{i=1}^{n}\sum_{j=1}^{n}[s_{ij}^C + \delta c_{ij}]U(i,j)y_s\kappa \\ &+ \sum_{i=1}^{n}[s_i^G + \delta g_i]U(i)\kappa.\end{aligned}$$

Considering the performance index $J^c = \int_{t_0}^{t} \Psi^T K \Psi d\tau$ is not difficult to show that

$$\begin{aligned}J^c &= \int_{t_0}^{t} \Psi^T K \Psi d\tau \\ &\le C_v^2 + \sum_{i=1}^{n}\sum_{j=1}^{n}\int_{t_0}^{t} \frac{|W_i x_{s_j}|\bar{h}_{ij}^2}{|W_i x_{s_j}|\bar{h}_{ij} + \nu}\kappa^2\nu d\tau \\ &+ \sum_{i=1}^{n}\sum_{j=1}^{n}\int_{t_0}^{t} \frac{|W_i y_{s_j}|\bar{c}_{ij}^2}{|W_i y_{s_j}|\bar{c}_{ij} + \nu}\kappa^2\nu d\tau \\ &+ \sum_{i=1}^{n}\int_{t_0}^{t} \frac{|W_i|\bar{g}_i^2}{|W_i|\bar{g}_i + \nu}\kappa^2\nu d\tau \\ &\le C_v^2 + \sum_{i=1}^{n}\sum_{j=1}^{n}\int_{t_0}^{t} \kappa^2\nu d\tau \\ &+ \sum_{i=1}^{n}\sum_{j=1}^{n}\int_{t_0}^{t} \kappa^2\nu d\tau + \sum_{i=1}^{n}\int_{t_0}^{t} \kappa^2\nu d\tau\end{aligned}$$

With the choices for κ and ν as in (4.15) or (4.16), ei the index is bounded or its time average is bounded the result follows. §

This strategy is easy to apply since the upper bound for each element, $|\delta h_{ij}|_{max}$, $|\delta c_{ij}|_{max}$, and $|\delta g_i|_{max}$, can be easily obtained by using the facts that $|\sin(.)| \leq 1$ and $|\cos(.)| \leq 1$.

Note that there are many possible choices for ν (see the table below, where $\mu_0 \geq 0, \upsilon_1 > 0$ and $\upsilon_2 \geq 0$). The impact of ν (and κ) on system performance is discussed later.

Table 4.1 Possible Choices for ν

μ_0	$\upsilon_1 e^{-\upsilon_2 t}$	$\upsilon_1 e^{-\upsilon_2 t^2}$	$\frac{\upsilon_1(1+t)}{e^{\upsilon_2 t}}$
$\frac{\upsilon_1 e^{-\upsilon_2}}{1+t}$	$\frac{\upsilon_1 e^{-\upsilon_2 t}}{1+t}$	$\frac{\upsilon_1 e^{-\upsilon_2 t^2}}{1+t}$	$\frac{\upsilon_1(1+t^2)}{e^{\upsilon_2 t}}$
$\frac{\upsilon_1 e^{-\upsilon_2}}{1+t^2}$	$\frac{\upsilon_1 e^{-\upsilon_2 t}}{1+t^2}$	$\frac{\upsilon_1 e^{-\upsilon_2 t^2}}{1+t^2}$	$\frac{\upsilon_1(1+t)}{e^{\upsilon_2 t^2}}$
$\frac{\upsilon_1 e^{-\upsilon_2}}{1+t^3}$	$\frac{\upsilon_1 e^{-\upsilon_2 t}}{1+t^3}$	$\frac{\upsilon_1 e^{-\upsilon_2 t^2}}{1+t^3}$	$\frac{\upsilon_1(1+t^2)}{e^{\upsilon_2 t^2}}$

The strategy presented herein exhibits the following features. The structure is simple and most of the required computations can be performed prior to real-time operation. As for the computation of H_s, C_s and G_s, one may choose them to be constant matrices/vector (or diagonal matrices for H_s and C_s), or simply zero. Additionally, time varying uncertainties can be easily handled by the strategy. Again since the rate function is utilized, the ROC is adjustable.

4.4 Tracking Performance Analysis

In addition to the tracking stability, it is important to explore the tracking performance that the strategies can achieve. The criteria for testing stability can also serve this purpose. The following is a brief discussion of this issue. Only adaptive control is considered. Referring to the proof of Theorem 4.1, it is found that the performance index for both the Estimation Algorithms 1 and 2 can be computed as

$$J^c(I, II) = \eta_0 + \eta_1 + \eta_2$$

where

$$\begin{aligned} \eta_0 &= W^T H(q(\tau); p) W \kappa^2(\tau)|_{\tau=t_0} \\ \eta_1 &= \sum_{i=1}^{s} \int_{t_0}^{t} (\hat{p}_i - p_i) W^T \Phi_i \kappa^2(\tau) d\tau \\ \eta_2 &= -W^T H(q(\tau); p) W \kappa^2(\tau)|_{\tau=t}. \end{aligned}$$

It is seen that only η_1 changes for the different estimation algorithms. When $\hat{p}_i$ is estimated by the I-Estimate (4.9),

$$\begin{aligned} \eta_1 &= -\sum_{i=1}^{s} \int_{t_0}^{t} (\hat{p}_i - p_i) W^T \Phi_i \kappa^2 d\tau \\ &= -\sum_{i=1}^{s} \left\{ \frac{\alpha_i}{2} I_i^2 + [p_i - \hat{p}_i(t_0)] I_i \right\} \triangleq \eta_1(I). \end{aligned}$$

For the PI-Estimate, since $\hat{p}_i$ is updated by (4.10),

$$\begin{aligned} \eta_1 &= -\sum_{i=1}^{s} \int_{t_0}^{t} (\hat{p}_i - p_i) W^T \Phi_i \kappa^2(\tau) d\tau \\ &= -\sum_{i=1}^{s} \left\{ \frac{\alpha_i}{2} I_i^2 + [p_i - \hat{p}_i(t_0)] I_i \right\} \\ &\quad - \beta_i \int_{t_0}^{t} (W^T \Phi)^2 \kappa^2 d\tau \triangleq \eta_1(II). \end{aligned}$$

Thus

$$\eta_1(II) = \eta_1(I) - \beta_i \int_{t_0}^{t} (W^T \Phi)^2 \kappa^2(\tau) d\tau \leq \eta_1(I).$$

Correspondingly it is indicated that

$$J^c(II) \leq J^c(I),$$

which implies that better tracking performance can b achieved by using the PI-Estimate. This conclusio agrees with the comment made in [3]. Simulation result presented in Figures 4.1-4.2 also verify this point (see [7 for more details).

At this point, we are also able to address the effec of the initial estimation on tracking performance. Tradi tionally, it is suggested that the initial estimate may b chosen arbitrarily (zero in general). This is because th stability is global and the initial estimate does not affec tracking stability. However, as clearly shown in (4.13) the initial estimate affects the overall tracking perfo mance in the sense that a "better" initial estimate result in a tighter bound J^c. Simply choosing $\hat{p}_i = 0$, as sug gested typically in the literature, is among the "worst choices. Choosing the nominal value of p_i as the initi estimate results in a smaller J^c, implying better perfo mance. This is also confirmed by simulation results (s [7]). These points, however, are not directly evident fro the Lyapunov stability method.

Finally, the impact of ν, $\kappa(t)$, K, and D on syste performance is discussed. It is noted that K and D a required to be symmetric positive definite. Their choic are related to the desired robustness, speed of respons and disturbance rejection properties. The roles of κ an ν are related to the rate of convergence. Note that sin the control torque τ is defined as in (4.8), if κ and ν a chosen such that ϵ and $\dot{\epsilon}$ rapidly tend to zero, then t control torque also rapidly tends to the desired value, τ However, if they are chosen so that the convergence rate is too fast, the control torques in the transition sta may exceed the admissible values. Hence some trade-o between ROC and control energy have to be made practice.

5. Concluding Remarks

This paper has demonstrated the application of the c teria established in [8] to robotic systems. Performan

analysis based on these criteria was also given. Additional applications of these results can be found in [7]. Note that the criteria and their applications are based on continuous systems. Given that discrete time systems are extensively encountered in practice, extensions of these results to discrete-time systems represent an important research effort. Due to the limited space, results concerning this aspect are omitted. Interested readers are referred to [7] for details.

Acknowledgement

This work was partly supported by NASA grant NAGW-2924.

References

[1] C. Abdallah, D. Dawson, P. Dorato and M. Jamshidi,"Survey of Robust Control for Rigid Robots," IEEE Control Systems Magazine, Vol. 11, No.2, 1991, pp. 24–30.

[2] M. Bodson and S. Sastry,"Adaptive Control: Convergence and Robustness," Prentice-Hall, Advanced Reference Series, 1989, pp. 229–231.

[3] S. Gutman,"Uncertain Dynamical Systems — A Lyapunov min-max Approach," IEEE Trans. on Automatic Control, Vol.24, 1979, pp. 511–522

[4] I.D. Landau and R. Horowitz,"Synthesis of Adaptive Controllers for Robot Manipulators Using Passive Feedback System Approach," Int. J. Adaptive Control and Signal Processing. Vol.3, No.1, 1989.

[5] J.J. Slotine and W. Li, Applied Nonlinear Control, Prentice Hall, Englewood Cliffs, 1991.

[6] Y.D. Song, R.H. Middleton and J.N. Anderson,"Study on the Exponential Path Tracking Control of Robot Manipulators via Direct Adaptive Methods," to appear in Int. J. of Robotics and Autonomous Systems, Vol. 9, 1992, pp.271-282.

[7] Y. D. Song and J. N. Anderson, "The Principle of Generalized Energy Accumulation and Its Application to the Motion Control of Robotic Systems," Tech Report No. MCTR-0792-02, July 1992.

[8] Y. D. Song and J. N. Anderson, "System Stability and Performance Analysis Based on Generalized Energy Accumulation: Part I — Criteria Development," IEEE 1st Int. Conf. on Control Applications, September, 1992.

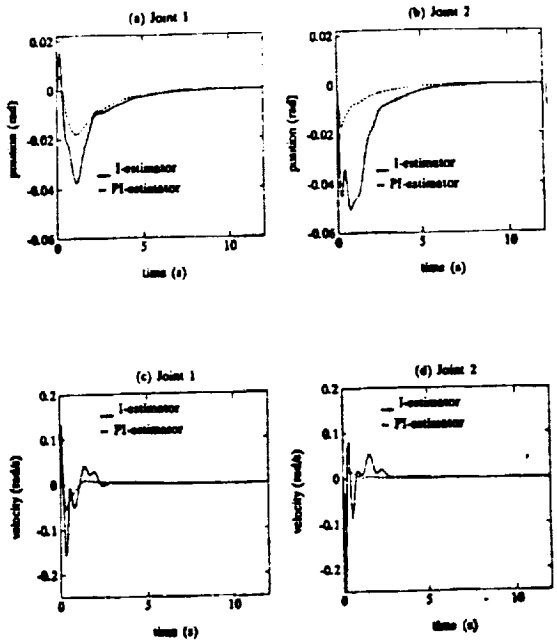

4.1 Tracking Errors with Adaptive Control

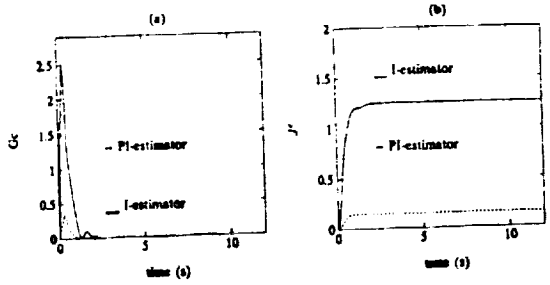

4.2 Performance Index with Adaptive Control

PREV. ANN.
92A 56836
OMIT

AIAA 92-4013

BOUNDARY LAYER STUDY ON NOZZLE WALL AT HYPERSONIC VELOCITIES

Kenneth M. Jones, Fred R. DeJarnette,
and Wayland C. Griffith
North Carolina State University
Raleigh, North Carolina

William J. Yanta
Naval Surface Warfare Center
Dahlgren Division, White Oak Detachment
Silver Spring, Maryland

AIAA 17th Aerospace Ground Testing Conference
July 6-8, 1992 / Nashville, TN

BOUNDARY LAYER STUDY ON NOZZLE WALL AT HYPERSONIC VELOCITIES

Kenneth M. Jones*, Fred R. DeJarnette†, and Wayland C. Griffith‡
Mars Mission Research Center
North Carolina State University
Raleigh, NC 27695-7921
919-515-5931

and

William J. Yanta**
Naval Surface Warfare Center
Dahlgren Division, White Oak Detachment
Silver Spring, MD 20903-5000
301-394-1928

Abstract

The boundary layer on the wall of Naval Surface Warfare Center (NSWC) Hypervelocity Tunnel 9 has been investigated with pitot pressure and total temperature measurements. Experimental results are presented for standard and supercooled Mach 14 runs. To the authors' knowledge this is the first published boundary layer data at supercooled conditions. The experimental results are compared to numerical predictions made with a Navier-Stokes algorithm including vibrational nonequilibrium and intermolecular force effects. For standard tunnel conditions, the numerical solutions agree very well with experimental data. For the supercooled cases, the numerical code predicts the total temperature well; however, it overpredicts the pitot pressure.

Nomenclature

E	energy per unit volume, J/m^3
M	Mach number
p	pressure, Pa
T	temperature, K
u	axial velocity, m/sec
v	radial velocity, m/sec
x	axial coordinate, m
y	radial coordinate, m
γ	ratio of specific heats
δ	boundary layer thickness, m
δ^*	displacement thickness, m
ρ	density, kg/m^3

Subscripts

c	core conditions
e	boundary layer edge conditions
o	supply conditions
rot	rotational
s	local conditions
t	total conditions
tr	translational
v	vibrational

Introduction

The recent interest in the development of high speed vehicles has been instrumental in the renewed study of hypersonic aerodynamics. The design of these proposed vehicles will probably be accomplished through the use of computational fluid dynamics (CFD). However, the computational techniques must be verified at conditions as close as possible to the actual flight regime of the vehicles. Thus, hypersonic experimental facilities are needed which can produce quality flow and test flow characteristics accurately at well defined conditions.

The most common method of producing high Mach number flow is to rapidly expand a gas at high pressure and temperature through an axisymmetric nozzle. The flow quality achieved by this process is almost exclusively dependent on nozzle design and construction. In most cases, the design of a nozzle has been performed by first calculating the inviscid core and then adding a boundary layer displacement thickness correction at each station to obtain the final physical wall coordinate. Since hypersonic nozzles have relatively thick boundary layers, the main difficulty in the nozzle design has been the accurate calculation of the boundary layer growth and the displacement thickness. Recent papers [1,2] discuss the accuracy of classical methods of nozzle design at high Mach numbers and propose the use of a Navier-Stokes solution algorithm to design these nozzles. They found that inviscid/boundary-layer codes were inaccurate above Mach 8.

---

* Research Assistant, Member AIAA
† Professor/Director of Mars Mission Research Center, Associate Fellow AIAA
‡ Professor Emeritus, Fellow AIAA
** Chief Technologist, Associate Fellow AIAA

The purpose of this investigation was to make actual measurements of the Pitot pressure distribution and total temperature distribution through the boundary layer on a hypersonic nozzle. The measurements would be used to develop a data base that could be used to validate numerical codes for nozzle design and analysis as well as other applications for the codes. In addition the investigation developed data at supercooled conditions that has never before been obtained. This data will help in the determination of whether supercooling is a viable means of obtaining higher Mach numbers in existing facilities.

Experiment

Test Facility

Experiments were conducted in the Hypervelocity Wind Tunnel No. 9 at the Naval Surface Warfare Center, Silver Spring, Maryland. Tunnel 9 (shown schematically in Figure 1) is a blowdown facility which uses nitrogen as the working fluid. The test section is over twelve feet long and five feet in diameter. The tunnel operates at Mach numbers of 8, 10 and 14 by means of interchangeable contoured nozzles. Maximum Reynolds numbers are approximately 50×10^6 per foot at Mach 8, 20×10^6 per foot at Mach 10, and 3.8×10^6 per foot at Mach 14 [3].

In Tunnel 9, the gas is pressurized and pre-heated at levels up to T_o = 1900 K and P_o = 1400 atm. Two metal diaphragms are ruptured to initiate the flow. After passage of the transient starting shocks, quasi-steady flow is established from 250 milliseconds to several seconds depending on the reservoir conditions selected. The throat-to-test cell distance is 40 feet (12 meters), giving a characteristic flow transient time of 6 to 8 seconds. The diameter of the potential core flow is approximately 3 feet [3] in the test section, which makes the boundary layer thickness approximately 12 inches.

Test Apparatus/Instrumentation

A tunnel mounted traversing mechanism [4] was used to obtain pitot pressure and temperature data in a continuous manner through the boundary layer. The system incorporates a hydraulically driven blade with a total travel of 33 inches. Probes mounted on the end of the blade can be moved across the tunnel flow from the test cell wall to a point two to three inches beyond the tunnel centerline. The traversing system was activated automatically at a pre-determined time after tunnel start up and traversed the boundary layer in 600 to 700 milliseconds. The traversing blade was instrumented with an extension, shown in Figure 2, to survey the boundary layer 15 inches up stream of the nozzle exit plane. The extension arm was designed to accommodate a test head (shown in Figure 3) which had provisions for two pitot pressure tubes and a fine wire temperature probe.

Pressure Measurements

A Pitot probe was mounted on either side of the temperature probe. A large Pitot probe was fabricated from 0.173 inch I.D./ 0.203 inch O.D. stainless steel tubing. The small Pitot probe was fabricated from 0.033 inch I.D./ 0.049 inch O.D. stainless steel tubing. The spacing between the two probe tips was 2.3125 inches and the probes were flat faced.

The boundary layer pitot pressures were measured with Kulite XCW-065-5A pressure transducers which were mounted in the traversing blade head to minimize tubing lengths and reduce pressure response time. Tubing diameters and lengths for pressure measurements were selected to minimize response time and reduce pipe organ oscillation effects. Procedures for tubing selection are given in [5], which produced response times generally below 5 msec. Since response time varies inversely with the pressure, selection of tubing sizes had to be matched to the local values of pressure. This was especially critical for the boundary layer survey, where the pressure varied significantly from the wall to the freestream. The use of two probes provided a check of probe response as well as measurement redundancy over a sizeable region of the survey.

No corrections are applied to the pitot pressures measured in the boundary layer. However, the possible variations attributable to different effects are summarized as follows. The effects of thermal transpiration errors due to temperature variations along the tube connecting the orifice and the transducer are negligible [6]. Errors in wall pressure resulting from orifice effects due to heat transfer to the wall are less than 3% [7]. Beckwith, et. al. [8] have shown that the Reynolds number based on free stream conditions and the probe height was a good correlation parameter for the correction due to viscous and rarefied flow effects. In this investigation, the Reynolds numbers were so high, that this effect could be neglected. An estimate of the uncertainty of the measured pressures P_o and Pitot are $\pm$ 0.5% and$\pm$ 0.3%, respectively [3,9].

Temperature Measurements

A fine-wire, total temperature probe was mounted in the center of the traversing probe to obtain direct, independent measurements of total temperature through the boundary layer. Temperature data can serve as an independent check on measurements obtained through other methods. The temperature probe is constructed of two thermocouples, known as the midpoint or sensing thermocouple and the support or reference thermocouple (Figure 4). The sensing thermocouple is formed by the junction of two 0.003 inch diameter wires strung between the probe supports,which are 0.3 inches apart. The reference thermocouple is composed of two 0.005 inch diameter wires

and is welded to the end of one support. The thermocouple wires are carried back to the probe mount through stainless tubing, which is electrically insulated with ceramic inserts. The thermocouple materials are alloys of Tungsten with 5% Rhenium by weight and Tungsten with 26% Rhenium by weight. The probe supports are also fabricated from the same alloys. These materials will withstand temperatures in excess of 3500 K and furthermore the high tensile strength of the alloy make it possible for the fine diameter wires to withstand the dynamic loads encountered in a blow down tunnel.

The temperature probe was designed to be small and streamlined to allow its insertion into the flow field without significantly altering the flow. The sensing thermocouple of the probe is treated as a simple one-dimensional rod exposed to a crossflow. Analysis of this is possible, with the temperatures measured at the two thermocouple locations providing the boundary conditions required for the solution of the one-dimensional heat transfer equation, that leads to the flow field stagnation temperature.The probe configuration minimizes radiation and conduction losses. Radiation is proportional to wire diameter and conduction is inversely proportional to wire length-to-diameter (L/D) ratio. With a small wire diameter of 0.003 inches and a large L/D of 100, the losses to radiation and conduction are low. The algorithm used to calculate total temperature from the probe accounts for radiation and conduction losses, as well as real gas effects[10]. The error in the temperature probe is estimated to be ± 5%[10].

Data Acquisition

All pressure transducers were calibrated prior to each tunnel run. As the tunnel was being evacuated from atmospheric pressure to approximately 1 mm Hg, transducer response was recorded at eight calibration points. The evacuation was temporarily halted when data were recorded to ensure uniform pressure in the test cell. Two MKS Baratron type 145 transducers, one with a range of 1000 mm Hg and the other with a range of 10 mm Hg, monitored the test cell pressure and were used as the reference standards. Then the method of least-squares was used to calculate a slope and intercept for each transducer.

The data for the test were recorded on the DARE VI (Data Acquisition and Recording Equipment) system. The DARE VI is a simultaneous-sample-and-hold, single amplifier -per- channel system with 14 bit resolution. The output signals from all DARE VI channels were amplified and fed through six-pole, low-pass Bessel filters with a cutoff frequency of 60 Hz. The data was collected at sample rates of 250 Hz per channel and 500 Hz per channel.

Some of the data from the Dare VI recording system was digitally filtered using a low pass sixth-order Butterworth filter. A cutoff frequency of 10 Hz was used for tunnel supply conditions, test cell pitot pressure and rake pitot pressures.

Test Procedures

Boundary layer surveys were conducted in two phases:

- Phase I surveys were conducted at Mach 14 standard conditions (Typical supply conditions: P_0 = 1344 atm, T_0 = 1800 K). These cases were used as a baseline for all other runs.
- Phase II surveys were conducted at Mach 14 with varying degrees of supercooling. The Mach 14 case with 29.4 K of supercooling has supply conditions: Po = 32.246 MPa , To = 680.78 K.

Numerical Prediction

A Navier-Stokes computational fluid dynamic algorithm [2,11] which includes the effects of intermolecular forces and vibrational nonequilibrium, was used to determine the flow field in Tunnel 9. The set of coupled governing equations are approximated by finite differences. These time-dependent equations are implicitly integrated forward in time on a grid of finite volumes until a steady-state solution is obtained. The numerical method uses a modified form of Steger-Warming flux vector splitting to accurately simulate the spatial derivatives appearing in the governing equations. In order to account for the intermolecular force effects associated with large densities, an empirical equation of state developed by Jacobsen, et. al. [12] for nitrogen is used. A turbulent boundary layer was assumed throughout the nozzle and was predicted using a Cebeci -Smith algebraic turbulence model [13]. The solution of the governing equations yields the variables ρ, ρu, ρv, E_v and E_{tr+rot}. Given these quantities, the translational-rotational temperature, pressure, vibrational temperature, and speed of sound are calculated. The code requires as input: T_o, P_o and the x,y coordinates for the nozzle contour and the wall temperature at each contour point .

Results and Discussion

For this study, measured pitot pressures and total temperature measurements through the boundary layer of a contoured nozzle are presented. Due to the magnitude of the data, only two representative cases will be presented. Experimental results will be presented for standard Mach 14 conditions(run 2240), P_0= 136.23 MPa, T_0= 1800.6 K and a Mach 14 run with 29.4 K of supercooling(run 2237), P_0=32.246 MPa, T_0= 680.78 K. Predictions from the Navier-Stokes code are compared with these experimental data.

As noted in reference [14], the real-gas effects in the expansion of nitrogen through a hypersonic nozzle are confined to the initial region where the Mach number is less than 9. In general, this region is between the settling chamber and one meter downstream of the nozzle throat. Beyond this point, the nitrogen behaves like a prefect gas (γ=1.4). This allows the use of the prefect-gas relations to reduce tunnel data in this region. Therefore, the local values of Mach number in the boundary layer were calculated from the Rayleigh pitot formula using the ratio of static pressure to pitot pressure.

$$\frac{p_t}{p_s} = \left[\frac{(\gamma+1)M^2}{2}\right]^{\frac{\gamma}{\gamma-1}} \left[\frac{\gamma+1}{2\gamma M^2-(\gamma-1)}\right]^{\frac{1}{\gamma-1}}$$

At present there is some question as to the accuracy of this method for supercooled data. The method does predict Mach numbers that agree well with the numerical solutions for standard cases as will be shown later.

Since the shock lies so close to the probe, it is almost impossible to accurately measure a static pressure through the boundary layer. Therefore, a constant static pressure through the boundary layer was assumed. Although the measured wall pressure was different from the boundary layer edge value, the wall pressure was corrected to be the edge value and assumed to be constant through the entire boundary layer. This is similar to the method used by Backx [15].

The Navier -Stokes algorithm [11] was run on a Cray Y-MP and required between 3 to 4 hours of CPU time to obtain a converged solution. The CPU time requirement was a function of the number of grid points employed. A total of ninety grid points was used in the radial direction,y. Grid points in the axial direction, x, varied from 444 to 730 depending on resolution requirements. It was determined that a very fine grid was required in the subsonic and throat region in order to capture the true centerline Mach number distribution. In the supersonic region, the grid was gradually expanded to a much coarser grid. The grid was body fitted and exponentially stretched in the radial direction. This allowed for the clustering of points near the wall in order to resolve the boundary layer. The minimum grid spacing in the radial direction was defined as the distance from the centerline to the nozzle wall divided by 2000.

Figures 5 and 6, show the comparison of tunnel supply temperature, T_0, and the probe temperature, T_{probe}, with tunnel run time. Since there are no chemical reactions taking place in the flow, T_0 should be constant in the core flow and be a good comparison for the accuracy of the temperature probe. As seen in Figure 5, a standard condition run, the probe temperature begins to track with T_0 as soon as the probe exits the boundary. In this case, the probe measurements are 3% higher than the measured T_0. For the 29.4 K supercooled run shown in Figure 6, the probe temperature tracks with T_0 upon exiting the boundary layer. In this case the probe temperatures are 3% lower than the measured T_0. These results are in agreement with Hill's predictions in reference [16].

Figure 7 shows the Mach contours for a standard Mach '14 run, T_0=1800.6 K, P_0=136.23 MPa. The numerical solution obtained a maximum Mach number of 14.3 compared to an experimental Mach number of 14.17. Figures 8 and 9 give the total temperature and pitot pressure profiles for the numerical and measured data. Figure 8 shows that the temperature probe measures a constant 1900 K in the core and starts to indicate a steady decrease in temperature at 0.3 meters from the nozzle wall. At the wall, the probe indicates an upturn in the temperature. The numerical solution predicts a total temperature of 1790 K in the core and a decrease in this core temperature starting at 0.18 meters from the nozzle wall. The numerical solution underpredicts the total temperature in the core by approximately 1% and overpredicts the total temperature through the boundary layer.

Figure 9 shows that the pitot pressure is a constant 0.087 MPa in the core and transitions smoothly into the boundary layer. This transition occurs at 0.32 meters from the nozzle wall. The numerical solution predicts a total pressure of 0.092 MPa in the core and a transition into the boundary layer at 0.24 meters off the wall. The numerical solution overpredicts the experimental pressure by 7%. The numerical pressure decreases at a much steeper rate than the experimental pressure through the boundary layer. Figure 10 shows the Mach number profile through the boundary layer. The numerical solution overpredicts the experimental core Mach number by 0.9%.

Figure 11 gives the Mach number contours for the supercooled run, T_0=680.78 K, P_0=32.246 MPa, with 29.7 K of supercooling. The numerical solution gives a maximum Mach number of 13.02, compared to a Mach number of 14.76 calculated from the total pressure measurements. A grid resolution study was conducted for this case to determine if a finer grid would give a better core Mach number. A final grid spacing of 0.01 inch was used in the subsonic and throat region; however, this had no effect on the exit Mach number. Use of the Rayleigh pitot formula to calculate the experimental Mach number from the total and static pressures may be in error for this case.

Figure 12 shows the comparison of numerical and experimental total temperatures. The temperature probe indicates a constant total temperature of 690 K in the core and a transition to the boundary layer at 0.22 meters from the nozzle wall. At the wall, the probe temperature again

appears to increase as it did in the standard run. The numerical method predicted a total temperature of 715 K in the core and a transition to the boundary layer at 0.22 meters off the wall. The computed total temperature is approximately 3% higher than the value measured with the fine-wire probe in the core and continues to overpredict the temperature through the boundary layer.

Figure 13 shows the comparison of the pitot pressures. The total pressure in the core increases up to the boundary layer then begins to decrease to the wall forming a "dog-leg" in the pressure profile. The boundary layer is thinned somewhat with this surge in pressure. This phenomena is observed in all the highly supercooled cases. This effect could be due to the supercooling or it could be due to running the tunnel too far off design conditions. This phenomena requires more investigation and additional pressure data to be obtained at varying degrees of supercooling to fill the gaps between the existing data points. The numerical solution predicts a total pressure in the core of 0.26 MPa compared to a maximum experimental value of 0.21 MPa. The numerical code predicts a near constant pressure through the core, whereas the experimental data shows the pressure increasing from 0.17 MPa in the central core to 0.21 MPa at the boundary layer edge. Through the boundary layer, the numerical solution underpredicts the measured pitot pressure. Figure 14 gives the Mach number profiles through the boundary layer.

In general, the total temperature profiles obtained experimentally look reasonable. When the traverse starts at the nozzle wall, the fine-wire probe appears to be sensing a temperature higher than the wall temperature (294 K). Since the temperature probe can only measure to within 0.25 inches of the wall, the temperature's approach to the wall is not known. Data needs to be collected in the region from the wall to 0.25 inches away from the wall in order to verify the validity of these data points. However,this upturn in temperature at the wall is not observed when the probe's traverse is started in the core flow. One explanation for the upturn in temperature could be due to wall effects heating up the probe during the tunnel startup.

In all the cases presented, the pitot pressures calculated by the numerical method are higher than values measured experimentally. Several factors may attribute to this discrepancy: (1) The turbulence model used in the numerical method does not predict the boundary layer thickness well as seen in the comparison of experimental and numerical boundary layer thickness, Table 1. The experimental definition of the boundary layer edge was the point where the core velocity decreased by 1%, or u_e=.99u_c. The difference in the displacement thickness, δ^* (based on the momentum integral method) has a significant effect on the core properties. (2) The virial equation of state for nitrogen used in the numerical method was developed for the range 63.15 to 1944 K and 0.0125 to 1,034 MPa. The supercooled conditions are within this range but at the lower end. At the low temperature and pressures of interest in supercooling, the inverse powers of the temperature becomes significant and could cause the overprediction of pressure at the low temperatures and densities. (3) The test facility is a blow down tunnel and develops a quasi-steady state flow. This means that the supply pressure and temperature could be changing slightly as the boundary lay measurements are taken. When the Navier-Stokes code is run, an averaged P_o and T_o is used. This could explain small variations in the numerical result but not what is seen in the present pressure predictions.

In general, the numerical method predicts the total temperature very close to the experimental values in the core and parallels the experimental values in the boundary layer. Again a change in boundary layer thickness could shift the two profiles to be on top of one another.

Concluding Remarks

This paper presents experimental pitot pressure and total temperature measurements through the boundary layer of a hypersonic nozzle. A non-equilibrium, Navier-Stokes algorithm is employed to simulate the flow in the nozzle and the calculated flow properties are compared to the experimental measurements. The numerical method predicts the total temperature very well. However, the numerically predicted pitot pressures vary significantly from the experimental results, especially for the supercooled runs.

Acknowledgements

Support for this work was provided by the NASA-AFOSR-ONR hypersonic training and research program under NASA grant number NAGW-1072. Computer time was provided by the North Carolina Supercomputer Center.

References

[1]Benton, J., Perkins, J., and Edwards, A., "Limitations of the Methods of Characteristics When Applied to Axisymmetric Hypersonic Nozzle Design," AIAA Paper No. 90-0192, 1990.

[2]Candler, G. and Perkins, J., "Effects of Vibrational Nonequilibrium on Axisymmetric Hypersonic Nozzle Design," AIAA Paper No. 91-0297, 1991.

[3]Ragsdale, W. C., "Hypervelocity Wind Tunnel 9 Test Planning Guide," Second Edition, Oct. 1989, NAVSWC, Silver Spring, MD, to be published.

[4]Voisinet, R. L. P., "Flowfield Surveying Techniques Used in the NSWC Hypervelocity Wind Tunnel No. 9," ICIASF '81 Record, IEE Publication 81 CH 1712-9, 1981, pp. 128-135.

[5]Hill, J. A. F., "Stability and Pressure Measurements in the NSWC Hypervelocity Tunnel," ICIASF '77 Record, IEEE Publication 77-CH-1251-8-AES, Sept. 1977.

[6]Arney, G.D.,Jr., and Bailey, A.B.,"Addendum to an Investigation of Equilibrium Pressures Along Unequally Heated Tubes," AEDC-TDR-62-188,Oct.1962.

[7]Potter, J.L., Kinslow, M., and Boylan, D.E.," An Influence of the Orifice on Measured Pressures in Rarefied Flow," AEDC-TDR-64-175,Sept. 1964.

[8]Beckwith, I.E., Harvey, W.D., and Clark, F.L., "Comparisons of Turbulent-Boundary-Layer Measurements at Mach Number 19.5 with Theory and an Assessment of Probe Errors," NASA TN D-6192, June 1971.

[9]Lafferty, J. F., "Supercooling II(WTR 1601) Flow Validation and Calibration," NSWC Wind Tunnel Data Report, March 1991. (Draft)

[10]Hollis, B.R.,Griffith, W.C.,and Yanta,W.J.,"A Fine-Wire Thermocouple Probe for Measurement of Stagnation Temperatures in Real Gas Hypersonic Flows of Nitrogen," ICIASF'91 Record, IEEE Publication 91CH3028-8, Oct. 1991.

[11]Canupp, P. W., Candler, C. V., Perkins, J. N., and Erickson, W. D., "Analysis of Hypersonic Nozzles Including Vibrational Nonequilibrium and Intermolecular Force Effects," AIAA Paper No. 92-0330, 1992.

[12]Jacobsen, R.T., Stewart, R.B., McCarty, R.D., and Hanley, H.J.M.,"Themophysical Properties of Nitrogen from the Fusion Line to 3500 R (1944 K)for Pressures to 150,000 psia (10342 x 10^5 N/m^2)," NBS Technical Note 648, National Bureau of Standards, 1973.

[13]Cebeci,T. and Smith, A. M.O., *Analysis of Turbulent Boundary Layers*, Academics Press, 1974.

[14]Culotta, S. and Enkenhus, K., "Analytical Expressions for the Thermodynamic Properties of Dense Nitrogen," VKI Technical Note 50,1968.

[15]Backx, E.,"Experimental Study of the Turbulent Boundary Layer at Mach 15 and 19.8 in a Conical Nozzle," VKI Technical Note 102,August 1974.

[16]Hill, J.A.F.,"Vibrational Excitation of N_2 by Small Probes in the Tunnel 9 Test Section," NOL Memo, 21 March 1974.

Table 1. Comparison of Boundary Thickness and Displacement Thickness

		Experimental		Numerical	
Run Conditions	Run Number	δ (m)	δ^* (m)	δ (m)	δ^* (m)
Supercooled	2237	0.2489	0.0874	0.2398	0.1091
Standard	2240	0.2743	0.0888	0.1768	0.1184

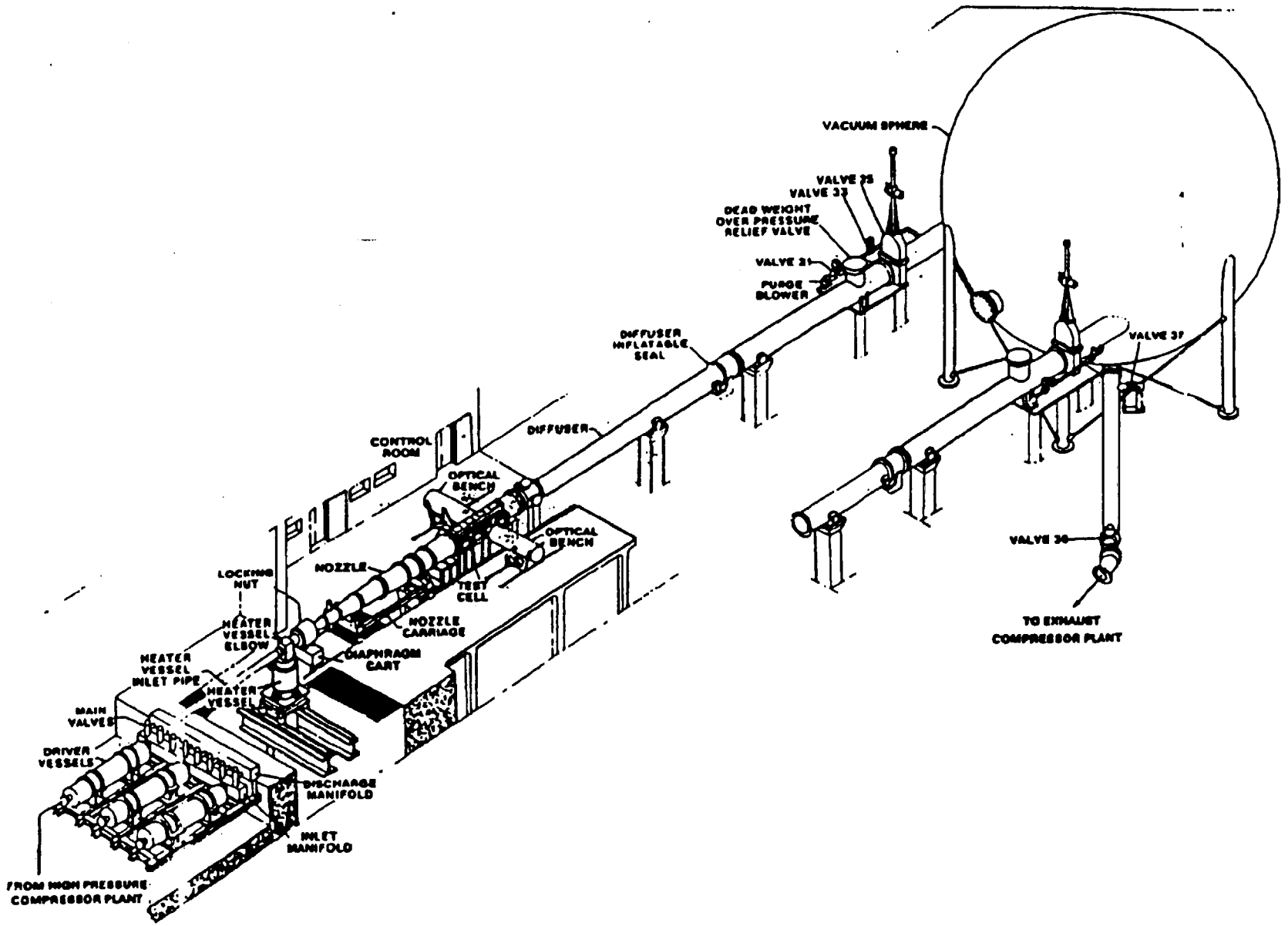

Fig. 1 NSWC hypervelocity wind tunnel no. 9

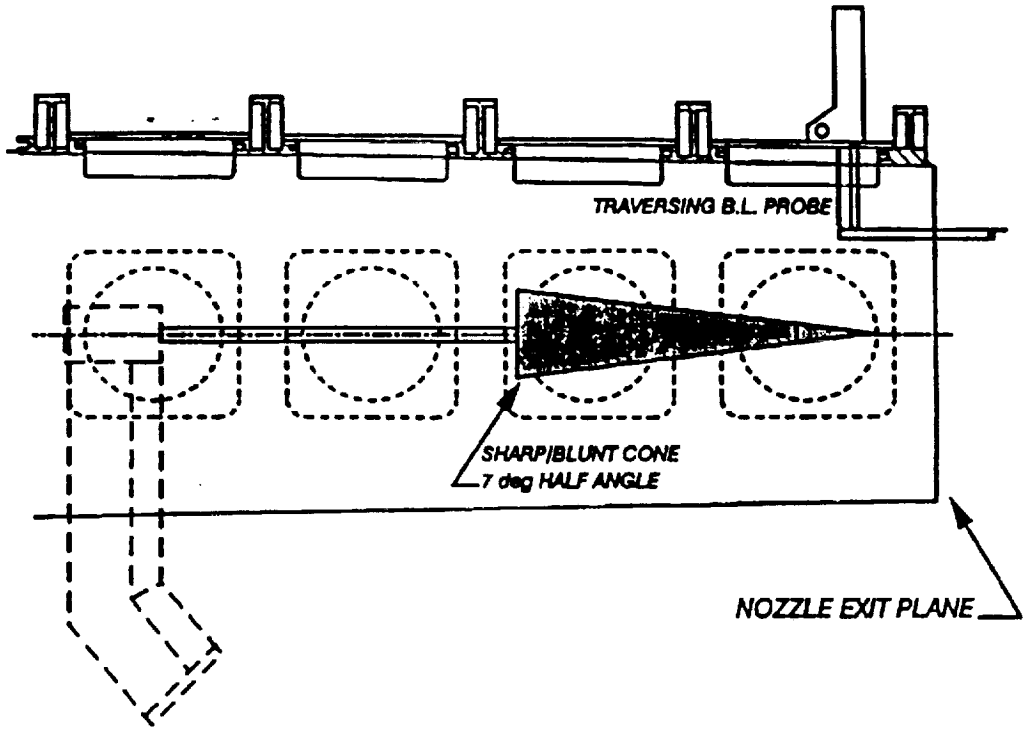

Fig. 2. Test cell set-up

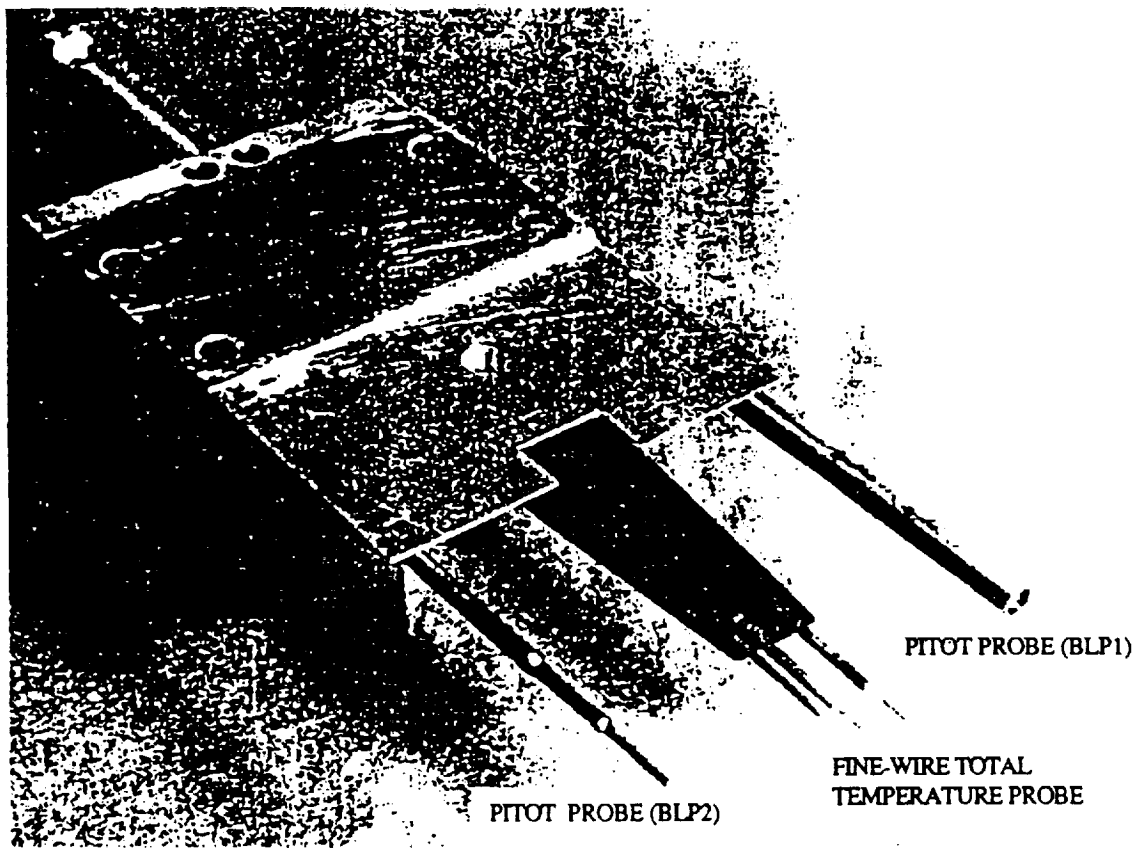

Fig. 3. Boundary layer probe

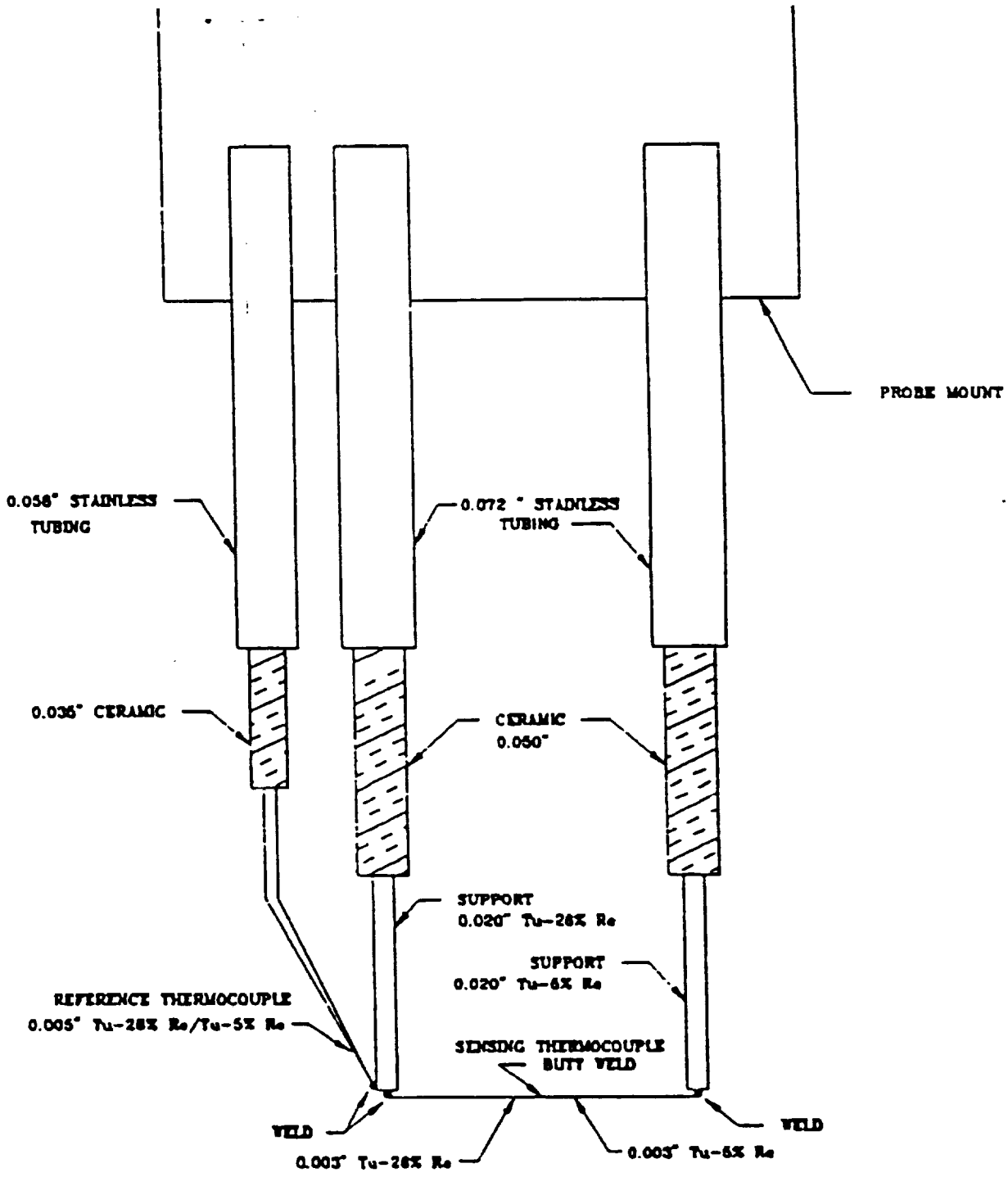

Fig. 4. Temperature probe schematic

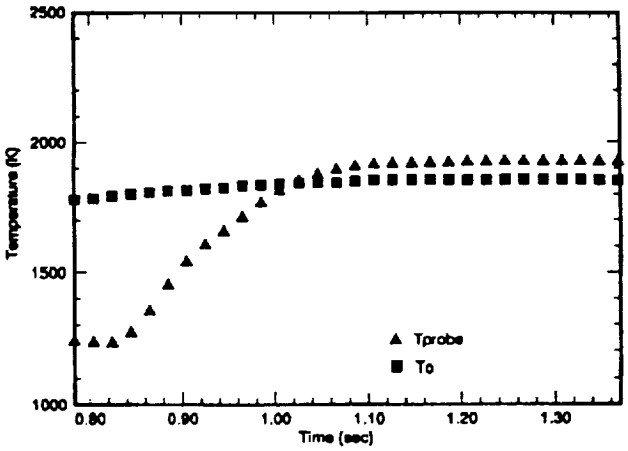

Fig. 5. Comparison of T_o and T_{probe} with respect to time for standard Mach 14 conditions, Run 2240

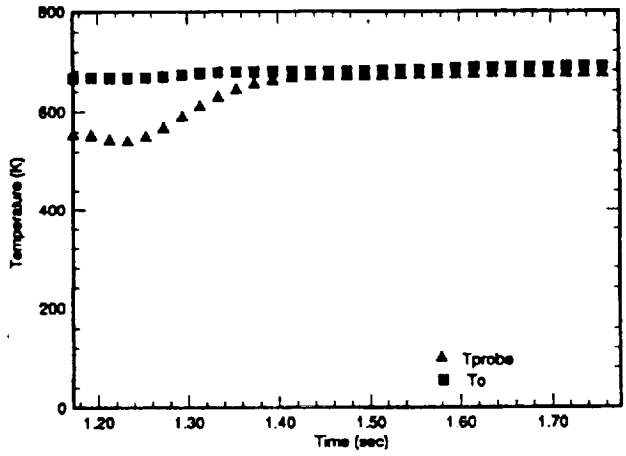

Fig. 6 Comparison of T_o and T_{probe} with respect to time for supercooled Mach 14 conditions, Run 2237

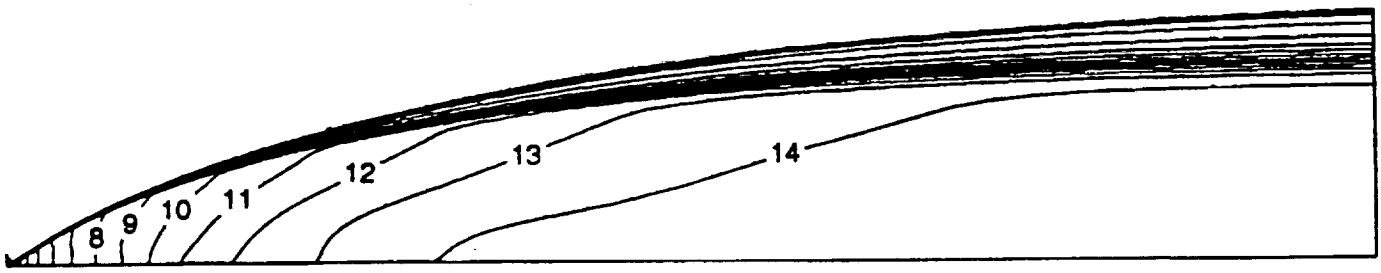

Fig. 7. Mach number contours for nonequilibrium, real gas model using Cebeci-Smith algebraic turbulence model for standard Mach 14 conditions, Run 2240, T_o = 1800.6°K, P_o = 136.23 mPa. Nozzle diameter has been scaled by a factor of 3. Experimental Mach number is 14.17, maximum predicted Mach number is 14.3

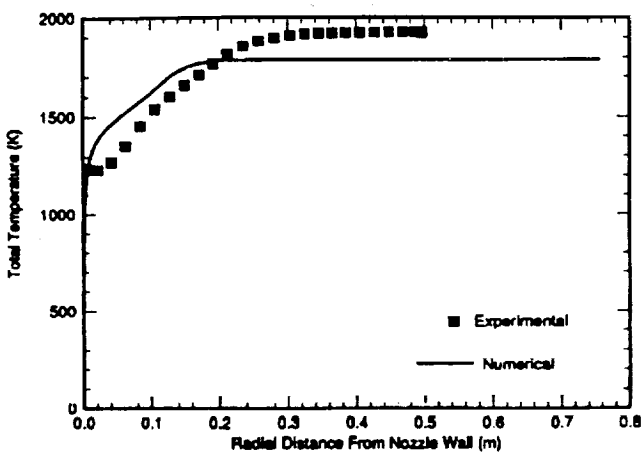

Fig. 8. Comparison of total temperature distribution through boundary layer for standard Mach 14 conditions, Run 2240

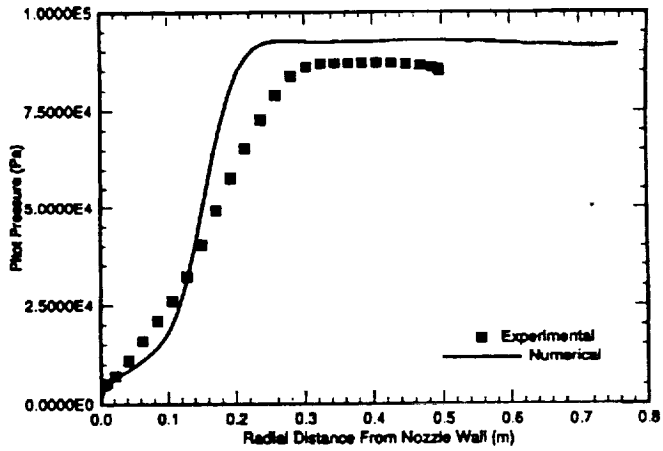

Fig. 9. Comparison of pitot pressure distribution through boundary layer for standard Mach 14 conditions, Run 2240

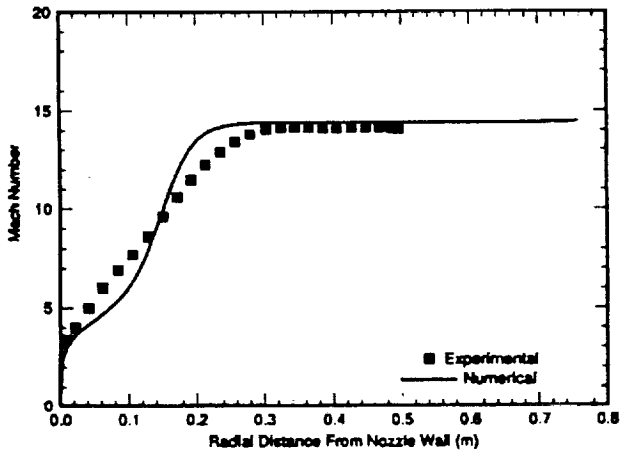

Fig. 10. Comparison of Mach number distribution through boundary layer for standard Mach 14 conditions, Run 2240

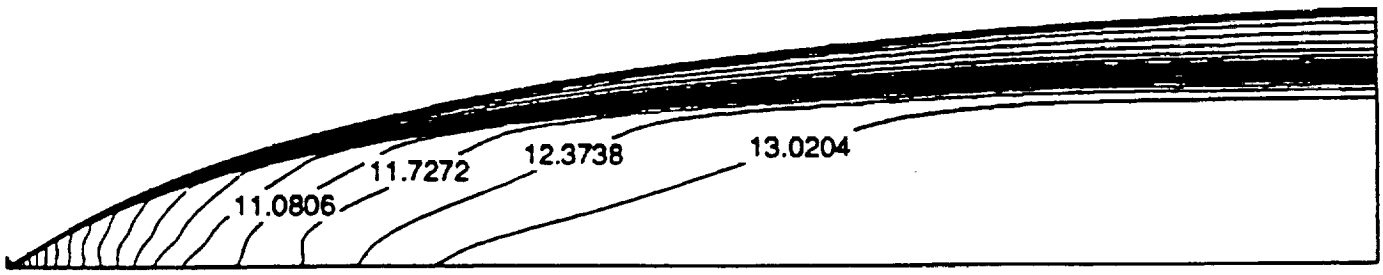

Fig. 11. Mach number contours for nonequilibrium, real gas model using Cebeci-Smith algebraic turbulence model for supercooled Mach 14, Run 2237, T_o = 680.78°K, P_o = 32.246 mPa with 29.4°K supercooling. Nozzle diameter has been scaled by a factor of 3. Experimental Mach number is 14.76, maximum predicted Mach number is 13.02.

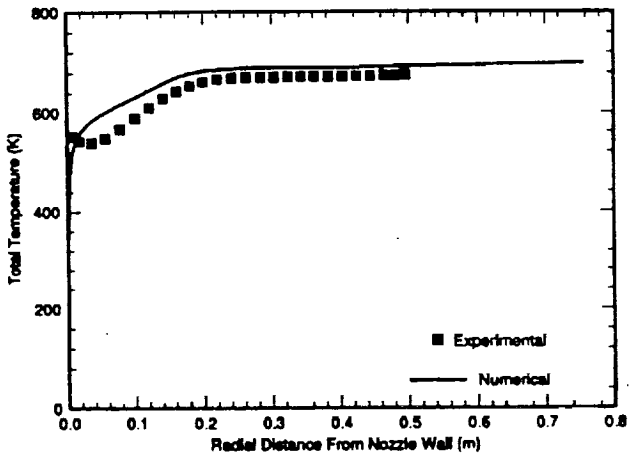

Fig. 12. Comparison of total temperture distribution through boundary layer for supercooled Mach 14, Run 2237

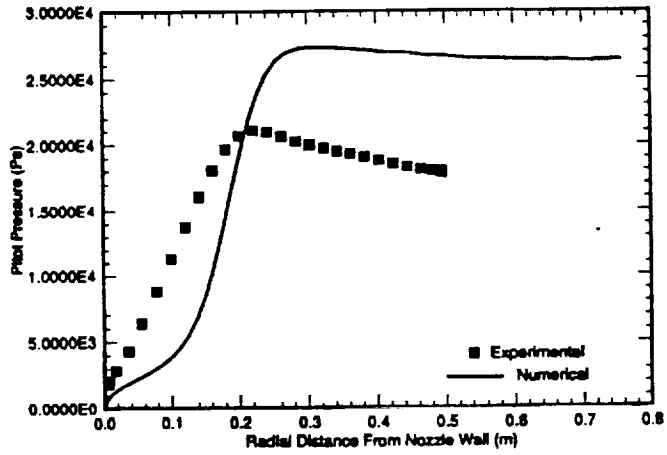

Fig. 13. Comparison of pitot pressure distribution through boundary layer for supercooled Mach 14, Run 2237

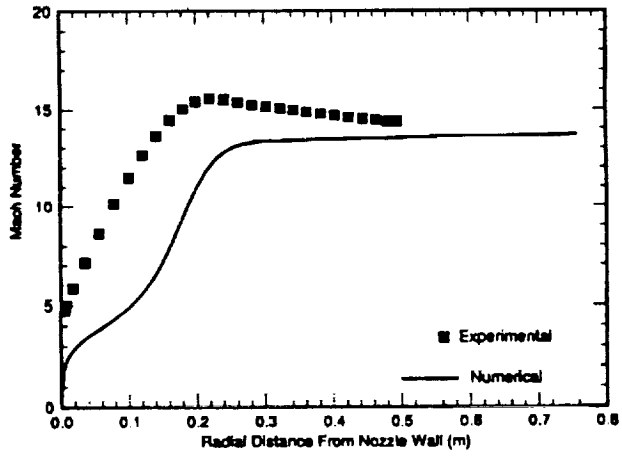

Fig. 14. Comparison of Mach number distribution through boundary layer for supercooled Mach 14, Run 2237

NIS OMIT

AIAA-93-0139
Axisymmetric Radiative Heat Transfer Calculations for Flows in Chemical Non-Equilibrium

Gregory J. Elbert and Pasquale Cinnella
Engineering Research Center for
Computational Field Simulation
Mississippi State, MS 39762

31st Aerospace Sciences Meeting
January 11-14, 1993/Reno, Nevada

Axisymmetric Radiative Heat Transfer Calculations for Flows in Chemical Non-Equilibrium

Gregory J. Elbert† and Pasquale Cinnella‡
ERC for Computational Field Simulation, Mississippi State, MS

ABSTRACT

In the present study, numerical techniques for the calculation of radiative heat transfer in axisymmetric flowfields are developed and applied to the simulation of hypersonic reactive flows. The present approach removes the need for simplified models such as the One-Dimensional Slab theory, and can be easily extended to three-dimensional flow problems. Preliminary results are presented for the Mach 47 flow past a sphere, and the predictions obtained from the axisymmetric algorithm are compared with those given by simplified radiative models. A non-negligible difference is found in the predicted values of heat flux at the stagnation point.

1. INTRODUCTION

In recent years, the need for accurate predictions of aerothermodynamic heating loads, and of radiative heat transfer in particular, has been spurred by interest in aerospace applications, such as the manned mission to Mars, and the re-establishment of human presence on the Moon[1]. Moreover, the design of thermal protection systems for the Aeroassisted Orbital Transfer Vehicle (AOTV), and for planetary probes such as Pioneer (for Venus) and Galileo (for Jupiter), is almost entirely driven by predictions of radiative heat transfer[2].

There are two major techniques utilized for the simulation of gasdynamic problems that include radiative heat transfer. Several investigators use an *uncoupled* approach, whereby the thermodynamic state of the flow is determined from a solver without radiative heat transfer, followed by a post-processing phase where the radiative field is evaluated[1,3,4]. On the other hand, the *fully coupled* approach is advocated by many[5,6], because the decoupling can significantly overestimate both radiative and conductive heat fluxes. Other factors that can play a significant role in the accuracy of radiative heat transfer predictions include: the need for detailed emission and absorption models, the importance of thermo-chemical non-equilibrium phenomena, the possibility of ablation, and the presence of three-dimensional effects away from the stagnation point[5].

The numerical simulation of hypersonic flowfields in thermo-chemical non-equilibrium without radiative transfer has been successfully attempted by Candler and MacCormack[7], and uncoupled calculations have been presented by Candler and Park[8]. Moss and Simmonds[2], and Gupta et al.[9] have used the viscous shock layer equations to solve axisymmetric reentry problems with fully coupled radiative heat transfer. However, the previous analyses employ the One-Dimensional Slab approximation, which is valid in the stagnation region only. Hartung[3] compares the 1D Slab model to a Modified Differential Approach, and shows that the former is a potential liability if used away from the stagnation point. Several researchers have developed fully coupled hypersonic/radiation simulations, but in all cases the 1D Slab approximation is employed[10,11].

In a related paper[6], the writers have successfully attempted truly two-dimensional numerical solutions to the radiative heat transfer equations, fully coupled with an existing thermo-chemical non-equilibrium flow solver[12], co-developed by the second author. The approach is compatible with existing spectrographic information and/or radiative models, which can be used as input in order to predict coupled radiative, conductive and diffusive heat transfers over relatively complex geometries. Preliminary results obtained for the inviscid flow over a cylinder at a freestream Mach number of $M_\infty = 47$ indicated that there is a significant difference between predictions obtained by means of the 1D Slab theory and fully two-dimensional radiative heat transfer calculations. Moreover, the inadequacy and inaccuracy of uncoupled approaches at that high Mach number was graphically demonstrated.

In the present study, the techniques developed for two-dimensional flowfields are extended to axisymmetric problems. The approach chosen has the distinctive advantage of being readily portable to three-dimensional problems as well, with a reasonable increase in computational requirements for the radiative source term at a point. Due to the computational costs associated with the development and testing of the new model, two simplifying assumptions are employed: a grey gas approximation has been used for the absorptivity coefficient, although provisions for multi band models are included; and thermodynamic equilibrium

---

†Research Assistant, Student Member AIAA

‡Assistant Professor of Aerospace Engineering, Member AIAA

has been assumed. Although it would be necessary to lift the above simplifications in order to obtain quantitatively accurate predictions of radiative heat transfer for geometries of practical interest, it is necessary to stress at this point that the objective of the present study is to develop the numerical tools for the simulation of axisymmetric flowfields via the inclusion of a truly multi-dimensional radiative source term.

In the following, the mathematical and physical foundations for the study of flows in chemical non-equilibrium, *including* radiative heat transfer effects, will be briefly outlined. A discussion of the numerical techniques employed for the discretization of the flow equations and the determination of the source term due to the presence of a radiation field will follow. A few preliminary results, both viscous and inviscid, will be presented in order to assess the performance of the present algorithm when compared with one-dimensional approximations.

2. GOVERNING EQUATIONS

2.1. Thermodynamic Model

In the following, a gas mixture composed of N thermally perfect species is considered. The *thermal equation of state* will be given by Dalton's Law, whereby the mixture pressure, p, is the summation of partial pressures

$$p = \sum_{i=1}^{N} \rho_i R_i T , \qquad (2.1)$$

where ρ_i is the species density, R_i is the species gas constant, and T is the temperature.

The state relationship of the pressure to the specific internal energy occurs implicitly through the temperature. For a given chemical composition and internal energy, the temperature must be evaluated from the *caloric equation of state*

$$e = \sum_{i=1}^{N} \frac{\rho_i}{\rho} \Big[\int_{T_{ref}}^{T} c_{v_i}(\tau)\, d\tau + h_{f_i} \Big] , \qquad (2.2)$$

where ρ is the mixture density, given as $\rho = \sum_i^N \rho_i$; c_{v_i} is the species specific heat at constant volume; and h_{f_i} is the heat of formation at reference temperature T_{ref}.

2.2. Gasdynamic Equations

The governing integro-differential equations for a reacting gas in radiative non-equilibrium have been derived by Simon[13] with the inclusion of relativistic effects. However, most hypersonic problems will be such that relativistic effects can be neglected[14], which amounts to considering the speed of light to be infinite. In those cases, radiative pressure and radiant energy density will be negligible, and the only contribution from radiative non-equilibrium to the gasdynamic equations will be the inclusion of the divergence of the radiant heat flux vector in the global energy equation. This additional term can be written as an integral involving the specific intensity of radiation I_ν, and treated as a source term.

Within this non-relativistic framework, the governing equations for a two-dimensional or axisymmetric flow with finite-rate chemistry may be written in vector conservation form, using generalized coordinates, as

$$\frac{\partial}{\partial t}\left(\frac{Q}{J}\right) + \frac{\partial(\tilde{F}-\tilde{F}_v)}{\partial \xi} + \frac{\partial(\tilde{G}-\tilde{G}_v)}{\partial \eta} = \frac{W}{J}, \qquad (2.3)$$

where Q is the vector of conserved variables, $\tilde{F}$, $\tilde{G}$ are the inviscid flux vectors, $\tilde{F}_v$, $\tilde{G}_v$ are the viscous flux vectors, and W is the vector of source terms. Equation (2.3) represents $N+3$ conservation equations, with the first N corresponding to species continuity, followed by momentum conservation, and the total energy conservation equation. In the above, J is the Jacobian of the coordinate transformation between the orthogonal Cartesian frame $(x,\ y)$ and the generalized curvilinear frame $(\xi,\ \eta)$. It is important to point out that the use of generalized coordinates allows for the simultaneous treatment of both two-dimensional and axisymmetric problems, without the introduction of additional terms in the latter instance. In the following, axisymmetric problems will be studied using the x-axis as the symmetry axis, and the computations will be performed in the $(x,\ y)$ plane.

The vectors Q and W are given by

$$Q = \begin{pmatrix} \rho_1 \\ \rho_2 \\ \vdots \\ \vdots \\ \rho_N \\ \rho u \\ \rho v \\ \rho e_0 \end{pmatrix}, \qquad W = \begin{pmatrix} w_1 \\ w_2 \\ \vdots \\ \vdots \\ w_N \\ 0 \\ 0 \\ -\nabla \cdot q^R \end{pmatrix}, \qquad (2.4)$$

where body forces have been neglected. In the above, u is the mass-averaged velocity vector (whose Cartesian components are u, v), and e_0 is the total energy per unit mass, $e_0 = e + (u^2+v^2)/2$. The source terms w_i represent chemical production for a species[12].

The term $\nabla \cdot q^R$ is the divergence of the radiant heat flux vector, which is given by

$$\nabla \cdot q^R = \int_0^\infty \int_0^{4\pi} \hat{R} \cdot \nabla I_\nu \, d\Omega \, d\nu , \qquad (2.5)$$

where $d\Omega$ is a differential solid angle located in the direction of propagation of the radiation, $\hat{R}$, and $I_\nu = I_\nu(t, \xi, \eta, \hat{R}_x, \hat{R}_y, \hat{R}_z, \nu)$ is the specific intensity of radiation, or the radiant energy flux, per unit solid angle and per unit frequency, across a surface normal to $\hat{R}$. For a given time and position, I_ν is a function of the direction cosines, $\hat{R}_x$, $\hat{R}_y$, $\hat{R}_z$, and of the frequency ν. Consequently, the integration in (2.5) is carried over all frequencies and all solid angles (or directions of propagation).

Expressions for the inviscid flux vectors $\tilde{F}$, $\tilde{G}$, and the viscous flux vectors $\tilde{F}_v$, $\tilde{G}_v$, and details on the modeling of viscosity, thermal conductivity and diffusion phenomena are given by Walters et al.[12].

The mathematical closure to the system of integro-differential equations (2.3) is provided by the equations of state, (2.1) and (2.2), and the equation of radiative transfer[14], providing a differential equation for the space variation of the specific intensity in terms of the gas properties.

2.3. Radiative Source Term

As previously stated, the presence of a radiation field manifests itself into the governing fluid dynamic equations (3.1) as a source term. Substitution of an expression for the specific intensity, derived from the formal solution of the equation of radiative transfer[14], into the divergence of the radiant heat flux vector, (2.5), yields

$$\begin{aligned}\nabla \cdot q^R =& 4\sigma\alpha_P T^4 \\ &- \int_0^\infty \alpha_\nu \left(\int_0^{4\pi} I_\nu(\infty) e^{-\int_0^{r_\infty} \alpha_\nu dz} d\Omega \right) d\nu \\ &- \int_0^\infty \alpha_\nu \left(\int_0^{4\pi} \int_0^{r_\infty} \alpha_\nu B_\nu \, e^{-\int_0^{w} \alpha_\nu dz} dw d\Omega \right) d\nu,\end{aligned} \tag{2.6}$$

where σ is the Stefan-Boltzmann constant, α_P is the Planck mean absorption coefficient per unit volume, α_ν is the absorption coefficient at frequency ν, and B_ν is the equilibrium specific intensity (Planck function). In the above, the notation r_∞ symbolizes a boundary point, whereas point 0 is the point under consideration. Moreover, w and z are dummy variables of integration, and the boundary condition $I_\nu = I_\nu(\infty)$ at $r = r_\infty$ has been imposed. It is apparent from this form of the radiative source term that its value at any point in the flowfield at a given time will depend upon the properties of all the points that are in its "line of sight": all the points lying in the portion of the flowfield that is swept by straight lines (rays) emanating from the point under consideration, and terminating either at solid boundaries or in the farfield.

The axisymmetric character of the problems under consideration allows for some simplification of the integrals in the radiative source term. Specifically, all the points in a three-dimensional space (x, y, z) can be considered as lying in planes $(x, \bar{y})$, where $\bar{y}$ is *any* axis perpendicular to x. Fig. 1 represents such a point P, which by virtue of the symmetry has the *same* thermophysical properties as point M, which lies in the plane (x, y). Consider a unit vector $\hat{l}$, in the direction *opposite* to the direction of propagation $\hat{R}$, emanating from a point C in the plane (x, y), and propagating in a three-dimensional space, as shown in the two-dimensional projection of the figure. Every point encountered on its trip towards a boundary can be traced back to an equivalent point in the (x, y) plane, as was done for point P. This fact allows the determination of the radiative source term based upon the thermophysical properties of points in the plane (x, y) *only*, as will be discussed in the following section.

The expression for the divergence of the radiant heat flux vector, (2.6), is relatively complex and difficult to evaluate numerically. In order to simplify its treatment, the 1D Slab approximation is introduced and almost universally adopted in practical calculations[15]. In summary, the approximation consists of neglecting two-dimensional (and three-dimensional) effects in proximity of the stagnation streamline, reducing the shock-layer region around a blunt body to a slab whose physical properties vary in one dimension only[14]. Consequently, the integration over direction of propagation is considerably simplified, and the final expression for the divergence of the radiant heat flux vector reads

$$\begin{aligned}&\nabla \cdot q^R = 4\sigma\alpha_P T^4 \\ &-2\pi \int_0^\infty \alpha_\nu \left[I_\nu(-\infty) E_2(-\eta^\nu_{-\infty}) + I_\nu(+\infty) E_2(+\eta^\nu_{+\infty}) \right] d\nu \\ &-2\pi \int_0^\infty \alpha_\nu \left[\int_{-\infty}^0 \alpha_\nu B_\nu E_1(-\eta^\nu) dx + \int_0^{+\infty} \alpha_\nu B_\nu E_1(\eta^\nu) dx \right] d\nu,\end{aligned} \tag{2.7}$$

where E_i is the integro-exponential function of order i, and η^ν is the optical thickness of the gas

$$E_i(z) = \int_0^1 w^{i-2} e^{-z/w} dw, \qquad \eta^\nu = \int_0^x \alpha_\nu dx \,. \tag{2.8}$$

In the above, the integration over direction of propagation Ω has been simplified and is taken into account by the presence of the integro-exponential function. The radius x originates at one boundary point ($-\infty$, e.g. the freestream) and ends at the other boundary point ($+\infty$, e.g. the body), going through the slab and passing through the location of the finite volume under consideration (point 0). The direction x is defined by the local normal to the body. In the derivation of the 1D Slab approximation, it is assumed that the flow properties vary only in the direction perpendicular to the slab

(i.e., from the freestream to the body). It is apparent that this assumption will be reasonable only in a small region close to the stagnation streamline, because the changes in the flowfield in the direction tangential to the body, in general, are far from being negligible.

In some cases, an even more drastic simplification is made to the modeling of radiative heat transfer: the gas is assumed to be emission-dominated[14]. This translates into the simple expression for the divergence of the radiant heat flux vector

$$\nabla \cdot q^R = 4\sigma\alpha_P T^4 , \qquad (2.9)$$

which is a local contribution only, and does not depend upon directions of propagations and/or lines of sight. A condition for a gas to be emission-dominated is that its optical thickness, η^ν, be small for the entire frequency spectrum. This is a reasonable assumption for some practical problems, but not very accurate in general[5].

3. NUMERICAL FORMULATION

3.1. Gasdynamic Equations

The governing partial differential equations for hypersonic flows out of chemical equilibrium that have been presented in §2.2 are discretized using the finite-volume technique[16], whereby their integral form is solved for the unknown volume averages of conserved variables in some small, but finite, control volume. The discretization of the inviscid fluxes is accomplished by means of flux-split techniques, and a thorough derivation of the algorithms can be found in Grossman and Cinnella[17]. Central differences in conjunction with the Thin Layer approximation are used for the viscous fluxes[12].

It may be useful to point out that the use of finite volumes simplifies considerably the treatment of axisymmetric problems, because no additional or corrective terms are necessary to "transform" the two-dimensional equations into the axisymmetric form. The only peculiarity in the axisymmetric case is the fact that the volumes terminating at the symmetry axis will have one face of zero area.

The discretized equations are advanced in time using an Approximate Factorization scheme. More details are given in Walters et al.[12].

3.2. Radiative Source Term

The numerical evaluation of the radiative source terms, (2.6), involves integrations over frequency, solid angle, and length (direction of propagation). This evaluation should be performed at every time step when time accuracy is of interest. However, for steady-state problems, the radiative source terms can be lagged for a few time steps. It might be useful to point out that the "ultimate" lagging, that is, the evaluation of the source terms at convergence only, is tantamount to a fully decoupled approach. This is the strategy employed by Candler and Park[8], among others, in conjunction with the one-dimensional approximation.

The integration over the frequency spectrum can be performed in its simplest form by means of the gray-gas approximation[14]. More realistic approaches include three-band and eight-band models[5], whereby the mean absorption coefficient is considered constant over a frequency band, and the integration reduces to a summation over the bands. Presently, preliminary results have been obtained for the one-band (gray-gas) model only, although provisions for multiband models are included.

The double integration over the geometric parameters (solid angle and length) is accomplished by superimposing a "radiation grid" on the discretized domain. In particular, for every finite volume in the calculation it is necessary to define the rays that will be considered for the integration over the angle, and the points along each ray for the integration over the length, including the boundary points in the farfield or at some solid wall. Specifically, given a computational cell and a direction of propagation, a ray is started from the cell center and continued until a boundary is reached. After locating the position of the boundary point at the intersection of the ray with the grid boundary, the points along the ray are distributed in accordance with the technique chosen for the line integration. The process is continued until all directions of propagation are exhausted, and is repeated for all volumes in the computational domain.

The integration over the solid angle (direction of propagation) is performed by partitioning the interval $[0, 4\pi]$ into equally distributed subintervals, which translates into the requirement that the rays be evenly distributed in three-dimensional space. This approach is tantamonut to using a composite Newton-Cotes quadrature. Several options have been implemented for the integration over the length, including composite trapezoidal and Simpson rules, the use of Richardson's extrapolation, and the implementation of a composite Gauss-Legendre formula.

In a previous paper[6], the authors have developed numerical techniques for the simulation of two-dimensional radiative heat transfer. While the basic algorithm remains unchanghed, three new problems have to be overcome in order to extend the previous methodology to axisymmetric flowfields. The first one is to develop a method for defining a uniform distribution of ray directions in three-dimensional space which would also lend itself easily to radiation grid refinement. The second problem is to develop a ray tracing algorithm which would accept a general 3D ray and map it back

into the computational plane. The third problem is determining the absolute length of the ray. These three topics will now be discussed.

Among all of the three-dimensional geometric figures which can be used to simulate a sphere, the icosahedron is the one composed of the maximum possible number of equilateral triangles[18]. It features 20 triangles, defined by 12 vertices. Ray directions can be created by connecting a line starting at the centroid of the icosahedron and passing through a prescribed point on the surface of one of the triangles. By uniformly distributing points on the surface of the triangles, the rays are approximately uniformly distributed in three-dimensional space. A uniform triangle discretization scheme[19,20] was employed for the specification of the points on each of the 20 triangles of the icosaedron. The points on the surface of a triangle are determined from a linear parametric representation[21]. A discretization parameter, K, which varies between 2 and infinity, is used to control the number of rays (points) in the discretization scheme. Care must be taken so as not to define duplicate rays from the edges of neighboring triangles. The previously mentioned need for equilateral triangles is apparent: if the triangles had an edge which was shorter (or longer) in length than the other edges, then the rays defined on that edge would be more (or less) clustered. Fig. 2 shows the discretization of one triangle for $K = 5$. It may be noted that the number of smaller equilateral triangles which share a portion of one of the vertices is $K - 1$.

Table 1 shows different values of the discretization parameter, K, and the corresponding number of rays (Ray3D), average angle between rays (Angle), and maximum deviation (Dev.). There are only 2 values of K, namely 2 and infinity, that will provide a perfectly uniform set of rays in 3D space. However, the maximum deviation is small and should not adversely affect the accuracy of the solid angle integration. Also shown in Table 1 is a reduced number of rays (RayAX), which is the number utilized for an axisymmetric problem. Specifically, the rays which are generated by the discretization scheme can be divided into two groups: the first one contains all of the rays which lie in the (x, y) plane, that is, rays having a zero component in the z-direction; and the second group contains all remaining rays, which have non-zero components in the z-direction. The rays in the second group are present in an even number, because each ray has a mirrored counterpart: for each ray with direction $(\hat{R}_x, \hat{R}_y, \hat{R}_z)$, there exists another ray with direction $(\hat{R}_x, \hat{R}_y, -\hat{R}_z)$. For axisymmetric problems, the path of a ray when mapped back into the computational plane is the same regardless of the sign of the z-component. This translates into using one ray instead of two in the solid angle integral, provided its weight is doubled in the quadrature formula. Correspondingly, computer storage is reduced, and the total number of rays utilized is close to half the original value, as shown in Table 1.

Unfortunately, the requirements for an axisymmetric calculation are heavier than those of a comparable two-dimensional problem. For example, the calculations of Cinnella and Elbert[6] employed 36 rays for a ray discretization angle of 10 degrees in two dimensions. An axisymmetric calculation having the same ray discretization angle will require 193 rays, corresponding to $K = 7$, and a full 3D calculation would require 362 rays.

Table 1

K	Ray3D	Angle	Dev.	RayAX
2	12	63.43	0.00	8
3	42	33.86	2.14	25
4	92	21.94	1.86	52
5	162	16.63	2.07	89
6	252	13.20	1.83	136
7	362	10.88	1.56	193
8	492	9.34	1.44	260
9	642	8.14	1.29	337
10	812	7.20	1.16	424
11	1002	6.49	1.08	521
12	1212	5.88	1.00	628
13	1442	5.38	0.91	745

The next problem that has to be solved is the mapping of 3D rays back to the computational plane. Fig. 3 shows a symbolic representation of a computational grid, with the radiation grid for one volume superimposed on it. The rays are straight lines in three dimensions; however, if they belong to the second group, when mapped back into the computational plane they appear curved. Rays from the first group, including those reflected by the axis of symmetry, remain straight.

Fig. 4 depicts a canted view of the problem, with a typical ray from the second group shown starting from point C and going out of the (x, y) plane in space. Also represented is the same ray mapped back to the computational plane. The coordinate of a generic point P along the ray is given by

$$\begin{aligned} x_P &= \hat{l}_x L + x_C \,, \\ y_P &= \hat{l}_y L + y_C \,, \\ z_P &= \hat{l}_z L \,, \end{aligned} \tag{3.1}$$

where L is the Euclidean distance between points C and P. The figure shows how point P along the ray

is mapped back into the originating plane to point M, given by

$$\begin{aligned} x_M &= x_P \,, \\ y_M &= \sqrt{y_P^2 + z_P^2} \,, \\ z_M &= 0 \,. \end{aligned} \tag{3.2}$$

At this stage, any point along a general ray in space is easily mapped back into the originating plane, and the cell to which it belongs can be found from the two-dimensional ray tracing algorithm described by Cinnella and Elbert[6].

The only problem that remains to be solved is the determination of the length of a generic ray. This piece of information is vital to allow a precise distribution of points along the ray, which must terminate at a boundary of the flowfield grid. The mapping algorithm previously described, in conjunction with the ray tracing algorithm, is used to obtain an initial guess for the ray length and for the cell whose boundary contains the endpoint. Given a ray direction, small steps are taken along the ray, the new point is located in a cell and the cell indices are monitored until one (or both) of the indices exceeds the grid dimensions. At this stage, a good guess for the length of the ray and the cell which contains the boundary point is known. The solution for the location of the endpoint E and the length of the ray is now reduced to finding the intersection of a line and a surface of revolution, as shown in Fig. 5. The surface generated by rotating the line (1, 2) about the axis of symmetry x can be described by a scalar parametric representation as

$$\begin{aligned} x(a,b) &= 0.5[x_2(1+a) + x_1(1-a)] \,, \\ y(a,b) &= 0.5[y_2(1+a) + y_1(1-a)]\cos(\pi b) \,, \\ z(a,b) &= 0.5[z_2(1+a) + z_1(1-a)]\sin(\pi b) \,, \end{aligned} \tag{3.3}$$

subject to

$$-1 \le a \le +1 \,, \qquad -1 \le b \le +1 \,. \tag{3.4}$$

A point on the ray can be described as

$$\begin{aligned} x(l) &= \hat{l}_x L + x_C \,, \\ y(l) &= \hat{l}_y L + y_C \,, \\ z(l) &= \hat{l}_z L \,, \end{aligned} \tag{3.5}$$

subject to

$$0 \le L \le \infty \,. \tag{3.6}$$

Equating (3.3) and (3.5), a system of 3 nonlinear equations is obtained for the unknowns a, b, and L. Solutions by means of Newton's method prove to be very efficient, with typically only 4 to 5 iterations needed for convergence.

The last step necessary for the numerical evaluation of the integrals that appear in the radiative source term is the determination of the thermophysical properties of every radiative grid point. This can be accomplished by imposing that the point under consideration assumes the properties of its host cell (finite volume). At this point, it is possible to perform truly axisymmetric simulations of radiative heat transfer.

4. NUMERICAL RESULTS

Preliminary results have been obtained for the inviscid and viscous flow at Mach 46.9 over a sphere in air at an altitude of 57.9 km. The sphere radius is 5 ft, or 1.524 m, the freestream temperature is $T_\infty = 262.9\ K$, the density is $\rho_\infty = 4.26\ 10^{-4}\ kg/m^3$, and the pressure is $p_\infty = 32.2\ N/m^2$. A surface temperature $T_w = 1500\ K$ is imposed as a boundary condition for both inviscid and viscous simulations. The gray-gas model for the absorption coefficent in equilibrium air given by Wang[22] has been employed.

Results have been obtained for the truly multi-dimensional radiative heat transfer case (which will be denoted as the Full radiative model), the 1D Slab approximation, and the emission-dominated case. Viscous calculations for a baseline case with no radiative heat transfer have also been performed. A Van Leer-type discretization of the inviscid fluxes was employed[17]. Unfortunately, only simulations that are first-order-accurate in space were obtained, due to severe convergence problems encountered at this extremely high Mach number. The thermophysical model used is a finite-rate chemistry model for air which includes five species and seventeen reactions[12], and is popular in hypersonic applications.

4.1. Inviscid Results

The present investigation employs a 41 × 61 grid, which corresponds to 40 volumes in the circumferential direction and 60 in the radial direction. The "radiation grid" at every volume corresponds to a triangle discretization parameter of $K = 5$, and employs 30 intervals of integration per ray, slightly clustered near the originating cell. The composite two-point Gauss-Legendre formula is used for the numerical quadrature along a ray, which results in 60 points being employed for the integration.

Fig. 6 shows the temperature along the first row of volumes off of the stagnation streamline for the three cases with radiation. It may be noticed that the shock location is in good agreement, but the temperature profiles are affected by the choice of the radiative transfer model. In particular, absorption is re-heating the gas in the shock layer when compared with the emission-dominated case. The Full radiative algorithm and the

1D Slab approximation predict essentially the same temperature profile.

The radiative heat loads are shown in Fig. 7, which depicts the component of the radiative heat flux vector normal to the body on the first row of volumes off of the body. Also represented is the tangential component for the Full radiative case. There is a significant change between the two-dimensional and the one-dimensional predictions. It should be reiterated at this point that both emission-dominated and 1D Slab results are to be considered in the stagnation region only. Nonetheless, these preliminary results seem to indicate that the approximations made in the 1D Slab theory may produce a significant error even at the stagnation point. More specifically, the radiative heat flux vector at the stagnation point has a dimensional value of 227 MW/m^2, when evaluated with the 1D Slab theory, and a value of 204 MW/m^2, when calculated by means of the Full radiative algorithm. The difference is about 11%.

The components of the heat flux vector normal to the body on the first row of volumes off of the stagnation streamline are represented in Fig. 8. The somewhat oscillatory behaviour of the Full radiative curve is probably due to the coarseness of both flowfield and radiative grids. Again, there is a significant difference between Full radiative and 1D Slab results, although the stagnation region is the place where the one-dimensional approximation should perform best.

The pressure coefficient on the body, not shown here, is in good qualitative agreement with Newtonian theory[15], and is not dramatically affected by radiation modeling.

4.2. Viscous Results

The viscous calculations employ a 61 × 91 grid, which corresponds to 60 volumes in the circumferential direction and 90 in the radial direction. The "radiation grid" at every volume corresponds to a discretization parameter of $K = 7$ for the Full radiative model. The composite two-point Gauss-Legendre formula is used for the numerical quadrature along a ray, with intervals of integration slightly clustered near the originating point. In this case, 80 points per ray are employed for the 1D Slab approximation, and 60 points per ray for the Full radiative model.

The Reynolds number for this case is 0.59 10^6, based on the sphere radius, or 0.815, based on the minimum cell width in the radial direction.

The density profiles along the stagnation streamline are shown in Fig. 9. In this case, both shock location and post-shock values are affected by the radiative model employed for the simulation. It is interesting to note that the thermal boundary layer is present only in roughly one-sixth of the shock layer. Also interesting is the comparison with the no radiation calculation, where the density does not increase after the shock, because no radiative cooling of the flow is present.

A logarithmic plot of the total enthalpy along the stagnation stramline is shown in Fig. 10. The significant decrease of total enthalpy after the shock, in what is essentially an inviscid region, is attributed to the radiative cooling. The no radiation case, also shown in the plot, confirms that the dissipation of total enthalpy in the shock layer is indeed negligible until its innermost region is reached, which corresponds to the thermal boundary layer.

The total (radiative plus conductive) heat transfer vector along the body surface is represented in Fig. 11. It may be noted that the magnitude of the conductive heat flux vector ranges from one tenth to one twentieth of its radiative counterpart, which confirms the fact that at this extreme Mach number the heat transfer is essentially radiative[5]. Moreover, the heat transfer vector goes to zero along the body more rapidly than its two-dimensional conterpart[23], which is probably due to three-dimensional relieving effects. It may be useful to point out that there is a 10% difference in radiative heat flux vector values at the stagnation point for this case between the different models (212 MW/m^2 for the Full radiative model versus 234 MW/m^2 for the 1D Slab).

The behaviour of the skin friction coefficient is shown in Fig. 12, where it can be seen that the presence of radiative heat transfer significantly reduces the skin friction, when compared to the non-radiative case. No significant difference in the values of skin friction is found among the different radiative models.

5. CONCLUDING REMARKS

This study has detailed the derivation and application of numerical techniques for the prediction of radiative heat transfer in hypersonic flows. A truly multidimensional algorithm has been proposed for the discretization of the radiative source term in the governing flow equations, and a fully coupled approach advocated for the solution of flowfield problems involving a significant amount of radiative heat transfer. The present methodology can be readily extended to three space dimensions.

Non-negligible differences between the multi-dimensional model and more simplified approaches such as the One-Dimensional Slab approximation have been registered for a few test cases. The simplifications in the thermophysical and radiative models (e.g. gray gas and thermodynamic equilibrium) prevent a quantitative description of the discrepancy between the present approach and the other geometrically simpler techniques. However, a qualitative comparison has been performed, by keeping all the problem variables equal with the exception of the radiative discretization algorithms, and

there is evidence that the simplified models are a potential liability for accurate estimates of radiative heat transfer in the hypersonic regime.

Future work is necessary in order to remove the simplifications to the physical models, and further validation of the present algorithm for both axisymmetric and fully three-dimensional geometries is being planned.

ACKNOWLEDGEMENTS

This work was funded in part by Mississippi State University, under a Research Initiation Program sponsored by the Office of Research, and in part by the National Science Foundation, which funds the Engineering Research Center for Computational Field Simulation.

REFERENCES

1. Hartung, L.C., Mitcheltree, R.A., and Gnoffo, P.A., "Stagnation Point Nonequilibrium Radiative Heating and the Influence of Energy Exchange Models," AIAA Paper No. 91-0571, 1991.
2. Moss, J.N., and Simmonds, A.L., "Galileo Probe Forebody Flowfield Predictions," *Progress in Astronautics and Aeronautics*, Vol. 85, pp. 419–445, 1983.
3. Hartung, L.C., and Hassan, H.A., "Radiation Transport Around Axisymmetric Blunt Body Vehicles Using a Modified Differential Approach," AIAA Paper No. 92-0119, 1992.
4. Fuehrer, P.L., and Edwards, D.K., "Computational Methodology for Radiation Heat Transfer in the Flowfield of an AOTV," AIAA Paper No. 91-1407, 1991.
5. Anderson, J.D.Jr., "An Engineering Survey of Radiating Shock Layers," *AIAA Journal*, Vol. 7, No. 9, pp. 1665–1675, 1969.
6 Cinnella, P., and Elbert, G.J., "Two-Dimensional Radiative Heat Transfer Calculations for Flows in Thermo-Chemical Non-Equilibrium," AIAA Paper No. 92-0121, 1992.
7. Candler, G.V., and MacCormack, R.W., "The Computation of Hypersonic Ionized Flows in Chemical and Thermal Nonequilibrium," AIAA Paper No. 88-0511, 1988.
8. Candler, G., and Park, C., "The Computation of Radiation form Nonequilibrium Hypersonic Flows," AIAA Paper No. 88-2678, 1988.
9. Gupta, R., Lee, K., Moss, J., and Sutton, K., "Viscous-Shock-Layer Solutions with Coupled Radiation and Ablation Injection for Earth Entry," AIAA Paper No. 90-1697, 1990.
10. Balakrishnan, A., Park, C., and Green, M.J., "Radiative Viscous Shock Layer Analysis of Fire, Apollo, and PAET Flight Data," *Progress in Aeronautics and Astronautics*, Vol. 103, pp. 514–540, 1986.
11. Hartung, L.C., "Development of a Nonequilibrium Radiative Heating Prediction Method for Coupled Flowfield Solutions," AIAA Paper No. 91-1406, 1991.
12. Walters, R.W., Cinnella, P., Slack, D.C., and Halt, D., "Characteristic-Based Algorithms for Flows in Thermo-Chemical Nonequilibrium," *AIAA Journal*, Vol. 30, No. 5, pp. 1304–1313, 1992.
13. Simon, R., "The Conservation Equations of a Classical Plasma in the Presence of Radiation," *Journal of Quantum Spectroscopy and Radiative Transfer*, Vol. 3, pp. 1–14, 1963.
14. Vincenti, W.C., and Kruger, C.H.Jr., "Introduction to Physical Gas Dynamics," Krieger, Malabar FL, 1986.
15. Anderson, J.D.Jr., "Hypersonic and High Temperature Gas Dynamics," McGraw-Hill, New York, 1989.
16. Walters, R.W., and Thomas, J.L., "Advances in Upwind Relaxation Methods," in *State-of-the-Art Surveys on Computational Mechanics*, (ed. A.K. Noor), ASME Publication, 1988.
17. Grossman, B., and Cinnella, P., "Flux-Split Algorithms for Flows with Non-equilibrium Chemistry and Vibrational Relaxation," *Journal of Computational Physics*, Vol. 88, No. 1, pp. 131–168, 1990.
18. Pottmann, H., and Eck, M., "Modified multiquadratic methods for scattered data interpolation over a sphere," in *Computer Aided Geometric Design*, Vol. 7, pp. 313–321, North-Holland, Amsterdam, 1990.
19. Boehm, W., "Generating the Bezier Points of Triangular Splines," in *Surfaces in Computer Aided Geometric Design*, (eds. R.E. Barnhill and W. Boehm), pp. 77–91, North-Holland, Amsterdam, 1983.
20. Desai, C.S., "Elementary Finite Element Method," Prentice-Hall, Englewood Cliffs NJ, 1979.
21. Kreyszig, E., "Advanced Engineering Mathematics," Wiley, New York, 1983.
22. Wang, K.C., "The 'piston problem' with thermal radiation," *Journal of Fluid Mechanics*, Vol. 20, Part 3, pp. 447–455, 1964.
23. Elbert, G.J., "Two Dimensional and Axisymmetric Radiative Heat Transfer for Hypersonic Flows in Chemical Nonequilibrium," Ph.D. Dissertation, Mississippi State University, 1992.

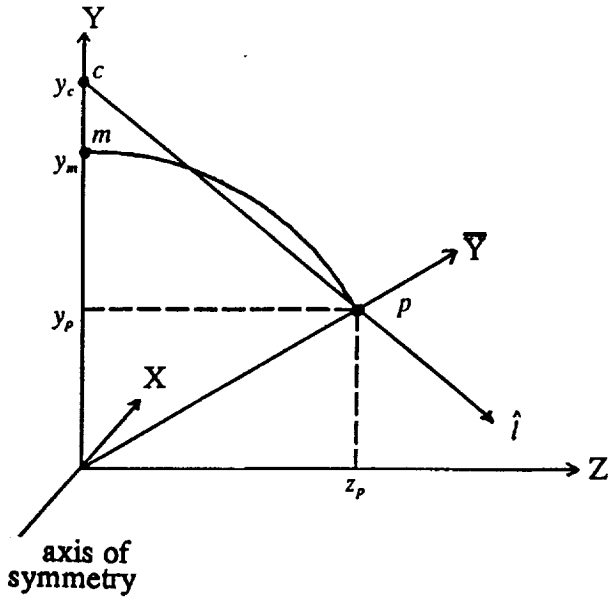

Fig. 1 Mapping of Point P to point M for an axisymmetric problem. Two-dimensional view.

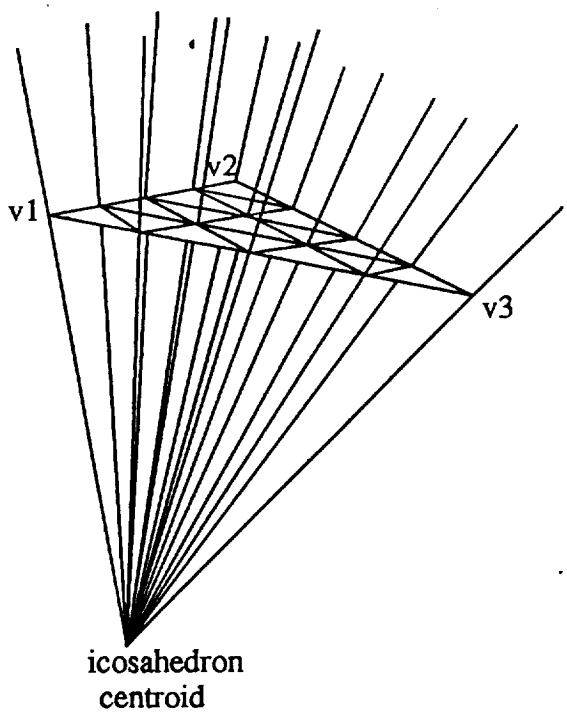

Fig. 2 Discretization of one triangle belonging to an icosaedron for $K = 5$.

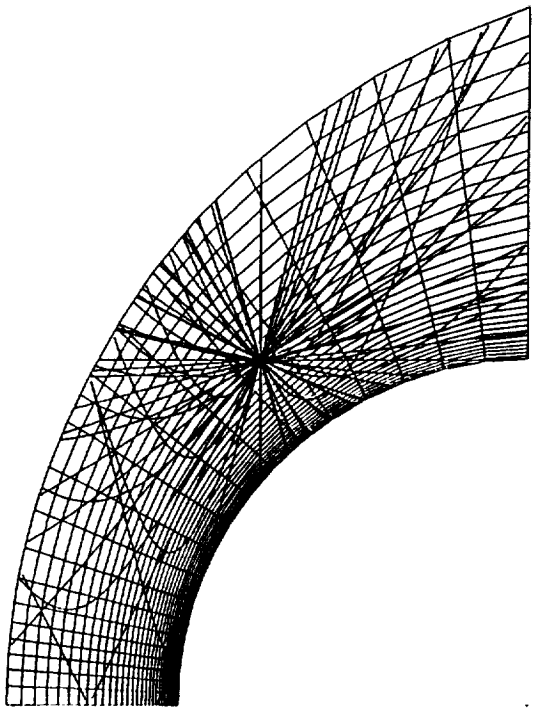

Fig. 3 Axisymmetric flowfield grid and radiative grid for one volume.

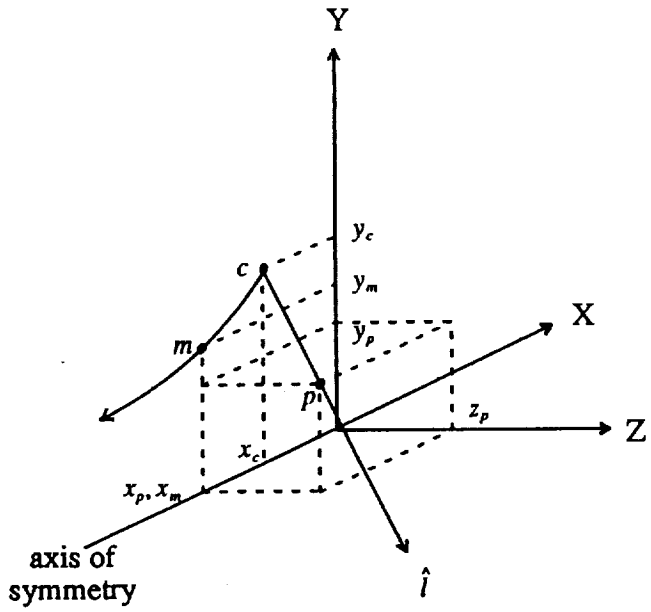

Fig. 4 Mapping of point P and ray $\hat{l}$ back to the plane (x, y).

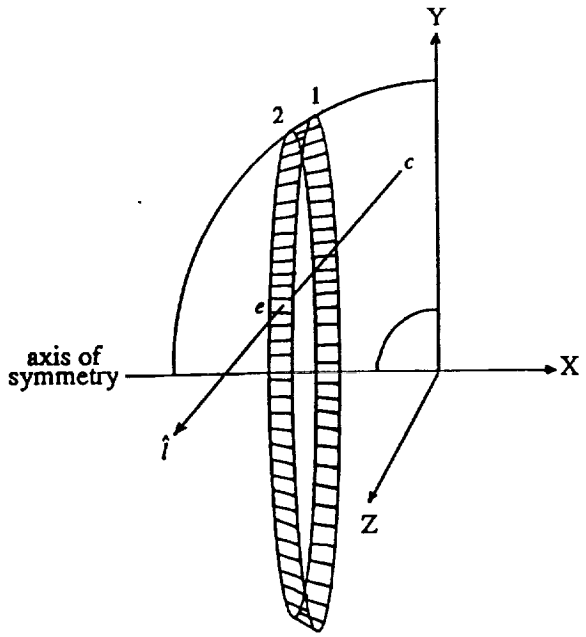

Fig. 5 Location of the endpoint E of a ray at a computational boundary.

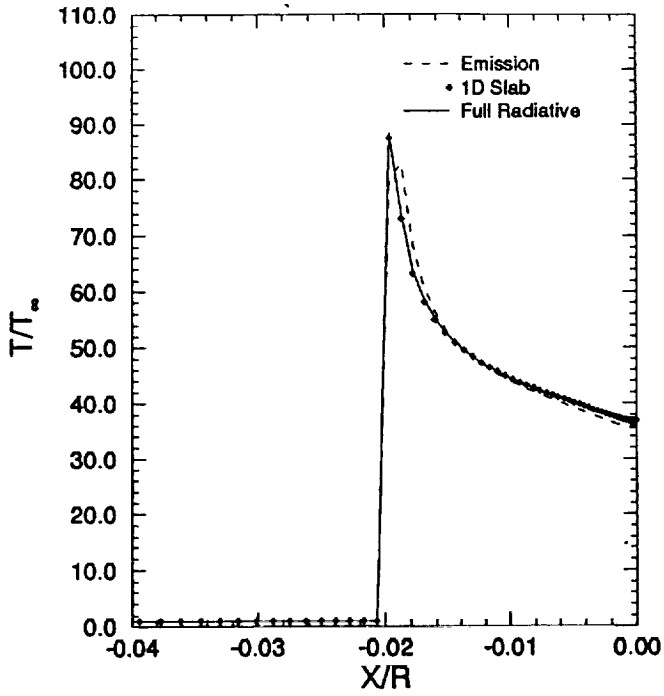

Fig. 6 Temperature along the stagnation streamline. Inviscid result.

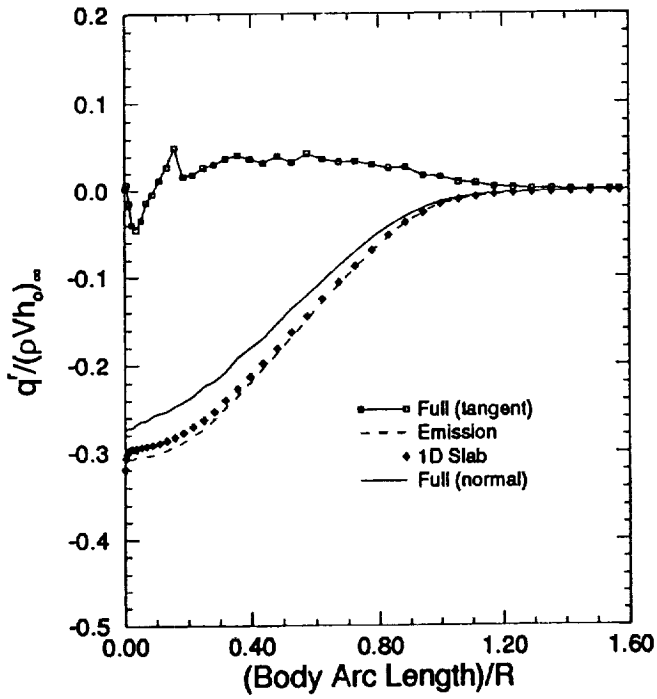

Fig. 7 Radiative heat transfer vector components along the body surface.

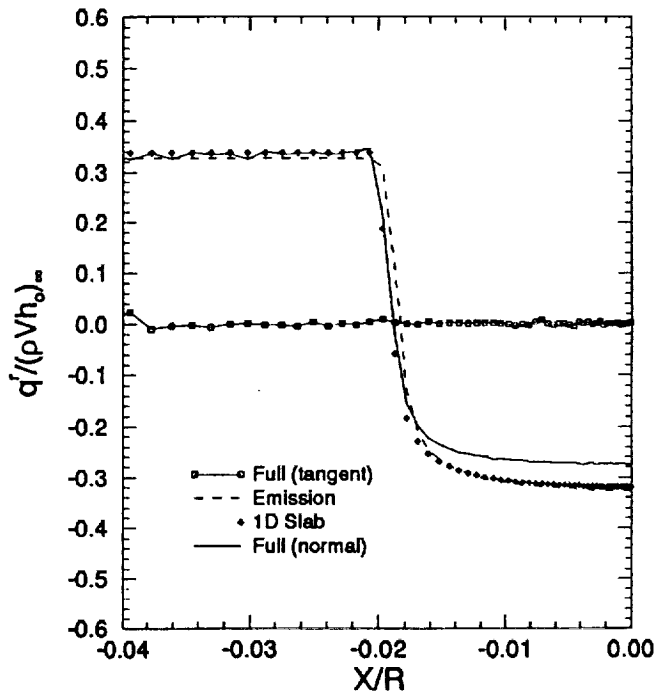

Fig. 8 Radiative heat transfer vector components along the stagnation streamline.

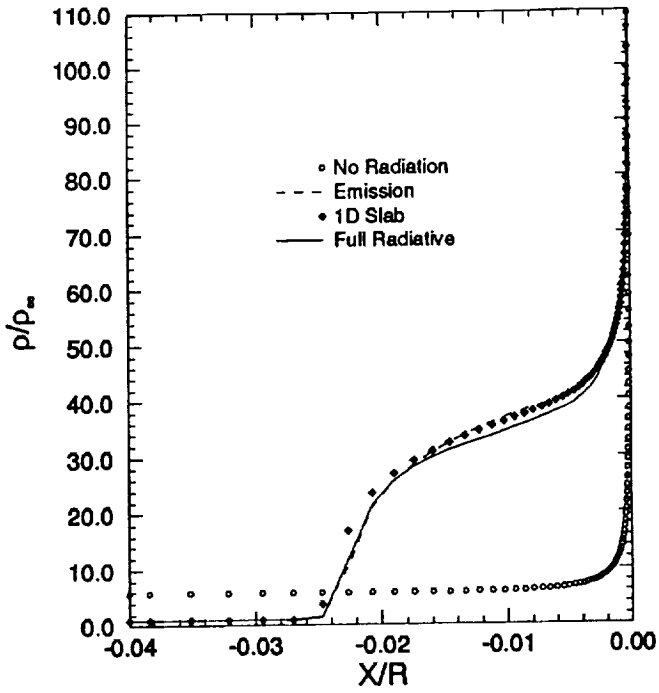

Fig. 9 Density along the stagnation streamline. Viscous result.

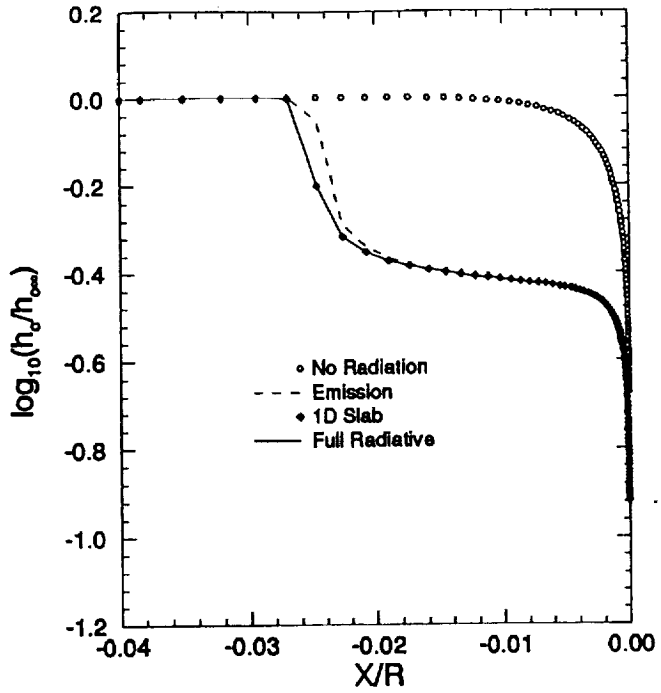

Fig. 10 Total enthalpy along the stagnation streamline. Viscous result.

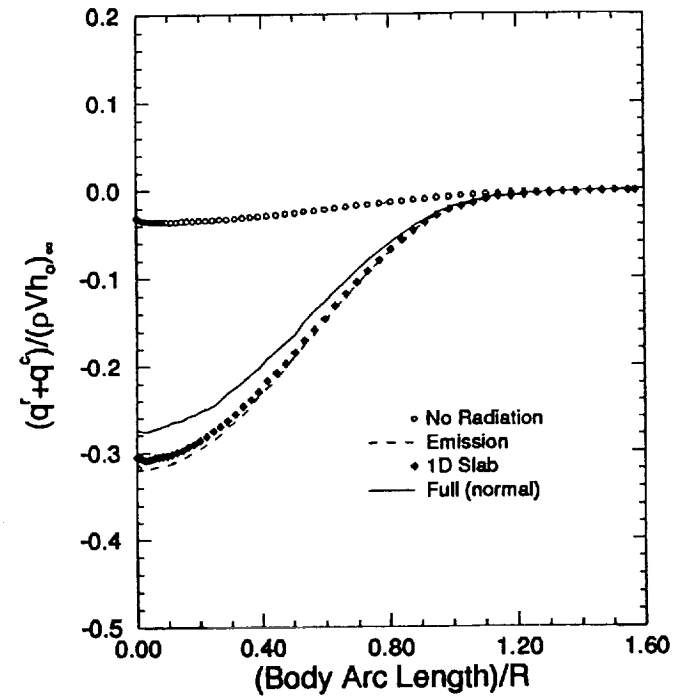

Fig. 11 Total (conductive plus radiative) heat transfer vector along the body surface.

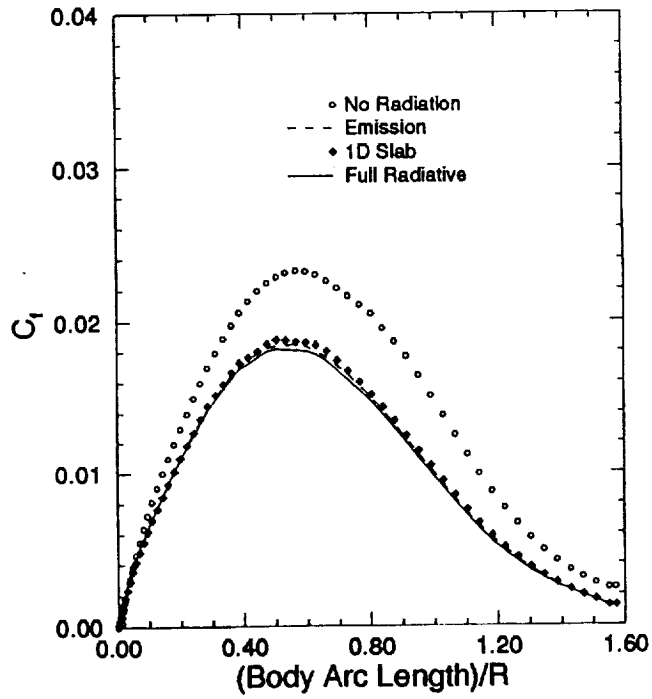

Fig. 12 Skin friction coefficient along the body surface.

A Multivariate PDF for Favre Averaging

H. A. HASSAN, North Carolina State University, Raleigh, North Carolina 27695-7910

Abstract – Present assumed PDF approaches for the calculation of compressible turbulent reacting flows use PDF's that do not yield Favre averaged quantities. Because of discrepancies between results of theory that uses such PDF's and experiment, there is a need to develop PDF's that are capable of producing Favre averaged quantities. A new PDF which combines the simplicity of the multivariate PDF of Girimaji and is capable of providing the desired Favre averaging is developed. This PDF is then used to calculate all necessary expressions involving composition needed for modeling compressible turbulent reacting flows.

When the pressure is constant, the proposed PDF gives exact analytical expressions for all averages involving chemical source terms.

INTRODUCTION

Recent interest in scramjet engines focused attention on the need to develop appropriate computational models capable of predicting supersonic turbulent reacting flows. Because of the high Mach numbers and short residence times, compressibility and chemical nonequilibrium effects play dominant roles in such engines. Understanding the roles of such phenomena is a prerequisite for determining the performance of such engines.

When compressibility effects are important, Favre averaging is used to simplify the Reynolds-averaged Navier-Stokes equations. This enables modeling procedures developed for low speed flows to be applied at the higher speeds. The procedure does not help in providing simple time averages for the chemical source terms. As a result, methods based on the probability density function (PDF) are used to calculate averages of the chemical source terms.

Calculation of PDF's from first principles has yet to be carried out for supersonic flows (Pope, 1985). Because of this, calculation of such flows have relied on assumed PDF's (Frankel et al., 1990, Baurle, et al., 1992a, 1992b, Narayan and Girimaji, 1992). Even when an assumed

Submitted to Combustion Science and Engineering

PDF is employed, the resulting averages are essentially time averages, i.e., the averages of the chemical source terms are expressed in terms of the time averaged concentrations and not the Favre averaged concentrations. Because of this, one is somehow forced to assume that the time averaged concentrations are essentially the corresponding Favre averaged quantities. Inevitably, such an assumption leads to errors which, so far, cannot be assessed.

Typical of the assumed PDF's is the multivariate β-PDF developed by Girimaji, (Girimaji, 1992a, 1992b). This is a joint β-PDF of the scaler mass fractions Y_k. For such a quantity, the relation between a time average, denoted by "–", and a Favre average, denoted by "~", can be expressed as

$$\bar{Y}_k = \tilde{Y}_k - \frac{\overline{\rho' Y_k'}}{\bar{\rho}}, \quad Y_k' = Y_k - \bar{Y}_k \tag{1}$$

where ρ is the density. Because there is no accepted procedure for modeling $\overline{\rho' Y_k'}$, $\bar{Y}_k$ was set equal to $\tilde{Y}_k$ in two recent investigations that used the PDF of Girimaji (Baurle et al., 1992b, Narayan and Girimaji, 1992).

The object of this investigation is to remedy this situation. By definition

$$\bar{\rho}_k = \bar{\rho}\,\tilde{Y}_k \tag{2}$$

$\bar{\rho}$ is given from the mass conservation equation. Thus, if we calculate $\bar{\rho}_s$, then equation (2) gives $\tilde{Y}_s$, which is the quantity appearing in the Favre averaged species conservation equations.

The plan of the paper is as follows. First, a joint PDF for the density and the species densities is developed. Next, equations are presented which determine all parameters appearing in the PDF. Finally, averages appearing in the governing equations that involve chemical source terms are evaluated.

PROPOSED JOINT PDF

As an illustration of the proposed approach, it is instructive to develop a multivariate PDF involving the density and the densities of the various species ρ_k. This PDF has the form

$$f = \frac{1}{C} \exp(-\rho)\, \rho^{\alpha-1} \prod_{k=1}^{N} \rho_k^{\beta_k - 1}\, \delta(\rho - \rho_s - \ldots - \rho_N) \tag{3}$$

All densities appearing in equation (3) are dimensionless quantities with δ being the Dirac delta function and C is determined from the requirement

$$\int_0^{\infty} \int_0^{\rho} \cdots \int_0^{\rho - s_{m-1}} \cdots \int_0^{\rho - s_{N-1}} f \, d\rho \, d\rho_1 \ldots d\rho_m \ldots d\rho_N = 1 \tag{4}$$

where

$$s_m = \sum_{k=1}^{m} \rho_k , \qquad m = 1, \ldots, N-1 \tag{5}$$

Carrying out the indicated integration in (4), we find

$$C = \left[\Gamma(\alpha + \gamma) \prod_{s=1}^{N} \Gamma(\beta_s) \right] \Big/ \Gamma(\gamma) \tag{6}$$

where

$$\gamma = \sum_{k=1}^{N} \beta_k \tag{7}$$

The average $\bar{\rho}_k$ and $\bar{\rho}$ follow from

$$\begin{aligned} \bar{\rho}_k &= \int \rho_k \, f \, d\rho \ldots d\rho_N \\ &= \beta_k(\alpha + \gamma)/\gamma \end{aligned} \tag{8}$$

and

$$\bar{\rho} = \int \rho\, f\, d\rho \ldots d\rho_N$$

$$= (\alpha + \gamma) \tag{9}$$

Thus

$$\frac{\bar{\rho}_k}{\bar{\rho}} = \tilde{Y}_k = \frac{\beta_k}{\gamma} \tag{10}$$

The variance of ρ_k is defined as

$$\overline{\rho_k'^2} = \overline{(\rho_k - \bar{\rho}_k)^2} = \overline{\rho_k^2} - (\bar{\rho}_k)^2 \tag{11}$$

Using the assumed expression for f, one finds

$$\overline{\rho_k'^2} = \frac{\beta_k(\beta_{k+1})(\alpha + \gamma)(\alpha + \gamma + 1)}{\gamma(\gamma + 1)} - \left[\frac{\beta_k(\alpha + \gamma)}{\gamma}\right]^2$$

$$= \frac{(\alpha + \gamma)}{\gamma}\,\beta_k\left[-\frac{\alpha\beta_k}{\gamma(\gamma + 1)} + \frac{\alpha + \gamma + 1}{\gamma + 1}\right] \tag{12}$$

Similarly, the covariance $\overline{\rho_k'\rho_m'}$ is given by

$$\overline{\rho_m'\rho_k'} = \frac{(\alpha + \gamma)}{\gamma}\,\beta_k\,\beta_m\left[-\frac{\alpha}{\gamma(\gamma + 1)}\right] \tag{13}$$

The sum of the variances, σ, is given by

$$\sigma = \frac{\bar{\rho}}{\gamma + 1}\left[-\alpha S + 1 + \bar{\rho}\right], \quad S = \Sigma\,(\bar{\rho}_k/\bar{\rho})^2 = \Sigma\,(\tilde{Y}_k)^2 \tag{14}$$

Thus, in combustion calculations, that employ conservation equations for $\bar{\rho}$ and $\tilde{Y}_k$, the unknowns α and γ can be determined from equations (9) and (14) as

$$\alpha = \frac{(1 + \bar{\rho})(\bar{\rho} - \sigma)}{\bar{\rho}S - \sigma}, \quad \gamma = \frac{(\bar{\rho})^2(S - 1) + \sigma - \bar{\rho}}{\bar{\rho}S - \sigma}$$

Thus, similar to the joint β-PDF developed by Girimaji (1991a,b) an equation for the sum of the variances is needed to close the system of governing equations.

MODEL EQUATION FOR σ

The starting point for such a derivation is the species conservation equation which can be written as

$$\frac{\partial \rho_k}{\partial t} + \frac{\partial}{\partial x_j}(\rho_k u_j) = \frac{\partial}{\partial x_j}\left[\rho D \frac{\partial}{\partial x_j}(\rho_k/\rho)\right] + \dot{w}_k \equiv S_k + \dot{w}_k \tag{15}$$

where u_j is the mean velocity component, D is the diffusion coefficient and $\dot{w}_k$ is the net rate of production of species k. Setting

$$\rho_k = \bar{\rho}_k + \rho_k', \quad u_j = \tilde{u}_j + u_j'' \tag{16}$$

and averaging, equation (15) takes the form

$$\frac{\partial \bar{\rho}_k}{\partial t} + \frac{\partial}{\partial x_j}\left[\overline{\rho_k u_j}\right] = \bar{S}_k + \bar{\dot{w}}_k \tag{17}$$

with

$$\overline{\rho_k u_j} = \bar{\rho}_k \tilde{u}_j + \bar{\rho}_k \bar{u}_i'' + \overline{\rho_k' u_k'} \tag{18}$$

Next, equation (15) is multiplied by ρ_s and the resulting equation is averaged. The result can be expressed as

$$\frac{\partial}{\partial t}\left[\{(\bar{\rho}_k)^2 + (\overline{\rho_k'^2})\}/2\right] + \bar{\rho}_k \frac{\partial}{\partial x_j}\left[\overline{\rho_k u_j}\right] + \overline{\rho_k' \frac{\partial}{\partial x_j}\left[(\rho_k u_j)'\right]} = \bar{\rho}_k\left[\bar{S}_k + \bar{\dot{w}}\right] + \overline{\rho_k'\left[S_k' + \dot{w}_k\right]} \tag{19}$$

The desired equation for $\rho_k'^2$ is obtained by multiplying equation (17) by $\bar{\rho}_k$ and subtracting from equation (19), i.e.,

$$\frac{\partial}{\partial t}\left[(\overline{\rho_k'^2})/2\right] + \overline{\rho_k' \frac{\partial}{\partial x_j}\left[(\rho_k u_j)'\right]} = \overline{\rho_k'\left[S_k' + \dot{w}_k'\right]} \tag{20}$$

Now

$$\overline{\rho_k' \frac{\partial}{\partial x_j}\left[(\rho_k u_j)'\right]} = \frac{\partial}{\partial x_j}\left[\tilde{u}_j \overline{\rho_k'^2} + \bar{\rho}_k \overline{\rho_k' u_j'} + \overline{u_j'' \rho_k'^2}\right] - \tilde{u}_j \frac{\partial}{\delta x_j}\left[\bar{\rho}_k'^2/2\right] - \bar{\rho}_k \overline{u_j'' \frac{\partial \rho_k'}{\partial x_j}} - \overline{u_j'' \frac{\partial}{\partial x_j}(\rho_k'^2/2)} \tag{21}$$

Similarly

$$\overline{\rho_k' S_k'} = \overline{\rho_k' \frac{\partial}{\partial x_j}\left(\rho D \frac{\partial Y_k}{\partial x_j}\right)'}$$

$$\simeq \overline{\rho_k' \frac{\partial}{\partial x_j}\left(D \frac{\partial \rho_k'}{\partial x_j}\right)}$$

$$= \frac{\partial}{\partial x_j}\left[D \frac{\partial}{\partial x_j}(\overline{\rho_k'^2}/2)\right] - D \overline{\frac{\partial \rho_k'}{\partial x_j}\frac{\partial \rho_k'}{\partial x_j}} \tag{22}$$

Equation (22) has terms of the type

$$\overline{u_j'' A_i'} = \overline{u_j' A'}$$

where A' is some function of the density ρ_k. These equations are modeled using the gradient diffusion assumption. Thus

$$\overline{u_j' A'} = - D_t \frac{\partial \bar{A}}{\partial x_j} \tag{23}$$

where D_t is a turbulent diffusion coefficient. Using equations (21)-(23), equation (20) can be expressed as

$$\frac{\partial}{\partial t}\left[(\overline{\rho_k'^2})/2\right] + \frac{\partial}{\partial x_j}\left[\tilde{u}_j \bar{\rho}_k'^2 - D_t \frac{\partial}{\partial x_j}(\bar{\rho}_k)^2/2 - D_t \frac{\partial}{\partial x_j}(\bar{\rho}_k'^2)\right] - \tilde{u}_j \frac{\partial}{\partial x_j}\left[\bar{\rho}_k'^2/2\right] + D_t \bar{\rho}_k \frac{\partial^2 \bar{\rho}_k}{\partial x_j \partial x_j}$$

$$+ D_t \frac{\partial^2}{\partial x_j \partial x_j} [\bar{\rho}_k'^2/2] = \frac{\partial}{\partial x_j}\left[D \frac{\partial}{\partial x_j} (\bar{\rho}_k'^2/2) \right] - D \overline{\frac{\partial \rho_k'}{\partial x_j} \frac{\partial \rho_k'}{\partial x_j}} + \overline{\rho_k' \dot{w}_k} \tag{24}$$

Summing with respect to k

$$\frac{\partial(\sigma/2)}{\partial t} + \frac{\partial}{\partial x_j}\left[\tilde{u}_j \sigma - D_t \frac{\partial(S/2)}{\partial x_j} - D_t \frac{\partial \sigma}{\partial x_j} \right] - \tilde{u}_j \frac{\partial(\sigma/2)}{\partial x_j} + D_t \Sigma \bar{\rho}_k \frac{\partial^2 \bar{\rho}_k}{\partial x_j \partial x_j}$$

$$+ D_t \frac{\partial^2(\sigma/2)}{\partial x_j \partial x_j} = \frac{\partial}{\partial x_j}\left[D \frac{\partial(\sigma/2)}{\partial x_j} \right] - \varepsilon + \Sigma \overline{\rho_k' \dot{w}_k} \tag{25}$$

when ε is the dissipation function and is modeled as

$$\varepsilon = \Sigma D \frac{\partial \rho_k'}{\partial x_j} \frac{\partial \rho_k'}{\partial x_j} = C_\sigma \frac{\sigma}{\tau} \tag{26}$$

where C_σ is a model constant and τ is a turbulent time scale.

AVERAGES INVOLVING PRODUCTION RATES

The chemical source terms appear in the conservation of species equations and the equation for the total variance, σ. The instantaneous production rate of species k follows from the law of mass action. Thus, if there are m reactions involving species k, i.e.,

$$\Sigma \upsilon_{kj}' M_k \rightleftarrows \Sigma \upsilon_{kj}'' M_k ; \quad j = 1, ..., m$$

where M_k designates species k, then, $\dot{w}_k$ is defined as

$$\dot{w}_k = W_k \sum_{j=1}^{m} (\upsilon_{kj}'' - \upsilon_{kj}') \left\{ K_{f_j} \prod_{s=1}^{N} (\rho_s/W_s)^{\upsilon_{s_j}'} - K_{b_j} \prod_{s=1}^{N} (\rho_s/W_s)^{\upsilon_{s_j}''} \right\} \tag{27}$$

In the above equation, W_k is the molecular weight and K_{f_j} and K_{b_j} are the forward and backward rate constants of reaction j. Both rate constants have the Arrhenius representation

$$K_j = A_j T^{\omega_j} \exp(-T_j/T) \tag{28}$$

where A_j, ω_j, and T_j are constants appropriate for reaction j.

If the pressure is constant throughout, then the equation of state for a perfect gas shows that $T \alpha 1/\rho$ (the average molecular weight is, in most cases, not very sensitive to changes in composition). In this case a closed form representation of $\bar{\dot{w}}_k$ and $\overline{\rho_k' \dot{w}}$ is possible. If, on the other hand, the pressure is not constant, one may assume that the joint PDF $F(\rho, T, \rho_k)$ has the representation

$$F(T,\rho,\rho_k) = g(T)\, f(\rho,\rho_k) \tag{29}$$

where $f(\rho,\rho_k)$ is that given in equation (3). In this case averages involving densities can be carried out in closed form independent of averages involving temperature. The motivation for this work is the need to develop computational approaches for the design and analysis of scramjet engines. In such engines, the assumption of constant pressure is not appropriate. Because of this the assumption indicated in equation (29) will be adopted. As will be seen from the following development, the extension of the results to a constant pressure situation is rather trivial.

Setting

$$m_j = \sum_s \upsilon'_{sj}, \quad n_j = \sum_s \upsilon''_{sj} \tag{30}$$

then $\bar{\dot{w}}_k$ can be represented as (Girimaji, 1991b)

$$\bar{\dot{w}} = W_k \sum_{j=1}^{m} (\upsilon''_{kj} - \upsilon'_{kj}) \left\{ \bar{K}_{f_j} \prod_{s=1}^{N} \left(W_s^{-\upsilon'_{sj}} \right) I_{f_j} - \bar{K}_{b_j} \prod_{s=1}^{N} \left(W_s^{-\upsilon''_{sj}} \right) I_{\upsilon_j} \right\} \tag{31}$$

where

$$I_{f_j} = \overline{\prod_{s=1}^{N} \rho_s^{\upsilon'_{sj}}}$$

$$= \frac{\Gamma(\alpha + \gamma + m_j) \prod_{s=1}^{N} \Gamma(\beta_s + \upsilon'_{sj})}{\Gamma(\gamma + m_j)} \cdot \frac{\Gamma(\gamma)}{\Gamma(\alpha + \gamma) \prod_{s=1}^{N} \Gamma(\beta_s)} \tag{32}$$

with a similar expression for I_{b_j}. Because υ'_{sj}, υ''_{sj} are integers, above expression can be simplified (Girimaji, 1991b). Using the relations

$$\frac{\Gamma(\alpha + \gamma + m_j)}{\Gamma(\alpha + \gamma)} = \prod_{r=1}^{m_j} (\alpha + \gamma + m_j - r)$$

$$\frac{\Gamma(\gamma + m_j)}{\Gamma(\gamma)} = \prod_{r=1}^{m_j} (\gamma + m_j - r)$$

$$\frac{\Gamma(\beta_s + \upsilon'_{sj})}{\Gamma(\beta_s)} = \prod_{r=1}^{\alpha'_{sj}} (\beta_s + \upsilon'_{sj} - r) \tag{33}$$

then I_{f_j} can be written as

$$I_{f_j} = \frac{\left[\prod_{r=1}^{m_j} (\alpha + \gamma + m_j - r)\right]\left[\prod_{s=1}^{N} \prod_{r=1}^{\upsilon'_{sj}} (\beta_s + \upsilon'_{sj} - r)\right]}{\prod_{s=1}^{m_j} (\gamma + m_j - r)} \tag{34}$$

The term $\overline{\rho'_k \dot{w}_k}$ can be expressed as

$$\overline{\rho'_k \dot{w}_k} = \overline{\rho_k \dot{w}_k} - \bar{\rho}_k \overline{\dot{w}_k} \tag{35}$$

with

$$\overline{\rho_k \dot{w}_k} = W_k \sum_{j=1}^{m} (\upsilon''_k - \upsilon'_k) \left\{ \bar{K}_{f_j} \prod_{s=1}^{N} W_s^{-\upsilon'_{sj}} J_{f_j} - \bar{K}_{b_j} \prod_{s=1}^{N} W_s^{-\upsilon'_{sj}} J_{b_j} \right\} \tag{36}$$

with

$$J_{f_j} = \frac{(\beta_k + \upsilon'_{kj})\ (\alpha + \gamma + m_j)}{(\gamma + m_j)}\ I_{f_j} \tag{37}$$

Similar relation holds for J_{b_j}.

When the pressure is constant, Equation (28) gives

$$K_j \propto \rho^{-\omega_j} \exp(-\delta_j \rho) \tag{38}$$

Thus, calculating the averages for $\bar{\dot{w}}_k$ and $\overline{\rho'_k \dot{w}_k}$ proceeds as above. However, in this case, one has to perform integrals of the type

$$\int \exp[-(1 + \delta_j)\rho]\rho^{\alpha - w_j} \rho_1^{\beta_1 - 1} \ldots \prod_{s=1}^{N} \rho_s^{\upsilon'_{sj}}\, d\rho \ldots d\rho_N \tag{39}$$

Above integration can be written as

$$\frac{\prod_{s=1}^{N} \Gamma(\beta_s + \upsilon'_{sj})}{\Gamma(\gamma)} \cdot \int_0^{\infty} \exp[-(1 + \delta_j)\rho]\rho^{\alpha+\gamma-\omega_j-1}\, d\rho$$

$$= \frac{1}{(1 + \delta_j)^{\alpha+\gamma-\omega_j}} \frac{\prod_{s=1}^{N} \Gamma(\beta_s + \upsilon'_{sj})}{\Gamma(\gamma)} \int_0^{\infty} \exp(-\xi)\xi^{\alpha+\gamma-\omega_j-1}\, d\xi$$

$$= \frac{1}{(1 + \delta_j)^{\alpha+\gamma-\omega_j}} \frac{\Gamma(\alpha + \gamma - \omega_j) \prod_{s=1}^{N} \Gamma(\beta_s + \upsilon'_{sj})}{\Gamma(\gamma)} \tag{40}$$

Thus, extending above formulas for $\bar{\dot{w}}_k$ and $\overline{\rho'_k \dot{w}_k}$ to the case where the pressure is constant is straightforward.

CONCLUDING REMARKS

The PDF proposed in this work makes it possible to formulate a consistent set of Favre averaged system of equations for the calculation of compressible reacting turbulent flows. As a result we have a procedure to correctly model the contribution of Favre averaging to terms involving the averages of chemical source terms. Appropriate expressions were also derived for averages involving chemical source terms in such a way that existing codes that used Girimaji's PDF can be modified with a minimum of effort.

There are a number of combustion problems where the pressure can be assumed constant. In this case assumptions similar to those indicated in equation (29) are not necessary and an exact representation of both $\bar{\dot{w}}_k$ and $\overline{\rho_k' \dot{w}_k}$ is possible.

ACKNOWLEDGEMENT

This work is supported in part by the following grants: NASA Grant NAG-1-244, the Mars Mission Center funded by NASA Grant NAGW-1331 and NASA Grant NAGW-2924 with North Carolina A&T State University.

REFERENCES

1. Baurle, R. A., Drummond, J. P., and Hassan, H. A. (1992a). An assumed pdf approach for the calculation of supersonic mixing layers. Paper AIAA-92-0182.
2. Baurle, R. A., Alexopoulos, G. A., Hassan, H. A., and Drummond, J. P. (1992b). An assumed joint-beta pdf approach for supersonic turbulent combustion. Paper AIAA-92-3844.
3. Frankel, S. H., Drummond, J. P., and Hassan, H. A. (1990). A hybrid Reynolds averaged/pdf closure model for supersonic turbulent combustion. Paper AIAA-90-1573.
4. Girimaji, S. S. (1991a). Assumed β-pdf model for turbulent mixing: validation and extension to multiple scalar mixing. *Combustion Science and Technology*, 78, 177-196.
5. Girimaji, S. S. (1991b). A simple recipe for modeling reaction-rates in flows with turbulent combustion. Paper AIAA-91-1792.

6. Pope, S. B. (1985). Pdf methods for turbulent reactive flows. *Progress in Energy and Combustion Science*, **11**, 119-192.

7. Narayan, J. R. and Girimaji, S. S. (1992). Turbulent reacting flow computations including turbulence-chemistry interactions. Paper AIAA-92-0342.

MODELING HUMAN RESPONSE ERRORS IN SYNTHETIC FLIGHT SIMULATOR DOMAIN

Celestine A. Ntuen
Human-Machine Systems Engineering Lab.
Department of Industrial Engineering
North Carolina A&T State University
Greensboro, NC 27411

This project is being supported by:

NASA Center of Research Excellence
(NASA-CORE)
School of Engineering
North Carolina A&T State University

Research Memorandum # HMSEL-CORE-0191

August 1992

Modeling Human Response Errors In Synthetic Flight Simulator Domain

Celestine A. Ntuen
HMSEL - NASA CORE

ABSTRACT

This paper presents a control theoretic approach to modeling human response errors (HRE) in the flight simulation domain. The human pilot is modeled as a supervisor of a highly automated system. The synthesis uses the theory of optimal control pilot modeling for integrating the pilot's observation error and the error due to the simulation model (experimental error). Methods for solving the HRE problem are suggested. Experimental verification of the models will be tested in a flight quality handling simulation.

I. INTRODUCTION

The use of flight simulator in pilot training is as old as flying itself. However, it was not until the late part of 1940s that the human pilot was considered as a part of the simulation model (ref. 3). In this respect, the human pilot is considered to be a complex servo-mechanical system whose position in the simulation loop represents that of a sub-optimal controller (ref. 1, 4, 5, 16).

Control theoretic models have been shown to be very robust mathematical tools for modeling servo systems (ref. 5, 7, 10, 17). Whether the human is modeled as an observer (ref. 5, 6, 7), a controller (ref. 6, 8, 14, 21), a supervisor (ref. 9, 13), or a problem solver in fault diagnosis domain (ref. 12, 13, 17), the most important goal is to predict the human performance and behavior in a human-machine interaction system (ref. 12, 15, 20).

The application of control model in the human pilot training simulation have been

promising and accepted as the conventional approach to modeling the pilot handling quality fidelity (ref. 6, 11). There is one important drawback in the current control models for flight simulators. That is, the performance of the model is based solely on the knowledge of the plant response before control is applied. In this sense, the human response error is a simplistic assumption of a Gaussian wide noise with zero mean and variance which depends on the plant dynamics.

In this paper consideration is given to human response error (HRE) models which are additive components of both the model representation error and the experiment error respectively. The HRE models are conceptualized with generality in mind thereby allowing the simulationist the flexibility to experiment on a variety of flight handling quality (FHQ) tests. Methods for solving the HRE problem are suggested.

Symbols

$a^j_i (i=o,i;j \in \{m, o\})$ characteristic gain function of the term in second-order error dynamic equation
B_m control vector for simulated model
B_r control vector for reference model
C_r coefficient matrix for the reference system output
D_r coefficient of error matrix for the reference system output
d cardinality index
$E(\cdot)$ expected value operator
e additive human response error term
e_m simulation model error
e_o observed model error
e_m expected latent error of expected input and conditional control
F cost functional of least-square equation for e_o
HRE Human Response Error
i index ($i \rightarrow o, 1$)
J_o HRE cost functional
j index operator, $j \in \{m, o\}$
K scaling factor
$L_m(\cdot)$ a function describing unknown dynamic input response
M expected value of v^2
m index for "model"
$N_m(\cdot)$ known part of system dynamics for the simulation model

n cardinality index
o index of observation in reference model
P covariance matrix of error estimate
U_m control vector for simulation model reference control vector
U_r control vector for reference model
v error term
R real number in Euclidian space
r reference model index
X_m simulation model state vector
X_r reference model state vector
Y_r output vector from reference model
$Z_m()$ response disparity distribution function
η_m simulation error term described by neurodynamic function of the operator
$\varphi_{xx}(\omega)$ auto correlation function of x(t)
$\varphi_{xy}(\omega)$ cross correlation function of x and y
$\phi_{xx}(\omega)$ power-spectral density of (t)
$\phi_{xx}(j\omega)$ cross-spectral density of x(t) and y(t)

II. THE HRE MODELING PROBLEM

A. The optimal control model for HRE problem (OCM/HRE)

The OCM/HRE system of interest are derived by the following dynamic equations,

$$\dot{X}_M = N_m(x,t) + L_m(x,u,t) + \eta(t) \ldots\ldots\ldots (1)$$

where $X \epsilon R^n$ is plant state vector whose components may represent aircraft dynamics such as velocity, flight path angle, and altitude; $U \epsilon R^n$ is a control vector whose components may represent flap deflection, pitch roll angle, and elevator deflection; $N_m(x,t)$ is a known part of the system dynamics in the model before control is applied (i.e., the initial system state); $L_m(x, u, t)$ represent (the unknown response plant dynamics when the control vector u is applied, and $\eta(t)$ is ϵR^n is an unknown disturbance vector or the neuromotor noise of he human pilot. The time variable t represents time. Equation (1) represents the OCM/HRE model.

B. The classical OCM

Following the classical optimal control model (OCM); see, e.g; Ref 5. Let us define a linear quadratic time invariant reference model which generates a desired trajectory (see ref. 2)

$$\dot{X}_r = A_r X_r + B_r U_r \quad \ldots\ldots (2)$$

and the measurement

$$Y_r = C_r X_r + D_r U_r \quad \ldots\ldots (3)$$

is observed in the reference model r, where X_r is the reference plant state vector, U_r is the reference pilot control vector, Y_r is the observed system output from the reference model (i.e; output vector utilized by the pilot in performing the control task). $A_r \epsilon R^{nxn}$ is a constant stable system matrix, $B_r \epsilon R^{nxd}$ is a constant control vector and $C_r \epsilon R^{pxn}$ and $D_r \epsilon R^{nxd}$; $Y_r \epsilon R^p$. Note that C_r is a known matrix;

$$Let \quad v = D_r U_r \quad \ldots\ldots (4)$$

$$with \; E(v) = o \quad \ldots\ldots (5)$$

$$E(vv^T) = M \quad \ldots\ldots (6)$$

where M is a known p x p positive matrix.

C. The HRE Model

We are interested in modeling the response errors in the system. Starting from the reference model; let us suppose that we had an estimate of the state before the simulation (measurements) are made; which we will call X_r, where

$$E\left[(X_r - \overline{X}_r)\,(X_r - \overline{X})^T\right] = J \quad \ldots\ldots (7)$$

where J is a known n x n positive matrix. Observing equation (3) shows that Y_r is a weighted-least-square of the estimate vector X. The usual criterion (ref. 2, 7) is a minimization of a quadratic form

$$F = 1/2\left[(X_r-\bar{X}_r)^T J^{-1}(X_r-\bar{X}_r) + (Y_r-C_r X_r)^T M^{-1}(Y_r-C_r X_r)\right] \quad \ldots\ldots(8)$$

To determine X_r, consider the differential of equation (8):

$$dF = dx_r^T \left[J^{-1}(X_r-\bar{X}_r) - C_r^T M^{-1}(Y_r-C_r X_r)\right] \quad \ldots\ldots(9)$$

In order that dJ = 0 for arbitrary dx^T_r the coefficient of dx^T_r in equation (9) must vanish:

$$(J^{-1} + C_r^T M^{-1} C_r) X_r = J^{-1} \bar{X}_r + C_r^T M^{-1} Y_r) = (J^{-1} + C_r^T M^{-1} C_r)\ \bar{X}_r + C_r^T M^{-1}\ (Y_r-C_r \bar{X}_r)$$

$$\hat{X}_r = \bar{X}_r + P\ C_r^T M^{-1}\ (Y_r-C_r \bar{X}_r) \quad \ldots\ldots(10)$$

$$\textit{Where}\quad P^{-1} = J^{-1} + C_r^T M^{-1} C_r \quad \ldots\ldots(11)$$

P is the covariance matrix of the error in the estimate $\bar{X}_r$, *that we have*

$$P = E\left[(\hat{X}_r-X_r)\ (\hat{X}-X_r)^T\right] \quad \ldots\ldots(11b)$$

Theorem 1: *The observation error estimate* $e_o = \bar{X}_r-X_r$ *(see ref.2).*

Proof:

By adding and subtracting X_r in the e_o term we have

$$e_o = \bar{X}_r-X_r + \hat{X}_r-\bar{X}_r \quad \ldots\ldots(12a)$$

$$= \bar{X}_r-X_r + PC_r^T M^{-1}\left[D_r\ U_r-C_r(\bar{X}_r-X_r)\right] \quad \ldots\ldots(12b)$$

Since $\bar{X}_r-X_r$ *and* $D_r\ U_r$ *are independent, it follows equation* (12b) *that*

$$E(e_o\ e_o^T) = (I-KC_r)\ J(I-KC_r)^T + KMK^T \quad \ldots\ldots(13)$$

and I is a unit matrix.

$$\text{where } K = PC_r M^{-1} \quad \ldots\ldots(14)$$

Premultiplying equation (11) by P and postmultiplying by J, we have

$$J = P + PC_r^T M^{-1} C_r J \quad \ldots\ldots(15)$$

$$\text{or } P + (I - KC_r)J \quad \ldots\ldots(16)$$

By using equation (16) in equation (13):

$$E(e_o e_o^T) = P - P C_r^T K^T + KMK^T = P - PC_r^T M^{-1} C_r P + PC_r^T M^{-1} C_r P = P \quad \ldots\ldots(17)$$

Thus, we have established a model for observation error, e_o in equation (12b and their computing properties in equations (13)-(17).

We are now interested in establishing the existence of model error e_m. To do this, we can introduce the command vector U(t) into equation (1). By rewriting equation (1) with the $B_m U_m(t)$ component we have:

$$\dot{X}_m = N_m(x,t) + L_m(x,u,t) - B_m U_m(t) + \eta(t) + B_m U_m(t) \quad \ldots\ldots(18)$$

$$\dot{X}_m = N_m(x,t) + Z_m(x,u,t) + B_m U_m(t) + \eta_m(t) \quad \ldots\ldots(19)$$

where the term $Z_m(x,u,t)$ is defined by

$$Z_m(x,u,t) = L_m(x,u,t) - B_m U_m(t) \quad \ldots\ldots(20)$$

$B_m \in R^{nxd}$ is a known constant matrix of rank d selected from the experimental model. Next, we define a model error e_m to be the difference between the plant state vector and the reference vector,

$$e_m = X_m - X_r \quad \ldots\ldots\ldots\ldots\ldots\ldots\ldots\ldots\ldots\ldots\ldots\ldots (21)$$

Therefore the total human response error (HRE) comprises of the model error and reference error vectors respectively. That is

$$\underline{\mathbf{HRE}} = e_m + e_o \quad \ldots\ldots\ldots\ldots\ldots\ldots\ldots\ldots\ldots\ldots\ldots\ldots (22)$$

D. Properties of HRE

There various properties of HRE that need to be investigated experimentally.

Case 1: If the model state vector X_m is absent, then $e_m = 0$ thus, HRE = e_o which is the classical method of state estimation. Thus HRE has all the properties discussed under section C above.

Case 2: If the reference state vector X_r is absent, then X_m describes the synthetic simulation model whose validity is by experimental observation only. In this case HRE = e_m. However, there is an error or experimental bias introduced by the difference between unknown (latent) response $L_m(x,u,t)$ and the input control $B_m U_m(t)$ as defined by $Z_m(x,u,t)$ in equation (20). Let $\hat{e}_m$ define this error such that

$$\hat{e}_m = E\left[(Z_m(x,u,t)\right] \quad \ldots\ldots\ldots\ldots\ldots\ldots\ldots\ldots\ldots\ldots (23)$$

$$Then, \quad HRE = e_m + \hat{e}_m \quad \ldots\ldots\ldots\ldots\ldots\ldots\ldots\ldots\ldots\ldots (24)$$

Case 3: If $e_m + e_o = 0$, then, we say that the simulation model described by X_m has a high fidelity. This is never attained in reality.

Case 4: The order of the system.
From equation (21): $e_m = X_m - X_r$, and the time rate of change of the error e_m, is

$$\dot{e}_m = \dot{X}_m - \dot{X}_r \quad \ldots\ldots\ldots\ldots\ldots\ldots\ldots\ldots\ldots\ldots\ldots\ldots (25)$$

$X_r(t_o)$, $X_m(t_o)$ given. Similarly;

$$\dot{e} = \dot{e}_m + \dot{e}_o \quad \ldots\ldots\ldots\ldots\ldots\ldots\ldots\ldots\ldots\ldots\ldots\ldots (26)$$

is the time rate of change of HRE. Clearly, HRE can be modeled as a second-order system with

the minimization criterion defined by

$$J_o = 1/2 \|e\|^2 \quad \ldots\ldots\ldots\ldots\ldots\ldots\ldots\ldots\ldots\ldots (27)$$

where e = HRE.

Case 5: HRE is a second-order error dynamic system. This property follows directly from case 4 above. Since e_o and e_m are independent, we can define the error dynamic equations by:

$$\ddot{e}_m = a_i^m \dot{e}_m + a_o^m e_m = 0 \quad \ldots\ldots\ldots\ldots\ldots\ldots\ldots\ldots (28)$$

$$\ddot{e}_o + a_i^o \dot{e}_o = a_o^o e_o = 0 \quad \ldots\ldots\ldots\ldots\ldots\ldots\ldots\ldots (29)$$

Where a_1^i (i = o, 1; j ϵ(m,o}) is the characteristic gain vector associated with each system of equation.

Case 6: $L_m(x,u,t)$ can be determined experimentally as follows: using the second-order gradient method, we guess a control parameter u(t=0) and determine X(t=0) from N_m(x(t=0), u(t=0) =0, and then L_m(X(0), u(0)). We can then determine the first and second derivatives of $L_m(x,u,t)$ with respect to u. Thus, we can approximate the (L_m vs u)-curve by a quadratic curve:

$$L_m^* = L_m(x_o, u_o, 0) + \left[\frac{\partial L_m}{\partial u}\right](u-u_o) + \left[\frac{\partial L_m}{\partial u}\right](u-u_o)^2 \quad \ldots\ldots (30)$$

Case 7: Time frequency property of **HRE**

Previous human response models in the aircraft simulation domain have been described by Taylor (ref. 18, 19) in terms of time frequency and power spectrum density functions. In a particular case in which $e_m = e_o$, the autocorrelation function describing HRE is found by

$$\varphi_{oo}(\tau) = \frac{1}{T} \int_{-T/2}^{T/2} f_o(t)\ f_o(t+\tau)\ dt \quad \ldots\ldots\ldots\ldots\ldots\ldots (31)$$

where $f_o(t)$ is fitted distribution describing the observation error, e_o. In this case the power

spectrum is

$$\phi_{oo}(\omega) = \frac{1}{T} \int_{-T/2}^{T/2} \varphi_{oo}(\tau) e^{j n \omega_o \tau} dt \quad \ldots\ldots\ldots\ldots\ldots\ldots (32)$$

If $e_o \neq e_m$ during the period of observation T;

$$\varphi_{mo}(\tau) = \frac{1}{T} \int_{-T/2}^{T/2} f_o(t)\ f_m(t + \tau) dt \quad \ldots\ldots\ldots\ldots\ldots (33)$$

defines the crosscorrelation function of $f_o(t)$ and $f_m(t)$; and

$$\phi_{mo}(j\ \omega) = \overline{F}_m(n)\ F_o(n) \quad \ldots\ldots\ldots\ldots\ldots\ldots\ldots\ldots (34)$$

where

$$\overline{F}(n) F_o(n) = \frac{1}{T} \int_{-T/2}^{T/2} Exp(-j\ n\ \omega_m) \varphi_{mo}(\tau) dt \quad \ldots\ldots\ldots\ldots (35)$$

CONCLUDING REMARKS

The discussion in this paper is geared towards modeling human response errors in a synthetic simulation domain in which flight handling qualities are the main tasks. The following conceptual contributions are prevalent to this paper.

1. We model the HRE as a component of two types of errors: the model error constructed around the simulation domain; and the reference error which is the theoretical state space model commonly used. In addition, we introduce the concept of experimental latent error which is the disparity between the theoretical input vector and the human input response at a given state space.

2. We discuss the various properties of HRE and their implications.

3. We formulate a cost minimization model of a simulation environment interms of the HRE function.

4. We demonstrate how the HRE model can be used in both the time and frequency domains.

It should be noted here that the discussions in this paper needs further theoretical proofs as well as actual experimentation to warrant their applications in flight handling quality characterization.

REFERENCES

1. S. Baron, "A Model Of Human Control And Monitoring Based On Modern Control Theory", J. Cybern. Inform. Sciences, Vol. 1(1), 1976, pp. 83-86.

2. A.E. Bryson and Y-C Ho, Applied Optimal Control, Revised Printing, New York: Hemisphere Publishing Corporation, 1975.

3. K.J.W. Craik, "Theory Of The Human Operator In Control Systems: I The Operator As An Engineering System", Brit. J. Psychology, Vol. 38, 1947, pp. 56-61.

4. R.E. Curry, W.C. Hoffman, and L.R. Young, "Pilot Modeling For Manned Simulation", AFFDL-TR-76-124, Vol. I, 1976.

5. R.A. Hess, "Aircraft Control-Display Analysis and Design Using The Optimal Control Model Of The Human Pilot", Trans. On Systems, Man and Cybernetics, Vol. SMC-11(7), July 1981, pp. 465-480.

6. R.A. Hess, "Prediction Of Pilot Opinion Ratings Using An Optimal Pilot Model", Human Factors, Vol. 19(5), 1977, pp. 459-475.

7. G. Johnannsen, and W.B. Rouse, "Mathematic Concepts for Modeling Human Behavior in Complex Man-Machine System", Human Factors, Vol. 21(6), 1979, pp. 262-268.

8. D.L. Kleinman, S. Baron, and W.H. Levison, "An Optimal Control Model Of Human Response", Part I & II", Automatica, Vol. 6, May 1970, pp. 357-369.

9. K.S. Krishnajumar, D. Sawal, J.E. Bailey, and J.A. Dohme, "A Simulator-Based Automated Helicopter Power Trainer-Synthesis and Verification", IEEE Trans. On Systems, Man and Cybernetics, Vol. 21(5), 1991, pp. 961-969.

10. W.H. Levison, S. Baron and D.K. Kleinman, "A Model For Human Controller Remnant", IEEE Trans. On Man-Machine System MMS-10, 1969, pp. 101-108.

11. F. Osafo-Charles, J.C. Aganwal, W.D. O'Neill and G.L. Gottlieb, "Application Of Time-Series Modeling To Human Operator Dynamics", IEEE Trans. On Systems, Man and Cybernetics, Vol. SMC-10(12), Dec. 1980, pp. 849-860.

12. A.V. Phatak and G.A. Bekey, "Model Of The Adaptive Behavior Of The Human Operator In Response To A Sudden Change In Control Situation", IEEE Trans. On Man-Machine Sytems, Vol. MMS-10(3), September 1969, pp. 89-95.

13. R.W. Pew and S. Baron, "Perspectives On Human Performance Modelling", Automatica, Vol. 19, 1983, pp. 663-676.

14. D.K. Schmidt, "Optimal Flight Control Synthesis-Via Pilot Modeling", J. Guidance Contr., Vol. 2(4), July-Aug. 1979, pp. 118-124.

15. S.M. Shinners, "Modeling Of Human Operator Performance Utilizing Time Senses Analysis", IEEE Trans. On Systems, Man and Cybernetics, Vol. SMC-4(5), Sept. 1974, pp. 446-458.

16. R.Sivan, J. Ish-Shalom, and J-K. Huang, "An Optimal Control Approach To The Design Of Moving Flight Simulators", IEEE Trans. On Systems, Man and Cybernetics, Vol. 12(6), 1992, p. 808-.

17. W.R. Sturgeon, "Controllers For Aircraft Motion Simulators", J. Guidance Control, Vol. 4(2), pp. 18-191, March 1981.

18. L.W. Taylor "A Look At Pilot Modeling Techniques At Low Frequencies, Presented At The 6th Annual Conf. On Manual Control, WPAFB, Ohio, April 7-9, 1970.

19. L.W. Taylor, "A Comparison Of Human Response Modeling In The Time And Frequency Domains", USC/NASA Conf. On Manual Control, Los Angeles, CA, March 1-3, 1967, NASA SP-144.

20. L.R. Young, D.M. Green, J.I. Elkind and J.A. Kelly, "Adaptive Dynamic Response Characteristics Of The Human Operator In simple Manual Control", IEEE Trans. On Human Factors In Electronics, 1964, pp. 6-13.

N93-19465

MODELING THE PERFORMANCE OF THE HUMAN (PILOT) INTERACTION IN A SYNTHETIC FLIGHT DOMAIN: INFORMATION THEORETIC APPROACH

Celestine A. Ntuen
Human-Machine Systems Engineering Lab.
Department of Industrial Engineering
North Carolina A&T State University
Greensboro, NC 27411

This project is being supported by:

NASA Center of Research Excellence
(NASA-CORE)
School of Engineering
North Carolina A&T State University

Research Memorandum # HMSEL-CORE-0194

October 1992

* Submitted to International Journal for Information Sciences for Review.

Information Theoretic Models of Human-Machine Interaction

ABSTRACT

Current advances in computing technology are devoid of formal methods that describe the theories of how information is shared between the humans and machines. Specifically, in the domain of human-machine interaction, a common mathematical foundation is lacking. The aim of this paper is to propose a formal method of human-machine (H-M) interaction paradigm from information view point. The methods presented are interpretation - and context - free and can be used both in experimental analysis as well as in modeling problems.

1. INTRODUCTION

The effectiveness of modern information technology depends in parts on the level of human-machine interaction. The human users of information systems (softwares) are faced with information state space which are complex. This complexity evolves around both human behavior and the machine state dynamics (see, e.g; [2,7]). Unfortunately, as many studies [11,14] indicate, the level of information loading continue to be the number one problem affecting the design of softwares. One reason to this problem is that software engineers and information scientists seem to ignore the formal approach to the design of H-M interface in the software development life cycle.

Suffice to say that even in a simple human-computer system environment, the issue of developing a formal method (mathematical theory) of interface paradigm still remains an enigma (see, e.g; [1,5,6]). Rasmussen [14] supports this view by observing that "in human-machine interaction, it appears to be necessary to consider the same distinction between signals and signs for the significance of human acts as it is for the information observed by a human. This dynamic interaction with the environment of complex behaviors calls for a very efficient feature

extraction and classification and dynamic coordination of the human-machine system with the task environment.

Most existing formal methods of H-M interaction are context specific and concentrate more on:

(a) the allocation of tasks to human operators and machines [1,5,10,19];

(b) display design and information presentation theories [1];

(c) communication bandwidth and dialogue protocols [13,15];

(d) group behavior theory [4,18];

(e) matching human behavior maps to information load [13,17].

The citations above have a common drawback in that no general method of H-M interaction exists. What is often described is the engineering process of H-M interaction which lacks the rigorous scientific theories. Methodologically, information theory is needed to characterize the H-M interaction environment. This problem is presented here in a context - and interpretation free format. The discussions are based on elementary functions of automaton.

2. PRELIMINARIES

The human-machine interaction (HMI) problem can be stated succinctly as follows: given a computer system C, and the human (as a controller, supervisor, user, etc.) H, we are interested in the design d; such that

$$d = \phi_H \wedge \phi_c \neq 0$$

$$and\ D = \phi_H \bigcup \phi_c$$

We use D to be the universe of design discourse; d to typify the interaction domain such d ϵ D;

ϕ_H and ϕ_c are the feature space characterizing the human and computer systems respectively. When the word "model" is used, we shall mean the elements of the computer system. Thus, ϕ_c is a model feature space whereas ϕ_H is a physical feature space. We also define the general feature space ϕ by the three element grammar defined by

$$\phi = \{ I, \lambda, P \}$$

where I is the information vector characterized by the four tupple

$$I = \{ S, M, U, V \}$$

with S as the information source (or sensory matrix); M the information modality which assigns "type" (logical, numerical, etc.) to the value of the information; U is the information control vector that triggers information occurrence; and V is a matrix of input-output data defined by

$$V: = \langle I^i \otimes I^o \rangle$$

I^i is the input data usually from the physical source (user-input) and I^o is the output data, usually from the model source (computer system). The operator "$\otimes$" is defined as concatenation, operator, e.g; $\{a\} \otimes \{b\} = \{ab\}\lambda$ defines the global state of the H-M system and is defined by

$$\lambda: = \langle T \otimes E \rangle$$

where T is the task vector and E is a environment disturbance. P is a performance matrix defined by column-wise concatenation operator $\|$ over the tupple elements defined by

$$P: \langle \delta \| \omega \| \beta \rangle$$

where δ is a Mealey automaton state-transition function [13] defined by

$$\delta: \lambda \times V_1 \rightarrow I^i$$

ω is a Mealey automaton output function defined by

$$\omega: \lambda \times V_2 \rightarrow I^o$$

β is a combination network on δ and ω defined by

$$\beta: \quad \delta \times \omega \rightarrow \beta$$

$$V_1 = \left(\frac{\partial T}{\partial V}\right) \left[\frac{dV}{dI^o}\right]$$
$$V_2 = \left(\frac{\partial T}{\partial V}\right) \left[\frac{dV}{dI^i}\right]$$

Note that $\frac{\partial T}{\partial V}$ uniquely defines the differential change in the task information with respect to input-output matrix V. For a example, in a supervisory control task, this differential may be a change in the domain of diagnostic problem solving such as reading pressure or temperature gauges. dv/dI^i is the qualitative change in output data assuming no new input data

3. FORMAL DESCRIPTION

The HMI system is described by the following sets:

Terminal-state function

$$Y: = \alpha_d(I, P, Z)$$

where α_d is a translation function mapping the features ϕ_H and ϕ_c in feature space d ϵ D. α_D is a many-to-many corresponding mapping with P as the evaluation function.

$$Z = \{ Z_1, \beta, Z_2 \}$$

where Z_1 is the physical task vector defined by

$$Z_1 : = \omega\ (\ I, \lambda\ )$$

Z_2 is the model for information combination defined by

$$Z_2 :\ \delta\ (\ I, \lambda\ )$$

DEFINITION. The interaction is said to be "symbiotic" optimal if

$$\left\{\ \forall c' \in \phi_c ;\ \exists\ h \in \phi_H \right\}\ \phi_h \wedge \phi_{c'} = \phi_{c'}$$

The algebraic relation is that for every model feature $\acute{c} \in \phi_c$, the human can interact successfully to perform a defined task. The concept of symbiosis is to measure the level of cooperation between the physical and model elements. This relation can be proved easily by invoking the laws of absorption which argues that if $\phi_{\acute{c}} \subseteq \phi_h$, then $\phi_{\acute{c}} \wedge \phi_h = \phi_{\acute{c}}$, where $\wedge$ is a conjunction operator.

DEFINITION. The performance matrix is a linear manifold structure of Z. This property is a fundamental approach to information aggregation. Note that $Z = \{Z_1, Z_2\}$ represents information structure associated with the physical (human) and the model (computer) elements. If the event, say $h \in H$ occurs with observation error e_h; and the event say $\acute{c}' \in C$ occurs with model error $e_{\acute{c}}$. By definition, $Z = \{\ Z_1 \rightarrow Z_1 + e_h,\ \beta,\ Z_2 \rightarrow Z_2 + e_{\acute{c}}\}$.

Since the systems is considered to be dynamic, this allows us to write, Z as a time dependent system of control automation:

$$\begin{aligned} \dot{Z} &= A\ Z + E \\ P &= G\ Z \end{aligned}$$

where A is the matrix derived by $\delta\ \|\omega\|\ \beta$, E is the error matrix derived by concatenation of e_h and $e_{\acute{c}}$, and G is a constant performance matrix. Note however that A and G are chosen to be semi-positive definitive and the values of Z are obtained via real time observation. An

example is the human pilot interacting with the pilot associate program in deciding on where to land an aircraft during a severe storm.

DEFINITION. Let ϕ be an Euclidian information space. Consider a subspace ϕ_s such that $\phi_s \wedge \phi = 0$. Then ϕ can be represented in the form

$$\phi = \varphi(z) + N$$

where $z \in \phi_s$, $\varphi(z) \in \phi_s$ and N is orthogonal to $\varphi(z)$. The property of ϕ is such that

$$E\{\varphi(z) + N\} = E\{\phi - \varphi(z)) \cdot \varphi(z)\} = 0$$

Further, the distance between ϕ and any point p in $\varphi(z)$ satisfies

$$E\{(\phi - p)^2\} \geq E\{(\phi - \varphi(z)) \cdot \varphi(z)\} = 0.$$

with the equality if $p = \varphi(z)$; $\varphi(z)$ is known as the projection of ϕ on ϕ_s. This definition stipulates the relationship between the human observer trying to project his or her corporal self into the domain of a model state space. An example of $\varphi(z)$ is a pilot undergoing a flight handling simulation exercise and ϕ_s is the model information characterizing the aircraft dynamics. The orthogonal vector N may represent the actual observation data during the experiment.

DEFINITION Let r(D) be a measure of H-M interaction design effectiveness. Then we define

$$r(D) = \frac{Min\{(\phi_c \wedge \phi_h), \phi_h\ 0\}}{Max\{\phi_c, \phi_h\}}$$

PROPOSITION. Let $r(\phi_c)$ and $r(\phi_h)$ represent the design effectiveness of model and human elements, then $r(\phi_c \wedge \phi_h) \leq r(\phi_c) + r(\phi_h)$

Proof. The result above follows the triangle law of inequality and the law of conjunction operator.

DEFINITION. Let m(D) be a measure of H-M interaction design efficiency. Then we define

$$m(D) = \frac{\omega(I_h, \lambda_h)}{Max\{Z_1, Z_2\},\ for\ all\ h \in H}$$

Note that efficiency is used here to measure the human elements that have been tested and validated for the system.

DEFINITION. Let s(D) be a measure of interaction "symbiosis" between H and C. Then s(D) is related to r(D) and m(D) by s(D) = r(D)/m (D); s(D) $\geq$ 0 and m (D) $\neq$ 0.

Note that if s(D) = 0 then r(D) = 0 implies that $\phi_c \wedge \phi_h = 0$.

DEFINITION. Let α_D be an information mapping function on the universe of design discourse D such that the probability $\wedge$(D) exists. $\wedge$(D) follows the usual definition of probability axioms, such that

$$\sum_{d \in D} \wedge(D) = 1.$$

We can therefore define the mapping function $\alpha_D(\phi_c, \phi_h)$ by the relation

$$\alpha_D(\phi_c, \phi_h) = \min\{\wedge(\phi_h),\ \wedge(\phi_c),\ \wedge(\phi_h \wedge \phi_c)\}$$

DEFINITION. Assume that information value can be measured on some distance metric n(ϕ). Further, assume the existence of optimal policy

$$\phi^* \in \phi_h \wedge \phi_c \quad \forall\ h \in H;\ \forall c \in C.$$

Define the design error e_d by $e_d = \phi_h - \phi_c$. e_d can be written in terms of ϕ^* by $e_d = (\phi_h + \phi^*) - (\phi_c - \phi^*)$. If there are d design variables observed in ϕ; then the d - norm error distance n(ϕ) is defined by

$$n(\phi) = \|d\| \quad , \quad that\ is$$

$$n(\phi) = \left[(\phi_h + \phi^*)^d + (\phi^* - \phi_c)^d\right]^{1/d}$$

PROPOSITION. If $\phi^* - \phi_c = 0$, then the distance measure $n(\phi)$ is said to be regular with respect to the human observer. In this case, the human is said to "gain" all the information in ϕ_c

Proof. If $\phi^* - \phi_c = 0$; then $\phi^* = \phi_c$. By definition, $\phi^* = \phi_h \wedge \phi_c$ that is $\phi_c = \phi_h \wedge \phi_c$. By rules of Boolean algebra; $\phi_c \subseteq \phi_h$; and $\phi = \phi_h$ is the universal set. Therefore $\phi \wedge \phi_c = \phi_c$. Hence, $n(\phi) = \{(\phi_h + \phi^*)^d\}^{1/d} = \phi_h + \phi^*$; this implies that $\phi^* = \phi_c$ is the gain. An example of this proposition is used in developing decision support systems. Here, ϕ_h is what the person using the system had known already, $\phi^* = \phi_c$ is the decision support information from the computer which is new to the human. If at the end of interaction, the human has learned all ϕ_c, by the proposition, information gain has taken place.

PROPOSITION. Let H_I be experimental or observation matrix which is a positive definite. Then $H_I = \phi_h \cdot \phi^{-1}{}_c$

Proof. Let the matrix function H_I: $R \circledast J \rightarrow R$ be induced in the natural way by multiplying the design matrix R by a unit matrix J. R is defined such that

$R \circledast J: = < \phi_h, \phi_c, J >, \forall h \in H, \forall c \in C$ with the definitions:

$\phi_h : = \phi_h \circledast J_h \rightarrow \phi_h$

$\phi_c : = \phi_c \circledast J_c \rightarrow \phi_h$

$J: = J_h \parallel J_c$, when "$\parallel$" means column wise concatenation. Without loss of meaning. Let us assume the relationship: J_h and J_c to be unit matrices defined on ϕ_h and ϕ_c respectively.

$$\phi_h \cdot \phi_c \cdot \phi_c^{-1} = \phi_h^{-1}(\phi_h \cdot J_h \, \phi_c \, J_c) \; \phi_c^{-1}\phi_h^{-1} \, J_h$$

The left hand side of equation is equal to $\phi_h \cdot J_c$. And the right hand side is simplified to

$J_h \cdot \phi_c \cdot H_I \cdot$. Thus, $\phi_h \cdot J_c = J_h \, \phi_c \, H_I \, J_h$

If we post concatenate J_h on both the left and right hand side of the equation above, we have

$\phi_h \cdot J = J_h \, \phi_c \, H_I \, J$

$\phi_h = J_h \, \phi_c \, H_I$

$$Hence \; H_I = \left(\phi_h \cdot J_h^{-1}\right)\phi_c^{-1}$$

$$H_I = \phi_h \cdot \phi_c^{-1} \; (since \; J_h^{-1} = J_h)$$

Note that the model information matrix has become a weighted matrix for the observation matrix. We assume that ϕ_h and ϕ_c have the same cardinality.

4. CONCLUSIONS

The development of information theoretic models based on abstraction and automaton theory, provides a framework for measuring the effectiveness and efficiency of human-machine interaction design. In addition, a general framework for formal methods of modeling H-M interaction is suggested.

As a prolegomenous discussion, the basic definitions and some propositions with proofs are presented. Specifically, the formal descriptions rely more on abstractions and equivalence formulations of formal method rather than inductive hypothesis. The presentation is open-ended in format. Thus, the concept presentation are useful in disciplines such as software engineering, fuzzy models, and decision support system (expert system) techniques.

REFERENCES

1. A.N. Badre, Selecting and Representing Information Structures for Visual presentation, IEEE Trans. on Man, Systems, and Cybernetics, Vol. SMC-12(2): 491-498 (1982).

2. A. Borgida, Features of Languages For The Development of Information Systems at The Conceptual level, IEEE Software, 2(1): 63-73 (1985).

3. T.L. Booth, Sequential Machines and Automata Theory, New York: John Wiley (1967)

4. T.T. Carey and R.E.A Mason, Information Systems Prototyping: Techniques, Tools and Methodologies, INFOR, 21(3): 17-191 (1983).

5. J. Contaz, Abstractions For User Interface Design, IEEE Computers 18(9): 21-34 (1985).

6. M.U. Faroq and W.D. Dominicu, A Survey of Formal Tools and Models For Developing User Interfaces, Int. J. Man-Machine Studies, 29: 479-496 (1988).

7. T.R.G. Greene, F. Schiele, and S.J. Payne, Formalisable Models of Users Knowledge in Human-Computer Interaction In: Van Der Veer, G.C; Green, T.R.G., Hoc, J-M, and Murray, D.M. (eds), Working with Computers: Theory versus Outcome: 3-46 (1988), Academic Press, London.

8. R.J.K. Jacob, Using Formal Specification In The Design of Human-Computer Interface, Communication of the ACM, 26(4)L 259-264 (1983).

9. A.P. Jajodzinski, A theoretical Basis of Representation of On-Line Computer Systems to Naive Users, Int. J. Man-Machine Studies. 18: 215-252 (1983).

10. D.E. Kieras, and P.G. Polson, An Approach To The Formal Analysis of User Complexity, Int J. Man-Machine Studies 22(4): 365-394 1985).

11. T.P. Moran, The Command Language Grammar: A Representation For The User Interface of Interactive Computer Systems, Int. J. Man-Machine Studies 15: 3-50 (1981).

12. N. Moray, Intelligent Aids, Mental Models, and the Theory of Machines, Int. J. Man-Machine Studies, 27: 619-629.

13. H. Oberquele, I. Kupka, and S. Maass, A View of Human-Machine Communication and Cooperation, Int. J. Man-Machine Studies, 19: 209-333 (1983).

14. J. Rasmussen, Information Processing and Human-Machine Interaction: An Approach To Cognitive Engineering, North-Holland, Amsterdam (1986).

15. M.L. Shaw, Attending to Multiple Sources of Information: The Integration of Information in Decision Making, Cognitive Psychology, 14: 353-409 (1982).

16. P. Reisner, Using A Formal Grammar In Human Factors Design of An Interactive Graphics System, IEEE Trans. on Software Engineering, SE-7: 229-240 (1981).

17. B. Shaiederman, Multiparty Grammars and Related Features for Defining Interactive Systems, IEEE Trans. on Man, Systems, and Cybernetics. SMC-12 (2): 148-154 (1982).

18. P.M. Wortman, Medical Diagnosis: An Information-Processing Approach, Computer and Biomedical Research, 5: 315-328 (1971).

19. B.P. Zeigler, Towards a Formal Theory of Modeling and Simulation: Structure Preserving Morphisms, Journal of the Association for Computing Machinery, 19(4): 74-764 (1972).

RECOGNITION OF PARTIALLY OCCLUDED THREAT OBJECTS USING THE ANNEALED HOPEFIELD NETWORK

by

Jung H. Kim*
Sung H. Yoon*
Eui H. Park**
Celestine A. Ntuen**

Human-Machine Systems Engineering Group
* Department of Electrical Engineering
** Department of Industrial Engineering
North Carolina A&T State University
Greensboro, NC 27411

This project is being supported by:
NASA Center of Research Excellence
(NASA-CORE)
School of Engineering
North Carolina A&T State University

Research Memorandum # HMSEL-CORE-0193

OCTOBER 1992

Recognition of partially occluded threat objects based on the annealed Hopfield network[1]

Jung H. Kim*, Sung H. Yoon*, Eui H. Park**, Celestine A. Ntuen**, and Shiu Cheung***

*Dept. of EE and **Dept. of IE
North Carolina A&T State University
Greensboro, NC 27411

***FAA Technical Center ACA-500
Atlantic City Airport, NJ 08405

ABSTRACT

Recognition of partially occluded objects has been an important issue to airport security because occlusion causes significant problems in identifying and locating objects during baggage inspection. Neural network approach is suitable for the problems in the sense that the inherent parallelism of Neural Networks pursues many hypotheses in parallel resulting in high computation rates. Moreover, they provide a greater degree of robustness or fault tolerance than conventional computers. The annealed Hopfield network which is derived from the mean field annealing(MFA) has been developed to find global solutions of a non-linear system. In the study, it has been proven that the system temperature of MFA is equivalent to the gain of sigmoid function of Hopfield network. In our early work, we developed the hybrid Hopfield network(HHN) on the purpose of fast and reliable matching[1]. However, HHN doesn't guarantee global solutions and yields false matching under heavily occluded conditions because HHN is depending on initial states by its nature. In this paper, we present the annealed Hopfield network(AHN) for occluded object matching problems. In AHN, the mean field theory is applied to the hybrid Hopfield network in order to improve computational complexity of the annealed Hopfield network and provide reliable matching under heavily occluded conditions. AHN is slower than HHN. However, AHN provides near global solutions without initial restrictions and provides less false matching than HHN. In conclusion, a new algorithm based upon a Neural Network approach was developed to demonstrate the feasibility of the automated inspection of threat objects from X-ray images. The robustness of the algorithm is proved by identifying occluded target objects with large tolerance of their features.

1. INTRODUCTION

Pattern recognition and computer vision theory has been considerably improved during the last decade such that the appearance of an automated vision system seems very close to our future[2,3]. However, because of the higher computational burden of image understanding algorithms, use of object recognition from an image is still limited to the restricted environment. In the mean time researchers developed a new idea of computation which imitates human brain structure, called a neural computing[4,5]. Techniques in neural computing are based on a new concept of distributed parallel computation, and applicable to any number crunching objectives. Hopfield network, one of the neural computations is very popular in real world application due to simple architecture and well defined time domain behavior[5-9]. The Hopfield network is composed of single-layer neurons with fully connected feedback connections. The neurons have the sigmoid gain characteristic, while the connectivity matrix corresponding to the connection is symmetric and the diagonal terms of the matrix are zero. Such networks always move in the direction of decreasing the energy of the networks and get stable states at the local minimum of the energy. Since the energy function of a Hopfield network has many local minima, the resultant network output is usually the closest local minimum to initial states. This nature of the Hopfield network must be the demerit in solving an optimization problem. In our early work, we developed the hybrid Hopfield network algorithm to improve deficiency of the original Hopfield network. The method yields a good solution by adding an adjusting procedure for the output neuron states of the

[1]This research has been supported by FAA under Contract DTF A01-87-c-00043, NSF under Grant ECD-8212696, and the NASA Center for Research Excellence of North Carolina A&T State University under Grant No. NAGW-1924.

Hopfield network. However, the method still does not guarantee global solutions. Simulated annealing is one heuristic technique to help escape the local minima by perturbing the energy function with the annealing temperature and artificial noise[10]. It is proven that the solution obtained by the simulated annealing is independent of the initial condition of the network and is usually very close to the global minimum[9]. Since the network should settle down at each temperature and the temperature decrement is very small, extraordinarily long time is required in the software computation. The mean field theory(MF) has been applied to the simulated annealing in the effort on reducing the computational time and many impressive outputs in image processing area have been reported. The MF has the analogy to the Hopfield networks[11]. It was proven that the system temperature of MF is equivalent to the neural gain. D. E. Van den Bout *et al.* also developed a new algorithm, the mean field annealing(MFA) which merges many features of simulated annealing and Hopfield networks[12]. They does not use a sigmoid function but use the normalization technique. However the normalization technique can be applied to the case in which the sum of a normalized subgroup is equal to 1. An occluded object matching problem is the one which can be cast into an optimization problem when the graph theory is applied to the problem. MFA can be used to solve the occluded object matching problem. Unfortunately, the problem is not suitable to normalization technique because the sum of normalized subgroups is zero or one. Thus, we use the sigmoid function, which is one of the important characteristic of Hopfield network. We can do an hardware implementation as well as an algorithm approach. We call this technique as the annealed Hopfield network(AHN).

2. ANNEALED HOPFIELD NETWORK

2.1 Feature extraction and graph formation

In boundary based approaches, corner points are important since the information of the shape is concentrated at the points having high curvatures. From the corner points, we can extract useful features such as a local feature of an angle between neighboring corners and relational features of distances between the corners. These two features which are invariant under transnational and rotational changes are used for the robust description of shape of the boundary. Corner points are usually detected in a curvature function space by capturing the points whose curvature values are above a certain threshold value. We developed a new corner detection algorithm which provides reliable and invariant corners for a matching procedure in the early study[9]. A graph can be constructed for a model object using corner points as nodes of the graph. Each node has a local feature as well as relational features with other nodes. For the matching process, a similar graph is constructed for the input image which may consist of one or several overlapped objects. Each model graph is then matched against the input image graph to find the best matching subgraph.

2.2 Hopfield Network versus Mean field theory

The continuous Hopfield network(CHN) is a deterministic model which retains the significant characteristics of the discrete Hopfield network. The discrete network(DHN) uses binary states. However, real neurons and real physical circuits have integrative time delays due to capacitance, and the time evolution of the state of such systems is represented by a differential equation, so called the equation of motion. The continuous network has flow of neuron states in a continuous domain while the discrete network has flow of neuron states in a discrete domain. It means that CHN is better than DHN for the optimization problems since CHN has a smooth energy function surface. A two dimensional array is constructed to apply a matching problem into the neural networks. The columns of the array label the nodes of an object model, and the rows indicate the nodes of an input object[14,15]. The number of column n is the number of nodes of a model object and the number of rows m is the number of nodes of input image. Therefore, the state of each neuron represents the measure of match between two nodes from each graph. The matching process can be characterized as minimizing the following energy function:

$$E = -\frac{1}{2}\sum_i\sum_j\sum_k\sum_l C_{ijkl}V_{ik}V_{jl} + \frac{q}{2}\left(\sum_i\sum_k\sum_{l\neq k} V_{ik}V_{il} + \sum_k\sum_i\sum_{j\neq i} V_{ik}V_{jk}\right) \quad (1)$$

where V_{ik} is a variable which converges to "1" if the ith node in the input image matches the kth node in the object model; otherwise, it converges to "0". The first term in Eq.(1) is a compatibility constraint. Local and relational feature which have different measures are normalized to give tolerance for ambiguity of the features as follows:

$$C_{ikjl} = W_1 \times F(f_i, f_k) + W_2 \times F(f_j, f_l) + W_3 \times F(r_{ij}, r_{kl}) \quad (2)$$

The fuzzy function F has a value 1 for a positive support and -1 for a negative support. The value of $F(x, y)$ is defined such that if the absolute value of the difference between x and y is less than a threshold θ, then $F(x, y)$ is set to 1, otherwise $F(x, y)$ is set to -1. The sum of the weights is 1. In our early work[], we uses two features such as angle and distance. Angle helps us to recognize the shape of object. However, false segmentation cause to generate different angles from those of original segmentation. In this paper, relational features are more emphasized than local features. AHN even works well without local features. The last two terms are included to enforce the uniqueness constraint so that each node in the object model eventually matches only one node in the input image and the summation of the outputs of the neurons in each row or column is no more than 1. Some papers concerning a matching problem with the Hopfield style neural network have used $\Sigma\Sigma(1-V_{ik})^2$ as an uniqueness constraint. This term implies global restriction. However, matching of occluded objects will not guarantee that every row or every column has only one active neuron. Thus the energy function of the occluded matching problem excludes the global restriction condition in Eq.(1). In a traveling salesman problem, uniqueness coefficient q is more weighted than the coefficient of the compatibility term because q contributes yielding valid solutions. However, conditions of valid solutions in the matching of occluded objects are indefinite, so the coefficient A is supposed to be more weighted in the matching problem. Eq.(1) can be cast into the discrete Hopfield energy function(DHN) as follows:

$$E = -\frac{1}{2}\sum_i\sum_j\sum_k\sum_l T_{ijkl}V_{ik}V_{jl} - \sum_i\sum_j I_{ik}V_{ik} \quad (26)$$

$$T_{ikjl} = C_{ijkl} - q\,(\delta_{ij} + \delta_{kl} - \delta_{ij}\delta_{kl})$$

where $\delta_{ij} = 1$ when $i = j$, otherwise $\delta_{ij} = 0$. Hopfield proved that the energy function is a Liapnov function. Thus the energy function converges to a local minimum when the states of neurons converge to stable states[13]. Unlike the other application[14,15], the constraint that $\Sigma\Sigma V_{ik}$ is equal to the number of column can not be used in the occluded object matching problem since occluded objects can lose a lot of segments of the original. The matching process of CHN can be characterized by the same energy function as that of DHN. Only an integral term is added to the energy function as follows:

$$\sum_i\sum_k (1/R_{ik}) \int_0^{V_{ik}} g^{-1}(V)dV \quad (4)$$

Where g is a sigmoid function and R_{ik} is the input resistance of a neuron. This term comes from the point of view that neural input state u_{ik} will lag because of the existence of capacitance in an analog electrical circuit. Thus, there is a resistance-capacitance charging equation, called the equation of motion that determines the rate of change of u_{ik}[14]. It is the first order differential equation. The equation of the motion is as follows[9]:

$$\frac{du_{ik}}{dt} = -u_{ik}/\lambda + \sum_j\sum_i T_{ikjl}V_{jl} + I_{ik} \quad (5)$$

where

$$g(u_{ik}) = \frac{1}{1 + \exp[-u_{ik}/\lambda]} \quad (6)$$

Now, let us consider MFA application. A motion equation is shown in Eq.(5) with the sigmoid function g. Our energy function of the matching problem is organized as Eq.(1). The output of each neuron for the matching problem has the value of 0 or 1 to represent measure of similarity. We will call output of each neuron a ***spin*** for the mean field annealing

approach. It was assumed that the *spin* interactions T_{ikjl} are symmetric and have no self-interaction (i.e., $T_{ikik} = 0$). The state space of each *spin* is:

$$s_{ik} \in \{0, 1\} \quad for\ 1 \le i,k \le N \tag{7}$$

where $N^2 = m \times n$. In simulated annealing, random perturbations move the system towards its thermal equilibrium at the current temperature. Assuming that all the *spin*s are at equilibrium, one can determine the equilibrium spin average of the *i*th *spin* $<s_{ik}>$ from the Boltzmann distribution and the change in the average system energy as s_{ik} flips from 0 to 1. To illustrate, let $H_0 = < H(s) > \big|_{Sik=0}$, $H_1 = < H(s) > \big|_{Sik=1}$. Since the system is Boltzmann distributed, the equilibrium value of $<s_{ik}>$ is calculated as follows:

$$\begin{aligned} <s_{ik}> &= Pr\{s_{ik}=0\}\times 0 + Pr\{s_{ik}=1\}\times 1 \\ &= \frac{\exp(-\frac{H_1}{T})}{\exp(-\frac{H_0}{T}) + \exp(-\frac{H_1}{T})} \\ &= \{1 + \exp[-\frac{(H_0-H_1)}{T}]\}^{-1} = \{1 + \exp[\frac{u_{ik}}{T}]\}^{-1} \end{aligned} \tag{8}$$

We define u_{ik} to represent the quantity $H_0 - H_1$, which is the mean or effective field experienced by the *ik*th *spin*. Unfortunately, it is in general difficult to compute u_{ik} for large N:

$$\begin{aligned} <H(s)> &= <\sum_i\sum_j\sum_k\sum_l T_{ikjl}s_{ik}s_{jl} + \sum_i\sum_k I_{ik}s_{ik}> \\ &= \sum_i\sum_k\sum_j\sum_l T_{ikjl}<s_{ik}s_{jl}> + \sum_i\sum_k I_{ik}<s_{ik}> \end{aligned} \tag{9}$$

The difficulty arises from the fact that s_{ik} and s_{jl} are not independent, so that their expected values are not separable in the above equation. However, when the number of interacting spins is large enough that the effect of any single *spin* on any other *spin* is very small in comparison to the total field, then the mean field approximation can be used:

$$<H(s)> = \sum_i\sum_k\sum_j\sum_l T_{ikjl}<s_{ik}><s_{jl}> + \sum_i\sum_k I_{ik}<s_{ik}> \tag{10}$$

The Eq.(8) and Eq.(10) has the same structure as Eq.(3) and Eq.(6). In addition, random perturbation to move the system towards its thermal equilibrium in simulated annealing is the same as updating rule of the Hopfield network. The only difference is that λ in eq. (6) is replaced with temperature T. It means that given T, flow to thermal equilibrium in MFA is the same as the flow of Hopfield network given λ. Therefore, if we find the stable points of states by slowly lowering λ from the high value, then we will find global solutions or near global solution of the network without initial restriction. We call this algorithm as the annealed Hopfield network(AHN).

2.3 The Critical Temperature(T_c) and Uniqueness Coefficient(q)

Setting the operating parameters for the annealed network significantly affects a final solution. Starting at too high a temperature above the critical temperature is just time-consuming since no progress is made toward a solution until the critical temperature is reached. Starting at too low a temperature can quench the system and quickly force it into a poor solution. In addition, neural networks often enforce problem constraints through penalty functions which must be weighted in importance against the remaining cost components of the objective function. Weighting penalties too heavily leads to valid but poor solutions, while reducing the penalties permits infeasible solutions to arise. In this section, techniques for estimating T_c and q are explained. D. E. Van Den Bout *et al.* use normalization technique to improve solutions of TSP[16]. However, the technique is hard to implement hardware since it is not natural flow in biological neural networks or the analog Hopfield

network model. In this paper, we use the sigmoid function and derive critical temperature from the function. The *spin* perturbations near T_c are small enough so that all the spins remain near their high temperature average of $1/N$. With this assumption, the effect mean field changes have on the *spins* are found from the sigmoid function in Eq.(8) to be

$$\frac{\partial s_{ik}}{\partial u_{ik}} = \frac{(N-1)}{N^2 T} \tag{11}$$

From Eq.(5),

$$\frac{\partial u_{ik}}{\partial s_{jl}} = \begin{cases} 0, & ik = jl \\ T_{ikjl}, & ik \neq jl \end{cases} \tag{12}$$

The change of s_{ik}, Δs_{ik} cause the change of inputs of the other neurons Δu_{jl} as follows:

$$\begin{aligned} \Delta u_{jl} &= \frac{\partial u_{jl}}{\partial s_{ik}} \Delta s_{ik} + \sum_{jl \neq ik}^{N} \frac{\partial u_{jll}}{\partial s_{jl}} \Delta s_{jl} \\ &= T_{ikjl} \Delta s_{ik} \end{aligned} \tag{13}$$

Now, the change of s_{jl}, Δs_{il} from the change of u_{jl} is:

$$\Delta s_{jl} = \frac{\partial s_{jl}}{\partial u_{jl}} \Delta u_{jl} = \frac{N-1}{N^2 T} T_{ikjl} \Delta s_{ik} \tag{14}$$

From the change of s_{jl}, Δs_{jl}, the new input of ikth neuron Δu_{ik}^{b} is calculated:

$$\begin{aligned} \Delta u_{ik}^{b} &= \frac{\partial u_{ik}}{\partial s_{ik}} \Delta s_{ik} + \sum_{jl \neq ik} \frac{\partial u_{ik}}{\partial s_{jl}} \Delta s_{jl} \\ &= \sum_{jl \neq ik} T_{ikjl} \frac{(N-1)}{N^2 T} T_{ikjl} \Delta s_{ik} = \Delta s_{ik} \frac{(N-1)}{N^2 T} \sum_{jl \neq ik} T_{ikjl}^{2} \end{aligned} \tag{15}$$

Finally, we get the new perturbation Δs_{ik}^{b} from the Eq.(15)

$$\begin{aligned} \Delta s_{ik}^{b} &= \frac{\partial s_{ik}}{\partial u_{ik}} \Delta u_{ik} = \frac{(N-1)}{N^2 T} \frac{(N-1)}{N^2 T} \Delta s_{ik} \sum_{ik \neq jl} T_{ikjl}^{2} \\ &= \frac{(N-1)^2}{N^4 T^2} \Delta s_{ik} \sum_{ik \neq jl} T_{ikjl}^{2} \end{aligned} \tag{16}$$

In fact, the Hopfield network in the object matching problem is a fully connected network and the flow of the output change of neurons are very complicated. The result is based on the assumption that output changes of all the other neurons caused by the change of the ikth neuron Δs_{ik} are fed back to the ikth neuron and force the change of the ikth neuron to be accelerated when a temperature is near Tc. Therefore, we ignore the effect of other neuron outputs to simplify this problem. Let an average of connection strength be w. At the critical temperature, the spin perturbation must persist so that $\Delta s_{ik}^{b} = \Delta s_{ik}$. This results in:

$$\Delta s_{ik}^{b} = \frac{(N-1)^2}{N^4 T^2} \Delta s_{ik} N^2 w^2 = \frac{(N-1)^2}{N^2 T^2} \Delta s_{ik} w^2 \tag{17}$$

At $T = T_c$, $\Delta s_{ik}^{b} = \Delta s_{ik}$

$$T_c = \frac{N-1}{N} |w| \approx |w| \tag{18}$$

for $N >> 1$. q is not emphasized because valid solution is not quite definite in this problem. Therefore q has relatively small

value as it does in the TSP problem. q is set to the unit value in the energy function.

3. EXPERIMENTAL RESULTS

Several models are obtained and used in the matching procedure to test the new algorithm. Figure-1 shows images of model objects and occluded images. Once images are obtained, boundary is extracted by the chain code method. After extracting the boundary, corner points are obtained by using the optimal boundary smoothing method based on the constrained regularization technique. Figure-2 shows the boundary and corner points of the model objects. The number of segments of the models and occluded images ranges from 6 to 25. From each segment, features are extracted: an angle as local feature and the distance between nodes as relational feature. The boundary segmentation algorithm is very reliable in the sense that it is not noise dependable and it keeps detecting the same corner points from an object in different scenes. However, some models in occluded images are occasionally oversegmented or lose some corner points under the same threshold value. They affect matching procedure as occluded parts does. A matching algorithm should be tolerable for the false segmentation occurred in preprocessing stage as well as occlusion. AHN shows good performance in the above situation. Fig.-2(c) and Fig.-3(d) shows robustness of the algorithm under over-segmentation as well as occlusion. The number of the model is 8 but in the occluded image, the model has 14 segments. 8 nodes of the model are exactly matched with those of images. Figure-3 shows output plots of AHN. Star signs indicate matched nodes between model and occluded images. The results show the desired matchings are successfully obtained.

We also experiment on the critical temperature to see if the parameter estimation is correct. As shown in Figure-5, annealing through the higher temperature is wasted work since it has no effect on the energy function. Instead, most of the optimization occurs near the critical temperature. There is a precipitous drop in the energy function around the critical temperature where a coagulation starts. Annealing through the low temperature does not improve the solution but serves only to saturate the neurons at 1 or 0. As shown in Figure-4, the experiment result of Figure-3(a) was 0.45 of T_c while the estimate of Tc was 0.7. This discrepancy may result from the small number of neurons of the example since we assume that the number of neurons are very large for mean field approximation. Therefore we have the T_c be the half of the estimated T_c to get a valid solution.

4. CONCLUSION

Issues related to the reliable matching have been discussed in this paper. Annealing the network allowed convergence to begin close to the critical temperature such that good solutions were found. By estimating the critical temperature, we can get a near optimal solution by few steps decreasing temperature. In conclusion, AHN gives a reliable matching of the corresponding segments between two objects. The method eliminates possibility for a part of an object to be matched to similar segments in a different object. We conclude that AHN is a robust approach to solve the two-dimensional occlusion problems.

5. REFERENCE

[1] "An Efficient Matching Algorithm by a Hybrid Hopfield Network for Object Recognition", *IEEE Int. Symp. on Circuits and Systems*, San Diego, CA, May 10-13, 1992.

[2] R. Chin and C. Dyer, "Model-based recognition in Robot vision," *ACM Computing Survey*, vol 187, No. 1, pp. 67-108, March 1986.

[3] H. Liu, M. Srinath, "Partial shape classification using contour matching in distance transformation," *IEEE Trans. PAMI*, vol. 12, No. 11, pp 1072-1079, Nov. 1990.

[4] Y. H. Pao, **Adaptive pattern recognition and Neural networks**, Addison Wesley Publishing Co., Inc, 1989.

[5] J. J. Hopfield, "Neural networks and physical system with emergent collective computational abilities," *Proc. Natl. Acad. Sci. USA* vol. 79, pp 2554-2558, April 1982.

[6] Y Zhou *et al.* "Image restoration using neural network," *IEEE Trans. Acoust., Speech, Signal Processing*, vol. ASSP-

36, No. 7, pp 1141-1151, July 1988.

[7] J. J. Hopfield and D. W. Tank, "Neural computation of decisions in optimization problems," *Biolog. Cybernet.*, vol. 52, pp. 141-152, 1985.

[8] J. J. Hopfield and D. W. Tank, "Computing with Neural circuits: A model," *Science*, vol. 233, pp. 625-633, 1986.

[9] J. J. Hopfield, "Neurons with graded response have collective computational properties like those of two-state neurons" *Proc. Natl. Acad. Sci. USA* vol. 81, pp 3088-3092, May 1984

[10] S. Kirkpatrick, C. D. Gelatt, Jr., and M. P. Vecchi,"Optimization by simulated annealing," *Science*, vol. 220, no. 4595, pp. 650-671, May 1983.

[11] Davi Geiger and Alan Yuille,"A common framework for Image Segmentation," *International Journal of Computer Vision*, 6.3, pp. 227-243, 1991.

[12] David E. Van Den Bout and Thomas K. Miller, III,"Graph partitioning using annealed neural networks", *IEEE Trans. on Neural Net.* vol. 1, No. 2, pp. 192-203, 1990.

[13] Kwanghoon et al. "Optimal curvature estimation using constrained regularization technique" *25th Asilomar Conference on SSC*, 1992 (In press)

[14] W. Lin, F. Liao, C. Taso, and T. Lingutle, "A hierarchical Multiple-view approach to three-dimensional object recognition," *IEEE Trans. on Neural Net.* vol. 2, pp. 84-92, 1991.

[15] W. Li and M. Nasrabadi, "Object recognition based on graph matching implemented by a hopfield-style neural network," *Int. J. Conf. Neural Networks., II* , pp. 287-290, June 18-22, 1989.

[16] David E. Van Den Bout and Thomas K. Miller, III,"Improving the performance of the Hopfield-Tank neural network through normalization and annealing" *Biolog. Cybernet.*, vol. 62, pp. 129-139, 1989.

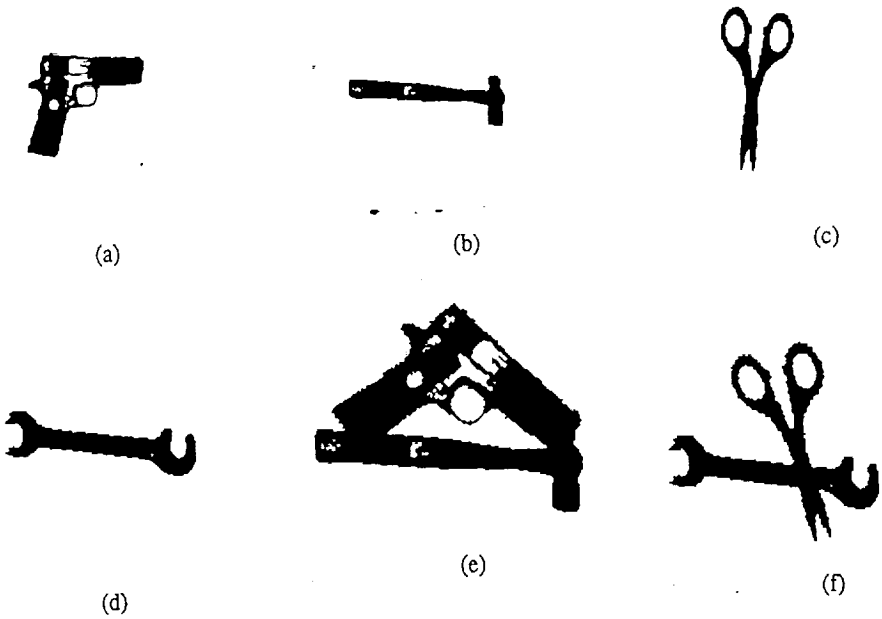

(a) (b) (c)

(d) (e) (f)

Figure-1: Model Images and Occluded Images

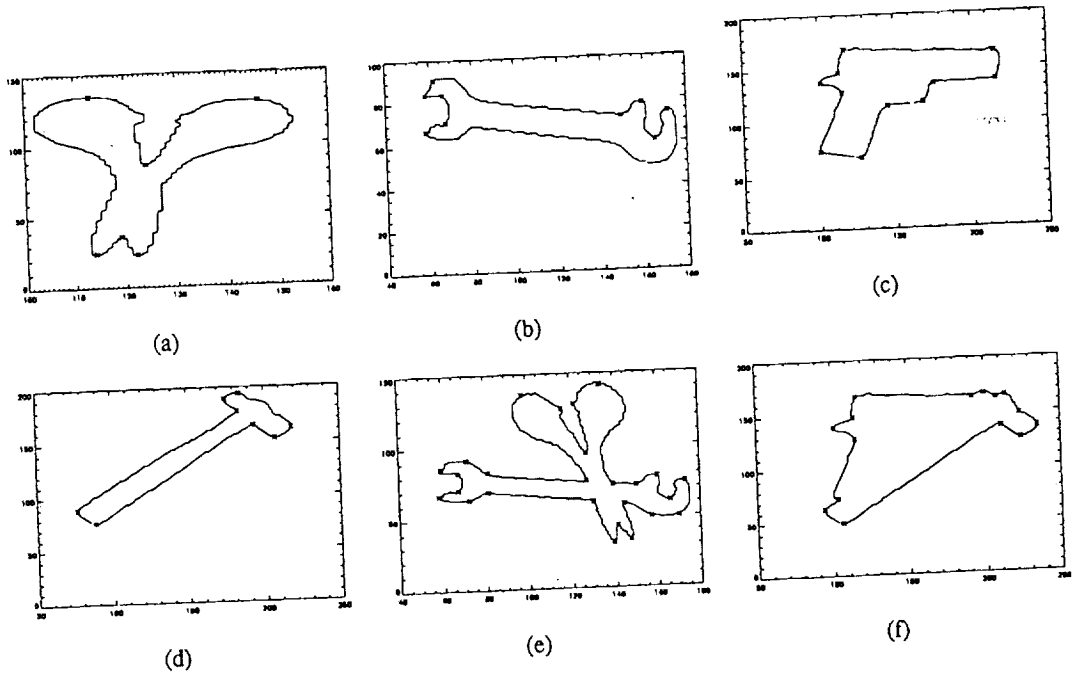

(a) (b) (c)

(d) (e) (f)

Figure-2: Boundary of Models and Occluded Images

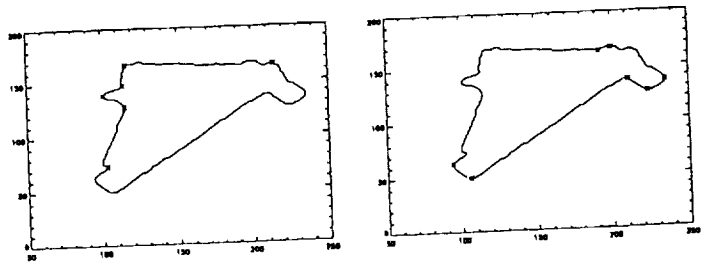

(a) (b)

Figure-3: Matched Nodes in Occluded images

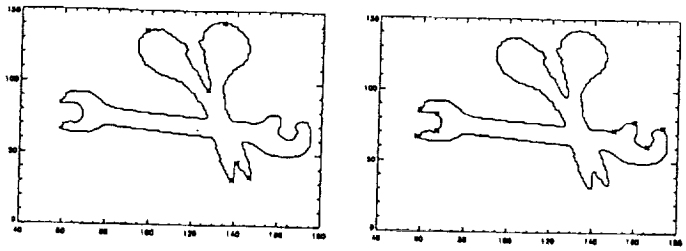

(c) (d)

Figure-3: Matched Nodes in Occluded images(continued)

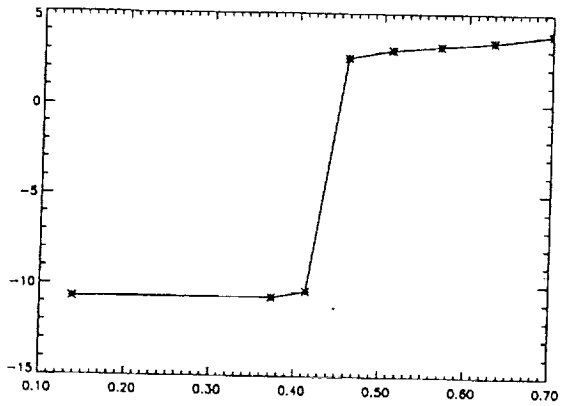

Figure-4: Energy vs. critical temperature